SYNTHESIS OF NANO MATERIALS AND NANO STRUCTURES FOR GAS SENSING APPLICATIONS

SUNIL KUMAR

A thesis submitted for the degree of

Doctor of Philosophy

Supervised by Prof. Vladimir Pavelyev

Nano-engineering Department

Samara National Research University

Samara, Russia

2021

D E C L A R A T I O N

I declare that this thesis has not been submitted as an exercise for a degree at this or any other university and it is entirely my own work.

I agree to deposit this thesis in the University's open access institutional repository or allow the library to do so on my behalf, subject to Russia Copyright Legislation and Samara National Research University Library conditions of use and acknowledgement.

Elements of this work that have been carried out jointly with others or by collaborators have been duly acknowledged in the text wherever included.

Sunil Kumar

A B S T R A C T

Carbon nanotubes have been of great interest, both from the fundamental point of view and for future applications. The most interesting features of these structures are their optical, chemical, mechanical and electronic characteristics, which opens a great prospect for future applications. These properties can even be measured on single nanotubes. For commercial application purpose, a large quantity of purified nanotubes is required.

A literature survey of published research on enhancing sensing parameters of gas sensor based on carbon nanotubes was performed to identify applications in which carbon nanotubes might improve on current sensor parameters, in either offering improved performance, reduced cost of manufacture, or both.

The objective of this thesis work is fabrication of gas sensor. NO_2 gas sensor which is based on single walled carbon nanotubes (SWCNTs) and its characterization for monitoring the concentration of NO_2 gas in the environment. The sensor development approach in this thesis has been creation of a resistive type NO_2 gas sensor using different functionalization techniques.

In order to enhance the important parameters of gas sensor such as sensitivity, response time and recovery time, a resistance-based sensor is developed using SWCNTs. various approaches were employed to improve the sensing parameters such as metal deposition, functionalization using polymers. The sensor's response is found to be much better compared to the previous existing functionalization technique which results in the development of simple and easy to handle and inexpensive NO_2 gas sensor.

PUBLICATIONS

1. **Sunil Kumar**, V. Pavelyev, P. Mishra, and N. Tripathi, "A Review on chemiresistive gas sensors based on Carbon Nanotubes: Device and Technology transformation," Sensors and Actuators: A Phys., vol. 283(2018), pp. 174–186. **DOI:** *https://doi.org/10.1016/j.sna.2018.09.061* **IF: 3.407** [**SCI, Scopus**] **[Q1]**

2. **Sunil Kumar**, Vladimir Pavelyev, Prabhash Mishra, Nishant Tripathi, "Thin Film Chemiresistive gas sensor on Single- walled carbon nanotubes- doped with Polyethylenimine (PEI) for NO_2 gas sensing," Bulletin of Materials Science, vol. 43 (2020) 1-7. **DOI:** *https://doi.org/10.1007/s12034-020-2043-6* **IF: 1.783** [**Scopus, SCIE**] **[Q2]**

3. **Sunil Kumar**, Vladimir Pavelyev, Prabhash Mishra, Nishant Tripathi, Vladimir Platonov; Prachi Sharma, F. Calle, "A review on 2D transition metal di-chalcogenides and metal oxide nanostructures based NO_2 gas sensors," Materials Science in Semiconductor Processing, vol. 107 (2020) 104865. **DOI:** *https://doi.org/10.1016/j.mssp.2019.104865*
   IF: 3.927 [**SCI, Scopus**] **[Q2]**

4. **Sunil Kumar**, Vladimir Pavelyev, Nishant Tripathi, Vladimir Platonov, Prachi Sharma, Rafiq Ahmad, Prabhash Mishra, Ajit Khosla, "Recent Advances in the Development of Carbon Nanotubes Based Flexible Sensors." Journal of The Electrochemical Society, vol. 167 (2020) 047506. **DOI:** *https://doi.org/10.1149/1945-7111/ab7331* **IF: 4.316** [**Scopus, Web of Science**] **[Q1]**

5. **Sunil Kumar**, V. Pavelyev, P. Mishra, and N. Tripathi, "Sensitive detection of nitrogen dioxide using gold nanoparticles decorated single walled carbon nanotubes," in CEUR Workshop Proceedings, (2017), vol. 1900, pp. 74–77. *DOI: 10.18287/1613-0073-2017-1900-74-77* **[Scopus]**

6. Mohammad Talib, Nishant Tripathi, Prachi Sharma, P.M.Z Hasan, Ammar A. Melaibari, Reem Darwesh, Aleksey V. Arsenin, Valentyn S. Volkov, Dmitry I. Yakubovsky, **Sunil Kumar**, Vladimir Pavelye, Prabhash Mishra, "Development of ultra-sensitive broadband photodetector: A detailed study on hidden photodetection-properties of TiS2 nanosheets," Journal of Materials Research and Technology., vol. 14(2021), pp. 1243-1254. DOI: https://doi.org/10.1016/j.jmrt.2021.07.032 **IF: 5.039** [**Scopus, Web of Science**] **[Q1]**

7. Nishant Tripathi, Vladimir Pavelyev, Prachi Sharma, **Sunil Kumar**, Anastasiia Rymzhina, Prabhash Mishra, "Review of titanium trisulfide (TiS3): A novel material for next generation electronic and optical devices," Materials Science in Semiconductor Processing, vol. 127 (2021) 105699. **DOI:** *https://doi.org/10.1016/j.mssp.2021.105699*
   IF: 3.927 [**SCI, Scopus**] **[Q2]**

8. Prachi Sharma, Vladimir Pavelyev, Sunil Kumar, Prabhash Mishra, S.S. Islam, Nishant Tripathi, "Analysis on the synthesis of vertically aligned carbon nanotubes: growth mechanism and techniques." Journal of Materials Science: Materials in Electronics (2020) 1-45. **DOI:** *https://doi.org/10.1007/s10854-020-03021-6* **IF: 2.478** [**SCI, Scopus**] **[Q2]**

9. Sunil Kumar, Nishant Tripathi, Prachi Sharma, Prabhash Mishra, Vladimir Pavelyev, Daria Shishkina, Vladimir Podlipnov, Sergey Stafeev, Anastasiia Rymzhina, Vladimir Platonov, "Development of transition metal dichalcogenides for modern photodetector devices," in IEEE Xplore, 2021 International Conference on Information Technology and Nanotechnology (ITNT), IEEE, Samara, Russia, 2021, (Accepted) (**Scopus, Web of Science).**

10. V S Pavelyev, K N Tukmakov, A N Agafonov, N Tripathi, S Kumar, " Technologies of microsystem technique and nanosensorics" 2020 IOP Conf. Series: Materials Science and Engineering 984 012011. ISSN No.: 1757-8981 [**Scopus**] DOI: https://doi.org/10.1088/1757-899X/984/1/012011

11. N.Tripathi, Vladimir Pavelyev, Andrei Mezhenin, Sunil Kumar, Mariia Sovetkina, Anastasiia Rymzhina, Vladimir Platonov, "Graphene-based Infrared Radiation Sensor for Household Electronic Applications," IEEE Xplore, 2020 International Conference on Information Technology and Nanotechnology (ITNT), IEEE, Samara, Russia, 2020, pp. 1-3[**Scopus**]. DOI: https://doi.org/10.1109/ITNT49337.2020.9253255.

12. Nishant Tripathi, V. Pavelye, V.S. But, S.A. Lebedev, Sunil Kumar, Prachi Sharma, P. Mishra, M.A. Sovetkina, S. A. Fomchenkov, V. V. Podlipnov, V. Platonov, "Analysis and optimization of photonics devices manufacturing technologies based on Carbon Nanotubes, Journal of physics: conference series, vol. 1368(2019) 22034 [**Scopus**].
DOI: https://doi.org/10.1088/1742-6596/1368/2/022034

D E D I C A T I O N

I dedicate this thesis to all the researchers working on development of COVID-19 vaccines.

A C K N O W L E D G E M E N T S

It is a genuine pleasure to express my deep sense of thanks and gratitude to my mentor, supervisor and guide Professor Vladimir Pavelyev., head of Nanoengineering department, Samara National Resesarch University, Samara, Russia. His dedication and keen interest above all his overwhelming attitude to help his students had been mainly responsible for completing my work. His timely advice, meticulous scrutiny, scholarly advice and scientific approach have helped me to a very great extent to accomplish this task. It is an honour to work under her supervision.

I owe a deep sense of gratitude to Dr. Nishant tripathi, Department of Nanoengineering, Samara National Research University, Samara, Russia, for his keen interest on me at every stage of my research. His prompt inspirations, timely suggestions with kindness, enthusiasm and dynamism have enabled me to complete my thesis.

I thank profusely to Dr. Prabhash Mishara, Dr. R.V. Skidanov, Vladimir Platonov, Irina Kozlova and Special thanks to all the Nanoengineering department lab team members who have shared their knowledge and supported me during this research.

I am very grateful to the thesis committee members, for their invaluable support, guidance and providing their precious time and efforts in reviewing my thesis and providing valuable suggestions.

Last but not least, a heartfelt thanks to my lovely parents, family and friends who have supported me with their unconditional love in this wonderful journey.

C O N T E N T S

Contents

List of Tables:

LIST OF FIGURES:

Chapter 1: MOTIVATION

1.1 MOTIVATION

Development of science and Technology is a continuous process. From the beginning of life, human race is evolving day by day. Development of logical thinking has brought the evolution in science and technology to make the tools more powerful that are making the life easier day by day. These tools work in the feedback process and take parts in the further development of science and technology. We are living in an age where we are playing with the part of the nature which is as small as it can be well fitted in the definition of invisible. This is the world of Nano.

Development of quantum mechanics and the allied sciences have made the microscopic tools so powerful that I can see the thing at the nano scale. This magical scale brings a lot of extraordinary features of the materials that they do not show at the macroscopic scale. Carbon nanotube is one of the rigorously researched materials in the contemporary worlds. Owing to their extraordinary properties, CNTs have become one of the frontrunners in the world of contemporary research. When considering the cross-sectional area of the CNT walls only, an elastic modulus approaching 1 TPa and a tensile strength of 100 GPa has been measured for individual MWNTs. This strength is over 10-fold higher than any industrial fibre. MWNTs are typically metallic and can carry currents of up to $109 A cm^{-2}$. Individual CNT walls can be metallic or semiconducting depending on the orientation of the graphene lattice with respect to the tube axis, which is called the chirality. Individual SWNTs can have a thermal conductivity of 3500 $W m^{-1} K^{-1}$ at room temperature, based on the wall area; this exceeds the thermal conductivity of diamond. Because of these ultimate properties, CNTs are being used in variety of nanosensors, biosensors, in optoelectronic devices

such as solar cells, photodetectors and light emitting diodes, in different types of high-performance electronic devices, as reinforcement in different composite systems etc.

Exposure of NO_2 gas have harmful reactions over our body parts like eye, throat etc. More exposure of this NO_2 gas can be the cause of death. So, protection from this NO_2 gas is very necessary and important. In this regard NO_2 detectors can help to a great extend to avoid the risk related to excess exposure of NO_2 gas. This idea provides me motivation to develop NO_2 gas sensors with better response employing various techniques such as metal decoration and Functionalization of SWCNTs surface. The SWCNTs were grown using chemical vapor deposition method. I have optimized the SWCNTs surface functionalization using vaious techniques in order to develop better NO_2 gas detector.

1.2 Aim

Development of a small size NO_2 - sensor with improved sensing parameters on the base of functionalized nanomaterials.

1.3 Tasks

1) Development and investigation of single walled Carbon Nanotubes (SWCNTs) decoration method based on the use of gold nanoparticles.
2) Development and investigation of single walled Carbon Nanotubes (SWCNTs) functionalization method based on the use of (Polyethylenimine) PEI.
3) Fabrication of Au decorated SWCNTs NO_2 sensor.
4) Fabrication of PEI functionalized SWNTs NO_2 sensor.
5) Response analysis of Au decorated SWCNTs sensor for NO_2 gas detection.

6) Response analysis of PEI functionalized SWCNTs sensor for NO_2 gas detection.

Scientific novelty:

1) Novel methods have been developed and investigated for functionalization of SWCNTs for NO_2 sensing.
2) The enhancement in the sensitivity of NO_2 -sensor after gold nanoparticles decoration on the surface of SWCNTs is demonstrated.
3) The improvement in the NO_2 gas sensing parameters such as sensitivity, response/recovery times and repetibilty after surface functionalization of SWCNTs with Polyethylenimine (PEI) Polymer is demonstrated.

Practical significance:

The development methods can be used for effective solution for noxious gas NO_2 detection problem.

The reliability of the results obtained:

The reliability of the results obtained and presented in the present work is confirmed by number of experiments and principal agreement with previously obtained scientific results.

Authors' contribution:

All the results presented in the dissertation were obtained by the author personally or with his definitive participation.

The following are submitted for defense:

1) Novel methods have been developed and investigated to functionalize the surface of SWCNTs NO_2 -sensor.

2) The enhancement in the sensitivity of sensor after gold nanoparticles decoration on the surface of SWCNTs is demonstrated.

3) The improvement in the sensing parameters such as sensitivity, response/recovery times and repetibilty after surface functionalization of SWCNTs with Polyethylenimine (PEI) polymer is demonstrated.

Publications and approbation of work:

In total, based on the results of the dissertation, 12 works were published, of which 7 articles were published in international peer revewed journals and 5 in international conference proceedings.

List of conferences:

ITNT conferences (2017-2021)

1. **Sunil Kumar**, V. Pavelyev, P. Mishra, and N. Tripathi, "Sensitive detection of nitrogen dioxide using gold nanoparticles decorated single walled carbon nanotubes," in CEUR Workshop Proceedings, (2017), vol. 1900, pp. 74–77. *DOI: 10.18287/1613-0073-2017-1900-74-77* **[Scopus]**

2. **Sunil Kumar**, Nishant Tripathi, Prachi Sharma, Prabhash Mishra, Vladimir Pavelyev, Daria Shishkina, Vladimir Podlipnov, Sergey Stafeev, Anastasiia Rymzhina, Vladimir Platonov, "Development of transition metal dichalcogenides for modern photodetector devices," in IEEE Xplore, 2021 International Conference on Information Technology and Nanotechnology (ITNT), IEEE, Samara, Russia, 2021, (Accepted) (**Scopus, Web of Science).**

3. N.Tripathi, Vladimir Pavelyev, Andrei Mezhenin, **Sunil Kumar**, Mariia Sovetkina, Anastasiia Rymzhina, Vladimir Platonov, "Graphene-based Infrared Radiation Sensor for Household Electronic Applications," IEEE Xplore, 2020 International Conference on Information Technology and Nanotechnology (ITNT), IEEE, Samara, Russia, 2020, pp. 1-3[**Scopus**]. DOI: https://doi.org/10.1109/ITNT49337.2020.9253255.

4. Nishant Tripathi, V. Pavelye, V.S. But, S.A. Lebedev, **Sunil Kumar**, Prachi Sharma, P. Mishra, M.A. Sovetkina, S. A. Fomchenkov, V. V. Podlipnov, V. Platonov, "Analysis and optimization of photonics devices manufacturing technologies based on Carbon Nanotubes, Journal of physics: conference series, vol. 1368(2019) 22034 [**Scopus**].
DOI: https://doi.org/10.1088/1742-6596/1368/2/022034

International Workshop on Navigation and Motion Control (NMC 2020) conference:

1. V S Pavelyev, K N Tukmakov, A N Agafonov, N Tripathi, **S Kumar**, " Technologies of microsystem technique and nanosensorics" 2020 IOP Conf. Series: Materials Science and Engineering 984 012011. ISSN No.: 1757-8981 [**Scopus**] DOI: https://doi.org/10.1088/1757-899X/984/1/012011

Chapter 2: Materials and Background

2.1 Introduction

The fundamental constituent or the building block of Carbon nanotubes is Carbon. This group IV element of periodic table is well known for its incredible ability to form crystalline solids and variety of other compounds. It is placed on sixth position in periodic table. Two out of its 6 electrons lie in 1s orbital, remaining electrons form sp^3, sp^2 or sp hybrid orbital (see Figure 2.1 (a)). These 4 valance electrons constitute allotropes of Carbon such as Carbon Nanotube, Diamond, Graphite, Graphene and Fullerenes [1]. Figure 2.1 (a) shows the orbital diagram of carbon atom. It's an important fact that existing electronic bonds are very poor in outer two orbitals as compare to first orbital. Due to weaker attraction of outer shell electrons than inner shell electrons, outer orbital electrons participate in electron hybridization. Small energy gradient between outer two orbitals (i.e. 2s and 2p) aids the overlapping of orbital wave functions favoring electron hybridization (see. Figure 2.1 (b)). There are three accessible mixing of atomic orbitals in carbon atom making hybrid orbitals typically referred as sp, sp^2 and sp^3 hybridization **(see** Figure 2.2 (a), 2.2(b) and 2.2(c)). In sp hybridization one 2s and one 2p electrons participate in mixing (forming sigma bonds) and leaving two 2p electrons free of mixing (pi bonds). Sp^2 hybridization involves mixing of one's orbital electron and two 2p electrons. In sp^3 hybridization all outer shell electrons of carbon atoms take part in mixing. The orbitals are focused on corners of a tetrahedron restricted to carbon atom. According to hybridization a carbon atom makes bonds with minimum 1 to maximum four partners to produce compounds. Structural quality of carbon-based compounds and allotropes also depends on type of hybridization. For sp^l hybridization, $(l + 1)$ σ bonds take charge to form generally one-dimensional local structure. The

linear chain compound of carbon i.e. 'Carbyne' is an example of sp hybridization. Sp^2 hybridization leads to formation of two-dimensional structures such as graphene.

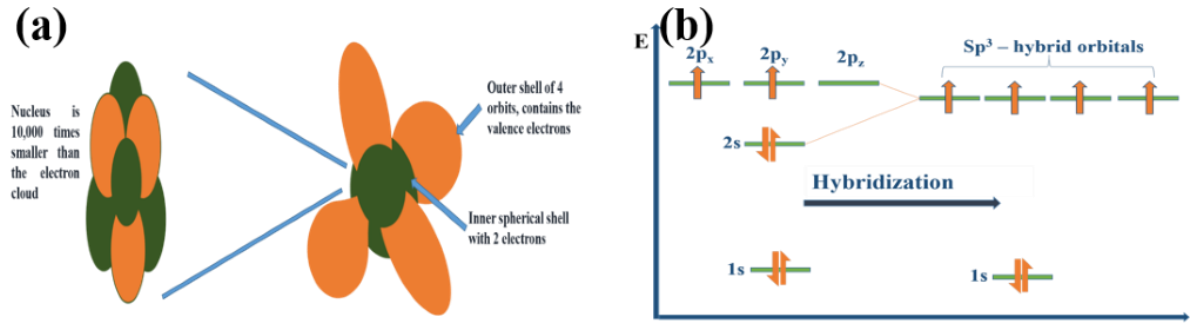

Figure 2. 1: (a) shows the basic structure of carbon atom; (b) shows atomic orbitals and sp^3 – hybridization.

3D structures such as Diamond is formed by sp^3 hybridization. It is also a noticed that in sp and sp^2 mixing one or two p orbital does not involve in hybridization, instead show their presence in the form π- bonds. Depending on orbital mixing Carbon have many allotropes and among these amorphous carbon, Diamond, Graphite, Graphene and Carbon Nanotube have received great amount of attention [2]. These allotropes of carbon exhibit a part or complete different property in nature. For their commendable and extraordinary multidimensional properties be it Carbon Nanotubes, graphene or diamond- others, allotropes of carbon have become hot cake for research investigations.

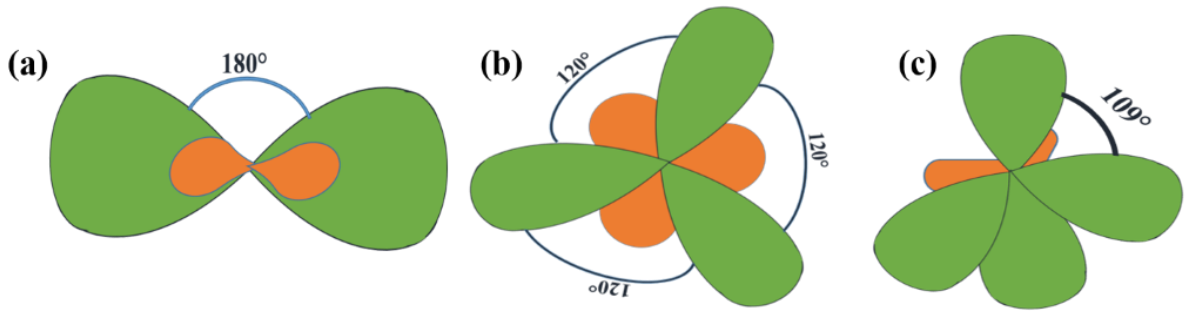

Figure 2. 2: Figure shows hybridization in Carbon atoms (a) Sp (b) Sp^2 and (c) Sp^3.

2.2 Graphite

The word graphite is taken from a Greek word 'graphein' i.e. 'write'. Pencil which is an attractive and widely used tool for writing and drawing is made from it. It was invented by Debye et. al. in 1917 [3]. Graphite is a combined structure of layers. Each layer is called Graphene [4]. In graphite structure, carbon atoms are situated in hexagonal fashion on XY plane [5-6]. The distance between carbon atoms in a single layer of graphite is 0.142nm. The separation distance between layers of graphite is approximately 0.335nm (see Figure 2.3 (a)) [7]. The graphene layers are held together by weak van der wall forces to form solid structure graphite. Each Carbon atom is situated on edge of hexagon having three σ-bond in sp^2 hybridization form in which three valance electrons participates in hybridization and one valance electron exists in p_z orbital creating two-dimensional electron gas in the form of π- bond or cloud. It is spread all over on individual XY plane of

graphite. Due to mobility of said electron gas, graphite shows electrical conductivity.

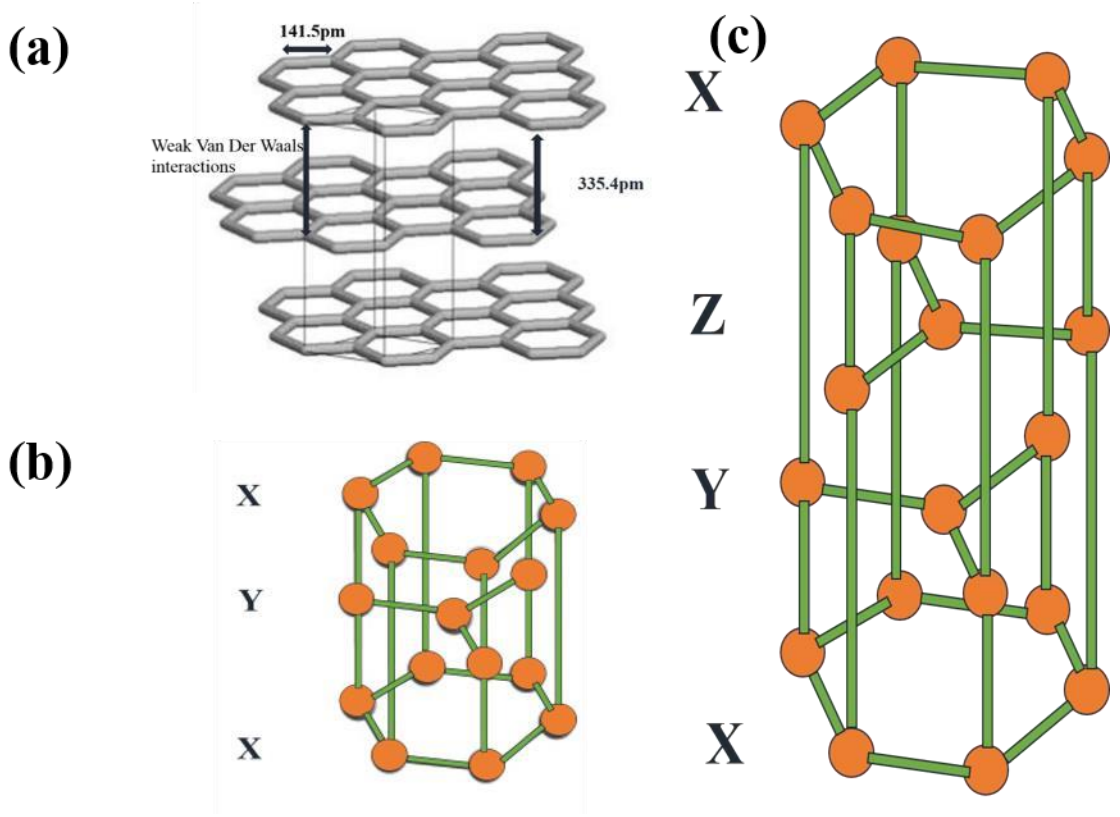

Figure 2. 3: (a) shows the Basic structure of graphite and figure (b) and (c) shows its hexagonal and rhombohedral structure

It is more reactive than diamond. The separation distance between nearest two carbon atoms on individual layer of graphite is around 0.142nm which is approximately equal to band order of 1.5 and two times larger than aromatic carbon atom's covalence radius. The separation gap among nearest two layer of graphite is approximately two times of van der Waals radius. The weak van der Waals interaction within layers of graphite causes the layers of graphite to easily move along the XY plane.

Generally, two types of graphite are found in nature abundantly: a stable form that is hexagonal or α- graphite and rhombohedral or β- graphite (see Figure 2.3 (b and (c))). β- graphite is more

abundant in nature than α- graphite. By heat treatment, β- graphite can be changed into α-Graphite. Other than these two, a few more types of graphite are found in nature. Some time, due to some disorder in stacking, no more attraction exists between layers and hence individual layer of graphene of graphite randomly turned around z- axis and move in XY plane resulting in a turbostratic structure.

2.3 Diamond

Diamond is an allotrope of carbon with sp^3 hybridization. Every carbon atom in diamond is bonded by 4 nearest carbon atoms. Each diamond cell has tetrahedron structure with bond length of 154.45pm. Mainly two types of structures of diamond are found (see Figure 2.4(a) and (b). cubic and hexagonal (see Figure 2.5) out of which cubic structure is more available than hexagonal [8-9]. Hexagonal shaped diamonds are very precious and rare to found. It was firstly found in 1967 in a meteorite. Still, there is a possible way to artificially synthesize hexagonal type diamond by graphite by heat treatment of graphite under high pressure with ambient temperature along vertical axis.

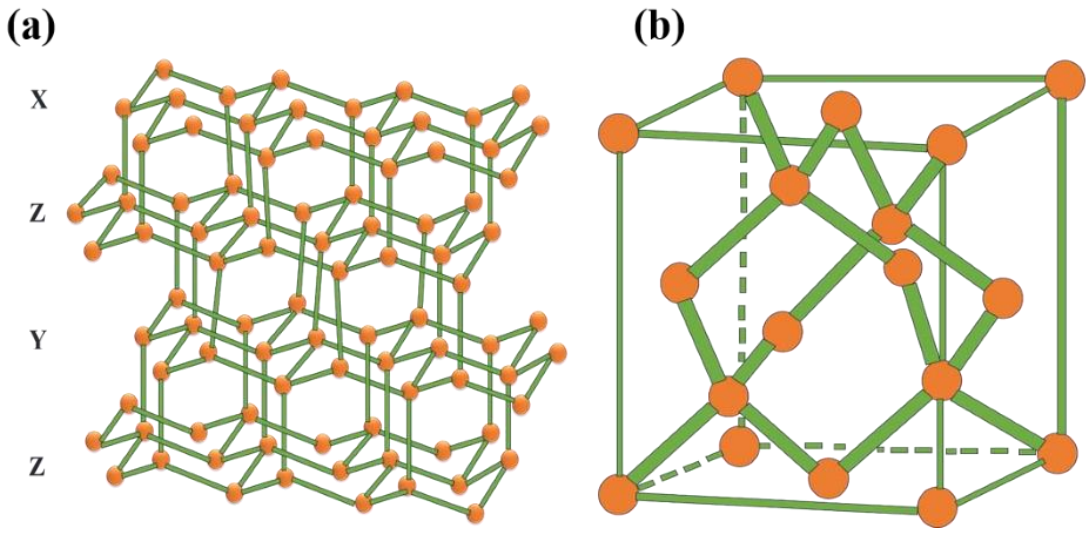

Figure 2. 4: (a) shows the lattice structure of cubic diamond and (b) shows its unit cell.

Some other structures are also found in which nitrogen molecules are mixed with carbon atoms. Some noticed nitrogen contained diamonds are Ia, Ib, IIa and IIb. If nitrogen contamination is like platelets, then it is Ia structure with composition C_3N. In Ib type nitrogen molecules are homogeniously spread all over the structure. And if diamond structure having null nitrogen then it is called IIa. Last one structure having very small probablaty to get in nature.

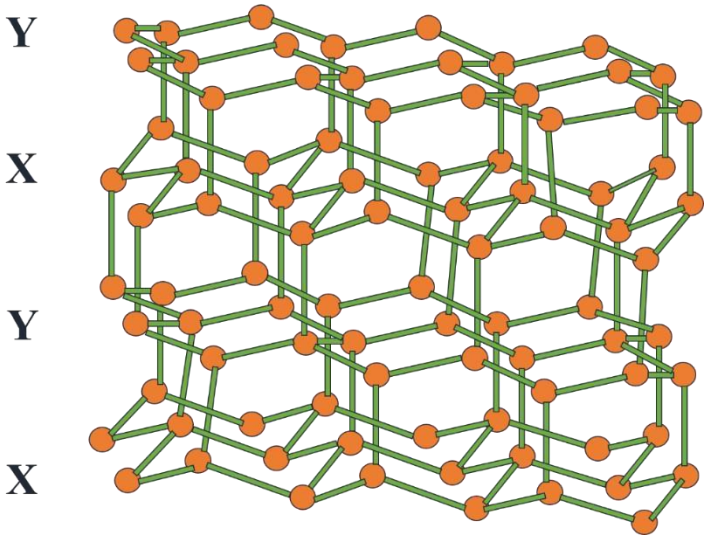

Figure 2. 5: The lattice structure of hexagonal diamond. The arrangement of atoms in the horizontal crystal plane somewhat resembles a "wavy" graphite structure.

Last one type i.e. IIb is semiconducting diamond. In that case, nitrogen is completely absent. Instead of nitrogen, IIb type of diamond structure have some contamination of aluminum. In a normal | diamond -unit cell eight atoms exist having face centered cubic packing. The lattice constant of diamond lattice is 356.68 pm [10-14]. Another noticeable point about Diamond's structure is that it's packed in a sphalerite kind instead of dense packing. Its structure is a penetration of two faces. Its Centered cubic lattices can be move along unit cell' space diagonal.

Another thing is that if diamond is heating with specific condition i.e. 3750° C temperature and 1840psi pressure, it is converted to graphite. It is also possible to make hexagonal structure like its cubic type structure from tetrahedrons of carbon with different configuration. In said configuration, cell is made with 4 carbon atoms with lattice parameters a_o= 252pm and c=412pm [11].

2.4 Graphene

As described in graphite section, if single layer of graphite is peeled off from bulk material, then it is called graphene. It is a single planar structure containing covalent bonded carbon atoms [15] thus also known as planar allotrope of carbon. Buckyball, nanotubes and graphite are allotropes of graphene. If graphene is folded in a shape of sphere, then it becomes the Buckyball or if rolled along any of its axis then it takes the form of nanotube. Stacked layers of graphene through its XY plane is graphite. Therefore, graphene may be called generator of three allotropes of carbon. Thus, it is vital to study the properties of graphene to understand the properties of Carbon Nanotubes and other two allotropes. The basic structure of graphene and corresponding electron spin with carbon atoms is shown in Figure 2.6 (a), (b) and (c). The 2s, $2p_x$ and $2p_y$ electrons interacts in hybridized fashion giving graphene its characteristic physical electrical properties (three sp^2 mixed orbitals with electron configuration are shown in Figure 2.6 (a)) [15].

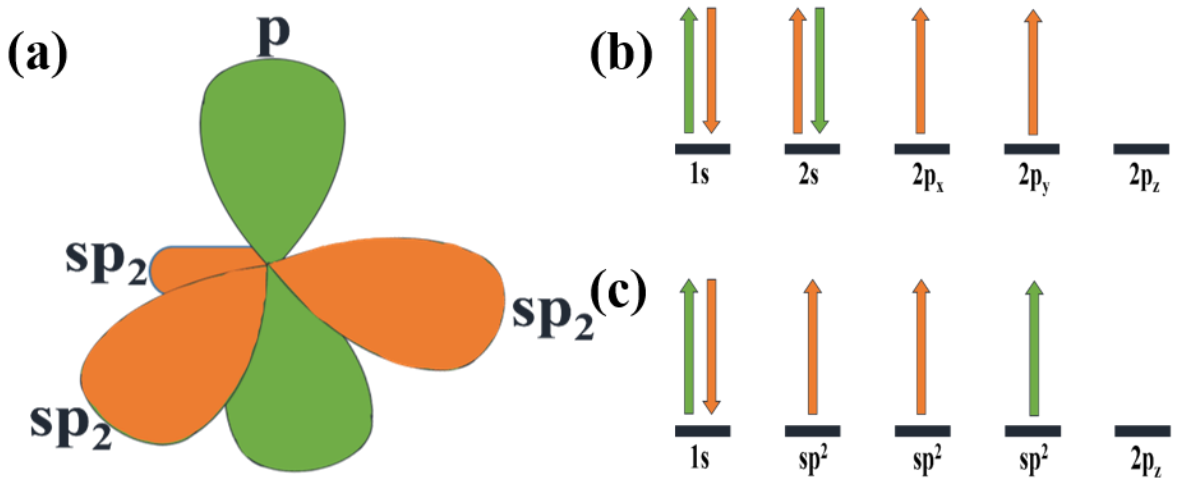

Figure 2. 6: figure (a) shows the basic atomic structure of graphene; (b) and (c) shows electronic spin in carbon atom and graphene cell respectively.

Sp^2 hybridization results in formation of very stable covalent bonds (σ-bonds) on graphene surface which is the reason of graphene and CNTs being the strongest material with superior mechanical properties among other materials known. Un-hybridized atomic $2p_z$ orbital forms say, π-bonds normal to XY plane due to electron gas delocalization. These π-bonds provide graphene its distinctive electronic properties [16]. Structurally Graphene has two types of lattice arrangements direct and reciprocal lattice.

2.4.1 **Direct Lattice**

Honeycomb structure of direct lattice graphene can be explained by ball and stick model (see fig. 1.7(a)). In ball and stick model carbon atoms are denoted by ball and sticks represent σ-bonds. σ-bonds of graphene have bond length around 1.42 Å. Such type of lattice may be considered as Bravais lattice. The basis of Bravais lattice is 2 (Point A and Point B in Figure 2.7(a)) given as two π electrons per unit cell and depicts enhanced electronic property of graphene [17].

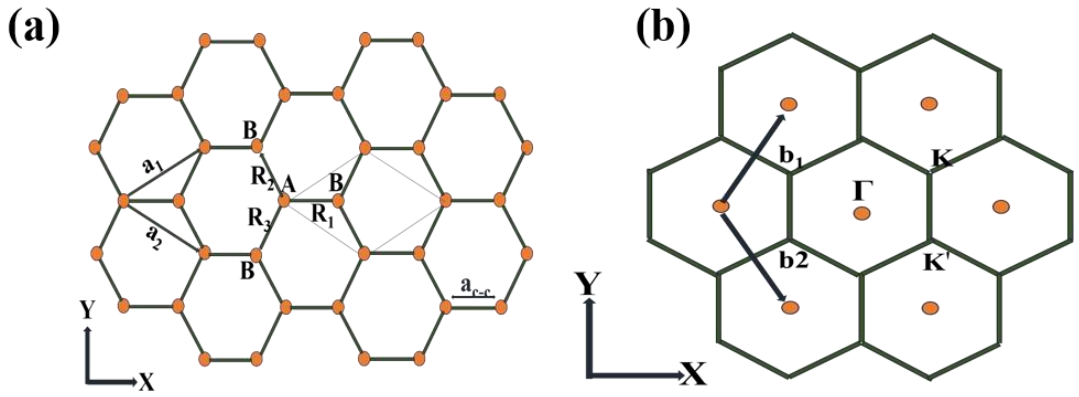

Figure 2. 7: Figure shows various lattice structures of graphene; (a) direct (b) reciprocal.

The primitive unit cell of said honeycomb lattice may be taken as equilateral parallelogram. The length of side of parallelogram is as following:

a = √3(length of a σ-bond)

= 2.46 Å.

The vectors of primitive unit cell are as following:

a_1 = (√3a/2, a/2), (1) a_2 = (√3a/2, a/ (-2)) (2)

Where vector $|a_1| = |a_2| = a$, describes the separation distance between two nearest carbon atoms.

R_1= (a/√3, 0) (3)

R_2= (-a_2+ R_1)

R_2= (-a/2√3, -a/2) (4)

R_3= (-a_1+ R_1) (5)

With $|R_1| = |R_2| = |R_3|$ = length of σ-bond.

2.4.2 **The Reciprocal Lattice**

The rotated lattice with angle of 90° with reference of direct lattice is called the reciprocal lattice of graphene (see Figure 2.7(b)) [17]. Similar to direct lattice, reciprocal lattice also has Carbon atoms arranged in honeycomb structure. The vectors of said lattice is given below:

$$\mathbf{b_1} = \mathbf{(2\pi/\sqrt{3}a,\ 2\pi/a)} \qquad \mathbf{(6)}$$

$$\mathbf{b_1} = \mathbf{(2\pi/\sqrt{3}a,\ -2\pi/a)} \qquad \mathbf{(7)}$$

Where $|b_1| = |b_2| = 4\pi/\sqrt{3}a$.

2.5 Fullerene

Fullerene, an extraordinary polymorphic form of carbon was invented by Harry Kroto in England in 1985 [18]. The hollow structure of sixty carbon atoms is breathing in discrete molecular form (see Figure 2.8).

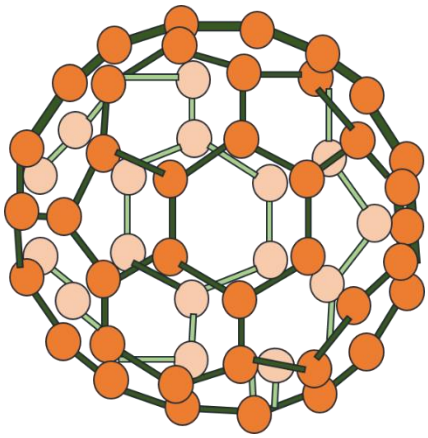

Figure 2. 8: Lattice structure of fullerene

Individual molecules of fullerene are presented by notation C_{60}. In crystal lattice of fullerene, combination of two types of structures i.e. honeycomb and pentagon is found. I can see a fullerene in Figure 2.13[19-21]. C_{60} molecule look like a symmetric soccer ball. In molecular configuration, it has twelve pentagons and twenty hexagons. These pentagons and hexagons are fashioned in a

specific manner. In C_{60} molecules, no two pentagons share a common wall. That type of C_{60} molecules is known as Buckminster- fullerene. Buckminster is added to given regard to Buckminster fuller whose invention is geodesic dom. It is observed that C_{60} is clone of said dome. Fullerene is itself a class of material that are configured with said molecules [22-23].

2.6 Carbon Nanotubes

The history of Carbon tubular structure starts after invention of electron microscopes in 1950 [24]. In 1952, a hollow tube of carbon was invented by a Russian researcher, Radushkevich ve Lucyanovich, however article did not gather much attention being it published in local language [25]. Related structure was again investigated by Baker, et al. in 1972 [26]. In 1976, Oberlain et al. described single cylinder hubs in graphite structure of carbon fibres [27]. Finally, in 1991 Sumio Iijima, an electron microscopist, discovered the cylindrical structure of carbon during analysis of fullerenes, another allotrope of carbon (Dupuis 2005). His discovery caught attention of worldwide researchers to the field of Nano Technology. Almost two years later, same group of researchers achieved another milestone in field of Nano Technology by inventing Single Wall CNTs (SWNTs).

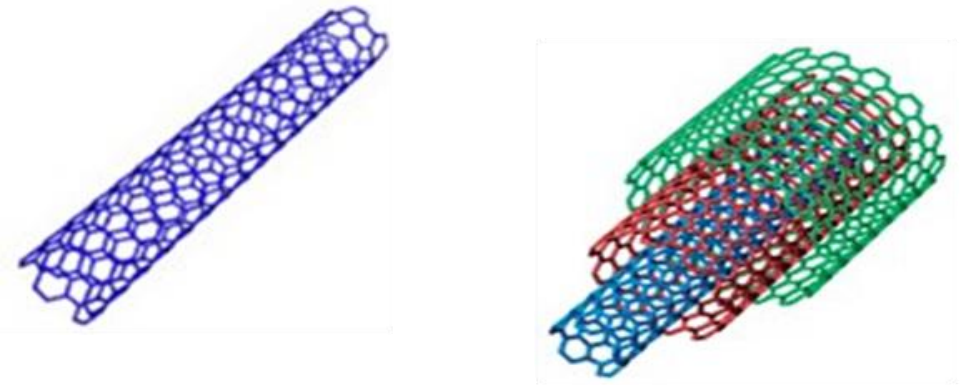

Figure 2. 9: Picture of SWNT.

Figure 2. 10: Picture of MWNT.

CNT is one of the essential allotropes of graphene and is formed when graphene sheet is rolled into a seamless hollow tube. Practically it is impossible to roll a graphene sheet into cylindrical structure because of ultra-small dimensions. It is only said to understand the structure of CNTs. Generally, diameter of CNTs lie between 0.5nm to 5nm thus termed as nanotubes. The length of CNTs however falls from 2nm to cm range [2]. CNTs are also called as a tubical fullerenes. Generally, CNTs are found in two structure (1) Single Wall Carbon Nanotubes (SWNTs) (see Figure 2.9) and (2) Multi Wall Carbon Nanotubes (MWNTs) (see Figure 2.10). If Single graphene sheet is rolled to make CNTs then it is called SWNTs and if more than one graphene sheets are concentrically rolled in 'Russian dolls model' then the tubes are called MWNTs. SWNTs are discussed below followed by introduction about MWNTs.

2.6.1 **SWNTs type and structure**

On the basis of structure, SWNTs are divided in three categories:

1. Zigzag
2. Armchair
3. Chiral

The types of SWNTs depend on the type of rolling of graphene sheets, which is the basis of the tubular structure of the CNTs. It is possible to calculate chirality (helicity) as well as diameter of SWNTs from a vector, called the chiral vector C_h. It is defined by $C_h = na_1+ma_2$ where n, m= 1,2,3. with notation as (n, m).

The diameter of SWNTs according to said model is calculated by the following equation:

$$d = \frac{|Chiral\ vector|}{\pi}$$

$$d = \frac{\sqrt{3} * b\sqrt{n * n + nm + m * m}}{\pi}$$

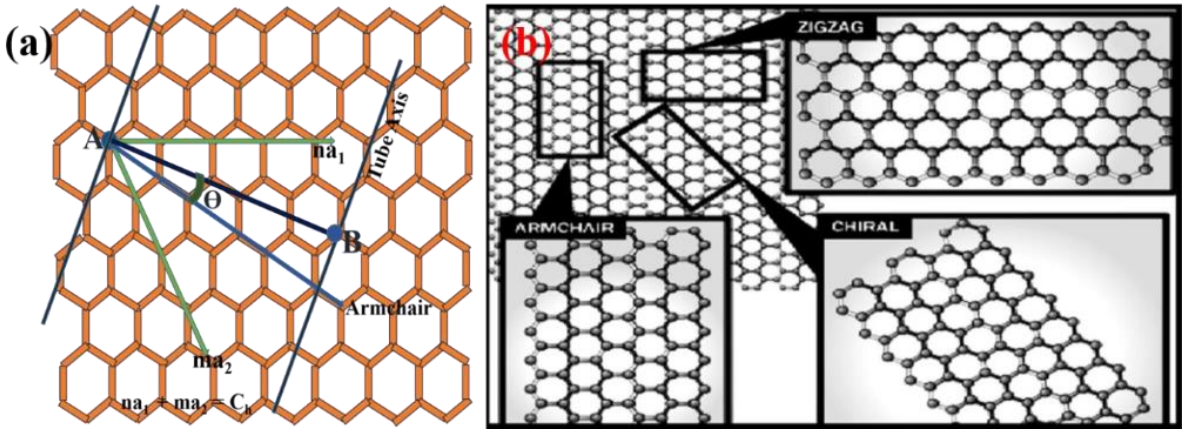

Figure 2. 11: Figure (a) shows the honeycomb structure of carbon atoms; (b) shows different type structure of CNTs.

Where b has the value 0.142nm which represents the carbon-carbon bond length. It is observed that CNTs diameter strongly depends on its chirality. A CNT having (5,5) chirality tends to have smaller diameter than a CNTs with (10,10) chirality. Steps to calculate of chirality as mentioned below:

1. Plot the tube axes. Tube axes are edges of nanotubes. If tube axes join with each other in the form of cylinder, then it becomes nanotubes (see Figure 2.11(a)).
2. Mark a point **A** along the tube axis, where tube axis interacts with carbon atoms.
3. Draw the armchair line (thin yellow line) by finding any point along the tube axis that travels across each hexagon, separating them into two equal halves.

4. Take a point **B** on second tube axis at intersection of tube axis and carbon atoms. It should be nearest intersection point from armchair line.
5. Draw a line AB representing the chiral vector $\mathbf{C_h}$. Chiral vector is equivalent to CNTs circumference.
6. Angle θ between armchair line and chiral vector decides the type of SWNTs.
7. If armchair line and chiral vector overlap each other i.e. when **θ= 0°** (**n=m**), then resultant SWNTs are called the armchair SWNTs (see Figure 2.11(b)).
8. If said wrapping angle **θ= 30°** (**m=0**), then Zigzag nanotubes are formed (see Figure 2.11(b)).

S. No.	Symbol	Name	Chiral CNT	Armchair CNTs	Zigzag CNTs
1.	C_h	Chiral Vector	$C_h = na_1 + ma_2 = (n,m)$	$C_h = (n,m)$	$C_h = (n,0)$
2.	C_h	Length of Chiral Vector	$C_h = \lvert C_h \rvert = a\sqrt{n^2+nm+m^2}$	$C_h = a\sqrt{3}n$	$C_h = an$
3.	d_t	Diameter	$d_t = \frac{a}{\pi}\sqrt{n^2+nm+m^2}$	$d_t = \frac{an}{\pi}\sqrt{3}$	$d_t = \frac{an}{\pi}$
4.	Θ	Chiral Angle	$\cos\theta = \frac{2n+m}{2\sqrt{n^2+nm+m^2}}$	$\theta = 30°$	$\theta = 0°$
5.	N	Number of hexagons/cells	$N = \frac{2C_h^2}{a^2 g_d}$	$N = 2n$	$N = 2n$

Table 2. 1: various parameters for SWNTs.

9. If wrapping angle θ is exist between 0° and 30°, then made SCNTs are called the Chiral Nanotubes (see Figure 2.11(b)). Among all types of CNTs, chiral type CNTs have superior place. Because chirality is an elemental theory to investigate different configured CNTs and their relative electronic band structures. So, it is important to understand the concept and its application to identify CNTs structure. Table 2.1 shows the parameters and their relatives' equations for CNTs.

2.6.2 **Chirality**

The word chirality comes from Greek language that means HAND. It is used to represent reflection symmetry between an object and its mirror image. In general, a chiral object is antisymmetric to its mirror image. For example, if I take the mirror image of our left hand and try to superimpose on left hand, it does not accurately superimpose which indicates hands to be chiral objects. Similarly, CNTs that are superimposed to their mirror image are called achiral CNTs. Zigzag and armchairs are examples of achiral CNTs.

2.6.3 **Electronic Properties of CNTs**

Electronic properties of CNTs provide great opportunities in nano-electronics research applications. Ultra-small dimensions and ultra-symmetric structures create remarkable quantum effects and electronic properties of the nanotubes. Due to circumferential confinement effect on tube, SWNTs and MWNTs [28-33] show the quality of quantum wire. Experimental investigations have proved that MWNTs and rope of SWNTs behaved like parallel assembly of single SWNTs. The electronic conductance for said assembly is given by

$$\mathbf{G = Go\ M = (2e^2/h)\ M}$$

Where, the calculated value of quantized conductance ***Go*** is 12.9 $k\Omega^{-1}$. Another parameter used in equation i.e. **M** is the measurement of exact conducting channels and its exact value for defect free ideal SWNT is 2. The value of M is determined by the intrinsic properties of nanotubes, coupling between tubes impurities, defects in structure of tubes, interaction with substrate and on contacts made for electronic connections. So, the experimental value of conductance is lesser than

the quantized value [34]. Many research groups reported about graphite's resistivity. It depends strongly on quantity of graphite taken for analysis. The best quality graphite has the resistivity around 0.4μΩmat room temperature [35]. In case of CNTs, the MWNTs as well as rope of SWNTs have much higher than the resistivity of best quality of graphite. It is also reported that the resistivity of said nanotubes decreases with temperature. These results were found due to random orientation of nanotubes on substrate. Same measurement was taking for purified CNTs aligned between four electrodes then it found much less than 0.4μΩm [34, 36]. In defect free nanotube, π electrons are more distributed as compare to graphite. It happens due to σ-π re-hybridization. And these conditions made graphene more conductive as compare to graphite [34]. So, CNTs are called 1-D conductor.

2.6.4 **Optical Properties of CNTs**

A defect less SWNTs have direct band gap. It also has well defined structure of sub band. Such type of structure is considered ideal for optical applications. Optical spectra for SWNTs may be obtained by resonant Raman spectroscopy [35] and by fluorescence spectroscopy [36]. An optical spectrum is obtained for grouped SWNTs shown in Figure 2.12 as well as for graphite for compression. Three important peaks which found in SWNTs are invisible in graphite. And attributed to symmetric transitions between the lowest sub bands in semiconducting (A and B)

and metallic (C) tubes. Generally, it is found that grown CNTs have a mixture semiconducting and metallic tubes.

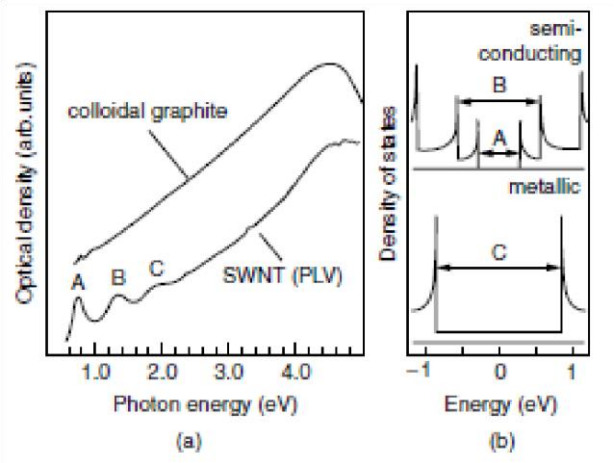

Figure 2. 12: UV-VIS-NIR spectra from different SWNT sample types. (a) Spectrum of SWNT rope material shown for comparison together with the spectrum of colloidal graphite (offset for clarity). (b) A, B, and C features can be attributed to symmetric transitions between the lowest sub bands in semiconducting (A, B) and metallic (C) tubes in representative density of states (DOS) [37].

Generally, it is found that grown CNTs have a mixture semiconducting and metallic tubes. In CNTs, measured peak position and intensity of optical spectra are giving information about electronic structures or tube chirality or (D, Θ). So, for detailed composition investigation of CNTs, optical spectra become must. For understanding the optical properties of CNTs, it is necessary to understand its band structure and DOS, which is already discussed in electronic dispersion section. The optical transportation only possible when electrons or holes are triggered from lower energy level to higher energy level. Required energy for optical transaction is donated by *Epq*. There two selection rules are decided for that. First, if p-q=0, it is defined for inter-band transitions. It is symmetric to fermi energy to polarized light along with tube axis. Second, it is

requires light normal to tube axis. But it is not appeared in optical spectra. It happens due to very weak transitions.

2.6.5 **Chemical Properties of CNTs**

Due to ultra-small dimension and ultra large specific area with σ-π re-hybridization, CNTs have strong sensitivity to chemicals and environmental interactions. It is important to study chemical properties of CNTs such as opening, wetting, filling, adsorption, charge transfer, doping, and intercalation for application purpose.

2.6.5.1 Opening

It is reported by several research groups that ends of CNTs are more reactive than the complete structure. CNTs ends have metallic catalyst particle with large curvature on its open end. So, many approaches have been focused to open CNTs end such as treatment with acids and plasma treatment etc. [38-40].

2.6.5.2 Wetting and Filling

CNTs are hydrophobicity in nature. Mostly aqueous solvents are unable to wet CNTs. But some organic elements, HNO_3, S, Cs, Rb, and Se as well as some oxides Bi_2O_2 are able to wet CNTs, if they are pressurized with capillary pressure. Using this technique some other no wetting elements may also be injected into CNTs. The capillary pressure for nanotube is proportional to $(1/D)$ **[**41-42**].**

2.6.5.3 Adsorption and Charge Transfer

It is expected that CNT have enhanced molecular adsorption as well charge transfer. Researchers have reported that CNTs shows a very good adsorption and charge transfer from oxygen to CNTs at room temperature. The localized sites on CNTs where pores exist, interstitial in tube bundles,

surface of a CNTs as well as a groove between two attached CNTs are the perfect places for charge transfer and for adsorption. In fact, said sites show the capability of CNTs for adsorption and charge transfer.

Above discussed property of CNTs is successfully used in NO_2, $C_6H_5NO_2$, C_6H_6, NH_3 as well as CH4 sensing. When these molecules interact with CNTs, the change in resistance of CNTs is observed. On that principle, it is possible to design electronic device for sensing application. [43-45].

2.6.5.4 Chemical Doping, Intercalation, and Modification

Above discussed adsorption method may be used for non-covalent bonding doping of CNTs to make p- type as well as n-type for enhanced electronic conductivity of CNTs. For enhancement of electronic conductivity, intercalation of the alkali metals is also used. Researchers reported on the behalf of experimental evidence that alkali metals diffuse into inter tube space or defects exist in CNTs, and hence enhanced the power of CNTs for charge transfer. To be enhanced the electrochemical capacity of CNTs, CNTs itself can be used for electrode purpose. In CNTs based electronic device, flow of electrons to production or harvesting the energy is generate by the reduction and oxidation reactions that occur at the electrodes [46-51].

2.6.6 **Defects in CNTs**

Defects being deterministic factor for the physical and chemical properties of the nanomaterial thereby it is considered significant. Although Nano materials like CNT is extremely perfect and have unique electrical and mechanical properties which changes due to presence of certain defects such as vacancies, heptagon–pentagon pairs type transformations, doping, and interstitials, edges

and adatoms (Figure 2.13) [52], resulting CNT's can be used for further applications like sensing purpose, hydrogen storage, drug delivery system etc.

2.6.7 **Structural Defect**

Structural defects in CNT's arise due to distortion caused in their topology by introducing pentagonal, heptagonal and octagonal ring in the hexagonal carbon network affecting the nanotube electrical properties resulting in conical structure with sharp tips due to presence of pentagonal ring at the peak of the nanotube (as shown in Figure 2.13 (a) & Figure 2.13 (b)). Also, different vertex angles are obtained by insertion of pentagon in a hexagonal carbon graphitic structure leading to 30° bend dictating that pentagon and hexagon are separated maximally that is they are placed opposite to each other (as shown in Figure 2.13 (c)) and 0° bend is obtained when both the structures are combined. Thereby, I can conclude by saying that vertex angles can suggest the count of hexagon – pentagon pairs present in the NT's. Spiral CNT (as shown in Figure 2.13 (d)) is an out of plane structure obtained by introducing pentagonal and heptagonal rings in the perfect graphitic sheet and then rolling it with a rotate angle. Toroidal CNT (as shown Figure 2.13 (e) is an in-plane structure obtained by connecting CNT's having various diameters by insertion of pentagons and hexagons [53].

2.6.7.1 Bond Rotation

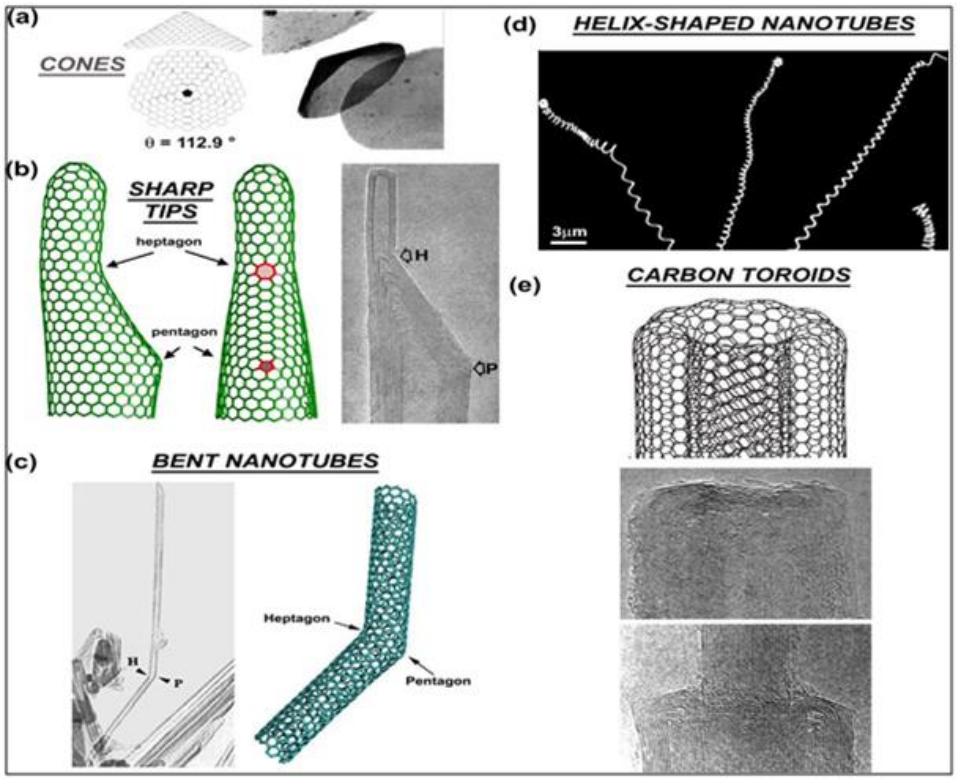

Figure 2. 13: TEM images and molecular models of different types of structural defects: (a) multi-layer graphitic cones constructed by adding one pentagon in the hexagonal carbon lattice; (b) CNT tip showing the influence of a pentagon and heptagon. The image shows the molecular models and a HRTEM image of a MWCNT displaying such structure has been reported in the literature [54]; (c) TEM image of a 30° bent MWCNT and molecular model of a bent nanotube created by adding a pentagon–heptagon pair. Only two defects result in the change of chirality and diameter of the tube before and after the kink; (d) image of carbon helices produced by the CVD process of triazine over cobalt oxide substrates; and (e) molecular model of a hemitoroidal nanotube cap, consisting of two concentric nanotubes joined together at their top rims, containing 5-7 rings, and hemitoroidal MWCNT caps found in cathode deposit (interlayer spacing approximately 0.34 nm) [54].

The thrower stone wales (TSW) type defects produced by bond rotation in the nanotube is due to 90° rotation of C-C bond in the hexagonal network such as in fullerenes, thereby resulting translation in two heptagons and pentagons (as shown in Figure 2.14 (a)) [52-56]. Unlike conicalend structure formed in structural defects, this TSW type defect does not result in large curvature deviations of the nanotube. SW type defects causes the plasticity failure at elevated

temperature and this can also alter the chirality of the CNT's, further elongation of the tube at the defect location can lead to collapse of nanotube. The significance of it is in innovation of nano-electronic devices [57].

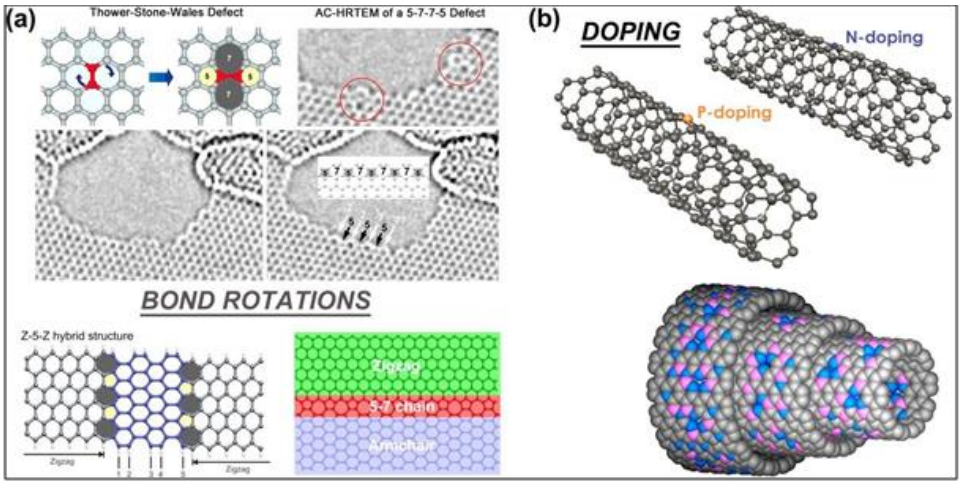

Figure 2. 14: Molecular model of the Thrower–Stone–Wales defect transforming four hexagons into two pentagons and two heptagons. Next to the model, a HRTEM image showing experimentally created 5-7-75 defects and 57575757 lines. Below, a hybrid graphene ribbon connecting zigzag ribbons with an armchair ribbon are shown; (b) molecular models of nitrogen- and phosphorous-doped carbon nanotubes as well as a random arrangement of BCN materials within concentric tubes [54].

2.6.7.2 Doping induced Defects

In order to increase the conductivity of CNT is to insert dopant atoms (as shown in Figure 2.14 (b)) in the carbon lattice or another method can be functionalization of nanotubes, which made it suitable for the biochemical and gas sensing purpose. Boron (p-type dopant) and N (n-type dopant) atoms in the internal CNT structure are used to sense the Carbon monoxide and water molecules. The Boron (B) atom doping is done by arc discharge method by using BN-rich as anode and the Nitrogen (N) atom doping is done pyrolyzing mixture of ferrocene-melamine at high temperature (J.-C. CHARLIER, 2002). As a result of doping both the nanotubes become metallic in nature with no bandgap in comparison to undoped lattice structure. Other atoms used

for doping purpose are P, S, Si in addition to B and N atoms; all these alter the reactivity of the nanotube by enhancing the binding energy of the sensing molecule with the doped species [58-62].

2.6.7.3 Non- sp^2 Carbon defects

These non-sp^2 hybridized defects in the CNT structure are formed due to dangling bonds, other than carbon atom found in the lattice structure or could be due to vacancies, adatoms and open or closed nanotube as shown in Figure 2.15. Adatoms are as dopants remains on the surface of the nanotubes in which lattice structure stay's undisturbed. Depending upon the relativeness between lower and upper occupied molecular orbit level of adatoms and tube's Fermi level, transmission or absorption of electrons of dopant atom occur.

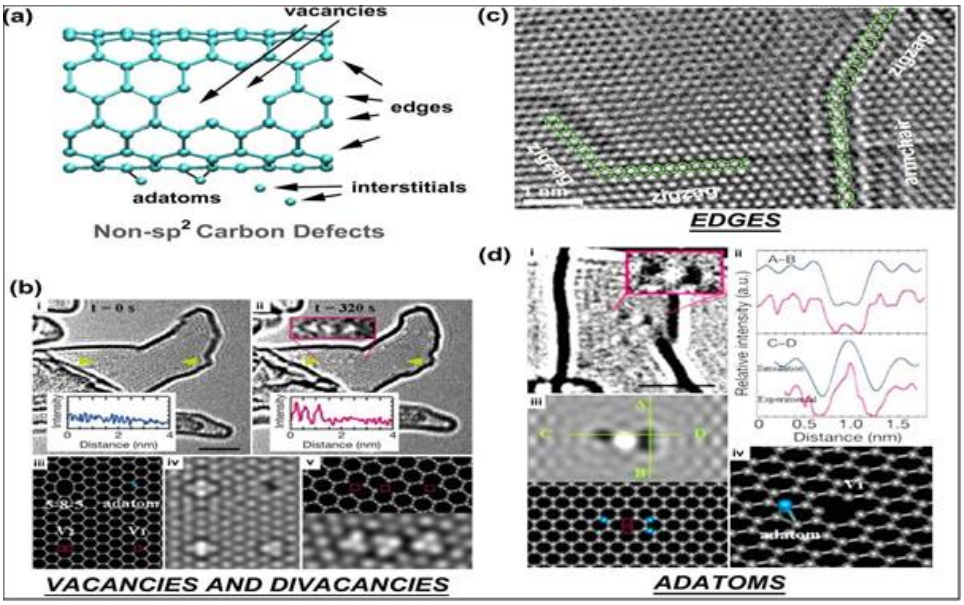

Figure 2. 15: (a) Molecular model of the different types of non-sp^2 defects: vacancies, divacancies, interstitials, adatoms, edges and interstitials; (b) experimental images showing the creation of vacancies in graphitic materials (bi and ii) and bii – inset, molecular models and HRTEM image simulations are also shown for clarity (c) HRTEM image of graphene edges exhibiting zigzag and armchair edges, that were obtained by applying Joule heating on an individual graphene nanoribbons inside the HRTEM; (di and ii) HRTEM image of adatoms on a

graphitic surface (see darker contrast spots); (diii and iv) HRTEM simulations and models of different configurations of adatoms on the surface of graphene that correspond to the experimental observations [54].

2.6.8 **Application of CNTs**

As mentioned above the peculiar, strong and powerful optical, electronic, mechanical as well as chemical properties make CNTs useful in innumerable applications. In current decade CNT shave become hot material for electronic, chemical, mechanical and optical applications. For their excellent electronics properties CNTs are capable of fabricating the basic solid-state devices with lesser dimensions than conventional silicon-based technology. The recently developed basic electronics devices based on CNTs are diode, tunnel diode, FETs and supercapacitors. It is also successfully used in fabrication of some other important applications Microwave amplifier, flat panel display, radio, X-Ray source, Radio, RAM as well transparent conductor [63-65]. CNTs also have very important invention in communications and information technology such as fibre lasers and nonlinear photonic. These inventions play role for routing, wavelength conversion and optical switching. It is also found applications such as photovoltaic devices, photodetectors and nono light sources [66-68]. CNTs also have proved to be promising material of the future in the field of Mechanical application. Worldwide researchers are working on NEMS (Nano Electromechanical System) technology based on CNTs. Researchers have successfully developed mechanical based on high frequency oscillators [69], rotational actuators [70], nanometer tweezers [71] and nanometer cargoes [72]. An outstanding invention of the ultraminiature sensors for observing the working force between two molecules [73] has taken place, to measure the force produced by magnetic resonance of single spin [74], measuring the displacement created by disturbance between individual atom. For their fairly high Young's modulus as well as specific weight, SWNTs have proved to be perfect for making the mechanical resonators for observing

the mechanical movement in quantum regime [75]. CNTs also have been part of surprising inventions in the field of electro chemistry. Several types of chemical sensors, humidity sensors, gas sensors for toxic gases and alcohol sensor are so far devolved. CNTs based chemical sensors have following advantages over conventional solid-state sensors.

- Existing sensors shows poor sensitivity at room temperature. Normal working temperature is in the range of 200°C to 500°C. But CNTs based sensor successfully work on room temperature.
- Existing toxic gas sensor shows limited maximum sensitivity however CNTs based sensor have shown order of higher sensitivities.
- The main drawback of using oxide-based gas sensors is use of microfabrication techniques to build the sensor which puts a limit on the size and geometry of the sensor. And in case of CNTs, due to its small dimensions no barrier created in front of design and geometry of device.
- For existing technology sensor fabrication cost is very high as compared with CNTs based sensors.
- Operating power for existing sensor is also very high. It is possible to operate CNTs based sensor at very low power.
- Existing toxic gas sensors shows very poor selectivity. Unspecific gas sensing mechanism, more or less many types of reducing gases are sensed. Response time is also very poor. These problems are resolved with CNTs based sensor technology.

References

1. A. Krueger, Carbon Materials and Nanotechnology, WILEY-VCH Verlag GmbH & Co. KGaA, Weinheim (2010)

2. M. Meyyappan, Carbon Nanotubes science and applications, NASA, Ames Research Center Moffett Field, CA, CRC Press (2004)

3. P. Debye, P. Scherrer, Interferenzen a regellos orientierten teilchen im Röntgenlicht. Phys. Z., 18 (1917) 291.

4. A.K.Geim, K.S. Novoselov, The rise of graphene, Nature Materials 6 (2007) 183.

5. International Committee for Characterization and Terminology of Carbon, Carbon, 28(5) (1990) 445.

6. J. C. Bokros, In Chemisfry and Physics of Carbon, (P. L. Walker, Jr.,ed.), Vol. 5, Marcel Dekker Inc., New York (1969).

7. H. O. Pierson, Handbook of Carbon, Graphite, Diamond and Fullerenes, Properties, Processing and Applications, Noyes Publications, Park Ridge, New Jersey, U.S.A. (1993).

8. G. Guy, Elements of Physical Metallurgy, Addison-Wesley Publishing, Reading, MA (1959).

9. D. Cullity, Elements of X-Ray Diffraction, Addison-Wesley Publishing, Reading, MA (1956).

10. K. E Spear, Diamond: Ceramic Coating of the Future, J. Am. Ceram. Sot., 72(2):171-191 (1969)

11. D. F. Eggers, Jr. and Halsey, G. D., Jr., Physical Chemistry, John Wiley & Sons, New York (1964)

12. F. Gardinier, Physical properties of superabrasives, Ceramic Bulletin, 67 (1988) 1006.

13. K. E. Spear, A. W. Phelps, W. B. White, Diamond polytypes and their vibrational spectra, J. Mater Res., 5 (1990) 2271.

14. J. B. Dawson, The Properties of Diamond, (J. E. Field, ed.), (1967) 539.

15. H.S. P. Wong, D. E. Jiakinwande, Carbon Nanotube and Graphene Device Physics, Cambridge University Press (2001).

16. L. Pauling, The Nature of Chemical Bonds, Cornell University Press (1960).

17. Bhushan, Nanoscience and Technology (Scanning probe microscopy in Nanoscience and Nano technology, Spriner (2011).

18. R. E. Smalley, Act. Chem. Res., 05 (1992) 2598.

19. R. F. Curl, R. E. Smalley, Handbook of carbon, graphite, diamond and fullerenes. Properties, processing and applications, Scientific American, (1991) 5463.

20. W. Kratschmer, L. D. Fostiropolous, D. R. Huffman, Solid C_{60}: a new form of carbon Nature, 347 (1990) 354358.

21. R.C. Haddon, Electronic structure, conductivity and superconductivity of alkali metal doped (C_{60}), Chem. Res., 25 (1992) 127.

22. R. D. Johnson, D. S. Bethune, C. S. Yannoni, Fullerene structure and dynamics: a magnetic resonance potpourri, Act. Chem. Res., 25 (1992) 169.

23. F. Diederich, R.L. Whetten, Beyond C_{60}: the higher fullerenes Act. Chem. Res., 25 (1992) 119.

24. G. L. Rogers, Gabor Diffraction Microscopy: the Hologram as a Generalized Zone-Plate, Nature, 166 (1950) 237.

25. L.V. Radushkevich, V.M. Lukyanovich. O strukture ugleroda, obrazujucegosja pri termiceskom razlozenii okisi ugleroda na zeleznom kontakte. Zurn Fisic Chim 26 (1952) 88.

26. R. J. Baker, G. A. Mengden, J. J. Bull, Karyotypic studies of thirty-eight species of North American snakes, Copeia, 1972 (1972) 257.

27. Oberlin, M. Endo, T. Koyama, Filamentous growth of carbon through benzene decomposition, Journal of Crystal Growth, 32 (1976) 3.

28. R. Saito, G. Dresselhaus, M.S. Dresselhaus, Physical Properties of Carbon Nanotubes, Imperial College Press, (1998)

29. P.L. McEuen, Disorder, pseudospins, and backscattering in carbon nanotubes. Physical Review Letters, 24 (1999) 5098.

30. M.S.E. Dresselhaus, Phonons in Carbon Nanotubes. Advances in Physics, 49 (2000) 705.

31. J. Hone, Quantized phonon spectrum of single-wall carbon nanotubes. Science, 289 (2000) 1730.

32. S.J. Tans, Individual single-wall carbon nanotubes as quantum wires, Nature, 386 (1997) 474.

33. S. Frank, Carbon nanotube quantum resistors, Science, 280 (1998) 1744.

34. H.T. Soh, Appl. Phys. Lett., 75 (1999) 627.

35. A.M. Rao, Diameter-selective Raman scattering from vibrational modes in carbon nanotubes Science, 275 (1997) 187.

36. S.M. Bachilo, Structure-assigned optical spectra of single-walled carbon nanotubes, Science, 298 (2002) 2361.

37. A. Hagen, T. Hertel, Quantitative Analysis of Optical Spectra from Individual Single-Wall Carbon Nanotubes, Nano Lett., 3 (2003) 383.

38. S. Paulson, In situ resistance measurements of strained carbon nanotubes, Appl. Phys. Lett., 75 (1999) 2936.

39. S.C. Tsang, A simple chemical method of opening and filling carbon nanotubes, Nature, 372 (1994) 159.

40. P.M. Ajayan, Opening carbon nanotubes with oxygen and implications for filling, Nature, 362 (1993) 522.

41. H. Hirura, Opening and purification of Carbon nanotubes in high yield, Adv. Mater., 7 (1995) 275.

42. P.M. Ajayan, Carbon nanotubes as removable templates for metal-oxide nanocomposites and nanostructures, Nature, 375 (1995) 564.

43. Dujardin, Capillarity and wetting of carbon nanotubes, Science, 265 (1994) 1850.

44. Ugarte, Nanocapillarity and chemistry in carbon nanotubes, Science, 274 (1996) 1897.

45. J. Zhao, A. Buldum, J. Han, J.P. Lu, Gas molecule adsorption in carbon nanotubes and nanotube bundles, Nanotechnology, 13 (2002) 195.

46. J. Zhao, J.P. Lu, J. Han, C. Yang, Noncovalent functionalization of carbon nanotubes by aromatic organic molecules, Appl. Phys. Lett., 82 (2003) 3746.

47. M. Kruger, Sensitivity of single multiwalled carbon nanotubes to the environment, N. J. of Phys., 5 (2003) 138.

48. J. Zhao, A. Buldum, J. Han, First-principles study of Li-intercalated carbon nanotube ropes, J. P. Lu, Phys. Rev. Lett., 85 (2000) 1706.

49. X. Liu, C. Lee, C. Zhou, J. Han, Carbon nanotube field-effect inverters, Appl. Phys. Lett., 79 (2001) 3329.

50. Frackowiak, Electrochemical storage of lithium in multiwalled carbon nanotubes, Carbon, 37 (1999) 61.

51. G.T. Wu, Structure and lithium insertion properties of carbon nanotubes, J. Electrochem. Soc., 146 (1999) 1696.

52. B. Bao, Carbon nanotubes science and Application, Chem. Phys. Lett., 307 (1999) 153.

53. J. M. Bonard , M. Croci, C. Klinke, R. Kurt , O. Noury, N. Weiss, Carbon nanotube films as electron field emitters, Carbon 40 (2002) 1715.

54. J. H. Lehman, M. Terrones, E. Mansfield, K. E. Hurst, V. Meunier, Evaluating the characteristics of multiwall carbon Nanotubes, Carbon, 4 9 (2011) 2581.

55. P. A Thrower, The study of defects in graphite by transmission electron spectroscopy, Chem Phys Carbon, 5 (1969) 217.

56. J.Stone, D. J. Wales, Theoretical studies of icosahedral C_{60} and some related species, Chem Phys Lett, 128 (1986) 501.

57. M. Terrones, G. Terrones, H. Terrones, Structure, chirality, and formation of giant icosahedral fullerenes and spherical graphitic onions. Struct Chem 13 (2002) 373.

58. C. O. Girit, J. C. Meyer, R. Erni, M. D. Rossell, C. Kisielowski, L. Yang, Graphene at the edge: stability and dynamics, Science 323 (2009) 1705.

59. M. Terrones, A. Jorio, M. Endo, A. M. Rao, Y. A. Kim, T. Hayashi, New direction in nanotube science. Mater Today, 7 (2004) 30.

60. C. E. Silva, D. A. Cullen, L. Gu, J. M. Romo-Herrera, E. M. Sandoval, F. L. Urias, Heterodoped nanotubes:

theory, synthesis, and characterization of phosphorus– nitrogen doped multiwalled carbon nanotubes. ACS Nano, 2 (2008) 441.

61. O. Maciel, J. C. Delgado, E. C. Silva, M. A. Pimenta, B. G. Sumpter, V. Meunier, Synthesis, electronic structure, and raman scattering of phosphorus-doped single-wall carbon nanotubes. Nano Lett, 9 (2009) 2267.

62. O. Maciel, N. Anderson, M.A. Pimenta, A. Hartschuh, H. Qian, M. Terrones, Electron and phonon renormalization near charged defects in carbon nanotubes, Nat Mater 7 (2008) 878.

63. S. Iijima, T. Ichihashi, A. Y. Pentagons, heptagons and negative curvature in graphite microtubule growth, Nature, 356 (1992) 776.

64. J. H. Ryu, J. S. Kang, K. C. Park, Carbon Nanotube Electron Emitter for X-ray Imaging, Materials, 5 (2012) 2353.

65. K. Jensen , J. Weldon , H. Garcia , A. Zettl, Nanotube Radio, Nano Lett., 11(2007) 3508.

66. T. Rueckes, K. Kim, E. Joselevich, G. Y. Tseng, C. L. Cheung, C. M. Lieber, Carbon Nanotube-Based Nonvolatile Random Access Memory for Molecular Computing, Science, 289 (2000) 5476.

67. N. Xi, K. La, Nano Optoelectronic Sensors and Devices: Nanophotonics from Design to Manufacturing, Elsevier, (2012).

68. Carbon Nanotubes and graphene for photonic applications, S. Yamashita, Y. Saito, J.H. Choi, Woodhead Publishing, (2013).

68. Carbon Nanotubes and graphene for photonic applications, S. Yamashita, Y. Saito, J.H. Choi, Woodhead Publishing, (2013).

69. D. Melisi, M. A. Nitti, M.Valentini, A. Valentini, T. Ligonzo, G. D. Pascali, M. Ambrico, Photodetectors based on carbon nanotubes deposited by using a spray technique on semi-insulating gallium arsenide, Journal of Nanotechnology, 5 (2014) 1999.

70. V. Sazonova, Y. Yaish, H. Üstünel, D. Roundy, T. A. Arias, P. L. McEuen, A tunable carbon nanotube electromechanical oscillator, Nature 431 (2004) 284.

71. M. Fennimore, T. D. Yuzvinsky, Wei-Qiang Han, M. S. Fuhrer, J. Cumings, A. Zettl, Rotational actuators based on carbon nanotubes, Nature, 424 (2003) 408.

72. P. Kim, C. M. Lieber, Nanotube Nanotweezers, Science, 286 (1999) 2148.

73. Qing Zhang, Carbon Nanotubes and Their Applications, Pan Stanford series on carbon-based nanomaterials, CRC Press, 1 (2012).

74. A.M. Popov, I.V. Lebedeva, A.A. Knizhnik, Yu.E. Lozovik, N.A. Poklonski, A.I. Siahlo, S.A. Vyrko, S.V. Ratkevich, Force and magnetic field sensor based on measurement of tunnelling conductance between ends of coaxial carbon nanotubes, Comput. Mater. Sci. 92 (2014) 84.

75. M. Poot, H.S.J. van der Zant, Mechanical systems in the quantum regime, Physics Reports 511 (2012) 273.

Chapter 3: Growth and Characterization techniques

3.1 Introduction

For developing a material with specific properties, it becomes most important to aware with its all-growth techniques, so that, it becomes possible to make material with best quality and yield for growth of CNTs, there are three main techniques used– Arc discharge, Laser ablation and Chemical vapour deposition (CVD). Amongst these, CVD is the most used technique so far. This thesis is based on CVD grown CNTs, so it is discussed in detail.

3.2 Growth Techniques of CNTs

3.2.1 Arc discharge method

Arc discharge method is a widely used method for CNTs growth. It was invented by Krätschmeret al. to produce high yield of fullerenes [1]. It was observed that, in addition to Fullerenes, some other allotropes of carbon were also present as the by-products. Later, Sumio Iijima, a microscopist, reported the presence of tubular allotrope of carbon i.e., CNTs in the by-products of arc discharge method [2]. So, arc discharge was the first known method for the growth of CNTs. This method was further developed and optimized for the exclusive growth of CNTs. Initially, CNTs in the soot form, were reported to be synthesized using this method [2]. Earlier, only MWCNTs were produced using this method, but at the later stage it has been successfully tuned for the growth of SWNTs [3]. Arc discharge method involves the Vaporization of Graphite in the inert atmosphere using electric arc. In specific cases, catalysts also take part in the synthesis of CNTs. At the heart of arc discharge system, there are two graphite rods situated inside the electric arc chamber. The diameters of graphite rods are of the order of 2mm and the separation

between these rods is kept about 1 mm [see Figure 3.1]. These graphite rods act as the electrodes and a high DC current around 50 to 100A is passed through them. Due to such high DC current, very high heat energy is produced which increases the temperature of system around 4000°C, which, in turn, vaporizes the carbon of the Graphite anode. These carbon vapors subsequently deposit on cathode in the form of different carbon nano structures such as CNTs, fullerenes and amorphous carbon. [4-7]. The composition of electrodes decides the type and quality of as-synthesized CNTs among the grown carbon nano structures. [8-9]. While pure graphite electrodes support the synthesis of MWCNTs, SWCNTs can be produced using Graphite electrodes mixed with metal catalysts. [1, 10-11]. The other properties of as-grown CNTs such as their diameter can be controlled by controlling other growth parameters. [12]

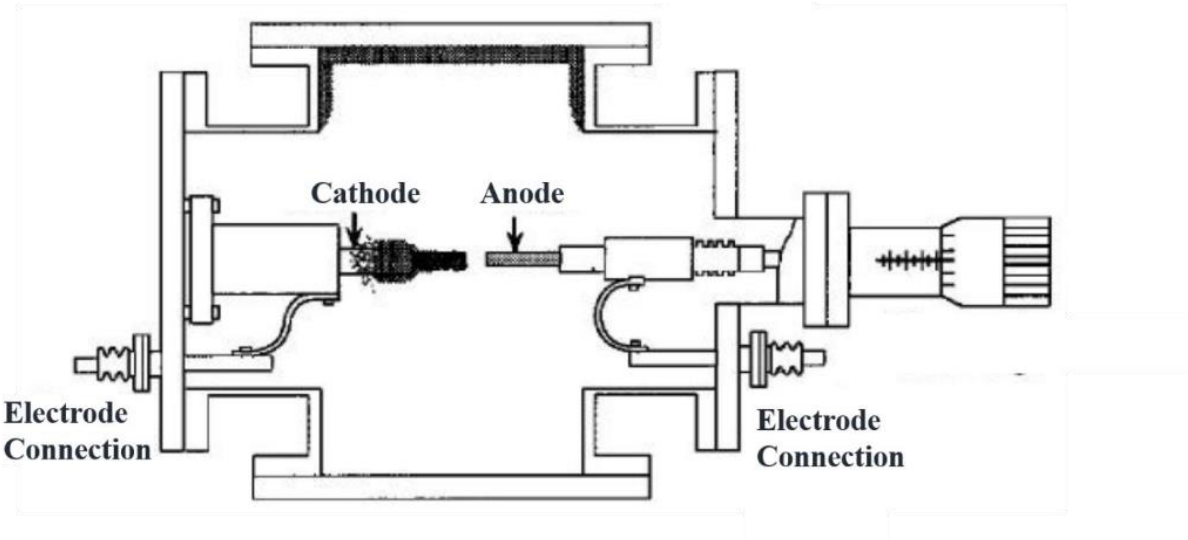

Figure 3. 1 Schematic diagram for Arc-discharge Method [58].

3.2.2 **Laser ablation**

Laser ablation method is quite similar to arc discharge method. In both techniques, carbon is vaporized and deposited at different places. The only difference in both the growth methods is the process of vaporization. In Laser ablation technique, a high intensity laser beam is used for

vaporization of Carbon instead of high DC current. A small amount of carbon is transmitted into its plasma. CNTs are synthesized into plasma plume with other allotropes of carbon. The plasma plume, subsequently, deposits on walls of the chamber. Mostly CO_2 and Nd: YAG laser sources are used in this technique in pulsed as well as in continuous modes [13-17]. Like arc discharge method, MWNTs as well as SWNTs can be deposited using this method. When pure carbon source is used, the growth of MWNTs takes place. On the other hand, use of metal catalyst mixed carbon source leads to the synthesis of mixture of MWNTs and SWNTs. Figure 3.2 shows the schematic diagram of laser equipment.

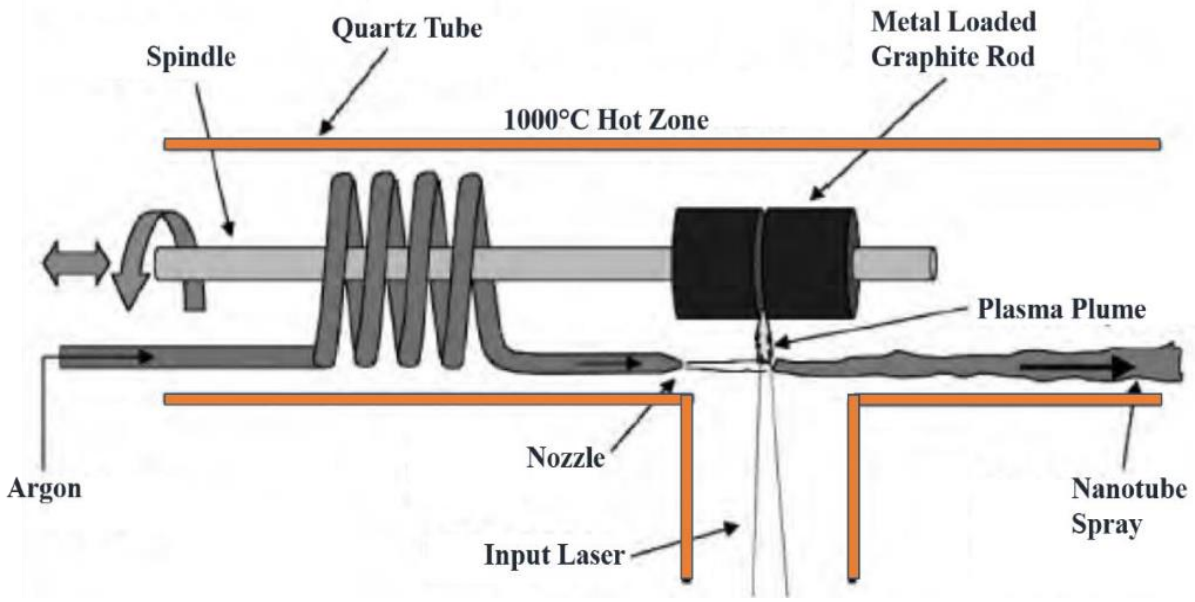

Figure 3. 2 shows the schematic diagram of Laser ablation technique [59].

3.2.3 **Chemical Vapour Deposition**

Chemical vapour deposition (CVD) is basically a film depositing equipment that has been alive for many years and is capable of depositing a number of materials. While the CVD method has been used since 1960's to produce carbon filaments and fibers, it was not until the early 1990's

that it was capable of producing CNTs. Chemical vapour deposition is a method where gaseous precursors react either in gas phase or at the substrate gas interface, producing thin film on the substrate There are many types of chemical vapour deposition systems exist in research world having different type of heating arrangements as well as some extra accessories. All type of CVDs has same working concept. Users customize CVD according to requirement. For the fabrication of CNTs, Thermal and Plasma Enhanced CVD are being used. The growth of CNTs by the CVD process requires three ingredients: the ablation precursor gas (also called feedstock), a catalyst surface, and a source of energy. The energy may be generated thermally (in Thermal CVD) or by plasma (in Plasma Enhanced CVD). I preferred using TCVD for CNTs growth (as CNTs are prone to be damaged by the plasma [29] which reduces their electrical performance).

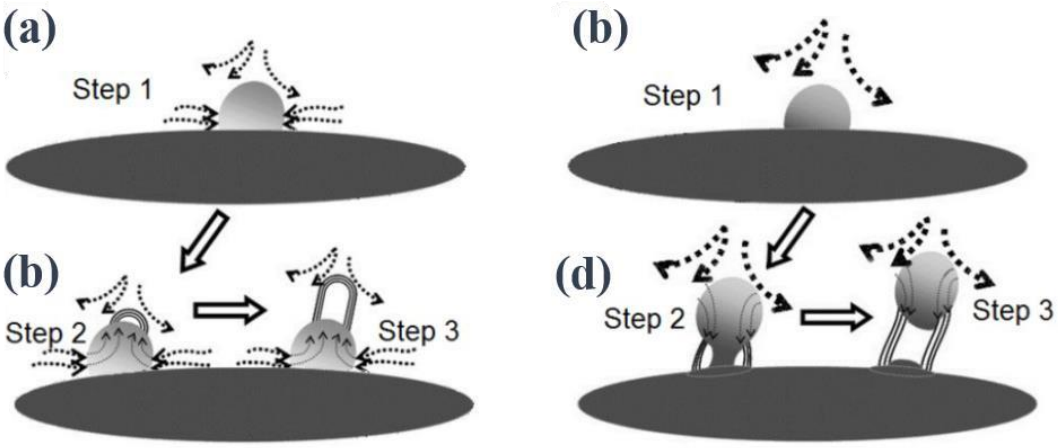

Figure 3. 3 Various stages of vapour-liquid-solid (VLS) growth mechanism. Catalyst particle in molten state absorbs carbon in vapour form (a) to form an alloy (b). As the particle becomes saturated with carbon, a solid CNT begins to extrude from the particle. The final location of the catalyst particle defines tip grown (c) or root grown (d) CNTs [61].

In TCVD, hydrocarbons are broken at high temperatures to produce the vapours of atomic carbon. These vapours get deposited on the metal catalyst deposited substrate via V-L-S growth process

to form carbon nanotubes. The VLS growth process involves three steps i.e., absorption, saturation and structure extrusion (see Figure 3.3). Any transition metal which have low melting temperature can be used as seed or catalyst for CNTs growth via VLS growth process. These catalysts have the capability to absorb vaporized carbon. [18-20]. These catalysts may be deposited on a substrate such as silicon, Al_2O_3 in the form of thin film by sputtering, dip coating or spin coating. Prior to deposition, the catalyst coated substrate is heated. Because of heat treatment, the continuous layer breaks down into lumps of nanoparticles to keep minimum surface energy. This process is known as catalyst activation or annealing. In some reports catalysts are reported to be injected directly into growth

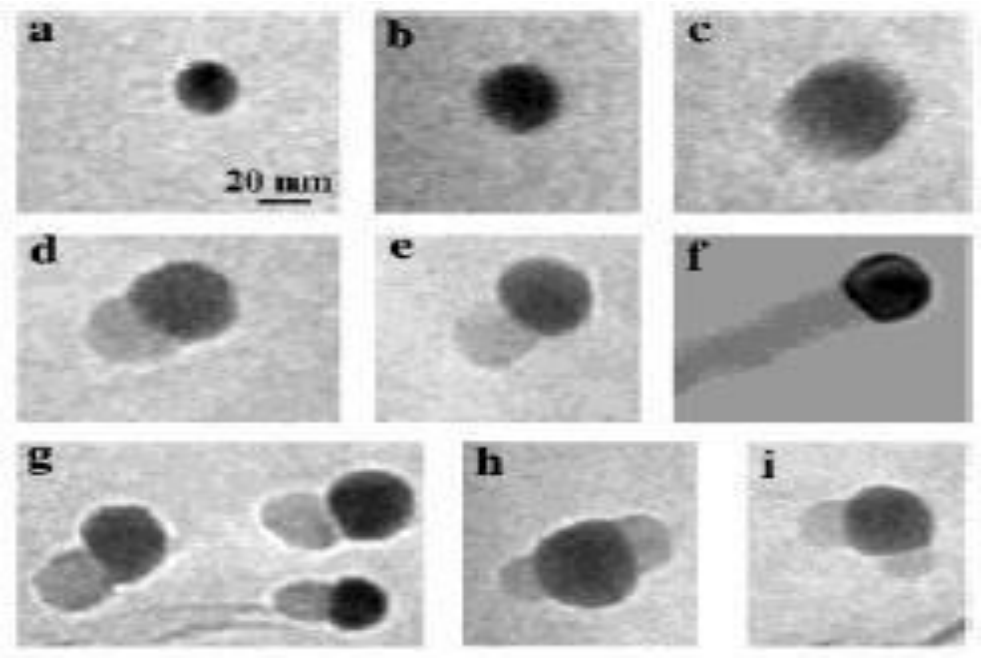

Figure 3. 4 Formation of germanium nanowires from gold nanoparticles via the vapour liquid solid growth mechanism. These transmission electron microscopy images reveal the extrusion of the germanium nanowires (c-i) from the saturated particle (b) [61].

chamber. Some oxide nano particles (SiO_2, Al_2O_3) have also been reported to act as catalyst for CNTs growth [21]. After putting the annealed catalyst film into the chamber, the chamber is evacuated. The precursor gas, which is usually a lower order hydrocarbon (such as methane, acetylene and ethylene) is then introduced into the chamber at an appropriate pressure. In some specific cases, Vaporized benzene or toluene can be used as the feedstock. Occasionally, an inert carrier gas is also used as the carrier, which also serves as an etchant for the excess amorphous carbon which gets deposited on the walls of the chamber. The temperature of the chamber is raised to few hundreds' degree Celsius. Such a high temperature induces the meatal catalysts nanoparticles to get into molten state. On the other hand, the high temperature also decomposes the hydrocarbon. Decomposition of hydrocarbon produces carbon vapours in the camber which get absorbed on the molten catalyst. As more and more carbon absorbed into the catalyst, its concentration exceeds the solubility of the catalyst particle. At this point, the catalyst particle beings to extrude a solid formation in the form of a CNTs as seen in Figure 3.3 (c, d). The schematic for CNTs growth via VLS process is given in Figure 3.3.

Depending on the final location of the catalyst particle, the nanotube is typically classified as either tip grown or root grown. Other one-dimension nanostructures can also be grown via VLS growth mechanism. The growth of a germanium nano wires from a gold nanoparticle is shown in Figure 3.4 (a-g) and the growth of multiple nanowires is shown in Figure 3.4 (h-i). The major benefit of using CVD for the synthesis of CNTs lies in its ability to be scaled-up in size, allowing the large production facilities to produce several kilograms of CNTs per day.

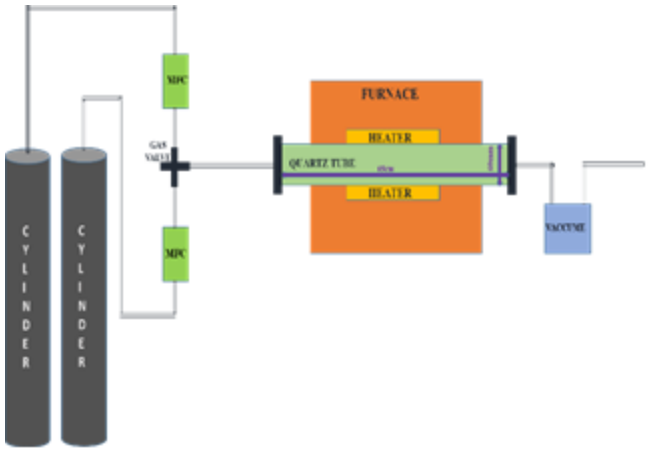

Figure 3. 5 Schematic diagram of Thermal CVD

TCVD setup includes a durable, high temperature compatible tube, usually made of quartz or alumina, which is heated by a box furnace or heating coils (see Figure 3.5). Hydrocarbons are channeled into the heated reactor zone via mass flow controllers and the eventual by-products are evacuated through a fume hood. TCVD can be used to grow MWNTs as well as SWNTs. CVD parameters such as temperature, pressure, flow of gases etc. play crucial role in deciding CNTs dimensions, structure as well as quality [22]. They have varying degrees of interaction with the growth conditions, which is further complicated by the fact that different research results often predict different behaviors. All of these make it a quite challenging task to find out the optimum growth conditions for producing CNTs with desired properties. The role of CVD parameters on CNTs growth will be discuses in later chapters of the thesis. In my research work self-designed thermal CVD is used. Picture and schematic diagram of said CVD is shown in Figure 3.5.

Now after gained knowledge about CVD system, a detailed dissection about various parameters used in CVD system is become necessary. So, in following section, I am going to present a detailed literature survey about various CVD parameters:

3.2.3.1 Mass production of CNTs

As CVD is known and already set in industries, CNT synthesis using CVD is a simplest process. Most R & D groups converted this process into mass production. Smalley et al. evolved the elevated pressure decomposition of carbon monoxide, technique known as 'HiPco' for bulk manufacturing of SWNTs [23]. In the said method, Fe penta-carbonyl catalyst release iron nano-particles in-situ at higher temperature range, although the high pressure (∼10 atm) of carbon monoxide offer the abundance of hydrocarbons, that notably increases the unbalancedness of CO molecules into C atoms and hence speed-up the SWCNT growth. The reported yield of HiPco route is ∼0.45 g/h [24]. The product is commercially offered at 'Carbon Nanotechnologies Inc.' (USA), which is reported to have a manufacturing capacity of 65 g/h [25]. Dai et al. has also enhanced SWNT's synthesis from methane spontaneous decomposition over Fe–Mo alloy, catalyst that is supported on sol–gel derived alumina-silica substrate. Said procedure yields around 1.5 g of SWNTs with 0.5 g of catalyst hybrid for 30 min of growth duration in CVD [26]. Maruyama et al. and 'Toray Industries Inc.' (Japan) have evolved alcohol CVD method [27], reported capacity of 15 g/h; while Hata et al. technique [28] reported (AIST (Japan)) approximate 100 g/h [25].

Endo et al. have developed their own method of benzene pyrolysis on iron catalyst [26] to an uninterrupted process for bulk production. In above procedure metal catalyst, benzene, and Ar/H_2gases are supplied from the upper end of an upright furnace, and the developed CNTs were deposited on the lower end. Simultaneously CNT growth took place when the catalyst particles were falling down (floating) through the furnace at 1100℃ [29]. The product was commercialized by 'Showa Denko KK' (Japan), they gave manufacturing capacity evidence of 16 kg/h [25]. Nagy et al. presented a method for acetylene CVD for various porous materials to grow CNTs at

industrial level [30, 31]. Fei et al. designed a nano-agglomerate fluidized-bed chamber in which constant breakdown of ethylene gas on Fe–Mo/vermiculite catalyst at 650℃ can produce up to 3 kg/h aligned MWNT. Not only mentioned universities and companies from, many other research groups also exist in CNTs production. To name some, Hyperion Catalysis International, Inc. USA (8 kg/h), Nano Carbon Technologies Co. Ltd. Japan (5 kg/h), Sun Nanotech Co. Ltd. China (0.6 kg/h), Shenzhen Nano Technologies Port Co. Ltd. China (5 kg/h) [25]. WTEC survey reported the combined synthetization of CNTs of the world today is approximately 300tons MWNTs and 7 tons SWNTs per year. The expected demand of CNTs growth for near future would reach around 1000tons/year. The current cost of available MWNTs is $1/g (Approx.), while that of SWNTs is $100/g (Approx.). At this rate, prevalent products based on CNTs would be about 10 times costlier. So, Researchers have great task to reduce cost of CNTs and hence CNTs based products. A good sign is that CVD-based CNTs technique is making headway fast, and innumerous companies are emerging. However, a noticeable point is that purity of grown CNTs decreases with the increasing yields, it becomes a common problem of mass-produced CNTs. It is easy to control the properties of CNTs in lab scale production but purity of CNTs decreasing and diameter distribution became broadens drastically, when same CNTs growth process moved to industrial level. So, more-easy, enhanced method must be found which could be transformed to large scale with the same quality and diameter distribution. Moreover, to fulfill present demand of CNTs, an environmental friendly, sustainable technology development is required.

3.3 CNT Characterization Instruments

3.3.1 Scanning Electron Microscope (SEM)

SEM is one of the most widely used techniques employed for the characterization of

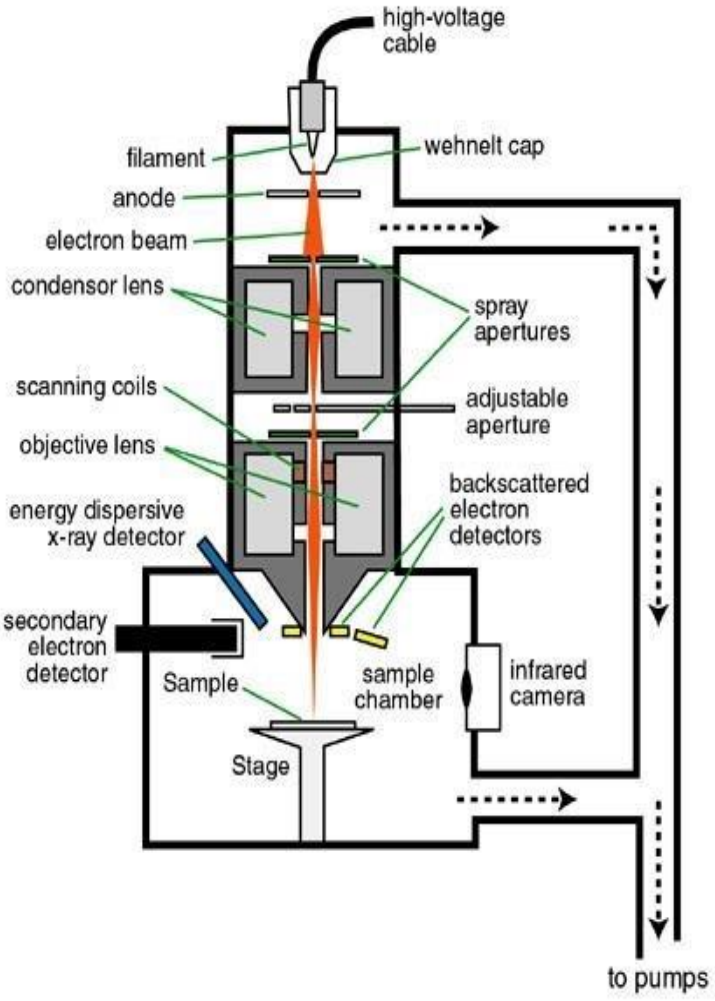

Figure 3. 6 The schematic diagram of SEM [60].

nanomaterials and nanostructures. The schematic diagram of SEM is shown in Figure 3.6. It was commercialized by Oxford Scientific Instruments in 1965 [32, 33]. The resolution of the SEM approaches a few nanometers, and the instruments can operate at magnifications that are easily adjusted from ~ 10 to over 600,000. Not only the SEM produces topographical information as

optical microscopes do, it also provides the chemical composition information near the surface. In a typical SEM, a source of electrons is focused into a beam, with a very fine spot size of ~5 nm and having energy ranging from a few hundred eV to 30KeV that is restored over the surface of the specimen by deflection coils. As the electrons strike and penetrate the surface, a number of interactions occur that result in the emission of electrons

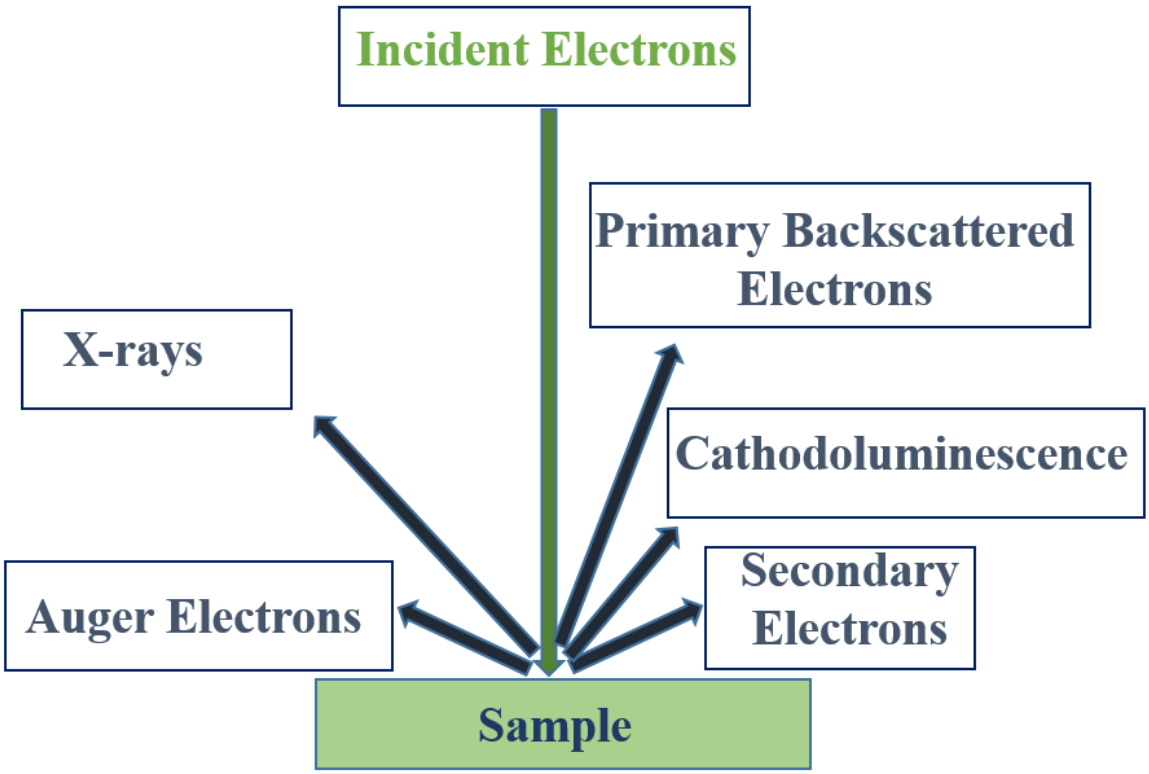

Figure 3. 7 Interaction between incident electron beam and material.

and photons from the sample (see Figure 3.7), and SEM images are produced by collecting the emitted electrons on a cathode ray tube (CRT). Various SEM techniques are differentiated on the basis of what is subsequently detected and imaged, and the principal images produce in the SEM are of three types: secondary electron images, backscattered electron images and elemental X-ray

maps. When a high-energy primary electron interacts with an atom, it does undergo either inelastic scattering with atomic electrons or elastic scattering with the atomic nucleus. In an inelastic collision with an electron, the primary electron transfers part of its energy to the other electron. When the energy transferred is large enough, the other electron will emit from the sample. If the emitted electron has energy of less than 50 eV, it is referred to as a secondary electron. Backscattered electrons are the high energy electrons that are elastically scattered and essentially possess the same energy as the incident or primary electrons. The probability of backscattering increases with the atomic number of the sample material. Although backscattering images cannot be used for elemental identification, useful contrast can develop between regions of the specimen that differ widely in atomic number (Z). An additional electron interaction in the SEM is that the primary electron collides with and ejects a core electron from an atom in the sample. The excited atom will decay to its ground state by emitting either a characteristic X-ray photon or an Auger electron, both of which have been used for chemical characterization and will be discussed later in this chapter. Combining with chemical analysis capabilities, SEM not only provides the image of the morphology and microstructures of bulk and nanostructured materials and devices but can also provide detailed information of chemical composition and distribution. The theoretical limit to an instrument's resolving power is determined by the wavelengths of the electron beam used and the numerical aperture of the system. The resolving power, R, of an instrument is defined as:

$$R = \frac{\lambda}{2NA}$$

Where λ is the wavelength of electrons used and NA is the numerical aperture, which is engraved on each objective and condenser lens system, and a measure of the electron gathering ability of the objective, or the electron providing ability of the condenser. The detailed information about

mostly used detectors in SEM for detection above mentioned electrons and phonons are following:

3.3.1.1 Everhart Thornley Detector (ETD)

ETD is always mounted on the top of sample stage to detect secondary and backscatter electrons. It is a scintillator photo-multiplier type detector. The detector's setting module have an adjuster for controlling Grid Voltage. When voltage is positive in range of +250V then Secondary electrons giving image. And in negative voltage range -25 to -150V backscattered electrons active to giving image. During loading and unloading of sample, the grid voltage as well as scintillator voltage are turned off. It is also switched of during vacuum mode change or SEM is operated in low vacuum.

3.3.1.2 Through the Lens Detector (TLD)

TLD works in four modes. But specifically, TLD is designed for high resolution imaging getting by Mode 2. The TLD detector have a grid voltage variation arrangement to customize the electron collection. To detect backscattered electrons, grid voltage should supply a negative voltage. Because negative grid voltage rippled the secondary electrons. Only backscattered electron reached to TLD detector. For detecting secondary electrons grid voltage puts on positive. The biasing possibility of grid is -150V for backscattered electrons while +150V for secondary electrons collection.

3.3.1.3 Low Vacuum Detector (LVD)

LVD is working as the standard detector for imaging in low vacuum mode. For enable LVD, it must be mounted on the objective pole piece of SEM. And hence, Low vacuum operation is enabling. It works in the whole pressure range from 0.08 to 1.5 Torr. It limits the field of view around 1nm at 5mm working distance. And minimum limited to 3mm. LVD detector have possibilities to utilize in all SEM imaging modes. Still, it gives most suitable images in mode1 and 3. The signal providing by LVD have both secondary as well as primary electrons Information.

3.3.1.4 Helix Detector

Helix Detector is an alternative detector for low vacuum mode. The Helix detector limits the field of view to about 0.5nm at the working distance of 5nm. Helix detector basically combination of LVD as well as Helix. LVD part have same operation as describes above. But it is designed for Mode 2(immersion). It gives superior imaging in immersion mode. It has power to give high resolution imaging in low vacuum.

FESEM is the one of the best techniques to investigate the morphology, length and diameter of CNTs without any sample preparation. SEM may also provide the information regarding impurities attached to CNTs. Lateral view of CNTs films may provide the information regarding the film thickness and orientation of CNTs.

3.3.2 Raman Spectroscopy

Raman spectroscopy is one of the main tools used for investigating the molecular vibrations. It is utilized to gain knowledge about chemical elements and structural forms to recognized materials

by characteristic fingerprinting. It is also used for quantitative information about materials amount in a sample. This equipment has potential of scanning of samples in all states as well as in all conditions; for example, as powder, vapours or liquids, as surface layers or in bulk form of nanoparticles, in different temperature states. Prior, IR absorption was widely used as compare to Raman scattering due to complexity in Raman spectroscopy. But enhancement in technology made Raman spectroscopy simple and compact and also reduced the problems substantially. Said improvement in Raman spectroscopy, together with the capability of investigation of different type samples without any preparation, made Raman spectroscopy powerful investigation tool in the field of material science. In 1928, Sir C.V. Raman reported the historical invention of inelastic light scattering. Raman scattering is inelastic scattering of light, i.e. scattering of light in which the photon energy

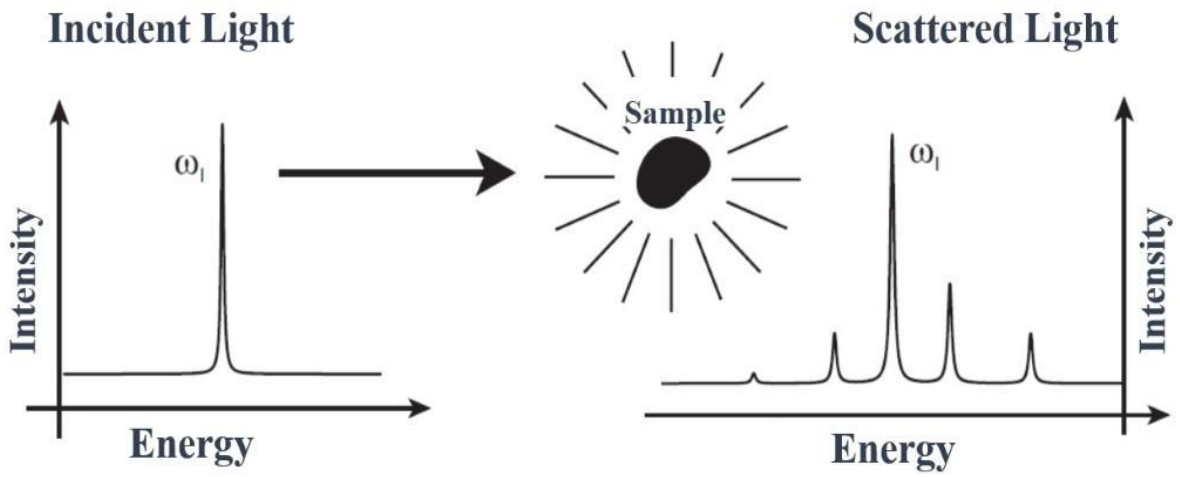

Figure 3. 8 Plot for Raman Scattering

changes (see Figure 3.8). The principle of the experiment is illustrated in Figure 3.9.A monochromatic beam of light impinge on the sample and the spectrum of the scattered light is

examined. Raman spectroscopy (RS) is a powerful, fast and non-destructive tool that provides information about vibrational, rotational, and other low-frequency modes in a sample [34-36]. Raman Scattering relies on a frequency change of incoming light photons after inelastic interaction with matter. If the scattered photon has the same frequency or energy as that of the coming light, said process of light interaction is called as elastic scattering. If the scattered photon has different frequency or energy than that of the incident light, then inelastic scattering take place. In RS, localized atom to atom bond structure is investigated by inelastic interaction of incoming photon with longitudinal or transverse modes of phonon. Spectral feature of phonon vibrations in solids can be analyzed by RS, which gives an opportunity for sample identification and phase quantification Interaction mechanism that causes a frequency change is illustrated in Figure 3.9.

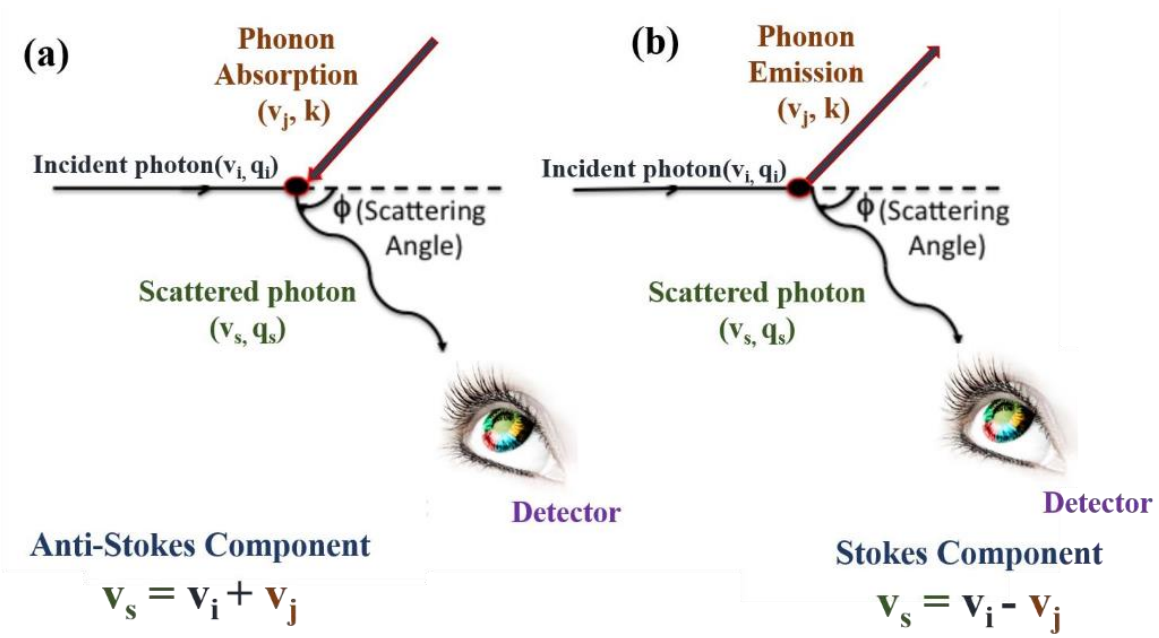

Figure 3. 9 Plot shows the sample identification and phase quantification interaction mechanism that causes a frequency change

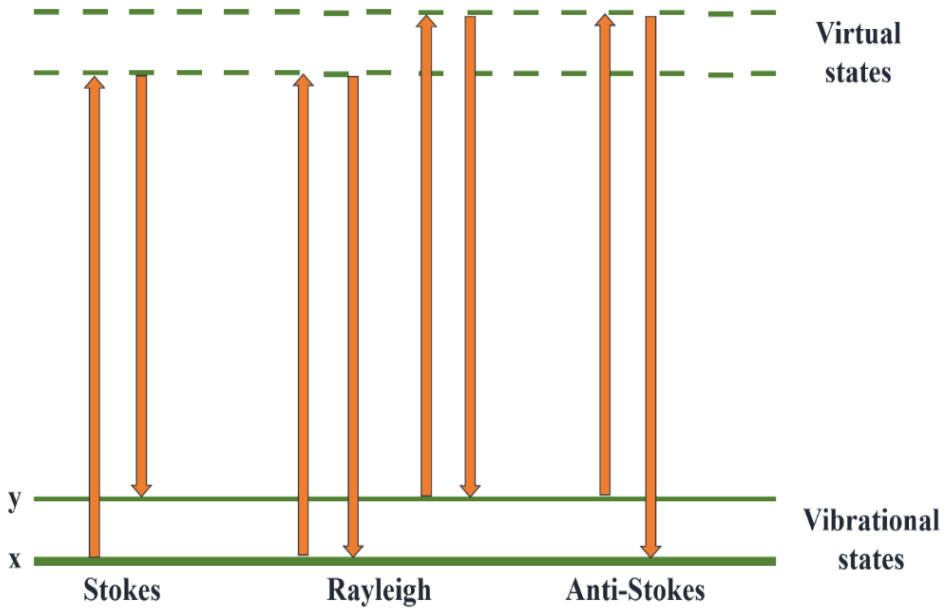

Figure 3. 10 Energy states diagram for scattering phenomenon.

If the light photon gains energy after the interaction by absorbing a phonon, the frequency of scattered photon is increases and this phenomenon is known as anti-stokes Raman scattering. If light photon losses energy after interaction by emitting a phonon, frequency of scattered photon is shifted down, this process is known as stokes Raman scattering. Since the anti-Stokes peaks are weaker than the Stokes peak, generally in Raman spectra Stokes peaks are displayed. Frequency shift is defined as; $\upsilon=\upsilon_s-\upsilon_i$, and it is equivalent to an energy change since $E=h\upsilon$. On the other hand, in Raman spectra, results are generally expressed by wavenumber instead of frequency. While frequency is equal to number of vibrations per second while wavenumber is equal to number of waves per centimeter.

Relation in between these two terms is:

$$\textbf{Wavenumber} = \frac{\textbf{Frequency}}{\textbf{c}}$$

Where the value of c is around 2.99×10^8 m/s i.e. the speed of the light in vacuum. Additionally, wavenumber is inversely proportional to the wavelength since;

$$\textbf{Frequency} = \frac{\textbf{c}}{\textbf{wavelength}}$$

Commonly used unit of the wavenumber is inverse centimeter (cm^{-1}). The energy difference in between the incident and the scattered photons corresponds to the energy of phonons in material. The frequency shift observed in scattering is directly related with vibrational energy of chemical bonds in between atoms within material. Hence, analysis of the scattered frequencies reveals information about the structure of the scattering medium. In crystalline structures, local bonds have well-defined energies. Due to narrow distribution of bonding energies, Raman spectra show narrow lines. However, in amorphous structures wide distribution of bonding energies is observed, thus broad scattering signal is obtained from this kind of disordered structures. In general, RS is very weak phenomenon. In 10^6-10^8 scattered photons only one Raman scattered photon comes out. In itself this does not make the process unachievable since with high-tech CCD detectors and lasers, very high-power densities can be incident to small objects. But it triggers the other un-acceptable things such as sample degradation and fluorescence. Figure 3.10 shows the fundamental phenomenon, which takes place for one vibration. In that figure, mention virtual energy states are imaginary states. These states are created by incident of laser light on sample. Laser source also determine the energy of said states. In general, mostly molecules are located at its lowest energy state. The Rayleigh have greatest intensity among all process, since major portion of scattered photons taken that way. They do not show any shift in energy. So, these types

of scattering are useless for investigation purpose. On illumination by a laser, the electrons present in a vibrational level get excited by the higher vibration level. During de-excitation process, some electrons return to the initial vibrational energy level. The photons generated during this type of de-excitation have the same wavelength as the incident photons. This is called Raleigh de excitation or Rayleigh scattering. Some electrons get de-excited to the lower vibrational level with respect to the initial vibrational level. The photon generated in this type of de-excitation have less wavelength than that of incident photons, this process is called anti-stock de-excitation or anti-stock scattering. Rest of the electrons get de-excited to higher vibrational level with respect to the initial vibrational level. The photons generated in the process have more wavelength than the wavelength of incident photons. This process is stoking de-excitation or stokes scattering. Intensity of anti-stokes scattering also become very poor. At higher temperature, both type scattering increases. Raman spectroscopy is divided into types, according to its way for sample collection i.e. dispersive Raman spectroscopy and FT-Raman spectroscopy. Both types have their own advantages as well as analyses specific samples.

3.3.2.1 Dispersive Raman Spectroscopy

For getting Raman spectra, it is become important to identify the scattered light beam into individual wavelengths. For this purpose, dispersive Raman spectroscopy used a grating. Raman scattered signals produced by samples are focusing on grating. This separated signal is sent to a detector. In that type of Raman spectroscopy visible lasers 473nm, 532nm, 633nm and 780nm are used in exciting the samples. The intensity of Raman scattering signal is inversely proportional to

(wavelength) [4]. So, using short wavelength lasers causing improvement in the Raman scattering signals.

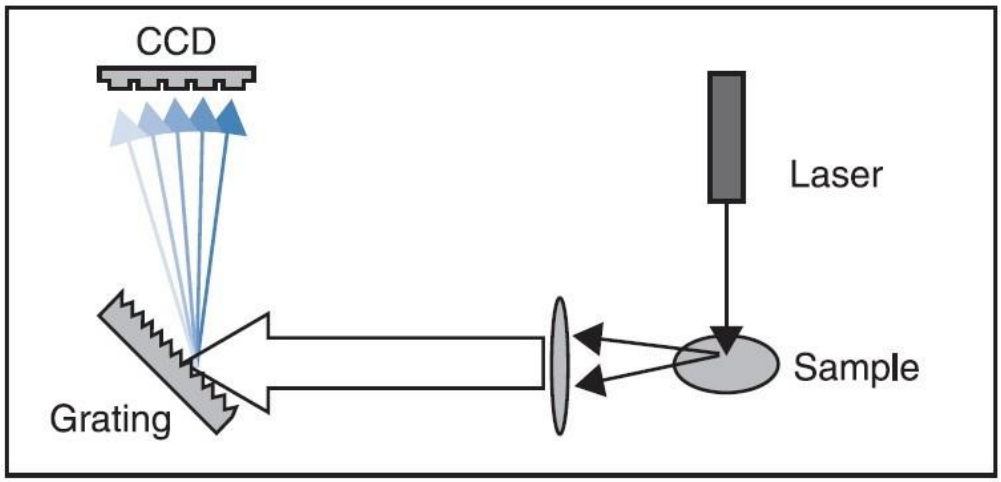

Figure 3. 11 Block diagram of Dispersive Raman Spectroscopy.

All type of Raman spectroscopy has a problem of fluorescence that produced unpredictably. It is very harmful for Raman signal because small quantity of fluorescence has power to overwhelm the expected Raman investigation. It is produced by overlapping of virtual energy level to upper level. So, as the wavelength of laser gets shorter the energy of laser increases, and hence intensity of fluorescence increased. Said phenomenon of fluorescence is depends on wavelength of laser. So, if a material produced fluorescence for one laser may be investigated by another wavelength. Grating plays a very important role in dispersive Raman spectroscopy. (see Figure 3.11). The resolution of a dispersive Raman spectroscopy and its throughput is very much depending upon grating. Grating is a surface on which grooves are created. These grooves distinguished the wavelengths in Raman scattering signals. For high resolution, it is become important that at least 2400 grooves are made on $1mm_2$grating. Dispersion angle of Raman signal is also very much

depending on number of grooves presenting in grating. For a good analysis dispersion should be as much as possible, so that area of surface become larger on which the different wavelength falls when they approach the detector. If detector size is fixed, user needs the spectrum beyond the resolution of instrument, in that case, all Raman wavelength does fall on detector. To overcome said limitation, either grating or detector should be movable. Performance of a grating is also strongly related to wavelength. So, resolution of equipment with respect to wavenumber is not linear. It increases at higher wavenumbers. So, resolution of equipment must be defined in respect of wavenumber. So, gratings must be grooved for optimization for a narrow wavenumber. It should be chosen for selective resolution and for selective laser wavelength. If user wants to use one grating for more than one laser than resolution of equipment needs compromising with sensitivity of instrument.

About CCD detector, the mostly used CCDs for dispersive Raman spectroscopy are made from silicon technology. The investigation area of the CCDs is made from 2-D arrays of pixels. Every pixel works as individual detector. Each wavelength light separated by grating is observed by different array element. CCD detectors have potential to detect 400nm to 1100nm wavelength light. If 780nm laser used in dispersive Raman spectroscopy then 3000cm^{-1} response produces radiation of 1018nm.

To make dispersive Raman spectroscopy for investigation of very small object or selective portion of sample, a microscope is connected with it. Minimum area analysed by a dispersive Raman is said spatial resolution. For achieving maximum spatial resolution, apertures of microscope should be of minimum diameter. But when light travel across such small aperture, diffraction of light

taking place, which limit the performance of instrument. Diffraction is a wavelength related issue. It depends on wavelength in following manner:

$$\text{Diffraction} = \frac{1.22 * \text{Wavelength}}{\text{Numerical Aperture of sample collection optics.}}$$

So, higher energies, short wavelengths laser sources are suitable for getting maximum spatial resolution i.e. less them 1μm. It is also possible, a minimum size aperture putting in a microscope's focal plane to make a confocal Raman spectroscopy (see Figure 3.12). Schematic plot of said confocal Raman microscope would be seen in Figure 3.12. In a confocal Raman spectroscopy, only light beam coming from optical focal point is allowed to fall on to the CCD. Remaining surrounding rays are eliminated by aperture. Confocal Raman spectroscopy is very beneficial for characterizing samples of polymer laminates and stacked structures.

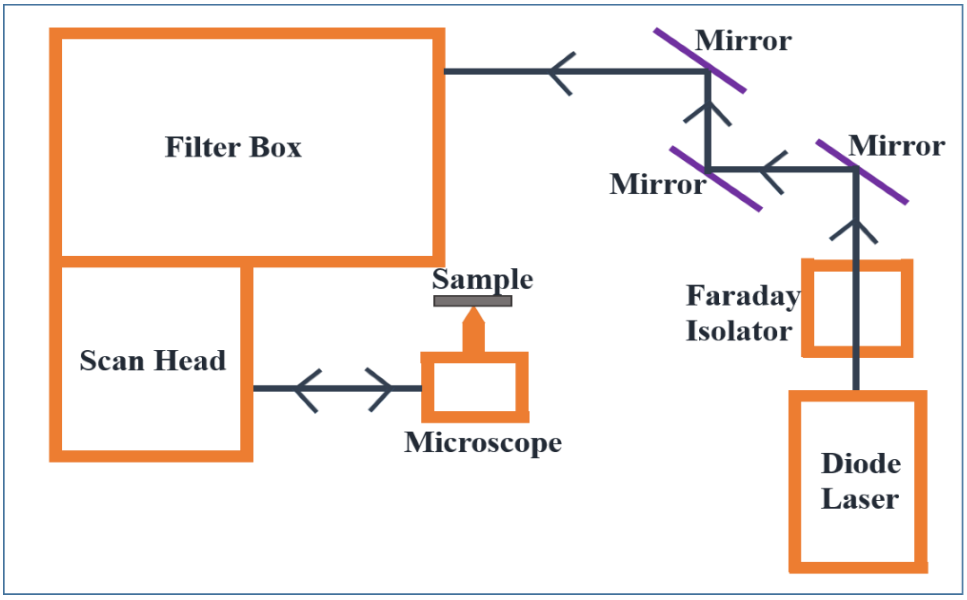

Figure 3. 12 Block diagram Confocal Raman spectroscopy.

3.3.2.2 FT-Raman Spectroscopy

After taking many precaution and laser selective criteria, however, fluorescence creates the interference with Raman signals. To overcome the problem of fluorescence, FT-Raman spectroscopy was assembled. In FT-Raman spectroscopy along wavelength (1μm) laser is employed for sample excitation instead of short length laser. Long wavelength lasers have less energy, so, chances of overlapping between virtual state and upper states decreases, and hence drastically control the problem of fluorescence. Including long wavelength laser source, FT-Raman spectroscopy also has an interferometer as well as very sensitive near- infrared detector. In FT-Raman spectroscopy most preferred detector is Indium gallium arsenide. Indium gallium arsenide detectors shows very high sensitivity, but these detectors are not good for near-infrared light as compare to silicon-based CCD for visible range.

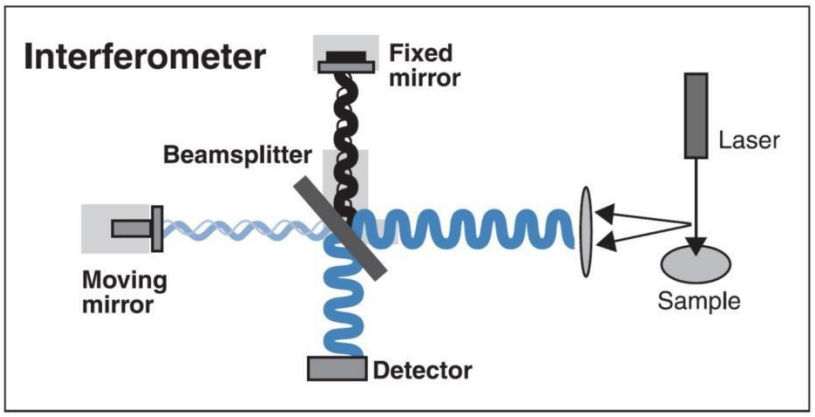

Figure 3. 13 Schematic diagram of Interferometer used in FT-Raman spectroscopy [57].

The benefit of said FT-Raman spectroscopy is to provide the sensitivity to week signals. FT-Raman spectroscopy also provides following advantages over dispersive Raman spectroscopy:

- It gives very high resolution with lesser throughput.
- All wavelengths measured in same time.
- It has increased signal to noise by compensating Raman Signal.
- Due inbuilt calibration property in interferometer, it has superior wavelength accuracy.

Another most important part of FT-Raman spectroscopy is interferometer. Interferometer is heart of FT-Raman spectroscopy. It is used to generate interferogram, which in turn is used to encode the individual frequency of Raman signal into a single signal (see Figure 3.13). Produced signal is observed in less than one second and averaging of signal is very rapid as well as accurate. Interferometer have a beam divider. It is optimized for radiation of near-infrared beam divider, split the Raman scattering into two parts, in which one part transmitted and remaining part reflected. Reflected portion going towards a fixed mirror and reflects off. From that mirror transmitted beam also get reflect off. Both beams meet at beam divider after travelling different distance. So, they produced interference in both constructive as well as destructive manner. The movable mirror has fixed frequency and movement, which modulate the interference. The produced interferogram have a special property. Every data point of interferogram have whole report about each frequency of Raman scattered signal.

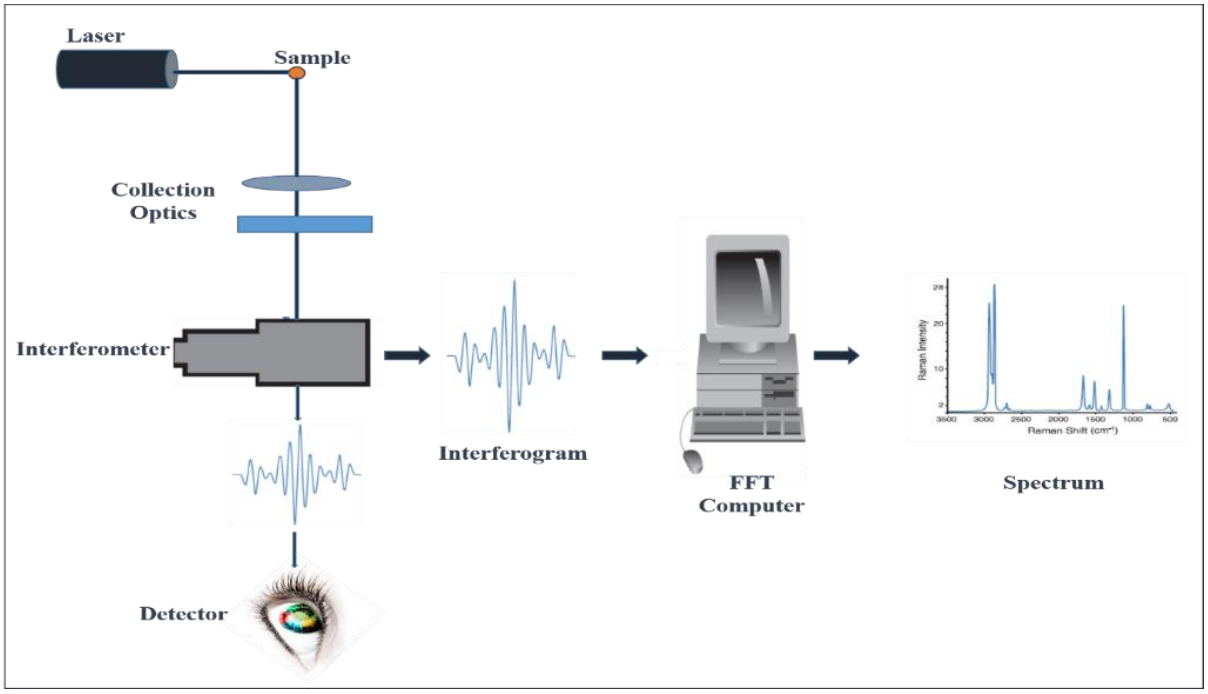

Figure 3. 14 Block diagram of FT-Raman spectroscopy [57].

Produced interferogram is in the encoded form of frequency spectra. It is decoded by Fourier transformation, a well-known mathematics technique. That part of decoding is done in computer (see Figure 3.14). Finally, having gone through the appropriate theory, all the details of the experimental Setup, I am now ready to consider the experimental Raman spectra of CNTs. Raman Spectroscopy provide major information about structure of CNTs, defects in CNTs as well as about purity. It is also used in in the identification between MWNTs and SWNTs as well as other carbon material [37]. In general, Raman spectroscopy is more fruitful for SWNTs as compare to MWNTs. For MWNTs it gives very complex spectra. Because MWNTs behave like a group of SWNTs, in the diameter range from very small to large [37]. The decoding of Raman spectra for MWNTs is based on well-established Raman spectra for SWNTs. It is reported in many articles that Raman spectroscopy have potential to provide qualitative as well quantitative information

about CNTs. An ideal Raman spectrum of CNTs have following important peaks (also see Figure 3.15):

- RBM
- D-Band
- G-Band
- G^{l}Band

3.3.2.3 Radial Breathing Mode (RBM)

The Radial Breathing Mode (RBM)(<200cm^{-1}) is one of the few strong lines in the SWNT Raman spectrum, and the only strong line which has no counterpart in graphite spectra. I found that it has a very simple diameter dependence $\omega_{RBM} = \alpha_{RBM}/dt$. RBM is strongly related to tube diameter. It is inversely proportional to diameter. For large diameter SWNTs, greater than 2nm, RBM may disappear [38]. And due to its radial motion of the atoms it is more strongly affected by the nanotube environment (e.g. other tubes as in a bundle or a supporting substrate) than the other high intensity modes. This, and the fact that the RBM is a direct manifestation of the one-dimensional tubular structure of the SWNT's makes it a very valuable probe for the nanotube properties and the majority of papers on the Raman effect in SWNT's concern. In case of RBM, Peak broadening is also having very meaningful information. Different effects can contribute to

broadening of the RBM-peak. The bundle-form of the nanotube sample will result in broadening with respect to the isolated tube case since the tube-tube interactions affect ω_{RBM} and the interactions depend on the position of the resonant tube in the bundle.

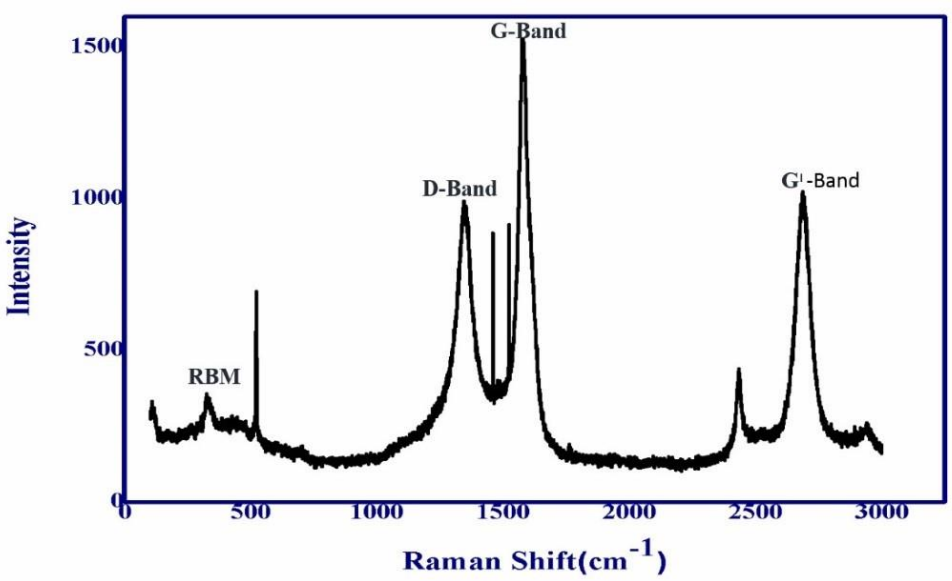

Figure 3. 15 Rama spectra of SWNTs [56].

The temperature of the sample gives rise to broadening due to phonon-phonon and electron phonon interactions, and it has been reported [39] that the peaks shift upon heating probably due to changes in the inter-and intra-tube interaction in the bundles and to a lesser degree due to thermal expansion of the tubes.

Thus, the peaks will broaden if there are temperature differences in the sample area for example because of different couplings to the substrate or due to the intensity profile of the impinging beam heating some areas more than others.

Additionally, defects in the tubes or other interactions also result in broadening of the peaks. In graphite the electron-phonon broadening is $\sim$6 cm^{-1}[40] and since several peaks are narrower, it is concluded that the electron-phonon broadening is smaller in nanotubes than in graphite. It should be noted that Raman studies on some nanotube samples consisting of bundles have found peaks not narrower than 20 cm^{-1}[41], and low-temperature measurements on highly defect free tubes report linewidths down to 0.35 cm^{-1}[42]. Thus, the width is highly dependent on the sample nature as well as on the measurement parameters.

3.3.2.4 G-Band

In Raman spectra, G-band, a bunch of peaks around 1582cm^{-1} also verify the existence of CNTs. G-band have capability to investigation of diameter dependent study of SWNTs without using RBM. In resonance, for a particular laser light, the metallic character of the CNTs also observed. For CNTs, G-band have six peaks. Out of six two peaks have maximum intensity and for simplicity, I consider only two peaks i.e. G^+ and G^-.

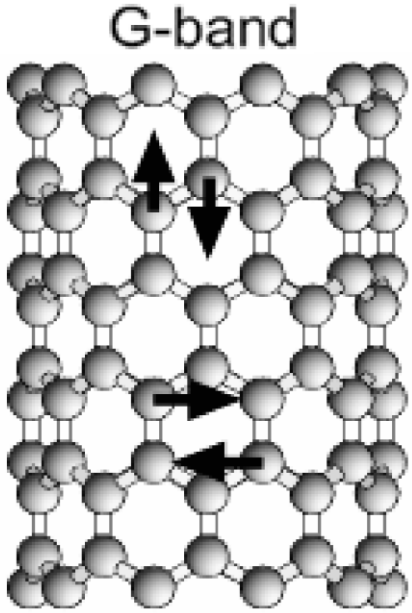

Figure 3. 16 Schematic picture showing the atomic vibrations for the G band modes (42) [55].

These peaks produced by symmetry breaking of the tangential vibration when the graphene sheet is rolled to make a cylindrically shaped tube. G^+ is originated through atomic displacements along the tube axis and G^- produced by atomic displacement along the circumferential direction (see Figure 3.16 and Figure 3.17). Figure 3.17 the line shape difference of G^- for semiconducting and multiwall CNTs and it is broadened for metallic with respect to semiconducting CNTs (see Figure 3.17), and its broadening coming from free electrons in nanotubes with metallic behavior [43-45]. If charged impurity exist in SWNTs then G-band for Semiconducting CNTs shows the behavior of metallic CNTs [46]. If talking about diameter dependent study of G-band then the frequency of G^+ does affected by diameter but in frequency of G^- band shifting with variation in diameter of CNTs is observed (see Figure 3.18 and Figure 3.19) [47-48]. Hence, G-band and its splitting may be used for diameter calculation of CNTs.

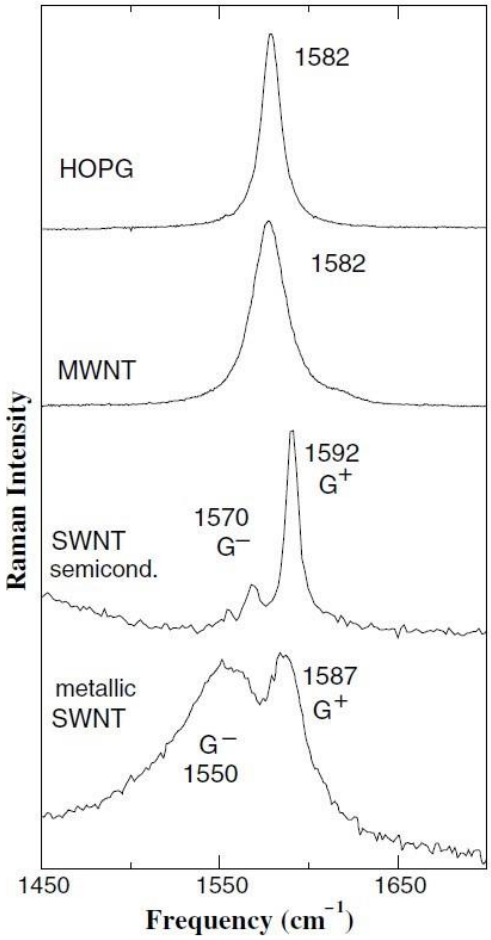

Figure 3. 17 G-band for highly ordered pyrolytic graphite (HOPG), MWNT bundles, one isolated semiconducting SWNT and one isolated metallic SWNT. The multi-peak G-band feature is not clear for MWNTs due to the large tube diameters [55].

Recently, some research group given evidence for formation of G-band from double resonance mechanism [49-50]. In that case, intensity of G-band very much depends on defects of CNTs, and the frequency of G-band is depending on energy of laser. These evidences create complication in use of Raman spectroscopy for SWNTs. However, it can be observed that double as well as single resonance shows the same intensity for defective material. For defect less materials, intensity of

single resonance is double as compare to double resonance phenomenon [51-52]. So, according to this report Raman spectroscopy is only effective for good quality of SWNTs.

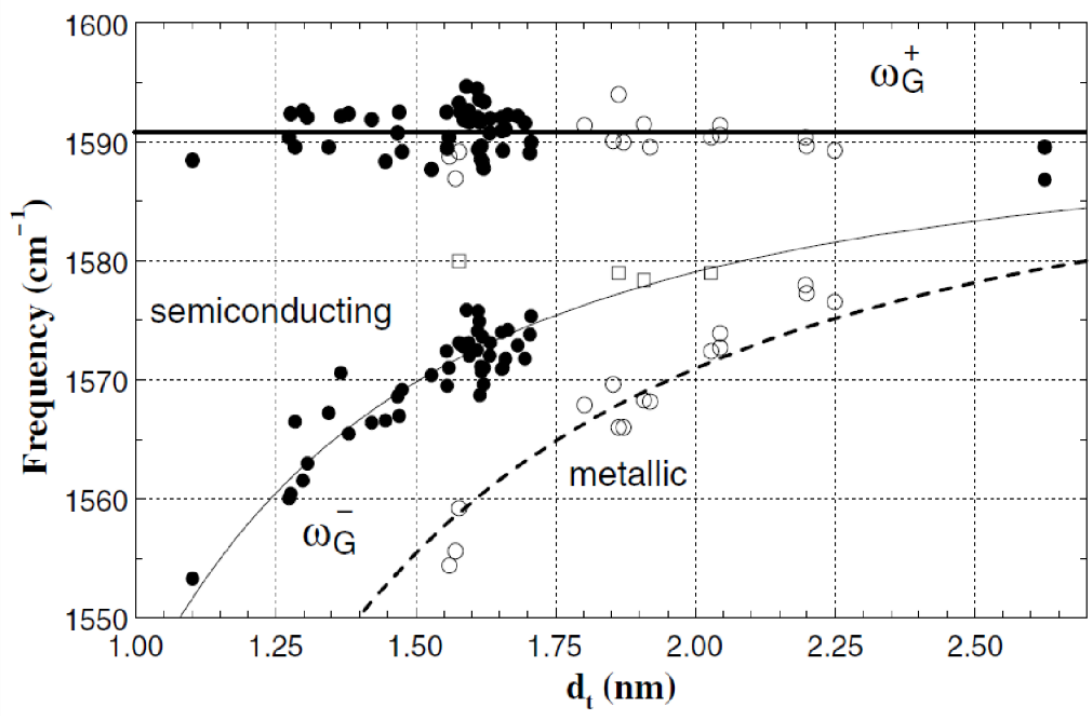

Figure 3. 18 Diameter dependence for ωG+ and ωG− for several isolated semiconducting and metallic SWNTs. Filled and open symbols apply for semiconducting and metallic tubes, respectively. The lines are fit to the experimental points [55].

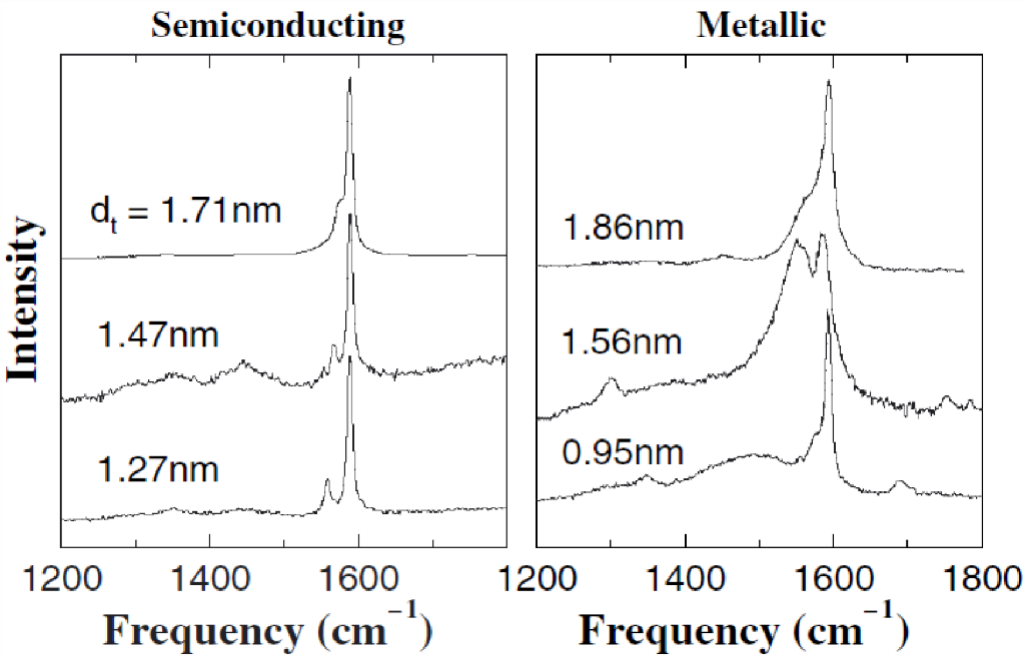

Figure 3. 19 Raman signal from three isolated semiconducting and three isolated metallic SWNTs showing the G and D band profiles. SWNTs in good resonance (strong signal with low signal to noise ratio) show practically no D band. Spectra in bad resonance shows noisy background with a peak at ~1450 cm−1 (e.g., see second trace for semiconducting SWNTs) [55].

3.3.2.5 Disorder Bands (D-Band and G/-Band)

A bunch of peaks appears in Raman spectra of CNTs around 1332$cm^{-1}$and 2700cm^{-1}. It represents the defects and disorders in structure of CNTs. It is highlighted in both type of CNTs. Due to double resonance criteria, D-band also appears due to some specific chirality [52]. In case of isolated SWNTs, D-band is splited into two parts. Split distance of D-band relates to energy of incident light. GI-Band shows an intrinsic property of graphite. The GI-B and is caused by two-phonon scattering around the K point of the Brillouin zone. This mode is known to be sensitive to increasing defect density, but not as significantly as the first-order mode. The mode has significant contributions from regions near the K and M points, yielding peaks at approximately

2700 $cm^{-1}$and approximately 2730 cm^{-1}, respectively [53]. The intensity of this peak depends strongly on the metallicity of the nanotube [54F]. It follows that these bands convey information about the nanotubes which cannot be accessed by the other phonon modes.

3.4 Conclusion

Development of science and Technology is a continuous process. From the beginning of life, human race is evolving day by day. Development of logical thinking has brought the evolution in science and technology to make the tools more powerful that are making the life easier day by day. These tools work in the feedback process and take parts in the further development of science and technology. We are living in an age where we are playing with the part of the nature which is as small as it can be well fitted in the definition of invisible. This is the world of Nano. Development of quantum mechanics and the allied sciences have made the microscopic tools so powerful that I can see the thing at the nano scale. This magical scale brings a lot of extraordinary features of the materials that they do not show at the macroscopic scale. Now a days, the research and development in all over the world is focused on the exploration of extraordinary features of the properties of materials that originate due to their size. Carbon nanotube is one of the rigorously researched materials in the contemporary worlds. Owing to their extraordinary properties, CNTs have become one of the frontrunners in the world of contemporary research. When considering the cross-sectional area of the CNT walls only, an elastic modulus approaching 1 TPa and a tensile strength of 100 GPa has been measured for individual MWNTs. This strength is over 10-fold higher than any industrial fiber. MWNTs are typically metallic and can carry currents of up to $109Acm^{-2}$. Individual CNT walls can be metallic or semiconducting depending on the orientation of the graphene lattice with respect to the tube axis, which is called the chirality. Individual SWNTs

can have a thermal conductivity of 3500 W m^{-1} K^{-1} at room temperature, based on the wall area; this exceeds the thermal conductivity of diamond. Because of these ultimate properties, CNTs are being used in variety of nano sensors, biosensors, in optoelectronic devices such as solar cells, photodetectors and light emitting diodes, in different types of high-performance electronic devices, as reinforcement in different composite systems etc. For the preparation of devices at nanoscale, where I deal with the ultra-small regime, control on synthesis and growth of CNTs, having precise specifications is very important. Chemical vapour deposition method is most widely used method to grow MWCNTs and SWCNTs. There are different factors such as dynamics of source as well as carrier gases, growth temperature, temperature ramp, catalyst engineering, substrate engineering etc. that affect the specifications of CNTs.

3.5 References

[1] Y. Saito, T. Yoshikawa, M. Inagaki, M. Tomita, T. Hayashi, Growth and structure of graphitic tubules and polyhedral particles in arc-discharge, Chemical Physics Letters, 204 (1993) 227.

[2] S. Iijjima, Helical microtubules of graphitic carbon, nature, 354 (6348) 56.

[3] C. Journet, W. K. Maser, P. Bernier, A. Loiseau, M. L. d. l. Chapelle, S. Lefrant, P. Deniard, R. Lee, J. E. Fischer, Large-scale production of single-walled carbon nanotubes by the electric-arc technique, Nature, 388 (1997) 756.

[4] Y. Saito, K. Nishikubo, K. Kawabata, and T. Matsumoto, Carbon nanocapsules and single-layered nanotubes produced with platinum-group metals (ru, rh, pd, os, ir, pt) by arc discharge, Journal of Applied Physics, 80 (1996) 3062.

[5] S. Farhat, M. L. de La Chapelle, A. Loiseau, C. D. Scott, S. Lefrant, C. Journet, P. Bernier, Diameter control of single-walled carbon nanotubes using argon–helium mixture gases, The Journal of Chemical Physics, 115 (6752) 2001.

[6] D. Tang, S. Xie, W. Liu, B. Chang, L. Sun, Z. Liu, G. Wan, and W. Zhou, Evidence for an open-ended nanotube growth model in arc discharge, Carbon, 38 (2000) 480.

[7] T. Ebbesen and P. Ajayan, Large-scale synthesis of carbon nanotubes, Nature, 358 (1992) 220.

[8] Y. Lu, C. Partridge, M. Meyyappan, and J. Li, A carbon nanotube sensor array for sensitive gas discrimination using principal component analysis, Journal of Electroanalytical Chemistry, 593 (2006)105.

[9] M. Cadek, R. Murphy, B. McCarthy, A. Drury, B. Lahr, R. Barklie, J. Coleman, W. Blau, Optimisation of the arc-discharge production of multi-walled carbon nanotubes, Carbon, 40 (2002) 923.

[10] C.-H. Kiang, W. A. Goddard, R. Beyers, and D. S. Bethune, Carbon nanotubes with single-layer walls, Carbon, 33 (1995) 903.

[11] C. Journet and P. Bernier, Production of carbon nanotubes, Applied Physics A: Materials Science & Processing, 67 (1998) 1.

[12] S. Farhat, M. L. de La Chapelle, A. Loiseau, C. D. Scott, S. Lefrant, C. Journet, and P. Bernier, Diameter control of single-walled carbon nanotubes using argon–elium mixture gases, The Journal of Chemical Physics,115 (2001) 6752.

[13] [13]Bolshakov, S. Uglov, A. Saveliev, V. Konov, A. Gorbunov,W. Pompe, A. Graff, A novel cw laser– powder method of carbon single-wall nanotubes production, Diamond and Related Materials,11(2002) 927.

[14] F. Kokai, K. Takahashi, M. Yudasaka, R. Yamada, T. Ichihashi, S. Iijima, Growth dynamics of singlewall carbon nanotubes synthesized by co2 laser vaporization,The Journal of Physical Chemistry B,103 (1999) 4346.

[15] M. Yudasaka, F. Kokai, K. Takahashi, R. Yamada, N. Sensui, T. Ichihashi, S. Iijima, Formation of single-wall carbon nanotubes: Comparison of CO2 laser ablation nd: Yag laser ablation," The Journal of Physical Chemistry B,103 (1999) 3576.

[16] P. Eklund, B. Pradhan, U. Kim, Q. Xiong, J. Fischer, A. Friedman, B. Holloway, K. Jordan, and M. Smith, Large-scale production of single-walled carbon nanotubes using ultrafast pulses from a free electron laser, Nano Letters, 2 (2002) 561.

[17] N. Braidy, M. El Khakani, and G. Botton, Effect of laser intensity on yield and physical characteristics of single wall carbon nanotubes produced by the nd: Yag laser vaporization method, Carbon, 40 (2002) 2835.

[18] T. De Los Arcos, F. Vonau, M. Garnier, V. Thommen, H.-G. Boyen, P. Oelhafen, Influence of iron– silicon interaction on the growth of carbon nanotubes produced by chemical vapor deposition, Applied physics letters, 80 (2002) 2383.

[19] M. Nihei, A. Kawabata, D. Kondo, M. Horibe, S. Sato, Y. Awano, Electrical properties of carbon nanotube bundles for future via interconnects, Japanese journal of applied physics, 44 (2005) 1626.

[20] T. Dikonimos Makris, L. Giorgi, R. Giorgi, N. Lisi, and E. Salernitano, CNT growth on alumina supported nickel catalyst by thermal CVD, Diamond and related materials, 14 (2005) 815.

[21] N. Tripathi, P Mishra, B Joshi, SS Islam,Catalyst free, excellent quality and narrow diameter of CNT growth on Al 2 O 3 by a thermal CVD technique,Physica E: Low-dimensional Systems and Nanostructures 62 (2014) 43.

[22] N. Tripathi, P Mishra, H Harsh, SS Islam, Fine-tuning control on CNT diameter distribution, length and density using thermal CVD growth at atmospheric pressure: an in-depth analysis on the role of flow rate and flow duration of acetylene (C2H2) gas, Applied Nanoscience, 5 (2015)19.
[23] K. Hernadi, A. Fonseca, J. B. Nagy, D. Bernaerts, A. A. Lucas, Fe-catalyzed carbon nanotube formation, Carbon, 34 (1996) 1249.
[24] M. J. Bronikowski, P. A. Willis, D. T. Colbert, K. A. Smith, and R. E. Smalley, J. Vac. Sci. Technol. A 19, 1800 (2001).
[25] WTEC Study Report on International Assessment of Research and Development of Carbon Nanotube Manufacturing and Applications, World Technology Evaluation Center Inc., USA (2007).
[26] A. M. Cassell, J. A. Raymakers, J. Kong, and H. Dai, J. Phys. Chem. B 103, 6484 (1999).
[27] S. Maruyama, R. Kojima, Y. Miyauchi, S. Chiashi, and M. Kohno, Chem. Phys. Lett. 360, 229 (2002).
[28] K. Hata, D. N. Futaba, K. Mizuno, T. Namai, M. Yumura, and S. Iijima, Science 306, 1362 (2004).
[29] M. Endo, Chemtech 18, 568 (1988).
[30] I. Willems, Z. Konya, J. F. Colomer, G. V. Tendeloo, N. Nagaraju, A. Fonseca, and J. B. Nagy, Chem. Phys. Lett. 317, 71 (2000).
[31] E. Couteau, K. Hernadi, J. W. Seo, L. T. Nga, C. Miko, R. Gaal, and L. Forro, Chem. Phys. Lett. 378, 9 (2003).
[32] D. C. Joy, G. R. Booker, Simultaneous display of micrograph and selected-area channelling pattern using the scanning electron microscope J. Phys. E: Sci. Instrum., 4 (1971) 837.
[33] N. Goldstein, C.M. Echer, A. P. Alivisatos, Melting in Semiconductor Nanocrystals, Science 256 (1992) 1425.
[34] M. Endo, H. Fijiwara, and E. Fukunaga, 18th Meeting Japanese, Carbon Society, Japanese Carbon Society, Saitama, December (1991), p. 34.
[35] M. Endo, K. Takeuchi, S. Igarashi, K. Kobori, M. Shiraishi, and H. W. Kroto, 19th Meeting Japanese Carbon Society, Japanese Carbon Society, Kyoto, December (1992), p. 192.
[36] M. Endo, K. Takeuchi, S. Igarashi, K. Kobori, M. Shiraishi, and H. W. Kroto, J. Phys. Chem. Solids 54, 1841 (1993).
[37] M. Jose-Yacaman, M. Miki-Yoshida, L. Rendon, and J. G. Santiesteban, Appl. Phys. Lett. 62, 657 (1993).
[38] Z. Liua, R. Cheb, Z. Xu, and L. Peng, Synth. Met. 128, 191 (2002).
[39] N. Li, X. Chen, L. Stoica, W. Xia, J. Qian, J. Abmann, W. Schuhmann, and M. Muhler, Adv. Mater. 19, 2957 (2007).
[40] O. A. Nerushev, S. Dittmar, R. E. Morjan, F. Rohmund, and E. E. B. Campbell, J. Appl. Phys. 93, 4185 (2003).
[41] R. E. Morjan, O. A. Nerushev, M. Sveningsson, F. Rohmund, L. K. L. Falk, and E. E. B. Campbell, Appl. Phys. A 78, 253 (2004).
[42] H. Dai, A. G. Rinzler, P. Nikolaev, A. Thess, D. T. Colbert, and R. E. Smalley, Chem. Phys. Lett. 260, 471 (1996).
[43] E. Flahaut, A. Govindaraj, A. Peigney, C. Laurent, and C. N. R. Rao, Chem. Phys. Lett. 300, 236 (1999).
[44] H. M. Cheng, F. Li, X. Sun, S. D. M. Brown, M. A. Pimenta, A. Marucci, G. Dresselhaus, and M. S. Dresselhaus, Chem. Phys. Lett. 289, 602 (1998).
[45] S. Maruyama, R. Kojima, Y. Miyauchi, S. Chiashi, and M. Kohno, Chem. Phys. Lett. 360, 229 (2002).
[46] S. Okubo, T. Sekine, S. Suzuki, Y. Achiba, K. Tsukagoshi, Y. Aoyagi, and H. Kataura, Jpn. J. Appl. Phys. 43, L396 (2004).
[47] A. Gruneis, M. H. Rummeli, C. Kramberger, A. Barreiro, T. Pichler, R. Pfeiffer, H. Kuzmany, T. Gemming, and B. Buchner, Carbon 44, 3177 (2006).
[48] A. G. Nasibulin, A. Moisala, H. Jiang, and E. I. Kauppinen, J. Nanopart. Res. 8, 465 (2006).
[49] Y. Murakami, Y. Miyauchi, S. Chiashi, and S. Maruyama, Chem. Phys. Lett. 377, 49 (2003).
[50] Y. Murakami, S. Chiashi, Y. Miyauchi, M. Hu, M. Ogura, T. Okubo, and S. Maruyama, Chem. Phys. Lett. 385, 298 (2004).
[51] S. Maruyama, E. Einarsson, Y. Murakami, and T. Edamura, Chem. Phys. Lett. 403, 320 (2005).
[52] R. Xiang, E. Einarsson, J. Okawa, Y. Miyauchi, and S. Maruyama, J. Phys. Chem. C 113, 7511 (2009).
[53] R. T. K. Baker, M. A. Barber, P. S. Harris, F. S. Feates, and R. J. Waite, J. Catalysis 26, 51 (1972).
[54] T. Murakami, T. Sako, H. Harima, K. Kisoda, K. Mitikami, and T. Isshiki, Thin Solid Films 464, 319 (2004).

[55] A. Jorio, Characterizing carbon nanotube samples with resonance Raman scat-tering, New J. Phys. 5 (2003) 139.1–139.17.

[56] Lourie, O., Wagner, H.D. Evaluation of Young's Modulus of Carbon Nanotubes by Micro-Raman Spectroscopy. Journal of Materials Research 13, 2418–2422 (1998). https://doi.org/10.1557/JMR.1998.0336.

[57] Li, Z.; Deen, M.J.; Kumar, S.; Selvaganapathy, P.R. Raman Spectroscopy for In-Line Water Quality Monitoring—Instrumentation and Potential. Sensors 2014, 14, 17275-17303. https://doi.org/10.3390/s140917275

[58] Rahman, G.; Najaf, Z.; Mehmood, A.; Bilal, S.; Shah, A.u.H.A.; Mian, S.A.; Ali, G. An Overview of the Recent Progress in the Synthesis and Applications of Carbon Nanotubes. C 2019, 5, 3. https://doi.org/10.3390/c5010003

[59] Szabó A, Perri C, Csató A, Giordano G, Vuono D, Nagy JB. Synthesis Methods of Carbon Nanotubes and Related Materials. Materials (Basel). 2010;3(5):3092-3140. Published 2010 May 7. doi:10.3390/ma3053092

[60] Suryanarayana C. (2017) Microstructure: An Introduction. In: Prasad N., Wanhill R. (eds) Aerospace Materials and Material Technologies. Indian Institute of Metals Series. Springer, Singapore. https://doi.org/10.1007/978-981-10-2143-5_6

[61] M. Kumar and Y. Ando, Chem. Phys. Lett. 374, 521 (2003).

Chapter 4: Literature survey

4.1 Introduction

Gas sensors or chemical sensors have a huge demand in the various fields such as in environment monitoring, biomedicine, pharmaceutics and space exploration [1]. The gas sensors are required to detect harmful and toxic gases in real time, and these can be done by gas sensors which possess good sensitivity and selectivity. Owing to the increasing air pollution and global warming, environment to detect toxic gases has emerged as an important area of scientific research [2]. In addition to this, gas sensors are instrumental to experiments involving imitation of atmospheric conditions of different planets, where they can detect and quantify the different gases present in the atmosphere [3,4,5]. In this regard, NASA Scientists in order to formulate atmospheric constituents of different planets, they are seeking the use of gassed-up gas sensors [6]. For the efficient and good gas sensing system, the following parameters are paramount: (1) portability of sensors (2) stability in performance; (3) lower detection limit; (4) high selectivity and sensitivity; (5) fast recovery as well as response; (6) low operating temperature; and (7) the effect of the temperature on sensor response should be minimum [7,8].

Ideal gas molecules adsorption and storage can be done by a material which has a pitted structure and high surface-to-volume ratio, hence, gas sensors based on nanomaterials, such as nanofibers, nanowires, CNTs and nanoparticles, have been widely explored [9,10,11,12]. There has been a considerable increase in the study of CNTs as gas sensors in order to meet the high demand for gas detection technologies [8,13].

The basic principles of gas sensors are desorption and adsorption of gas molecules on sensing materials [4,5]. CNTs, belong to the fullerene structure, are suitable material for gas sensing applications because it has large surface-to-area as per requirement of gas sensing applications [5]. Extraordinary electrical, mechanical and thermal properties of CNTs have led to extensive research in different fields. Electronic transport in CNTs, which is nearly one-dimensional structures, mainly takes place through quantum effects and ballistic transport along the nanotube axis with no scattering [4,14]. Due to one-dimensional structure of carbon nanotubes (CNTs), they have an anisotropic dielectric property which enables them to carry high current with negligible heating effect. Many experiments have shown that whenever CNTs and CNT based composites are exposed to different gases, their properties change [15]. Charge transfer and

chemical doping are usually responsible for high sensitivity of CNTs towards gases [16,17]. When electron-donating molecules such as NH_3 and electron acceptor molecules such as NO_2 interact with p-type semiconducting CNTs, the electron concentration of the bulk semiconductor changes, thereby changing the conductance of CNTs. This forms the ground for the application of CNTs as dynamic sensors [5,18]. The covalent sp^2 hybridization bonds formed between the individual carbon atoms along the CNTs walls has led to high mechanical strength. In comparison, the tensile strength of MWNT is approximately 50 times greater than that of steel [19]. CNTs have been extensively considered in the areas such as actuators, sensors and other engineering applications because of their above-mentioned exclusive characteristics and behavior [8,20].

Carbon nanotubes can be characterized into two groups: SWNTs (single walled nanotubes) and MWNTs (multi walled nanotubes. Hata et al; found in 2004 that the diameter of SWNTs lies in the range of 0.8 to 2 nm, on the other hand the diameter of MWNTs varies between 5 to 100 nm [21]. Along with this, the length of CNTs usually varies from several nanometers to few millimeters. MWNTs are formed of many concentric cylinders and it has two different structures called as parched and Russian doll model. Table 4.1 shows the different properties of CNTs. This review paper is formed as follows: First section shows the various synthesis approach of CNTs and diverse fabrication techniques for CNTs gas sensors, Second section will discuss CNTs functionalization and CNTs-based nanocomposites for gas sensing applications. The discussion includes analysis of the following parameters of CNTs based sensors: sensitivity, selectivity, accuracy and resolution.

Table 4. 1: Values of different properties of carbon nanotubes (CNTs).

Sl.no	**Type**	**Properties**	**Remarks**	**Ref.**
1.	MWNTs	(a) Thermal Conductivity = 3 000 W/m.K (b) Tensile Strength = (11–63) Gpa	The typical MWNTs with the current carrying capacity up to 10^9 A cm^{-2} are	[22, 23, 24]

		(c) bending strength = 28.5 Gpa	metallic in nature.	
2.	SWNTs	(a) Thermal Conductivity = 3 500 W/m.K (b) Tensile Strength = (13–52) Gpa (c) bending strength = 80 Gpa	The chiral angle between tube axis and hexagon of SWNTs determine its nature such as metallic or semiconducting.	[25,26,27]

Owing to global warming there is a great demand for renewable sources of energy. There has been tremendous growth in the research of organic solar cells and carbon nanotubes (CNTs) which plays an important role in organic solar cells development [28-31]. In the recent years, there has been a tremendous increase in the interest of flexible and wearable devices because of their potential utilization in the field of energy [32-39], like smart electronics [40-42], biomedical devices [43-45], artificial skins [46-48] and essentially sensing products. The computational capacity and speed of the modern flexible smart devices can be enhanced by using positive attributes derived from merging of technologies such as electronic engineering, electrical, textile technology and nanotechnology. The fabrication of wearable electronics is possible by virtue of their wearability, flexibility and thread line nature. There is a huge increase in the demand of these applications, correspondingly leading to an increase in the demand and criteria for the development and efficient completion of such sensors. Unlike the continuous emphasis on miniaturization process of conventional microelectronics for increasing integration density and eventual performance, the focus of macroelectronics is on the large-area and low-cost development of flexible and wearable devices [49-51]. There are many electronic devices which are fabricated on stretchable, flexible and plastic substrates such as wearable electronics, electronic paper, flexible

display, smart packages, implantable medical implements and skin-like sensors. These emerging technologies could entirely change people's attitude towards electronics [52-55].

The flexible or wearable electronics is an emerging technology with promising applications in large-area electronics which is compatible with the curved surfaces and movable parts. Rapid progress in the design of ultrathin electronics and optoelectronics devices, biocompatible encapsulating layers, sensors and actuators have accelerated the possibility of development of flexible electronics interface for the complex geometry and curved structures [56-62]. Figure 4.1 summarizes the application of carbon nanotubes on the flexible substrates for various electronic fields. Conventional sensors are rigid and consequently there is hindrance owing to rigidity in capturing analytes and also it suffers from poor quality transduction. In contrast the flexible sensors can capture analytes gases more efficiently and can generate high-quality signals. A radical change in the methodology of material design, including active materials and conductors design as well as selection and synthesis of flexible substrates are required for the production of flexible sensors. Majority of inflexible materials become deformable once they are refined and oriented into nanostructures [63-64]. For example, in the year 2011 Rogers showed that the flexible rigidity of silicon (Si) wafer (=200 μm) is fifteen order greater than that of silicon nanomembranes (Si NMs) (2 nm) [65].

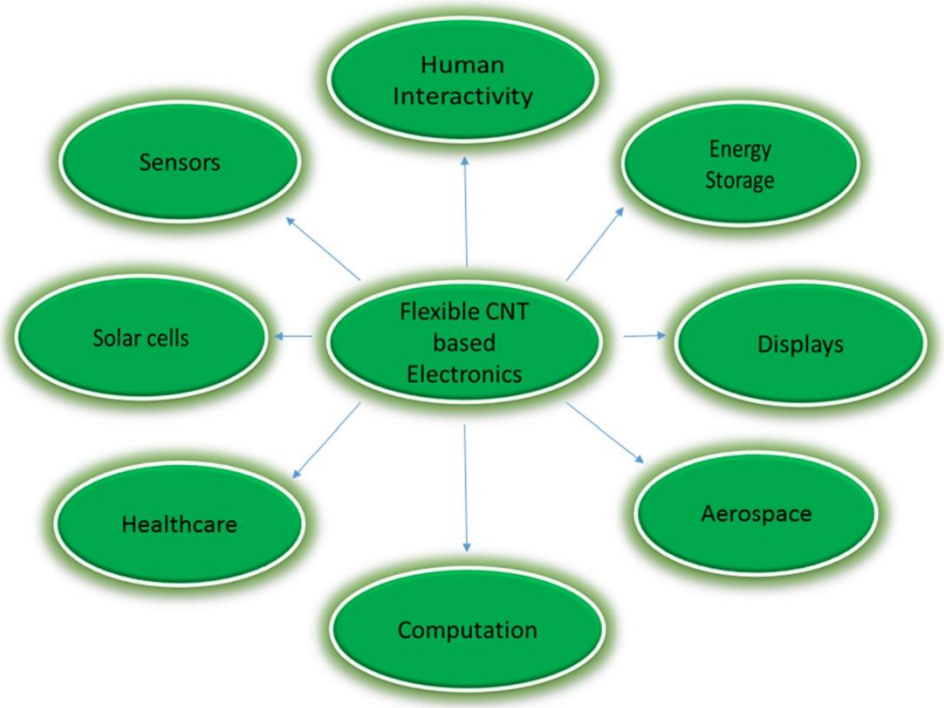

Figure 4. 1: Schematic explanation of development of flexible or wearable electronics across the broad range of applications.

There are some non-transition metal oxides which have been utilized as active materials such as SnO_2, Ga_2O_3, ZnO and In_2O_3. There are many active emerging materials which are suitable as flexible sensors, for example, two-dimensional nanostructure-based semiconductors including graphene [66-68], black phosphorus [69], transition metal dichalcogenides (TMDs) [70-72] and one-dimensional nanostructure material such as nanowires [73-77] all offer particular electrical and optical conduct aspects.

Carbon nanotubes (CNTs) have attributed intensive interest in various research areas from battery electrodes or flexible supercapacitor to high performance artificial muscles because of their great mechanical and electrical properties. By virtue of ultimate fibrils structures and small sizes, macro assemblies of CNTs can build diverse organizing structures which provide plenty of opportunities for the realization of CNTs based functional materials and devices. Unfortunately, as per the literature, this CNT based strain sensors suffered from low sensitivity, non-linearity and poor restorability [78-81].

During past years, the merits derived from the nanoscale thickness and large surface to volume ratio of 2D nanostructures materials have demonstrated great capabilities for gas sensing

devices. As a result, 4s sensor performance i.e., selectivity, speed (response and recovery times), sensitivity, and stability have gained significant momentum. For example, at room temperature graphene sensors have enabled an ultimate sensitivity towards detecting individual molecule. This sensor is capable of rapid desorption and adsorption of a single NO_2 gas molecule from the graphene surface. Moreover, the use of these novel 2D nanostructures such as graphene, MoS2 nanosheets, and phospherene has successfully decreased the working mode temperature for gas sensors, approximately up to the room temperature which is normally impossible to achieve by semiconducting metal oxides [82-86].

Since 1970's, the semiconductor metal oxides (such as ZnO, WO_3, SnO_2) in the form of porous polycrystalline layers have been established as the standard sensing films for conductometric gas sensors. The innovation in the field of nanotechnology has improved the knowledge of materials and phenomena at the nanometric scale, and the generation of novel metal oxide-based gas sensor in the early 2000s [87]. Nanostructured metal oxides promised to have enhanced signals due to their surface like nature, at the same time more stable at high operating temperature compared to their bulk counterparts. The majority of the research activities were performed on n-type semiconductors like WO3, TiO_2, ZnO and SnO_2, the most investigated material for chemical sensing [88]. On the other hand, the p-type metal oxides were less investigated as compared to n-type ones, owing to the lower expected performances related to the nature of charge carriers [89-91].

Some of the issues related to metal oxide-based gas sensors devices are well known and out of them one is that the metal oxide-based gas sensor suffers from the effects of baseline resistance drift and from poisoning interactions, which makes metal oxide surface progressively slow and less accessible to reactive gases. Although metal oxide-based gas sensors have very good sensitivity, but they suffered from poor selectivity between similar gases. Many gas species may cause similar changes in the resistance, making it impossible for single sensor to sense the present gas correctly. This problem may be partially solved by the formation of arrays by combining multiple and different sensors [92-93].

The formation of heterostructures by combining various metal oxides materials give a unique structure and fulfilled the necessity of further improved sensitivity, selectivity and other various important sensing parameters of resistive type gas sensors. Heterostructure nanomaterial

is a special branch of nanostructures which exhibits very good interactions between closely packed interfaces, resulting in superior performances compared to single materials. The fabrication of composite nanostructures, interacting n-type and p-type metal oxides, allows combining the different properties of the individual components [94-95].

The physical interface between two dissimilar materials at microscopic scale is known as heterojunction. It is well known through solid state physics that by contacting two dissimilar semiconducting materials at the interface, the fermi levels equilibrate at the same energy, often resulting in the charge transfer and hence formation of depletion layer. The formation of depletion layer zone is one of the most noticeable effects, but many other factors are also responsible for the improvement of sensing performance in these heterostructure devices.

The advancement of research in material science has led to the development of new forms of electronics. In macroelectronics, one of the key components of thin-film transistors (TFTs) is its channel and in the last decade there has been considerable research for materials such as polysilicon, organic semiconductor and amorphous silicon [96-100]. In the recent years, there is a great increase in the research interest for the nanomaterials including one dimensional carbon nanotubes, quantum dots [101-102], and two dimensional (2D) materials as they render much improved performance than organic semiconductors. Particularly, owing to their remarkably superior carrier mobility, stability and outstanding mechanical flexibility the carbon nanotubes (CNTs) carry on great promise for highly beneficial flexible or stretchable microelectronics. Carbon nanotubes molecular scale wires have high mechanical strength and stiffness [103-108].

The seamless cylindrical single walled carbon nanotubes (SWNTs) are obtained when the graphene sheet is rolled along the vector $C_h = na_1 + ma_2$, where graphene with hexagonal crystal lattice having a_1 and a_2 as basis vector. Two structural parameters, such as diameter and chirality of the nanotubes were defined by the indices (n,m). Theoretically, the carbon nanotubes can depict different electrical characteristics depending on the indices (n,m) such that when the difference of indices (n-m) equals to the multiples of 3 than the characteristics shown is metallic and for all the other values it is semiconducting. Further, for the semiconducting nanotube the band gap is inversely proportional to its diameter [109].

For the molecular electronic devices, the SWNTs is an ideal candidate because of its unique structure property-e.g., semiconducting SWNTs plays as a channel material for field effect

transistor (FET) while the metallic nanotubes act as interconnects [110-112]. In addition, various researchers have already revealed that as compared with conventional materials, the SWNTs exhibit very exciting electronic properties. In case of metallic SWNTs, the current carrying capacity can reach up to 10^9 A cm^{-2} which is much better than the best conducting metals such as copper and aluminium. Also, semiconducting SWNTs exhibits field effect mobility up to 10^4 cm^2 V^{-1} s^{-1} which is much more as compared with silicon [113-117].

Numerous flexible substrates which are often selected for sensing applications are of polymers like poly (dimethyl siloxane) (PDMS), [118-120] polyetheretherketone, Polycarbonate, polyethersulfone (PES),[121] Polyethylene naphthalate (PEN),[122-123] polyimide (PI) and also of polyester resins such as polyethylene terephthalate (PET) [124-125]. Materials such as nylon rope [126] and paper are also used as substrate for sensing applications. The various essential characteristics of a material to be suitable for practical sensing applications are chemical resistance, flexibility, transparency and thermal resistance [127]. The critical functioning of an electronic device depends on the conducting material which allows the communication among the various components of electronic devices. The core materials for sensing application can be nanowires, nanoparticles, nanotube or thin films [128].

The interactions between CNTs and polymers having large molecules with functional groups can be electrostatics or covalent, hydrogen bonding or π-stacking. This chemical interaction of polymers and CNTs leads to the formation of strong components coupling. Consequently, modifying the surface of the CNTs tube and inter-tube interactions. This strong coupling has been reported in CNTs-conducting polymer interactions. Conducting polymers are organic polymers with conjugated π-system and repeating monomer units. The charge transfer largely depends on the level of doping concentration. The typical examples are polyphenylene vinylene (PPV), polyacetylene and polyaniline [129]. Alternatively, the interaction between CNTs and polymers can be a weak van der waal force of attraction. The decoration of CNTs with polymers brings about entropic interactions among the layers of polymers.

In this chapter, I analyze the latest developments in the area of flexible and stretchable electronics with carbon nanotubes as channel material for various sensors. Our aim is to emphasize on numerous types of available flexible sensors based on carbon nanotubes. Instead of compiling all consistent earlier work, this paper is focused on significant work that may offer essential future

trends of carbon nanotubes based flexible sensors. The analysis presented here is expected to promote a more persuasive transaction of ideas and more profound interest in this developing field. The choice of materials and the fabrication of devices are also covered. I also present the comprehensive summary of engineering technologies with a priority on fabrication of flexible sensors. This chapter is formulated as: "flexible electronics application based on carbon nanotube network," in this section I examine the progress made in the field of flexible or stretchable sensors based on carbon nanotubes. In the conclusion section, I have concluded with the present-day leftover question and future potential in the field of flexible electronics.

According to a 2018 report of the World Health Organization (WHO), air pollution is one of the major environmental risks to health. Diseases like stroke and cancer are killing millions of people every year owing to inhalation of microscopic pollutants present in the air, which can easily penetrate into the circulatory and respiratory systems, damaging heart, brain, and lungs. According to this report, the majority of the world's population is living in places where WHO air quality guidelines are not met [130]. The major contributors to deteriorating air are nitrogen oxides (NO_x) such as nitrogen dioxide (NO_2) and nitrogen oxide (NO) [131]. Anthropogenic activities, especially combustion practices are responsible for the presence of the most prevalent and toxic form of NO_x gases, i.e., NO_2 in the atmosphere. Excessive exposure to NO_2 has adverse effects on both human and wildlife. The trace amount detection of NO_2 in the medical field is highly desirable because of its ability to give fingerprints for chronic obstructive pulmonary disease (COPD). The indoor threshold limit value (TLV) for NO_2 as stated by occupational safety and health administration is 5 ppm. Besides, the long term (LTEV) and short-term exposure (STEV) values for NO_2 are 3 and 5 ppm, respectively, as stated by ACGIH (American Conference of Governmental Industrial Hygienists is also known as Association Advancing Occupational and Environmental Health) [132]. In the modern world, with the abrupt rise of industry and rapid increments in the number of automobiles, NO_2 has become a major contributor to pollution. NO_2 is also responsible for the formation of acid rain and ozone-depleting substances emitted through human activities [133-136]. And it raises the demands for NO_2 detectors.

Over the past decades, extensive work has been done on metal oxide-based NO_2 gas sensors. The presence of active sites on the surface of metal oxides is responsible for their gas sensing properties. Thus, the gas sensing mechanism mainly depends on the amount of

crystallinity, particle size and the number of defects present in metal oxide nanostructures. Different nanostructures of metal oxides such as nanorods, nanoparticles and nanoflowers, have been used in NO_2 gas sensor fabrication because of their inherent properties like low cost, high chemical and thermal stabilities, nontoxicity and high chemical sensitivities which are attributed to the presence of high-density free charge carriers [137]. The low surface area of bulk silicon makes it's unsuitable for sensing applications. However, metal-assisted chemical etching method is used for obtaining porous silicon which shows fast response and selectivity towards NO_2 [138].

The mechanism of resistive NO_2 gas sensing based on metal oxides and TMDs is as follows: an electronic device whose electrical resistance is a function of ambient gas concentration is generally used as a resistive gas sensor. The detection of various ambient gases with variations of their concentration is particularly achieved by resistive gas sensors. The main part of the sensor is an active layer. The active layer can be made up of various materials which could be organic, inorganic or a hybrid combination of the two. The function of transducers is to convert variations in chemical interactions (i.e., electrostatic interactions, the formation of H-bonds, etc.) to a measurable signal (electrical, optical, etc.) or physical property (i.e., conductivity, refractive index, etc.) corresponding to gas concentration [139-142]. Several mechanisms are involved in a gas sensor operation such as sensing and transduction (optical, electrochemical, capacitive, resistive, etc.). However, the main disadvantage of the resistive gas sensors includes limited sensitivity and poor or no selectivity. Various strategies have been employed to overcome these shortcomings, e.g., formation of porous sensing layers, varying the operating temperature of the sensor, etc. [143].

In the beginning, the fascinating properties of graphene and its derivatives attracted researchers to develop NO_2 detector based on them, but the absence of an electronic bandgap in graphene has forced researchers to find some alternative elements such as 2D materials with semiconducting properties. In this process, transition metals di-chalcogenides (TMDs) being semiconducting in nature and an MX_2 structure, where ‘M’ stands for transition metal atoms (such as W, Mo, Ti, Ta) and ‘X’ stands for a chalcogen atom (such as S, Se, Te). The robustness of MoS_2 makes it the most studied TMD material. The use of TMD materials in fields such as flexible electronics, optoelectronics, high-end electronics, energy harvesting, personalized medicine, spintronic and DNA sequencing have been possible due to their strong spin-orbit coupling, a

unique combination of atomic-scale thickness, favourable electronic and mechanical properties and direct bandgap structure [144-150].

With progress in nanotechnology over the years, significant progress has been made in sensing technology with conducting polymers, carbon nanotubes and 2D materials and oxide nanostructures. Nowadays, in materials engineering, the use of transition metals di-chalcogenides (TMDs) and metal oxides has become the most impressive way for improving the performance of solid-state materials-based gas sensors. The use of metal oxides and TMDs is known to improve the selectivity, sensitivity, response and repeatability, of gas sensors [151-153]. Many solid-state gas sensors have been developed for detecting different toxic gases. Among these transition metals di-chalcogenides (TMDs) and metal oxides based chemiresistive gas sensors are quite promising. These sensors have low response time, high sensitivity, selectivity, cost-effective and great suitability for the design of movable apparatus. These unique properties make the sensor more suitable for advanced applications like an artificial nose, portable instruments and alarm systems [154-155].

Several strategies have been employed to enhance the performance of metal oxide-based sensors such as (1) one dimensional metal oxide nanostructures show improved thermal stability; (2) surface modification of noble metals is known to improve the response-recovery kinetics and sensitivity of the overall device; and (3) the morphology of deposit films and catalytic reactivity can be modified by doping the metal oxides with transition metals [156-159]. In recent years, nanostructured metal oxides have attracted huge attention to their application in NO_2 gas sensors [160-165].

The mechanism behind enhancement in sensor response can be attributed to the modulation behaviour of p-n junction as well as the contact resistances. The total variation in sensor resistance during molecule desorption/adsorption processes could be ascribed to occupation modulation of sorption sites and periodic tailoring of p-n junctions. For example, when n-type MoS_2 is exposed to air, the surface adsorbed oxygen will capture electrons from the conduction band to generate oxygen anions (O_2^-), resulting in the formation of an electron shell depletion region (EDR) on the surface. Hence, this procedure leads to an n-type semiconducting core region as low resistance and EDR as high resistance regions. In the case of p-type semiconductors, the adsorbed oxygen anions from the hole accumulation region (HAR) as a low resistance region near the material surface

because of the electrostatic interaction between oppositely charged species. Prior to NO_2 gas exposure, p-n junction results in an extension of charge depletion layer by recombination of electrons and holes. Considering that molecular NO_2 adsorption proceeds in the form of NO_2^- via continuous electron withdrawal from rGO or MoS_2, both HAR and EDR would be extended, accompanying a negative and positive impact on the resistance increase, respectively. However, upon exposure to NO_2 gas, the effect of HAR on total resistance change dominates over EDR, thereby leading to a net decrease of overall resistance [166-167]. This effect can be ascribed to more reluctance in MoS_2 to its resistance change than rGO.

The advancements in the material engineering for achieving the optimum performance or even possibly achieve new function for feasible utilization involve hybridization of two or more materials, which is the most interesting progress to vanquish the flaws of a particular material [168-169]. The recent success to use scalable techniques and solution precessing for preparing 2D TMDs nanosheets has created a great opportunity for developing functional composite nanostructures by exploiting them as building blocks [170]. In the last ten years, most of the studies have focused on the construction of functional composites of reduced graphene oxide (rGO) and graphene oxide (GO) for various applications. Success in the development of graphene-based nanostructures has inspired many researchers to explore various ways of incorporating ultrathin layers of TMDs in different materials [171-176]. Generally, the research based on TMDs is concentrated on: (1) the assembly or synthesis of TMD sheets of hierarchical nanostructures, (2) layered composites of TMD nanostructures, (3) developing in-plane doped or 2D alloyed heterostructures.

In the last decade, NO_2 sensor development has been reviewed by numerous researchers based on a diverse range of materials, i.e., metal oxide nanoparticles, 2D materials like MoS_2, carbon nanotubes [177-182], nanowires [183-184], polymers [185-186], and so on. The progress of the NO_2 gas sensor can be analyzed by the number of scientific publications in the last decade as shown in Figure 4.2. In this chapter, our aspiration is to provide a summary and comprehensive study of the promptly rising research direction and broad perspective of the crucial challenges, prospects and knowledge in this encouraging area of NO_2 gas sensors. The gas sensors on NO_2 have been developed based on many materials and hybrid structures, but here our focus will be on NO_2 gas sensors on 2D TMDs and metal oxide-based nanostructures. The progress in various

characteristics such as structure, method of preparation, concentration, sensitivity, operating temperature and recovery and response time for NO_2 gas sensors based on 2D-TMDs and hybrid structure is summarized in Table 4.2. Table 4.3 shows a comparison of various sensor parameters for NO_2 gas sensors developed from metal oxides and their composites.

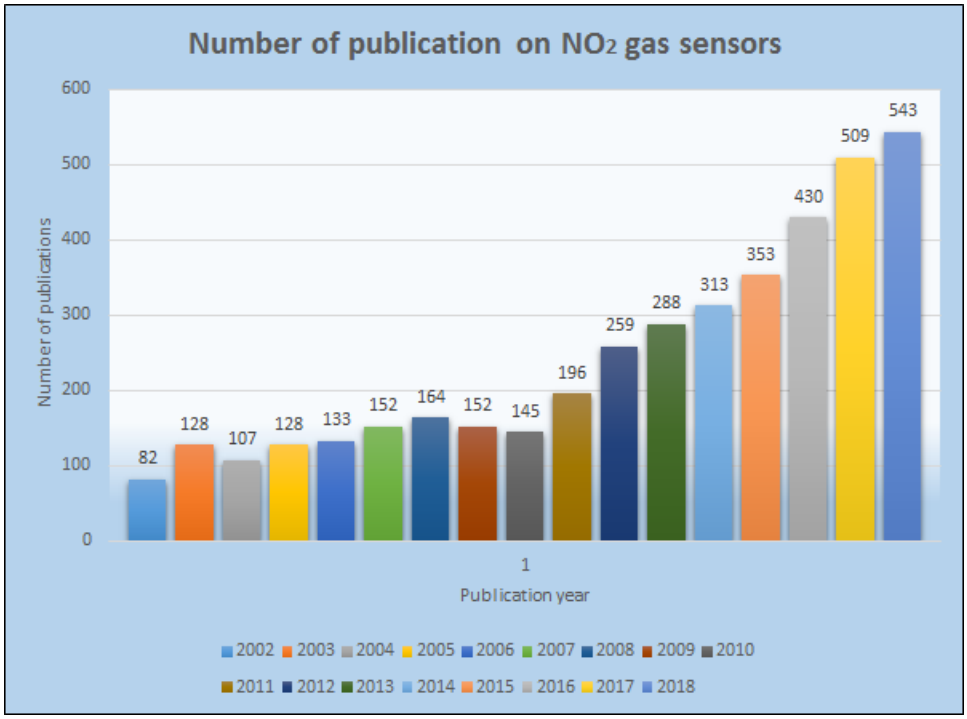

Figure 4. 2: The number of publications on NO_2 gas sensors from 2002 to 2018 (internet search of the web of science on 1st January 2019). Keywords for search: NO_2 gas sensor.

Table 4. 2: NO_2 gas sensors based on 2D transition metal di-chalcogenides (TMDs).

Sl. no	Method of preparation	Structure	Materials	Concentration	Response time/Recovery time	Response	Operating temperature (°C)	References
1.	Hydrothermal	3D flower	MoS_2	50 ppm	–/–	78%	150	[144]

2.	Aerogel conductometric	Composite	WS_2/GA	2 ppm	100 s/300 s	3%	180	[145]
3.	Hydrothermal-CTAB	3D flower	MoS_2	50 ppm	−/−	60%	100	[146]
4.	Sulphurisation	Vertically aligned	MoS_2/ZnO NWs	50 ppm	5 min/-	31.2%	200	[148]
5.	Hydrothermal	Nanosheets	WS_2	0.1 ppm	−/−	9.3%	RT	[187]
6.	Wet chemical	Hybrid	MoS_2-RGO	3 ppm	8 s/20 s	1.23	160	[188]
7.	Hydrothermal	Hollow	MoS_2	100 ppm	79 s/225 s	40.3%	150	[189]
8.	Two-step CVD	Bilayer	MoS_2	1 ppm	11.3/5.3 min	2.6%	RT	[190]
9.	Solvothermal	Nanocomposite	RGO-MoS_2-CdS	0.2 ppm	25 s/34 s	27.4%	75	[191]
10.	CVD	Monolayer	MoS_2	400 ppb	16 s/65 s	670%	RT (625 nm, 4 mW/cm^2	[192]
11.	CVD	Nanowires	MoS_2	5 ppm	16 s/172 s	18.1%	60	[193]
12.	Redox reaction	Nanoparticle	MoS_2–Au	2.5 ppm	4/14 min	30%	RT	[194]
13.	Annealing	Nanocomposite	NiO/WO_3	30 ppm	2.5 s/1.1 s	4.8	RT	[195]

14.	Electrospinning	Nanofiber	WS_2@MTCNFs	1 ppm	3.73 min/-	15%	RT	[196]
15.	Chemical etching + CVD	Nanosheet	MoS_2/PSi NWs	50 ppm	−/−	28.4%	RT	[197]
16.	Wet chemical	Nanostructure	MoS_2/ZnO	5 ppm	40 s/1000 s	3050 %	RT	[198]
17.	Nucleation controlled	Microflowers	MoS_2–MoO_3	10 ppm	~19 s/~182 s	33.6%	RT	[199]
18.	CVD	flakes	VA-MoS_2	50 ppm	−/−	48.32 %	100	[200]

Table 4. 3: NO_2 gas sensors based on Metal-oxide based nanostructures.

Sl.no	**Method of preparation**	**Structure**	**Materials**	**Concent-ration**	**Response time/Recovery time**	**Response**	**Operating temperature (°C)**	**Ref.**
1.	Facile solvothermal	Microspheres	ZnO/SnO_2	100 ppm	~33 s/~7 s	258	200	[160]
2.	Spray deposition	Heterojunction	ZnO/m-SWCNT	10 ppm	74 s/-		RT	[201]
3.	Surface etching	Microwire (MW)	ZnO	10-50 ppm	221 s/118 s	~411%	-	[162]
4.	Facile two-step synthesis	Actinomorphic flower	$ZnO/ZnFe_2O_4$	0.1 ppm	7 s/15 s	250	200	[163]
5.	Hydrothermal	Silk Fibroin(SF)	ZnO/SF	20 ppm	26 s/16 s	85	RT	[164]
6.	Drop casting	Heterostructures	Silicon/ZnO	200 ppb	50 s/-	35%	25	[165]
7.	Modified polymer-	Heterostructures	ZnO-Ag	0.5-5 ppm	~250 s/~200 s	1.545 ppm^{-1}	RT (470 nm/75 mW/cm^2)	[202]

	network gel method							
8.	Thermal reduction	Nanosheets	ZnO/rGO	50 ppm	25 s/15 s	9.61	RT	[203]
9.	Facile Hydrothermal	Nanowire	ZnO	1-30 ppm	25 s/21 s	3.3	250	[204]
10.	Facile three-step process	Nanowire	ZnO-CuO	10 ppm	~400 s/~300 s	48.4	350	[205]
11.	Thermal evaporation	Heterostructure	ZnO/CuO	100 ppm	14 s/197 s	175%	150	[206]
12.	Sol-gel spin coating	Thin film	ZnO	100 ppm	3 s/137 s	12.3	200	[207]
13.	Thermal evaporation	Nanorods	ZnO	100 ppm	35 s/206 s	622	200	[183]

14.	Thermal evaporation	Nanowires	ZnO	100 ppm	17 s/290 s	101	200	[183]
15.	Facile Two-step Hydrothermal	Hierarchical nanostructures	SnO_2@ZnO	5 ppb	60 s/45 s	0.2	150	[184]
16.	Electrospinning	Nanowebs	SnO_2-NiO	1,5,10 ppm	330,173,163 s/ 261,301,204 s	10.5,22.8, 36	300	[208]
17.	Oil bath precipitation	Brick-like	In_2O_3	500 ppb	114 s/49 s	402	50	[209]
18.	Precipitation-calcination	Mesoporous sheets	ZnO	1 ppm	3/2.5 min	130%	RT	[210]
19.	Hydrothermal	Nanowires	Pd-ZnO	1 ppm	141 s/177 s	13.5	100	[157]
20.	Thermal reduction	Nanowalls	ZnO/rGO	50 ppm	-37 s/2 s	35.31	RT(365 nm/1.2mW/cm^2	[211]
21.	Thermal annealing	Film	ZnO/rGO	100 ppm	6.2/15.5 min	47.4%	RT	[212]
22.	Sol-gel spin coating	Thin film	Al:ZnO	100 ppm	8 s/121 s	18.5	200	[213]

23.	Hydrothermal	Nanowire	Au-ZnO	1 ppm	29 s/18 s	31.4	150	[383]
24.	Sol-gel	Thin film	G-ZnO	5 ppm	150 s/315 s	894%	150	[214]
25.	OFET	Nanostructure	P3HT-ZnO@GO	1,5 ppm	-/-	32,210%	RT	[215]
26.	Microwave assisted hydrothermal	Hollow spheres	ZnO-BP	1 ppb	2 s/16 s	130.7%	RT	[216]
27.	Brush coating	Nanoparticles	ZnO	234 ppm	2 s/20 s	275%	280	[217]
28.	Thermal evaporation and sol-gel	Nanorods	Pd/ZnO-SnO_2	5 ppm	17.74 s/60 s	5.52	300	[218]
29.	Wet chemical and refluxing	Nanochains	CuO-ZnO/rGO	40 ppm	40 s/-	62.9%	RT	[219]
30.	Soft chemical synthetic	Flower shaped thin film	ZnO	10 ppm	65 s/54 s	55	200	[161]

4.2 Procedure for developing sensors

4.2.1 Growth of CNTs

There are three main principles for the growth of high-quality carbon nanotubes: CVD, laser ablation and electric arc discharge. Laser ablation and Arc discharge are essentially the modified version of Physical Vapor deposition (PVD) technique which comprises condensation of hot gaseous, carbon atoms usually achieved by heating solid carbon. However, arc discharge and laser ablation methods are not suitable for laboratory research because of the complex instrument requirement and a large amount of power consumption. In addition, this process takes place at very high-temperatures so the final product is accompanied with amorphous carbon impurities and catalysts [220-222]. Due to high operating temperatures of these two methods of CNTs growth, the process is difficult to control, thus MWNTs are obtained as a network of misaligned nanotubes. Also, by laser ablation and arc discharge techniques, I cannot deposit CNTs on a substrate, which is essential requirement for making any device based on CNTs. For utilizing CNTs deposited by arc discharge or laser ablation technique, I require several post CNTs deposit steps such as purification and deposition of CNTs on substrate, which increases the cost of device fabrication. Such kind of post treatment and steps are not required in case of CVD technique, that's why CVD

method has become most crucial commercial method for growing CNTs [223-224]. CVD is a deposition process of growing solid from gases or variety of gases using a heterogeneous reaction. Depending on the deposition conditions, this reaction begins at the gas-solid substrate and the growth technique can be controlled by the contained by diffusion and surface kinematics. In order to fabricate a thin layer of metals, semiconductors or insulators on a different substrate, CVD is a preferred technique. This process can be easily calibrated up to industrial production which can't be achieved by laser ablation and arc discharge method. For large turnout, and relatively pure growth of CNTs at a moderate temperature. Stable nature of the reaction basically convoluted in CVD, which offers better growth control. In addition, through a careful designing of catalysts pattern on the substrate, it is easier to regulate the size, shape and calibration of nanotubes. CVD is an irreversible deposition system in which hydrocarbons such as CH_4, C_2H_2, benzene, CO, ethanol or ethylene are used as a source of carbon and as precursor gases flow into the cell [225-226]. These hydrocarbon gases are decomposed into reactive species at a temperature around 500-1000 °C depending on the required thickness of carbon nanotubes to be grown. CNTs formation takes place when the receptive species react in the existence of transition metal catalysts like Co, Ni, and Fe. In addition to these catalysts, other metal catalysts which have been used are: Ta, W, Re, Hf, Mn, Sc, V, Ti, Cr, Mo, Nb, Y, Zr, etc. Green plant extract has been used as catalyst for the synthesis of carbon nanotubes [227]. Besides, a combination of these metals can also be used as a catalyst to grow CNTs [228-229].

There are two different modes of CNTs growth as reported by Nessim, such as "growth then place" and "growth in place". The advantages of growth in place i.e CVD technique over the laser ablation and arc discharge includes the growth of vertically aligned CNTs (VACNT), better physical interaction with the substrate, control and tuning of CNT position on catalyst dots and rapid growth. There are many advantages of CVD method over the Laser Ablation and Arc discharge methods; (1) the reactor design and reaction process are simple and also control and manipulation of reaction process is simple. (2) The availability of raw material in the form of gases are abundant. (3) In terms of unit price, the CVD process is cheap as it requires less operating temperature and also not difficult to produce targets. (4) This process is unique for producing vertically aligned carbon nanotubes and other two processes are incapable of producing aligned carbon nanotubes. (5) The nature of operation is similar to chemical unit operations that's why the process can be designed for continuous operation and easily scaled up to large industrial

production. (6) The CVD ease out the further process of further collection and separation and also eliminate the post refining process to at large extent because this process is capable of producing CNTs directly on the substrates. In some cases, refining is required for further purification [230]. Compared with other two methods to grow CNTs; CVD requires the relatively lower temperature to grow CNTs, therefore this method is suitable for scaling up the growth of SWNTs. Quality of SWNTs can be improved by optimizing the catalysts. The CVD synthesis process can be discussed into two groups: surface synthesis and bulk synthesis on flat substrates. The superiority of surface synthesis process is that the eventual outcome is cleaner than the one developed by bulk synthesis. Additionally, the most important advantage of surface synthesis which makes it more relevant for device fabrication is that it provides better alignment of carbon nanotubes and control over the diameter [231-232].

4.2.2 **Purification of CNTs**

As I mentioned above, in arc discharge and laser ablation technique, the growth of CNTs is accompanied with a number of undesired materials which can have deteriorating impacts on the fundamental properties of CNTs. The CNTs, produced from arc discharge and laser ablation methods, for sensor application require an additional step of obtaining high-quality CNTs, which is necessary for making CNT-based devices more reliable. Purification mechanism for as grown CNTs is very complex [233-234]. Carbonaceous contamination and metallic impurities are the most commonly found impurities. A byproduct of the reaction process is carbonaceous impurities while the metallic impurities are the leftover catalysts.

Chemical oxidation is the first step of purification to remove the carbonaceous impurities. Acids which are frequently used in this process are nitric and hydrochloric acids. Additional steps which are involved in the purification are decanting, centrifugation or filtration, succeeded by cleaning in deionized water [235-236]. For removing the metallic impurities the sample is heated up to the vaporization temperature of contaminant such that the impurities are evaporated. For deeper refinement of gas or vapor, oxidation is useful. Finally, in order to reduce the agglomeration of nanotubes, the nanotubes are gently treated in an ultrasonic bath. Comprehensive purification and higher CNTs yield are obtained by frequently combining the above approaches.

The process for separating carbonaceous impurities out of the surface of carbon nanotubes (CNTs) includes the following steps: (1) a specimen consisting of CNTs, in which at least a component of the exterior surfaces of said nanotubes are partly or entirely covered with carbonaceous impurities, and also the structure of carbonaceous coatings is unlike from that of CNTs. (2) In the next step an intercalant is added to the sample, in which the said intercalant inserts into interstitial sites between CNTs and carbonaceous coatings, thereby generating intercalated carbon layers; and (3) An exfoliation initiator is added to the sample which reacts with intercalant in said intercalated carbon layers, the reaction between intercalant present between carbon nanotubes and carbonaceous coating and exfoliation initiator exfoliates carbonaceous coating, thereby removing carbonaceous coatings from the outer surfaces of CNTs.

Mostly purification methods are based on "wet-chemical" treatment as this method allows large scale processing [237]. However, this method leads to a lot of defects in the nanotubes because of the involvement of strong acids. Therefore, procedures such as filtering and drying after the chemical etching substantially lower the quality of carbon nanotubes. Another simple way of purification of carbon nanostructured materials is "dry" oxidation at a high temperature in the presence of air. Most important use of this process is to remove the metal catalysts present by wet oxidation. The metal molecules cause the low-temperature deterioration of the CNT in the presence of oxygen, which decreases yield dramatically.

4.2.3 **Development of CNTs-based gas sensors**

Generally, there are three different techniques applied to fabricate CNTs based gas sensor devices. (1) Casting technique, (2) Di-electrophoresis (DEP), (3) Screen printing. In case of casting technique, Resistive gas sensors were developed by Li et al. [238] by directly casting SWNTs on interdigitated electrodes (IDEs). Photolithography is used to fabricate electrodes by evaporation of Ti and Au on silicon electrodes. Before integrating SWNTs into IDEs, the as grown SWNTs were first purified with acids and then by air erosion. As a result, the impact of impurities on sensors characteristics was minimized because of the relative purity (up to 99.6%) of SWNTs. Dimethylformamide (DMF) is used as a dispersion medium for purified nanotubes and after that drop-deposited on the electrode range. The subsequent evaporation of DMF leads to the formation of nanotubes network.

In case of screen printing, CNTs composition is blended with organic binders (Ethyl Cellulose, Terpineol) and on electrodes coated tube the glass frits are printed. Annealing is done under N_2 atmosphere in order to remove the organic binders. This technique was first used by Lee et al. for developing a gas sensor based on MWNTs for detecting NO_2 gas [8].

Dielectrophoresis (DEP) method is another technique to produce CNTs based devices. In this technique, a force is applied on non-conducting substance. Under the influence of non-uniform electric field and also, this force does not need the particle to be charged. All particles display dielectrophoretic exertion in the presence of electric field. However, the vitality of force bank on many things such as on particles shape, particle size, particles electrical properties further on the frequency of the electric field. DEP can also be used to influence the CNTs for separation, orientation, and positioning of CNTs. Consequently, the field of a peculiar frequency can be used to manipulate molecules with considerable selectivity. Moreover, an adjustment in DEP force as an operation of frequency can be used to study electrical properties of the particles. It has been demonstrated by Suehiro et al. [239] described that the DEP fabrication method can provide a good electrical network between electrodes and CNTs. Spray deposition technique and transfer printing were used by Ahmed Abdelhalim for developing carbon nanotubes thin film on elastic substrates [240]. Spray coating is the best choice when the demands are low cost and large scalability because it is a simple and rapid method to deposit carbon nanotube layers. In comparison with the spin coating and dip coating approaches, the spray deposition does not compromise with the efficient uses of the material nor with the surface roughness [241-242]. In spite of all these efficiencies of spray deposition techniques, they lack certain features which are very critical for large scale production of films. In the spray deposition process colloidal suspension is consistently distributed over the substrate and dispersing liquid is vaporized by heating, thus leaving the colloidal deposit to form the patina. In the case of pattern transfer, the carbon nanotube films are relocated from the glass to the PDMS and it is accomplished by jutting delicately the PDMs layer to the glass where CNTs are deposited, while ensuring that no bubbles appear on the surface. The PDMS layer with the relocated CNTs layer is placed on the plastic substrate and finally heated. Temperature is very important factor in relocating the CNT from PDMs to the plastic substrate [243-245].

4.3 Various types of CNT-based gas sensors

Types of detection gases

4.3.1 Oxidizing gases

An innovative gas sensor established on thin film carbon nanotubes with enhanced sub ppm sensitivity, selectivity and stability at rationally low temperature was successfully developed and tested by [246]. In this regard, carbon nanotubes narrow films were developed by rf PECVD. Carbon nanotubes were grown by depositing 5 nm thick Ni as a catalyst on Si3N4/Si substrate. The electrical resistance was measured using Keithley 2001 multimeter as a function of the operating temperatures, using three distinct thermal analyses. Figure 4.3 (a) displays that if the heating and cooling thermal period is maintained in the temperature range of 25–250 °C, then the sensor response is constantly varying (AA' and CC') but when the temperature increases more than 250 °C then uniform microstructural dislocation of the structure takes place. It happens because of the transition of the material from metal to semiconductor. This hypothesis is based on empirical testimony. Figure 4.3 (b) displays the dynamic response of gas sensor at operating temperature 165 °C at a concentration of NO_2 lies in the range 10 to 100 ppb. It is evident from the figure that the sensor is receptive to NO_2 concentration as low as 10 ppb. When the concentration of NO_2 is decreased or increased gradually in this spectrum, the sensor feedback is reproducible and steady. It was also concluded that the narrow film grown by r.f PECVD demonstrates that the CNTs are important material for detecting toxic/harmful gases such as NO_2 with detection limit as low as 10 ppb. By choosing appropriate thermal analysis protocols the sensitivity of NO_2 thin film can be improved.

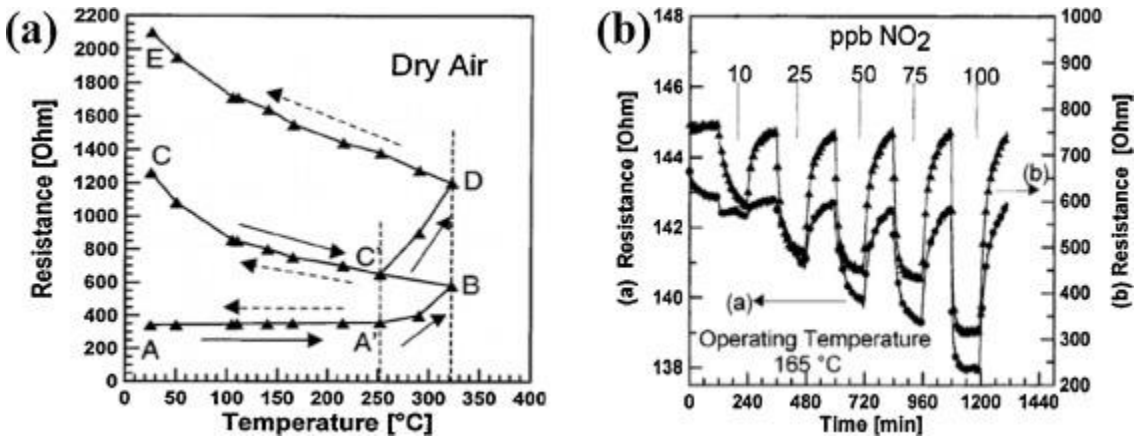

Figure 4. 3: Fig. 1. (a) Change of the CNTs' film resistance as an objective of temperature; (b) resistance change at different concentrations of NO_2. Copyright permission from [246].

Xian Li et al. developed an innovative NO_2 resistive room temperature (RT) gas sensor utilizing metallic single-walled carbon nanotubes (m-SWCNT) as electrodes and ZnO wire as sensing material. There are many studies showing that (ZnO) zinc oxide nanostructures are exemplary material which acapable of detecting NO_2 [247]. Interestingly, it was found that ZnO wire gave n-type response that on Au/Ti electrodes while on m-SWNTs electrode gave p-type of response to NO_2 gas molecules. It was fond that the ZnO/Au device depicts less response to NO_2 gas in comparison to ZnO/m-SWNTs device. SWNTs electrodes were fabricated on the substrate by employing airbrush by spray deposition technique. Annealing at 300 °C was done for the better interface contact of the substrate Si/SiO_2. Applying the same spray deposition technique ZnO was accumulated on the m-SWNTs electrode to obtain ZnO/m-SWNTs sensing device. The standard photolithography process of fabrication was used to obtain Au/Ti interdigitated electrode for ZnO/Au gas sensor. Figure 4.4 Shows the NO_2 sensing response for the ZnO/m-SWNTs device. (a) The real time resistance shift for the different concentrations of NO_2 and (b) sensing response (excellent repeatability for 3 cycles of 2.5 ppm NO_2). Figure 4.5 Shows the NO_2 sensing response for the device ZnO/Au. (a) Shows the real time resistance shift for the various concentrations of NO_2. (b) Sensing response (excellent repeatability for 3 cycles of 2.5 ppm NO_2). In case of ZnO/Au device, the interface barrier is high so I can ignore the Relectrode and Rmaterials on the other hand in case of ZnO/m-SWNTs interface because of low work function the junction schottky barrier is weaker than that of ZnO/Au and even disappeared. In Spite of all these the resistance of m-SWNTs is high and makes a significant addition in the overall resistance, which cannot be neglected. That's why m-SWNTs plays a crucial role in NO_2 sensing. After analyzing the response of the two devices

I can conclude that the ZnO/m-SWNTs device has faster response to NO_2 gas as compared with a traditional ZnO/Au device. The traditional sensing device ZnO/Au has reverse sensing response and may be associated with diverse schottky barrier features at ZnO/m-SWNTs interface.

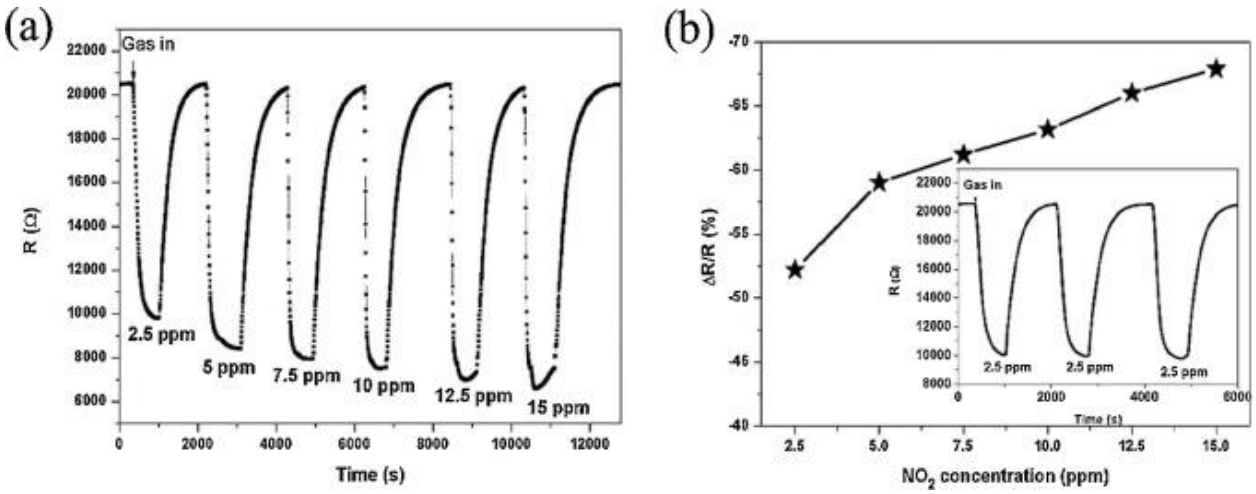

Figure 4. 4: ZnO/m-SWNTs device sensing properties for NO_2 (a) real time resistance response under the different concentration of NO_2 and (b) sensing response (inserted repeatability response for 2.5 ppm NO_2). Copyright permission from [247].

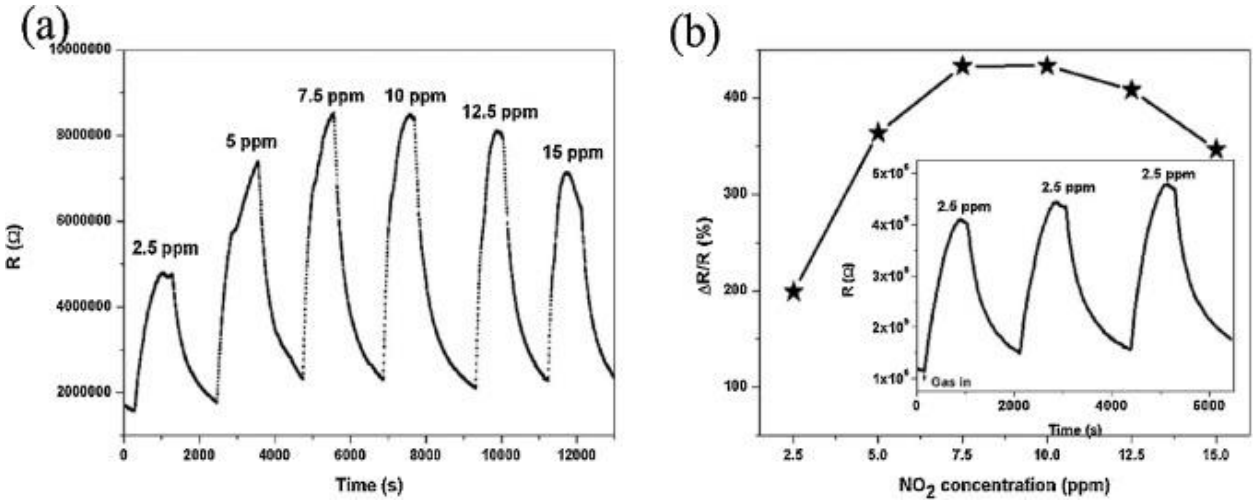

Figure 4. 5: NO_2 sensing properties for ZnO nanowire on Au/Ti electrodes (a) for the different concentrations of NO_2 the real time resistance change (b) sensing response (inserted repeatability response for 2.5 ppm NO_2). Copyright permission from [247].

In 2017, Choi et al. demonstrated a NO_2 sensor based on SWCNTs which are highly selective and sensitive [248]. Sputtering and thermal treatment were used to decorate Pt nanoparticles (NPs) on the SWNTs under atmosphere. The dependence of operating temperature on the sensing capability of SWNTs were studied using NO_2 as representative oxidizing gas. The

complete schematic process of the development of the Pt-NPs decorated SWNTs sensor is depicted in the Figure 4.6 As shown below. Sputtering technique was used of decorating 10 nm thick Pt-NPs on the surface of SWNTs under Ar ambient atmosphere. The Pt-NPs decoration of SWNTs sensor enhanced the sensitivity and selectivity. It was found that in comparison to pure SWNTs sensor, the Pt-NPs decorated SWNTs sensor response was ~5 fold higher for 2 ppm NO_2 gas. In addition, for 2 ppm NO_2 gas the PT-NPs decorated SWNTs sensor shown ~63% response at 100 °C. The increase in the NO_2 sensing mechanism at higher temperature is mainly attributed due to the special catalytic role played by the Pt-NPs and there is modulation in the SWNs conduction channel due to the presence of Pt-NPs which also plays an integral role in sensing mechanism.

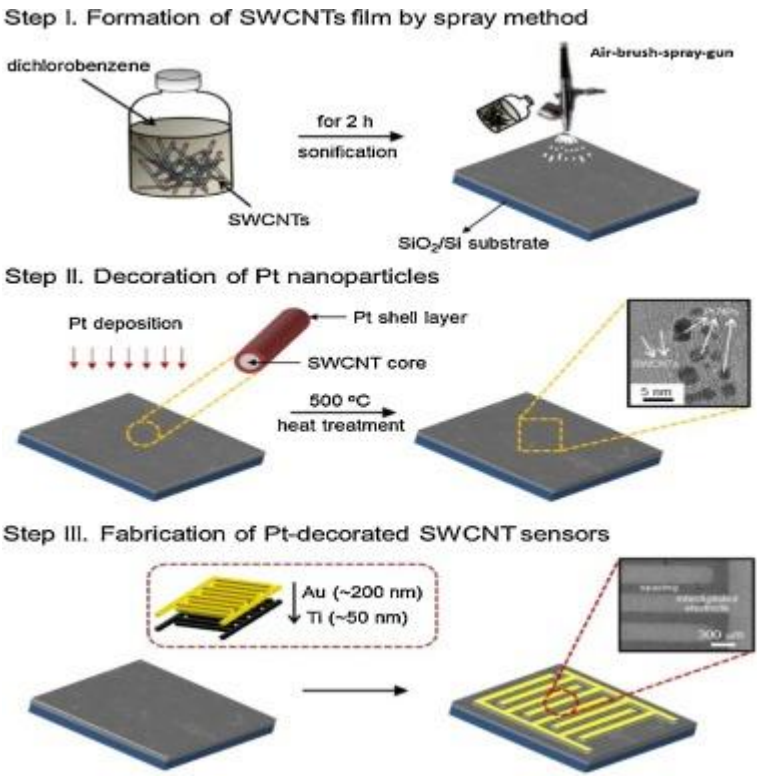

Figure 4. 6: Schematic diagram of the different steps involved in the fabrication of Pt-NPs decorated SWNTs sensor. Copyright permission from [248].

Kwon et al. developed a NO_2 sensor based on MWCNTs decorated with ZnO [249]. It was prepared by using thermal evaporation of ZnO powder in the presence of MWCNTs. The complete measures for the readying of ZnO decorated MWCNTs is depicted in Figure 4.7. Various gas sensing properties such as cross sensitivity, response and response recovery time of the ZnO/MWCNTs composites were studied and compared with the bare MWCNTs sensors. It was

demonstrated that ZnO decoration on the MWCNTs surface has resulted in the increase in the NO_2 detection capacity of the MWNTs based sensor. The presence of ZnO particles on the MWCNTs surface was established by structural analysis such as XRD and TEM also confirms the ZnO decoration on MWCNT surface. The ZnO decorated MWCNTs sensor showed better sensitivity of NO_2 gas compared to bare MWCNTs sensors. Moreover, a stable response was found for different reducing gases such as ethanol, H2S, acetone, CO and H2 by the ZnO decorated MWCNTs sensors. Some mechanisms which leads to the increase in the sensitivity of ZnO decorated MWNTs gas sensor is notable change in the hole collection layer of MWCNTs.

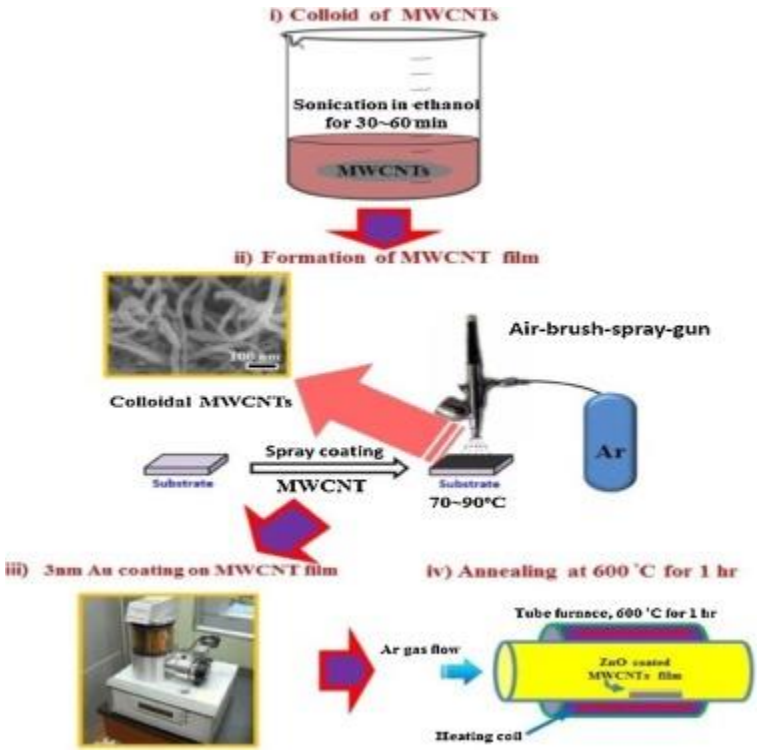

Figure 4. 7: Schematic description of development of ZnO-decorated MWNTs sensor. Copyright permission from [249].

Sharma et al. developed SnO_2 modified carbon nanotubes-based gas sensors for trace level NO_2 detection [250]. The chemical bath deposition (CBD) techniques were utilized to develop the composite films of SnO_2 nanoparticles. The mixing of various molarities (2 mg, 5 mg, 7 mg, and 10 mg) of functionalized MWNTs with the processed tin alloy dilution helped in the formation of

MWNTs-modified SnO_2 thin films. Glass substrate was used for the growth of hybrid thin films of MWNTs-SnO_2 nanoparticles by spin coating. The film used had the thickness of ~600 nm. Thermal treatment was performed at 150 °C for 5 min after each coating to vaporize the organic precursors. Eventually, for obtaining the appropriate crystallinity in the desired thicker film, the sample was heated at 300 °C for 1 h. A simplified sensor network, with dimensions, is demonstrated in Figure 4.8. The sensors were labelled as pure SnO_2, pure MWNTs, MWNTs-SnO_2 (2 mg), MWNTs-SnO_2 (5 mg), MWNTs-SnO_2 (7 mg), and MWNTs-SnO_2 (10 mg). The output characteristics of hybrid sensor structures towards the NO_2 were studied by changing the concentration of MWNTs. It is realized from Figure 4.9 that the blending of 2 mg of MWNTs in SnO_2 leads to the decrease in initial resistance (Ra) of the hybrid sensor from 2.4 MΩ to 1.2 MΩ. It was also noted that as the concentration of MWNTs increases to 5, 7 and 10 mg, the initial resistances farther reduces to 94 KΩ, 90 KΩ and 15 KΩ, respectively. In the hybrid structures, at the interface a depletion layer is formed between p-type MWNTs and n-type SnO_2. There is a decrease in the channel width of SnO_2 because of the formation of depletion layer, thereby exhibiting high resistance (Ra) as compared to the bare SnO_2 sensors. With the rise in temperature, both the rate of surface-assimilation and desorption of gases increases giving quicker response and recovery. A hybrid MWNTs-SnO_2 gas sensor which is able to detect 100 ppb NO_2 at room temperature was formulated apart from having high sensitivity and favorable recovery characteristics. Pure SnO_2 based sensors exhibited low recovery and response time at RT. At higher temperature there was increase in the response of pure SnO_2 sensors. However, the hybrid MWNTs-SnO_2 sensors show good sensing response to NO_2 gas at room temperature with quicker response and recovery rates. The maximum response was obtained for hybrid MWNTs-SnO_2 (5 mg) sensor at a temperature as low as 50 °C. As compared with traditional SnO_2 based sensor, the hybrid MWNTs-SnO_2 sensor which was proposed in this study was more capable in detecting NO_2 gas at room temperature with increased response characteristics.

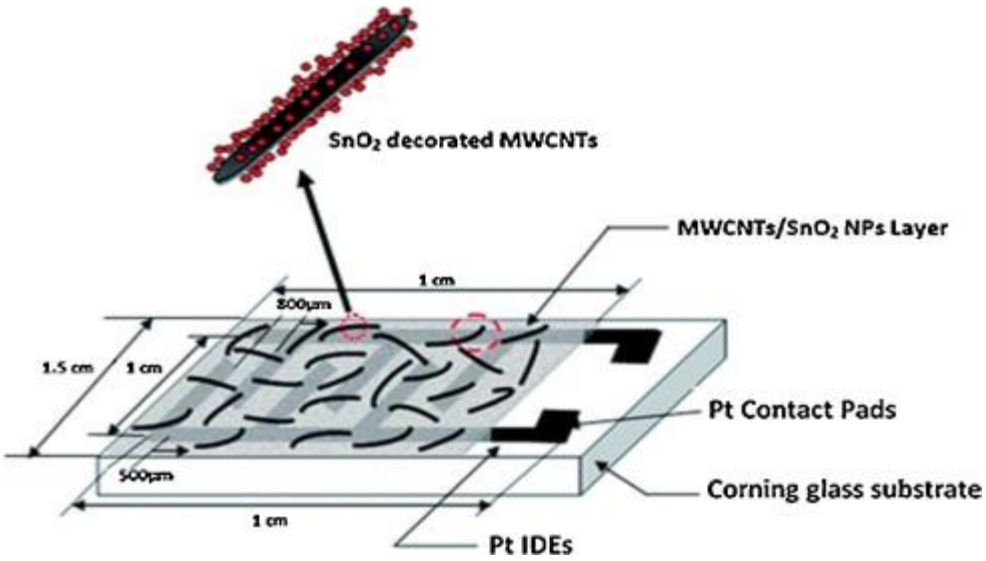

Figure 4. 8: Schematic of the MWNTs-SnO_2 hybrid sensor structure. Copyright permission from [250].

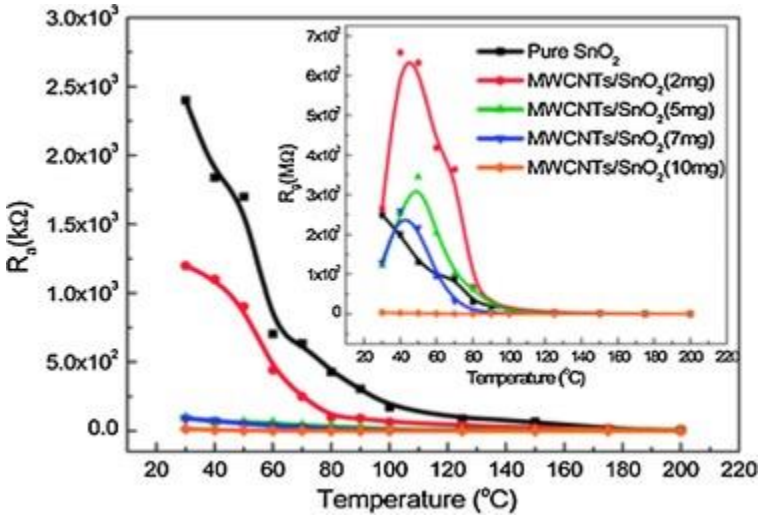

Figure 4. 9: Deviation of sensor resistance in the presence of air (R_a) and 100 ppb NO_2 gas (R_g shown in inset) with temperature for pristine SnO_2 and all the MWNTs-SnO_2 composite sensor networks. Copyright permission from [250].

Nguyet et al. designed and developed n-p-n heterojunction gas sensor of CNTs and SnO_2 nanowires (NWs) to investigate their performance in the presence of NO_2 gases [251]. The designed device is realized by firstly using thermal chemical vapor deposition technique was used to grow SnO_2 NWs on Pt electrodes than to make the connection between two electrodes the MWCNTs or SWCNTs were deposited by spray deposition technique. The potential and electrical

model were used to explain the sensing response of the heterojunction sensor. In this model it was assumed that the heterojunction between n-type SnO_2 and p-type CNTs would acts as distinctive p-n junction diode. The name of the structure is n-p-n because the current has to pass through two heterojunctions. Simultaneously, both CNTs and SnO_2 NWs acts as electrical resistances; as they are in serial contact. The p-type CNTs has a bandgap of (~0.1–0.5 eV) [252] which is much smaller than the bandgap of n-type SnO_2 ($Eg = 3.6$ eV, at 300 K) [253]. The carrier density of CNTs film (2.8×10^{22} cm^{-3}) is much higher than that of SnO_2 (3.6×10^{18} cm^{-3}) [253]. Therefore, the n-p-n heterojunctions can be treated as composed of two Schottky diodes in an opposite position agreement. The measured current is primarily dictated by the leakage current because under the reverse bias voltage arrangement one of the two diodes will operate in reverse bias during gas sensing measurements. Individual materials has great impact on the sensing functioning if there is no bias applied between CNTs and SnO_2 junction. Nevertheless, the heterojunction potential barrier has remarkable contribution on sensing performance of heterojunction sensor, which is much higher than that of pristine sensors. This also explains why a three-junction sensor has more sensitivity as compared with two junctions. The results revealed that the SWCNTs/SnO_2 NWs device showed lesser response to NO_2 compared with MWCNTs/SnO_2 NWs sensor. Also, with the increase in working temperature the sensitivity decreases because of the deformation of rectifying characteristics of CNTs/SnO_2 heterojunction.

Agarwal et al. developed a reliable and flexible NO_2 gas sensor based on SWCNTs using a membrane filter substrate polytetrafluoroethylene (PTFE) [254]. The preparation of SWNT thin film was realized by using a cost-effective spray coating method, followed by polyethyleneimine (PEI) noncovalent functionalization of SWCNTs and fabrication of metal contacts using a shadow mask. It was found that for the concentration of 0.75 ppm of NO_2 the response of the sensor was found to be 21.6% in 5 min, and the sensitivity of the sensor increased to 167.6% when the gas concentration reaches to 5 ppm. With the introduction of analyte (NO_2), the response and recovery times of the gas sensor is measured as time to reach 90% (10%) of its final value. NO_2 with 0.75 ppm concentration, the recovery and response times were found to be 13 min and ~4 min respectively. In comparison with silicon-based gas sensors the PTFE-based sensor has advantage of porosity in the PTFE substrate. As the relative humidity increases the performance of the sensor deteriorates due to the electron donating nature of water molecules.

Jing et al. showed that when some industrial chemicals such as HCl and Cl_2 are exposed to SWNTs coated with various polymers, then SWNTs are capable of detecting these industrial chemicals [255]. Owing to chemical and physical nature as well as the nature of the interaction between gas molecules and nanotubes, in the form of chemiresistor the SWNTs are not able to sense all the vapors and gases. CNTs have shown changes in electrical conductance when it is exposed to NH_3 or NO_2, hence providing a foundation for detecting other gases. There are some industrial chemicals such as Cl_2 and HCl which do not react with pristine SWNTs as suggested by various previous reports. Qi et al. found that SWNTs coated with polyethyleneimine (PEI) was sensitive towards NO_2 while insensitive to NH3; while Nafion coated SWNTs was able to sense NH_3 but insensitive towards NO_2 [25]. Chlorosulfonated polyethylene coated SWNT sensor was able to sense industrial Cl_2 while SWNTs sensor coated with hydroxypropyl cellulose was able to detect HCl. A simple sensing medium was developed using polymer coated SWNTs. Since pristine SWNTs was not able to detect all concerned gas species so it became obvious to search for different options such as doping, coating so that a broad application coverage can be achieved. In this paper [255], it was successfully demonstrated that polymer coated SWNTs sensors were able to respond via change in the conductivity upon exposure to Cl_2 and HCl vapors at a sensitivity level of 2 ppm and above. The polymer coating used here are: Chlorosulfonated polyethylene and hydroxypropyl cellulose for selective sensing of Cl_2 and HCl respectively. Limited selectivity of some analytes was achieved in this paper [255]. Further work is in the process to push the sensitivity at lower levels and to explore different ways to enhance the selectivity.

In the year 2017, Sharma et al. synthesized a hybrid gas sensor of non-covalently anchored MWCNTs with hexa-decafluorinated cobalt phthalocyanines F_{16}CoPc/MWCNTs−COOH for detecting Cl_2 gas [256]. The commercially available F_{16}CoPc and MWCNTs were procured from Sigma-Aldrich and acidification of MWCNTs bearing an acidic group (−COOH) were obtained by following the multi-step method developed by smalley and co-workers. F_{16}CoPc/MWCNTs−COOH hybrid were synthesized by using solution assembly method through π-π stacking between MWCNTs−COOH and F_{16}CoPc in dimethylformamide (DMF). F_{16}CoPc solution with DMF were obtained by dissolving 5 ml DMF with varied amount of F_{16}CoPc (0.1 to 0.5 wt %) followed by ultra-sonication. In the suspensions of MWCNTs−COOH and DMF the solution was added dropwise, and the consequent mixture was sonicated at RT. The mixture was washed and filtered with DMF after proper sonication to remove the excess of F_{16}CoPc derivatives,

afterwards washed with ethanol for multiple times and finally dehydrated to achieve intended F_{16}CoPc/MWCNTs−COOH hybrid. It was found that the as prepared F_{16}CoPc/MWCNTs−COOH hybrid chemiresistive sensor was a highly reversible, selective and sensitive towards Cl_2 gas and also the sensor displayed sensitivity of ~63% for 2 ppm of Cl_2 gas and limit of detection as low as 0.05 ppb. In this, cobalt metal ion was found to be playing a significant part in improving the sensitivity features of the fabricated hybrid sensor. The increase in the sensitivity of the hybrid F16CoPc/MWCNTs−COOH sensor towards Cl_2 gas were described by employing various characterization such as X-ray photoelectron spectroscopy (XPS), Raman and electrochemical impedance spectroscopy (EIS) studies. These studies reveled the effective charge carry-over between chlorine and F16CoPc/MWCNTs−COOH sensor. These results highlight the prospect of such hybrid material in establishing new economical Cl_2 sensors with outstanding gas sensing quality.

In year 2013 Jung et al., reported the use of MWNTs for detecting oxygen molecules. A noble technique was used for growing MWNTs and its sensing performance was analyzed by exposing the sensor with O_2 gas [257]. It was found that electrical resistance of the sensor decreases linearly with the exposure to O_2 gas. The MWNTs network has large surface area and hence large space for MWNTs and O_2 interaction which thereby increases the sensor characteristics such as linear sensitivity, repeatability, stability and fast response time.

The various parameters such as resolution, functionalization ways, operating temperature, response and recovery time has been discussed in Table 4.4.

Table 4. 4: Comparison of different parameters such as resolution, response and recovery time, etc.

Sl.no	**CNTs type**	**Detected gas**	**Functionalization ways**	**Response**	**Response time (s)**	**Recovery time (s)**	**Operating temperature**	**References**
1.	MWCNTs	NO_2	Chemical	5.5×10^3	2.3 min	6.8 min	50 °C	[250]

			solution deposition (CSD)					
2.	m-SWCNTs	NO_2	Spray deposition	ZnO/m-SWCNT showed better response then ZnO/Au	120 s	–	RT	[247]
3.	SWCNTs	NO_2	Sputtering	~63%	180 s	1200 s	100 °C	[248]
4.	MWCNTs	NO_2	Thermal evaporation	1.023	93.1 s	285.2 s	–	[249]
5.	MWCNTs/SnO_2	NO_2 (250 ppb)	Spray deposition	17.9 %	125 s	65 s	100 °C	[251]
6.	SWCNTs/ SnO_2	NO_2 (250 ppb)	Spray deposition	13.3 %	115 s	75 s	100 °C	[251]
7.	SWCNTs	NO_2 (0.75 ppm to 5 ppm)	Spray coating	21.58% – 167.7%	~240 s to 300 s	780 s to 900 s	RT	[254]
8.	ZnO-T − CNT	NH_3	Dripping procedure	~330	18.4 s	35 s	RT	[258]

9.	MWCNTs	NH_3 (100 ppm, 250 ppm, 500 ppm)	Plasma treatment	22.5%, 27.9%, and 31.4% respectively	260 s, 312 s and 330 s, respectively	–	RT	[259]
10.	CNTs	CO and NH_3	mixing	Detected 7 ppm of CO and 20 ppm of NH3	16 s	–	RT	[260]
11.	CNTs	CO and NH_3	Dispersion	38.4%	4 s and 4.3 s	–	RT	[261]

4.3.2 **Reducing gases**

The study by Sanghun et al. presented that how sensitivity and selectivity of the sensor to detect NH_3 can be manipulated by functionalizing CNTs with polymers like Nafion or Polyethyleneimine (PEI) without a change in the surface assimilation properties of gas molecules on CNTs [262]. I–V characteristics study showed that the as prepared structure exhibits p-type conduction even after functionalizing with PEI, inconsistent to the particular SWNTs in which PEI layer changes the nature from p-type to n-type [25]. Results suggested that PEI layer declines both hole molality as well as hole mobility because of the decrease in conductance by ten times due to PEI coating. Nonetheless, there was no noticeable change in I–V characteristic after Nafion coatings. There was a rapid increase in the conductance of PEI laminated devices when exposed to NO_2 molecules, while there was a decrease in conductance in devices coated with Nafion when exposed to NH_3 molecules. However, it was also noted that neither of the device exhibited noticeable changes when exposed to N_2, O_2, Ar or H_2 (the dominant constituents of air) [25]; this

study proved high selectivity of PEI coated SWNTs. Langmuir constant to ascertain the degree of surface assimilation at detected pressure is correlated to binding energy Eg. The functionalization of SWNTs network with PEI has no influence on Langmuir constant indicating that PEI coating does not changes neither the binding energy Eg nor the number of adsorbed molecules at given gas concentrations. In the event of NH_3 exposure, the Nafion coating neither stabilises the surface-assimilation of NH_3 on SWNTs substrate nor modifies the carrier molarity or mobility in the carbon nanotubes. In the end, it was concluded that functionalizing CNTs with Nafion or PEI does not modify surface-assimilation properties of gases on carbon nanotubes.

Bannov et al. developed a high performance ammonia (NH_3) gas sensor based on carbon nanotubes using oxygen plasma treatment [259]. Plasma enhanced chemical vapor deposition (PECVD) technique were used to deposit MWCNTs on the Si/SiO_2 substrate followed by plasma co-polymerization of maleic anhydride and acetylene, achieving core-shell carbon nanotubes covered with functional groups. The presence of D and G bands in the Raman spectrum of the sample confirms the presence of MWCNTs. In case of untreated sensor, the response to 100 ppm, 250 ppm and 500 ppm in the presence of NH_3 was 7.1%, 9.0% and 11.7%, respectively. On the other hand, plasma treated sensors response to 100 ppm, 250 ppm and 500 ppm of NH_3 was 22.5%, 27.9% and 31.4%, respectively, which is almost 3 times increase in the sensor response. Response time for the various concentration of NH_3 such as 100 pm, 250 ppm and 500 ppm were found to be 60 s, 72 s and 247 s respectively in case of untreated samples. In case of plasma treated samples, the response were found to be 260 s, 312 s and 330 s respectively. Plasma modification of sample has increased the response time and the reason for this could be the coverage of active carbon layer which in turn plays a role of barrier for the Ammonia gas. The two successively plasma treatment of MWCNT has led to significant increase in the response in wide range of NH_3. The modification of MWCNTs to core-shell carbon nanostructures is by the oxygen plasma treatment while the deposition of functional groups C=O, C-O and COOH is due to plasma co-polymerization technique. The role of functional group is to capture the electrons from the adsorbed gas on the sensor substrate, while the core shell structure forms the conductive network. The combination led to significant improvement in the sensing response.

Schütt et al. developed a hybrid sensing material (ZnO-T − CNT) which are extremely effective for selective, ultrasensitive and fast sensing of NH_3 gas at RT [258]. In this work, the

highly efficient material was developed by functionalizing the hybrid material tetrapodal ZnO (ZnO-T) networks with the CNTs. The improvement in the response to NH_3 gas was found to be of 1 order of magnitude (from 37.5–330) due to the presence of 2 wt. % of CNTs. Further increase in the wt. % of CNTs lead to decline in the gas response to ~110, which is still greater than the pristine ZnO-T networks (~38). The hybrid sensor ZnO-T-CNT also established excellent selectivity which is more significant for environment observing in which unlike gases are present. A long-time stability was obtained for the developed ZnO-T-CNT sensing material owing to the operation at RT.

Hyang et al. developed a sensor for detecting poisonous gases using CNTs with Pd nanoparticles [260]. Drop-casting method was used, wherein reduced carbon nanotubes with Pd nanoparticles were spread on electrodes of a network for detection of CO and NH_3 at room temperature. After exposing toxic gases on the CNT-Pd sensor, the particles are adsorbed transferring electrons between the adsorbed gas particles and the CNT-Pd sensor. It was argued that due to the formation of Schottky contact by Pd nanoparticles on carbon nanotubes, it changes the hole-carrier mobility of CNTs. The other possibility of Pd nanoparticles may be spillover which in turn enhances the sensing capabilities of CNT-Pd sensors. There is a surge in the electrical resistance of the CNTs due to decrease in hole carrier concentration in CNTs when a reducing gas such as NH_3 interacts with p-type semiconducting CNTs. On the other hand, electrical resistance decreases upon exposure to CO molecules. Purification of CNTs with carboxylic acids lead to the formation of defects and consequently the defect sites and COOH functionality play a crucial part in CO sensing, consequently there is decrease in electrical resistance even though CO is an electron donating gas. The carboxylic group and imperfectness of sites play a significant role in electrical variation when there is CO exposure on CNT sensor. However, there is an increase in electrical resistance of CNT-Pd sensor when the exposed gas is NH_3. Contrary to the pure CNTs sensors, Pd-CNT sensors exhibit a rapid response, linear sensitivity, good repeatability and a low sensitivity extent over different concentrations of CO and NH_3.

Lin et al. developed a hybrid sensor at room temperature with the sensitivity of CoP CNTs for CO was 5 times faster than that of pure Co3O4 nanoparticles based on Co_3O_4/polyethylenimine-carbon nanotubes composites (CoP CNTs) for detecting gases such as CO and NH_3 at room temperature [261]. Hydrothermal technique was used for synthesizing

Co3O4 nanoparticles supported on Polyethyleneimine (PCNTs). It was found that under an optimized condition, the CoP CNTs composites show fast response, higher sensitivity and lower detection limit. Similarly, the response to NH_3 gas by CoP CNTs was faster than that of pure Co_3O_4 based device. It is believed that in future, CoP CNTs may have applications in the fields of catalyst and fuel cell.

In the same year, Huang et al. developed a three-terminal CNT gas sensor for N_2 detection [263]. Vertically aligned CNTs were grown by thermal vapor deposition (CVD) technique, RF sputtering was used for depositing 5 nm thick layer of Fe which acts as a catalyst on the (100) n-type of a silicon substrate. The typical cross-sectional SEM image shows that the length and diameter of grown MWNTs are 47 nm and 30 nm respectively. The electrical resistance variation study of p-type CNTs under the exposure of N_2 molecules was studied. N_2 has been classified as reducing gas species [20]. It was established that under negative gate bias voltage the sensitivity exhibited by the sensor was higher than when the gate voltage was positive. This tendency was more evident when the N_2 pressure was higher. Hence, I can say that negative gate bias voltage not only provided more holes to the CNTs but also enhanced the gas binding locations inside the CNTs mat. CNTs absorbed more N_2 molecules when there was a high pressure of N_2 molecules, this leads to the high resistance contributing to the increase in the sensitivity. It was also observed that under the positive applied gate voltage the sensitivity decreases. CNTs based three terminal gas sensors was used for exploring N_2 absorption characteristics. After monitoring N_2 gas it was seen that at the high drain-source voltage the sensitivity of sensor increased as compared to a low bias voltage. Sensitivity was further improved by supplying more negative gate voltage which in turn adds more holes to CNTs mat. In terms of sensitivity, three terminal CNTs gas sensors have more sensitivity as compared to two terminal CNTs based gas sensors. The reasons for this behavior can explained by the well-established device physics, e.g., change in threshold voltage (Vt), variation in drain current (Id), mobility, etc. [264].

Sayago et al. developed a hydrogen sensor based on carbon nanotubes in which four different sensors were developed with metallic catalysts Nickel (Ni) and Yttrium(Y) in various ratios, such as (1) SWNTs (Ni/Y = 2:0.25) doped with Pd using sputtering (2) SWNTs functionalized with Pd (1:1); (3) pristine SWNTs; (4) SWNTs functionalized with Pd (1:4) [265]. The SWNTs were grown by arc discharge method and used as sensing material for the detection

of H_2. Contrasting behavior has been observed for various types of sensors prepared. It was observed that at room temperature SWNTs and Pd doped SWNTs don't detect H_2 molecules. Sensor (2), as well as Sensor (4), has shown a response to H_2 gas molecules but Sensor (4) has an improved response than Sensor (2) possibly because of the greater concentration of Palladium. The dependency of H_2 sensing has been noticed with increase in temperature. Sensor (3) starts detecting H_2 molecules only when the temperature reaches 250 °C. It was found that Pd doped SWNTs sensor detects H_2 molecules neither at room temperature nor at a higher temperature. It was concluded that at the hydrogen concentrations used, all the sensors demonstrate poor responses and their resistance change with H_2 concentration was not considerable. The sensor (3) represents the best sensitivity (20%). The temperature response needs to be analyzed for H_2 sensing of Pd doped SWNTs sensor.

Alshammari et al. developed an ethanol sensor based on carbon nanotubes inkjet printed on flexible substrate [266]. The fabrication of the sensor involves two steps: Firstly, the carbon nanotube an active layer and electrodes were printed on PET substrate. Secondly, the carbon nanotubes were functionalized with poly (3, 4-ethylenedioxythiophene) polystyrene sulfonate (PEDOT: PSS) and carboxylic acids (COOH). Schematic development of flexible CNTs sensor is shown in Figure 4.10 as shown below. An enhanced ethanol sensing carbon nanotube sensor based on inkjet printing were demonstrated. It was found that the polymer functionalized sensor showed better sensitivity and response to ethanol as compared with other functionalization method. Important reasons for improvement in sensing performance are nanocomposite element good dispersion, network configuration and the effect of gas molecules on the electronic properties of carbon nanotubes and polymer. The performance of the gas sensor can be tuned according to the properties of carbon nanotube, properties of composite material and polymer.

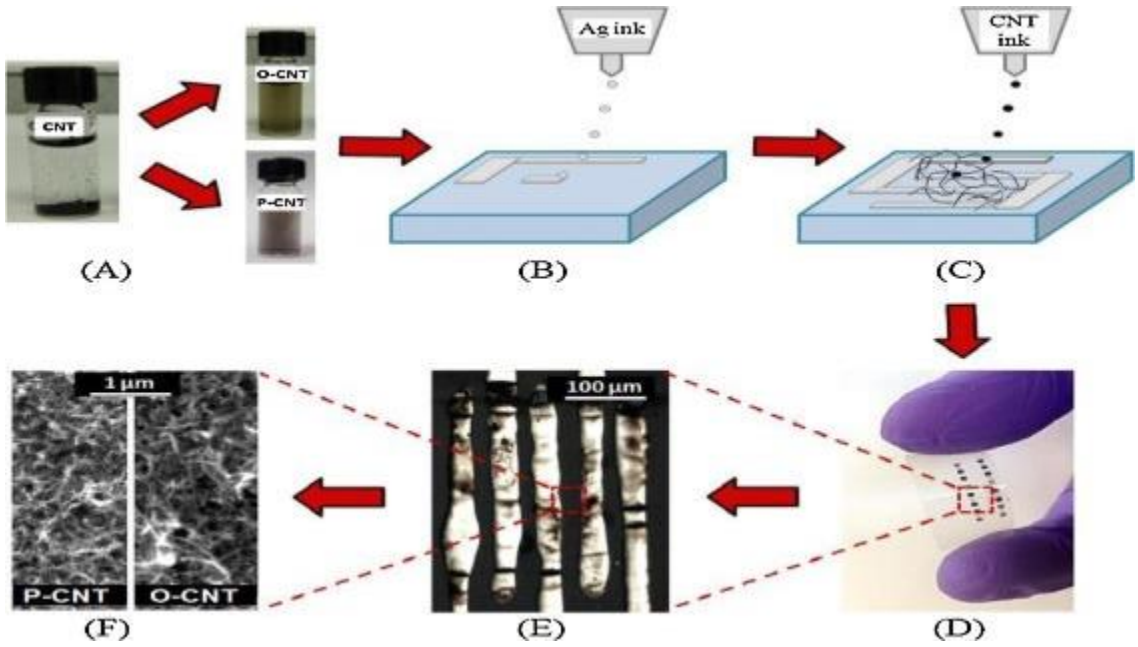

Figure 4. 10: Ink printed CNTs based flexible gas sensor, (a) shows functionalization of CNTs with carboxylic acid and PEDOT: PSS, (b) Printing of Ag electrodes, (c) CNTs printing process, (d) sensor on flexible substrate photograph, (e) shows the optical image of the interdigitated silver electrode, (f) the printed carbon nanotube SEM image. Copyright permission from [266].

D.W.H. Fam et al. formulated a sensor formed on CNTs decorated with silver nanoparticles for selective sensing of hydrogen sulphide. In this paper [267], a selective detection of H_2S gas was achieved by coating silver (Ag) layer on the SWNTs as conducting channel. It was observed that Ag decorated SWNTs gave strong electrical conductance upon the exposure to H_2S gases in comparison to other intrusive gases such as CO and NO. H_2S will form Ag_2S when it is in the contact with the nanotube surface because it is assumed that Silver has a firm attraction towards H_2S gases. Figure 4.11 Shows that for Ag decorated SWNTs sensors, Id decreases when there is an exposure to H_2S gas. On the other hand, for the undecorated SWNTs gas sensors, Id increases upon the exposure of H_2S gas. The interaction of Sulphur (S) with the Ag nanoparticles has led to the generation of more electrons which in turn increases the current density around the Ag particles which attributes to the decrease in Id. At the nanoparticle-SWNTs interface there is an electron-hole recombination which leads to the decrease in the hole density and hence decreases Id. Figure 4.12(a) shows the response of devices coated with gold Ag-SWNTs and COOH-SWNTs upon exposure to NO and CO, respectively. It can be seen from the figure that for the sensor Ag-SWNTs,

the Id decreases under NO exposure. There is a charge transfer between SWNTs and NO particles mainly due to decrease in Id. It can also be noticed that there is almost no response from the functionalized SWNTs upon the exposure to NO. This may be by the virtue of high attraction among NO particles (alongside single unpaired electrons) and Ag (alongside a lone electron). Large difference found between the response of Ag-SWNTs and functionalized SWNTs. Figure 4.12(b) shows that there is an increase in Id when there is CO gas exposed upon the Ag-SWNTs and it is mainly due to the existence of electropositive species around the SWNTs structure. Additional charge carriers induced on the SWNTs network are mainly due to physisorption of gaseous molecules such as CO, NO, and H_2S on the SWNTs network. In conclusion, an uncomplicated resistive sensor which works at room temperature, where SWNTs decorated with Ag nanoparticles is selective to the H_2S gas. One most important thing which can be concluded from Figure 4.11, Figure 4.12 is that among all the fabricated devices, only Ag-SWNTs device showed a significant decrease in Id due to a bond between S and Ag molecules. Furthermore, shift in Id values was considerably larger for H_2S in comparison to that for NO and CO particles. This shows that the interaction among H_2S and Ag-coated SWNTs is stronger than that for CO and NO particles. The empirical conclusion proved that a simple resistive sensor based on SWNTs with low operating power can be achieved by proper functionalization.

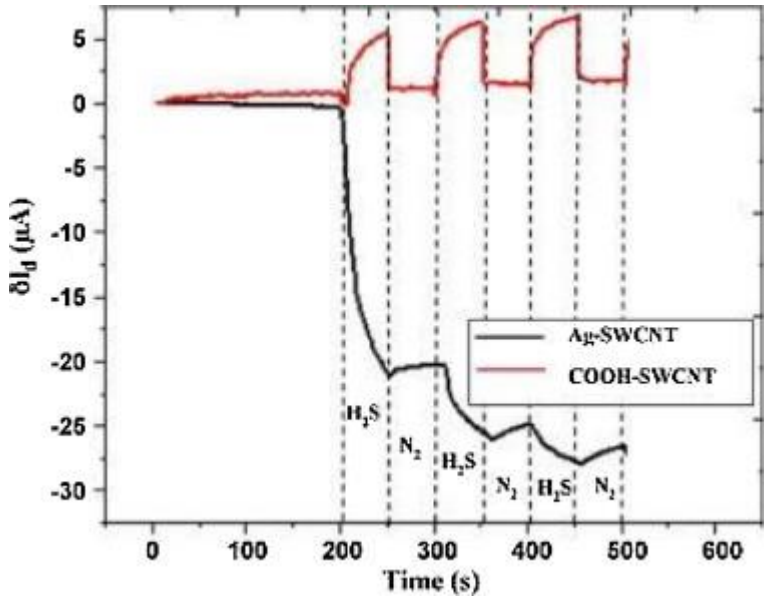

Figure 4. 11: Gas exposure upon device structure: In comparison with undecorated SWCNT device the Ag decorated SWCNT device displays unretrievable decline (of 20 A) in the current due to Ag_2S formation. Copyright permission from [267].

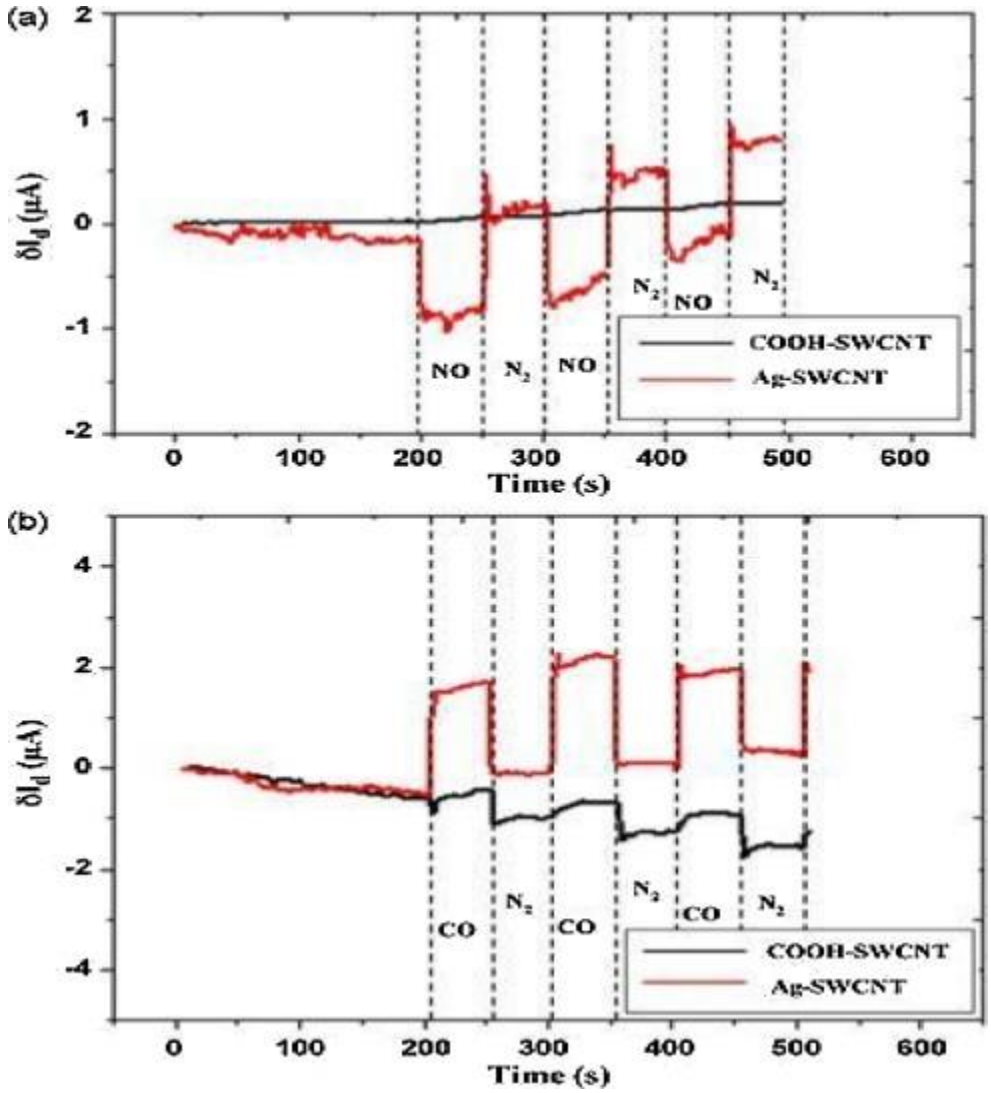

Figure 4. 12: The interfering plot analysts of Drain current–time: (a) NO and (b) CO shows H_2S selectivity of Ag decorated SWCNT owing to negligible I_d shift upon NO and CO exposure as compared to H_2S exposure. Copyright permission from [267].

A room temperature sensor based on CNTs and cobalt oxides was developed by Jung et al. for detecting Hydrogen (H_2) gas [268]. Hydrogen has so many promising features which makes it suitable for many applications. Nonetheless, one of the main challenges of using H_2 is safety because of its undesirable properties such as being odorless, colorless and flammable. Early detection of H_2 is very essential because H_2 can cause explosion, if present in the air with the concentration higher than 4%. CNTs were grown by CVD techniques in which He and C_2H_2 were used as carrier and as main component gases, respectively. Co_3O_4 was deposited by

electrodeposition technique and after deposition thermal treatment was carried out at 300 °C for 30 min as shown in Figure 4.13. It was observed that the thermally treated CNTs/Co_3O_4 composite sensor at room temperature has significantly higher response as compared to one which was not heated. The increase in response was almost 40%, whereas in case of unheated composite, it was only 8% at 35% of H_2 concentration. Typically, pristine CNTs has minimum reaction to H_2 at room temperature. But Kim et al. found that the room temperature sensing of CNT based sensor for H_2 sensing is possible after functionalization of CNTs with OH or COOH groups [269]. The possible reason for increased response is the annealing treatment of composite Co_3O_4/CNTs. Annealing treatment to the CNTs/Co_3O_4 composites has led to the formation of defects and the presence of defects or oxygen functional group plays an essential part in maximizing the feedback of CNTs/metal composites. The Co_3O_4/CNTs composites at room temperature display good H_2 detection properties such as reliable reversibility, stable repeatability, high gas response and fast response and recovery time.

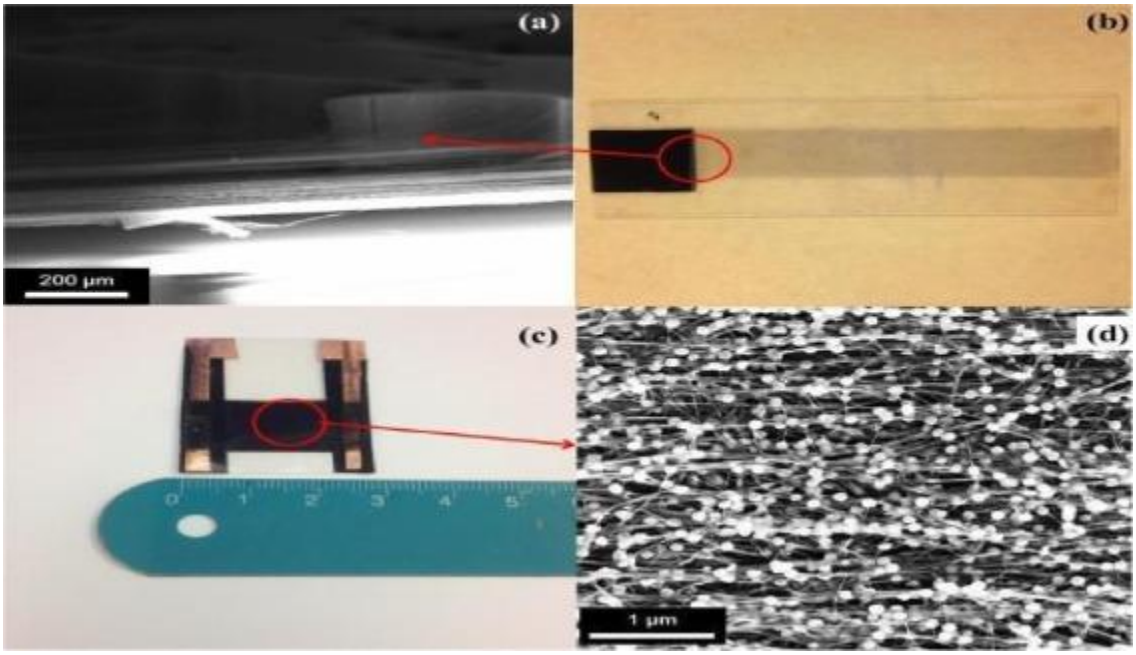

Figure 4. 13: SEM images of (a) and (b) a CNT sheet plucked from the CNT forest, (c) fabricated sensor and (d) CNTs/Co_3O_4 composites. Copyright permission from [268].

Various CNT sensors were analyzed in this section. A survey of sensing capacity of different gases/agents is shown in the Table 4.5.

Table 4. 5: Survey of CNT detection strength to various gases/agent.

Agents/gas	**Reference**	**Agents/gas**	**Reference**
NO_2	[247,248,251,254]	NH_3	[261,284,285,286]
CO_2	[270,271]	O_2	[287,276]
CH_4	[272,273]	H_2	[288, 289]
N_2	[274,275]	Ar	[290,291]
CO	[276, 277]	NO	[292,293,294]
He	[278,279]	SF_6	[295,296]
DNA	[280]	Methanol	[297,298]
Humidity	[281]	Cancer	[299,300]
Supercapacitor	[282]	Ethanol	[301,302,303]
Chlorine	[283]	Glucose	[304]

4.4 Development of Carbon Nanotubes Based Flexible Sensors

4.4.1 Flexible Electronic Applications Based on Carbon Nanotubes: Development and Physics

Tasaltin et al. (2014) developed an innovative flexible volatile organic compound (VOC) sensor. The electrospraying technique was employed for depositing amine altered multi-walled carbon nanotubes (MWNT-NH_2) and gold nanoparticles (AuNP) on polyimide (PI) substrate [305]. Photolithography was used for fabrication of interdigitated electrodes (IDE) on polyimide substrate. Then, the substrate was administered with oxygen plasma etching followed by the deposition of AuNP and MWCNT-NH_2 solution by electrospraying. The chemical behaviour of the sensor were studied for polar (ethanol, propanol; water) and non-polar ($CHCl_3$, hexane, toluene and trichloroethylene) VOCs. As indicated in Figure 4.14 there are 16 finger pairs for IDE with dimensions: electrode thickness of 100 nm, electrode width of 5 mm and spacing between the electrodes as 100 μm. It was observed that at room temperature the MWCNT-NH_2 and AuNP composite films had the highest sensitivity towards Chloroform (CHL) and Trichloroethylene (TCE). The sensing mechanism was shaped for the electrical charge translocation between adsorbed VOC molecules and MWCNT-NH_2 networks. The sensing mechanism of the sensors occurs in two stages. In the first stage, the AuNPs to be wrapped around MWCNT-NH_2 behaves

as filter and determine the gases that will reach the surface of MWCNT-NH_2. In the second stage, the interactions of the organic functional group and VOCs on the MWCNT-NH_2 determine the sensing behaviour. For example, AuNPs assumed to adsorb HEX vapour and do not allow it to reach MWCNT-NH_2, small resistance change was observed. The sensor was bent at various angles to examine the mechanical flexibility of the sensor. The I-V curve was obtained by the manual bending of the sample by hand at 90° upto 100 times and it was observed that there was a minor increase in the resistance, this indicates the bending of the sensor had a very negligible effect on the sensing performance of the sensor.

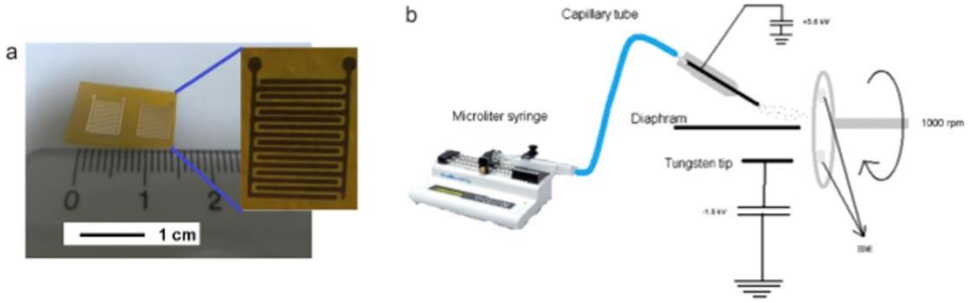

Figure 4. 14: (a) IDE electrodes image prepared on the flexible substrate and (b) Electrospraying system schematic diagram. Copyright permission from [305].

A simple and low-cost flexible sensor was developed in the year 2015 by Zhang et al [306]. The sensor was fabricated on the poly-dimethylsiloxane (PDMS) substrate based on carbon nanotubes and nanoparticles (NPs) of Ag composites. Synthesis of Ag nanoparticles was achieved by reducing $AgNO_3$ particles with sodium citrate. The colloidal solution consists of Ag nanoparticles altered CNTs were obtained by the addition of 0.5 mg CNTs into the $AgNO_3$ solution. The strain sensor fabrication process is depicted in Figure 4.15. Firstly, the Ag NPs modified CNTs solution containing drip was dropped on the glass slides and the excess liquid present in the solution was evaporated by keeping the slide in air for 2 h. This followed by fumigation in culture dish using trimethylchlorosilane (TMCS). The silylation of the sample by TMCS is the most important process, during this process a successful relocation of the Ag nanoparticles altered CNTs nanocomposites takes place from slide to PDMS. The developed sensor displays high stability, stretchability and sensitivity. The stretchability of the strain was found to be 95.6% and the gauge factor was found to be in the range of 2.1 to 39.8 and both are

higher than the typical strain sensors. It was also found that by manipulating the concentration of Ag NPs the linearity and stretchability of the sensor can be changed. The high sensitivity characteristics of the developed strain sensor can be used for highly sensitive strain sensors applications and also for capturing human body motions. To understand the change in the resistance of the strain sensor during the stretching and releasing process, a simple method is used to describe the sensing principle. A conductive network is formed by depositing plenty of Ag NPs modified CNTs and dispersive Ag NPs on PDMS. The resistance of the nanocomposite is constant and will not change during the deformation, whereas the junction resistance acts as a variable resistor and its value is affected by deformation. Hence the total resistance of the whole sample will change with the deformation.

Figure 4. 15: The strain sensor fabrication process over PDMS substrate with CNTs modified of Ag NPs. The final product is illustrated at the center of the figure. Copyright permission from [306].

In the same year 2015, yaqoob et al., (2015) explore the fabrication and evaluation of a highly flexible NO_2 gas detector on a polyethylene terephthalate (PET) substrate with hybrid tungsten trioxide (WO_3) NPs-MWNTs [307]. The hybrid viscous gel of WO_3 -MWNTs NPs is

obtained with the help of α-terpineol by blending the commercial MWNTs and hydrothermally synthesized WO^3 NPs. The hybrid gel was casted on the PET substrate for the fabrication of flexible sensor. Figure 4.16a show the complete schematic diagram of sensor fabrication technique. Two gold electrodes were deposited by using magnetron sputtering with radio frequency on a PET substrate with the dimension of 3 cm long, 1.5 cm wide and 0.1 mm thick. Later on, the as prepared viscous gel is casted between the electrodes. The residual α-terpineol solvent was removed by heating the device to 100 °C on a very hot lamina for one night after casting the fabricated device. Figure 4.16b shows the FESEM image of the MWNTs-WO_3 NPs hybrid fabricated on the PET substrate. MWNTs are properly dispersers and it is mainly credited by the good colloidal stability of α-terpineol and its enhanced dispersity property [308]. Due to the presence of long MWNTs which can cover the small size WO_3 NPs hybrid, there are very few amounts of visible WO_3 NPs. Figure 4.16c explained the mechanical dynamic flexibility of the sensor under bent and unbent situations for 5 ppm NO_2. During the unbent condition the maximum response of 14% was obtained and when the bending angle reached to 90° there was small (1.4%) degradation in response of sensor. Owing to degraded binding energy and little charge relocation between NO_2 gas molecules and strained carbon atoms at 90° might be responsible for degradation in response. On the other hand, there was subsequent enhancement in recovery time mainly due to the maximizing angles which causes the adsorbed NO_2 molecules on the detecting material surface vacate quickly in comparison with unbent. Good repeatability of all bending angles was obtained with very less drift. At room temperature, the gas sensing properties of the fabricated sensors were carried out in an open atmosphere. NO_2 is a highly oxidizing gas that traps electrons and subsequently decreases or increases the conductance of the sensing layer. In this case, the conductance increases when NO_2 gas interacts with the sensing layer. The sensing mechanism can be explained as when the sensor was placed in an open atmosphere, oxygen molecules trap the electrons from the surface of the sensing layer and leaves oxygen absorbents (O_2^-). The NO_2 gas takes the electrons from the interacting surface, dissociates in the form of NO and leaves oxygen absorbents (O_2^-). This O_2^- anion becomes the active sites for the absorption NO_2 gas molecules. Subsequently, NO again converted into NO_2 after reacting with half O_2 molecules. However, MWCNTs-WO_3 NPs hybrid can create p-n heterojunction with the n-type WO_3 and p-type MWCNTs. Later, this p-n heterojunction forms a depletion layer. This depletion layer plays an important role in the sensing mechanism by providing more space for the adsorption of NO_2

molecules. The interaction of NO_2 gas molecules with WO_3 NPs causes the withdrawal of electrons from nanojunction thereby making it unstable. The WO_3 NPs fill the electron vacancy by collecting loose electrons from MWCNTs and become stable again. This phenomenon occurs continuously following by NO_2 gas exposure resulting in a remarkable increase of sensing response.

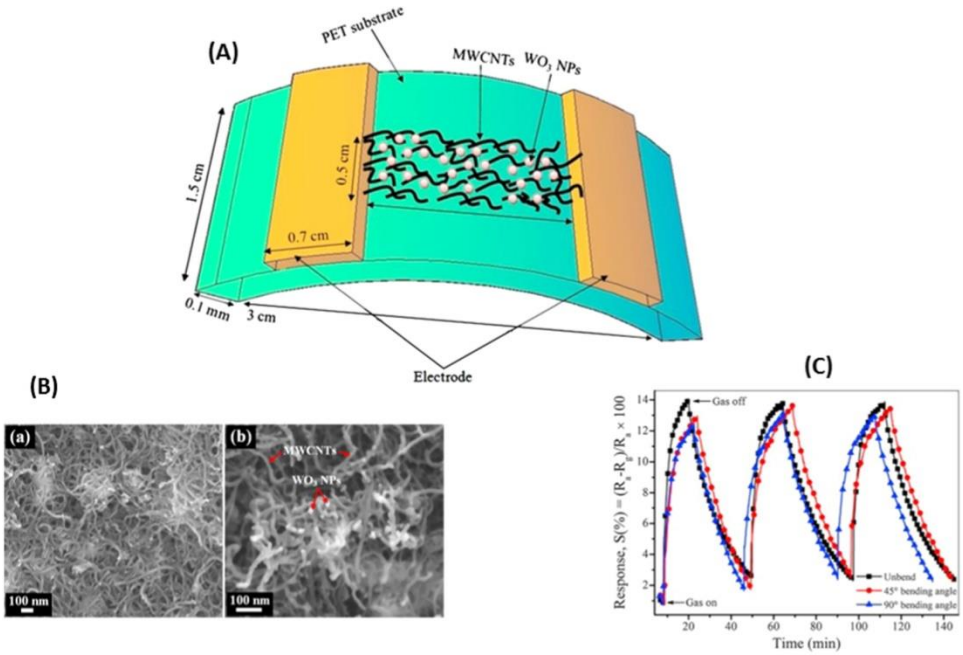

Figure 4. 16: (a) The flexible sensor Schematic diagram. (b) Hybrid sensor FESEM images with (a). Showing lower magnification and (b). Showing higher magnification. (c) Flexibility analysis of sensor at 5 ppm NO_2. Copyright permission from [307].

A sensitive flexible gas sensor based on Cu-SWNTs operating at room temperature presented by Asad et al., (2015) [309]. The SWNTs are decorated with reduced Cu NPs and deposited on a PET flexible substrate by spin coating method in order to achieve a cheap and facile sensor. Figure 4.17 shows the schematic diagram of the Cu-SWNTs sensor based on a flexible substrate PET. Interdigital transducers (IDTs) of aluminium are used as electrodes for Cu-SWNTs gas sensors. To fabricate IDTs on the flexible substrate micro-scale patterning is employed on PET substrate. Magnetron sputtering, a photolithography technique was used to pattern the photoresist layer on the substrate and Al layer was coated on the substrate followed by the lift off process, by the immersion of substrate in the sonicated acetone. At last, as prepared Cu-SWNTs were spin

coated on the substrate followed by annealing at 80 °C for 30 min. It was found that as developed sensor Cu-SWNTs showed an enhanced response to various concentrations of H_2S gas between 5 ppm and 150 ppm. For 5 ppm concentration of target gas a fast recovery time and response time of 15 s and 10 s, respectively were achieved. At room temperature for 20 ppm H_2S, the as developed sensor showed stable, reproducible and fast responses. Flexibility performance of the sensor was performed by bending the samples at various radii and it was found that neither the sensing performance degraded, nor the resistance of the sensor changed. This fabricated sensor can be integrated with the microelectronics circuits because of its low power consumption and high sensitivity. The Cu decoration modifies the electronic structure of the system i.e., the fermi level is raised into the conduction band and SWNTs becomes electrons rich. The results indicate that fermi level of H_2S/Cu-SWNTs system shifts 0.5 eV towards higher energy in comparison to pristine SWNTs. After the adsorption process, in comparison to Cu-SWNTs, the H_2S/Cu-SWNTs becomes n-type with more occupied conduction bands. Owing to the large overlap between the 3p and 4s orbitals, H_2S is strongly hybridized with Cu. As a result, a SWCNT decorated with Cu NPs is an excellent candidate for H_2S gas sensing.

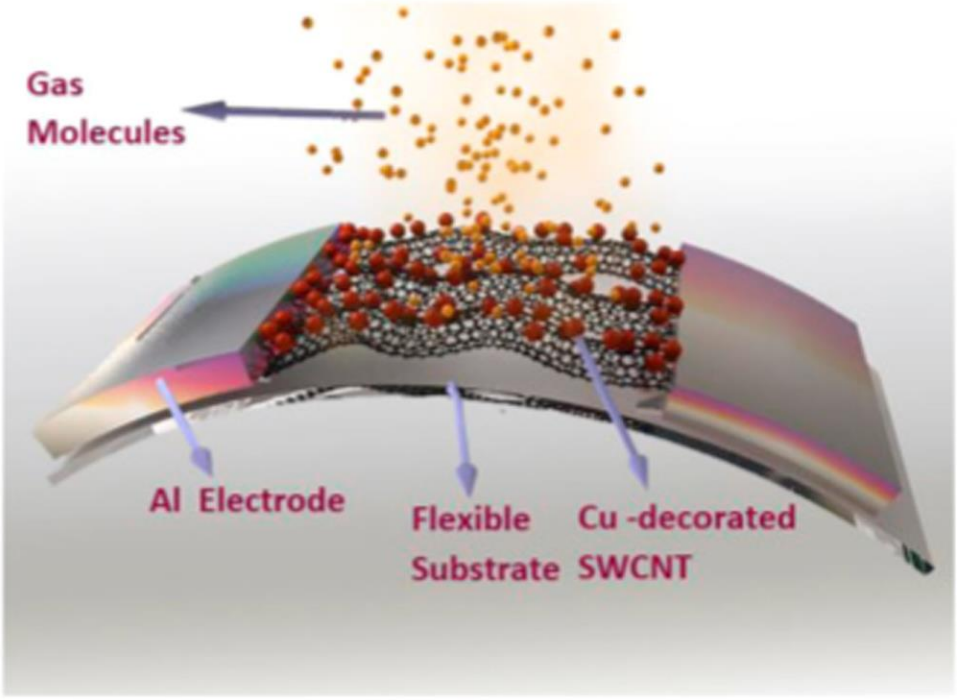

Figure 4. 17: The schematic diagram of the flexible sensor based on Cu decorated SWNTs. Copyright permission from [309].

In the year 2015, Cagatay et al. developed a flexible thin film capacitive sensor based on carbon nanotubes, by spray deposition techniques, for wearable smart skin [310]. Polyimide polymer was used as a flexible substrate and micro-structured PDMS as dielectric spacer between the electrodes. Wearable smart skin development largely depends on set of requirements. However, the general interest is to develop large area fabrication of flexible device economically. Considering, the above important criteria, in this paper the author revised an elastic capacitive tactile sensor composed of micro-structured PDMS as dielectric spacer which is wrapped between two transparent conducting sheets. The capacitance was measured during the sensor operation and it was found that the sensor can detect pressures lower than 0.5 KPa and forces lower than 10 mN. The complete evaluation of the sensor was done by measuring different physical dimensions of the sensor. It was found that under the influence of 1 N force the change in the capacitance of up to 20% was accomplished. Good reliability was demonstrated with long term cyclic tests. To examine the flexibility performance of the sensor, under various bending radii the mechanical characterization of the sensor was performed, and it was found that response was quite stable throughout the measurement. This work stands for the realization of low-cost flexible sensors which fully works under different bending and temperature conditions, for advance electronic applications such as wearable smart skin.

A flexible and transparent chemical sensor based on PANI/FMWCNT has been developed by Wan et al. (2015) [311] with 85% transparency and excellent performance even after 500 bending/extending cycles. The carbon nanotubes network was deposited on nanostructured polyaniline (PANI) nanorods. The nanocomposite film is incorporated by in situ, the oxidative polymerization of aniline in the presence of functional multi-walled carbon nanotubes (FMWNT) suspension and simultaneous deposition over the flexible polyethylene terephthalate substrate. Different quasi-one- dimensional and one-dimensional nanomaterial have been explored for the development of transparent and flexible electronic devices. Carbon nanotube (CNT) based network films are widespread used owing to their outstanding electrical conductivity, good flexibility, optical transparency, chemical stability, high surface area and intrinsic mobility [312,313]. There are many encouraging properties of organic polymers which makes it suitable

for use in organic electronic devices such as inherent compatibility with plastic substrates, scalable and low-cost manufacturing and low temperature synthesis process, which make them worthy for wearable sensing devices [314]. However, there are some drawbacks of conducting polymers such as limited environment instability and optical transparency. For example, the transparency of polyaniline (PANI) is 65% which is not sufficient to replace indium tin oxide (ITO) films for wearable electronics applications. It was found that at room temperature, the as prepared PANI/F-MWNT nanocomposites assembled portable electronic device showed splendid transparency of (85% with 500 nm thickness) along with sufficient flexibility. The schematic diagram flow of the flexible sensor based on nanocomposite PANI/F-MWCNT on flexible PET substrate is illustrated in Figure 4.18. The high surface-to-volume ratio of the CNT and PANI composites and also the synergistic properties of CNT and PANI a quasi-one-dimensional nanostructure which perform as a dependable and productive sensing channel are responsible for transparency, good sensing performance and flexibility of sensor. It is likely that this research will be continued to other conducting polymer containing nanocomposites, initiating the space for developing sensitive, low-cost and reliable sensors which can be integrated with flexible, wearable and transparent electronic devices. It has been widely investigated that NH_3 is a strong electron donor chemical. The emeraldine salt form of PANI transforms into its emeraldine base form in the presence of NH_3 atmosphere, resulting in dramatic decrease in conductance. The particle like PANI aggregates, FMWCNT film devices with different polymerization time upon exposure to 100 ppm NH_3 at room temperature. It was found that the PANI/FMWCNT nanocomposite network film devices have higher gas sensitivity than the particle-like PANI aggregates and FMWCNT film devices.

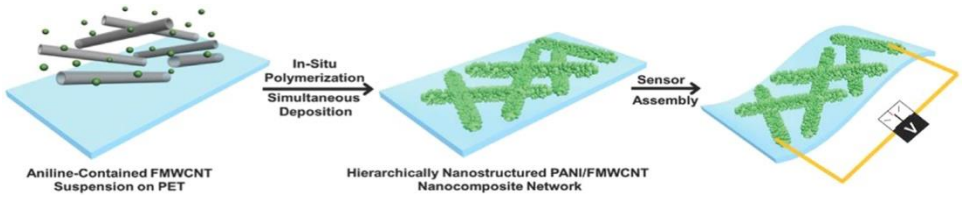

Figure 4. 18: Schematic graphical representation of the development of flexible sensor based on nanocomposite PANI/F-MWCNT on flexible polyethylene terephthalate (PET) substrate. Copyright permission from [311].

Lin et al. (2015) developed a carbon nanotube (CNTs) based CO_2 sensor on a flexible low-cost polyimide (PI) substrate which provides fast response at room temperature [315]. The Si

substrate was oxidised to form SiO_2 layer. A catalyst Fe layer of 10 nm was deposited on SiO_2 substrate by using sputtering technique. Subsequently, carbon nanotubes (CNTs) were grown on the Si substrate by standard chemical vapor deposition technique. Then, the flexible substrate polyimide (PI) was coated with acrylic adhesive. Now the transfer of CNTs grown on the SiO_2 surface will take place by stacking the acrylic adhesive deposited polyimide substrate. Ultimately, the Si substrate is removed, and the CNTs transferred on flexible sensor. It was found that the flexible sensor possesses a high sensitivity of 2.23% at room temperature when the ambient gas was 800 ppm. This article presents the feasibility of flexible CNT gas sensor using the transfer process.

In the following year 2016, Yaqoob et al., [316] investigated the fabrication of elastic NO_2 hybrid gas sensor supported on a tungsten trioxide (WO_3) nanoparticle (NPs) decorated on MWNTs and reduced graphene oxide (RGO) on a PET/PI (polyimide) substrate. The α-terpineol was used to mix the commercially available MWNTs and synthesized GO powder using sonication for 1 h. Additionally, after adding WO3 NPs powder of 3 mg, the solution was sonicated for another one hour. The complete sensor fabrication method is demonstrated in Figure 4.19. A commercial PI tape was fixed on the Si substrate. Magnetron sputtering with radio frequency and photolithography techniques was employed to deposit two finger gold electrodes on PI/Si substrate. The as prepared hybrid solution was drop casted on the electrode between the fingers and subsequently dried by placing on 100 °C heated hot plate. Each sample was dried for 1 h at different temperatures (100, 150, 200 and 250 °C). Finally, the PI is transferred to the PET substrate by cautiously peeled off from the Si substrate. Figure 4.19 depicts the schematic diagram and the optical image of the sensor. It was found that at room temperature as developed flexible sensor had superior mechanical flexibility and increased sensing properties. The fabricated flexible sensor is relevant contender for high performance fabrication of practical NO_2 sensors and is also feasible for diverse fields such as automobiles, aircraft, portable electronic devices and aeronautics because it has less humidity effect on the sensing surface and excellent resulting selectivity. At room temperature, the gas sensing properties of the fabricated sensors were carried out in open atmosphere. NO_2 is a highly oxidizing gas that traps electrons and subsequently decreases or increases conductance in the sensing layer. In this case, the conductance increases when NO_2 gas interacts with sensing layer. The sensing mechanism can be explained as when the sensor was placed in an open atmosphere, oxygen molecules traps the electrons from the surface of sensing

layer and leave oxygen absorbents (O_2^-). The NO_2 gas takes the electrons from the interacting surface and dissociates in the form of NO and leaving oxygen absorbents (O_2^-). This O_2^- anion becomes the active sites to absorb NO_2 gas molecules. Subsequently, NO again converted into NO_2 after reacting with half O_2 molecules. This phenomenon occurs continuously following NO_2 gas exposure.

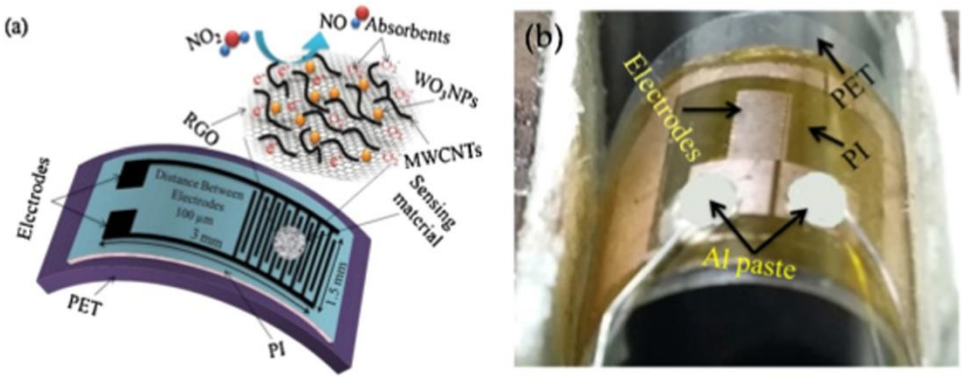

Figure 4. 19: (a) Sensor schematic diagram and (b) Optical image of the hybrid NO_2 sensor. Copyright permission from [316].

The study by Chiou et al. (2017) investigates the behaviour of the flexible polymer/multi walled carbon nanotubes (MWCNTs) composite sensor array as a function of operating temperature [317]. Copper was used as sensing electrode with 35 μm, line spacing was 220 μm and 220 μm line width. The flexible polymer/MWCNTs gas sensor offers many benefits which includes reproducibility, cost effectiveness, low power consumption, lightweight, and flexibility specific to its application in the electrical nose and mobile consumer products. In polymer/MWNTs composite films the gas adsorption and interaction mechanism are mainly governed by two principles: namely, chemisorption and physisorption. These two principles depend on the operating temperatures. In this paper the effect of operating temperature was studied on the polymer/MWCNTs sensor. There is a reduction in the influence of the ambient temperature but also reduces the response because of the higher operating temperature. Both these factors could impact the sensitivity polymer/MWCNTs gas sensor array.

Hua et al. (2017) developed a flexible gas sensor based on Fe_2O_3 composite film and single walled carbon nanotubes (SWNTs) [318]. High performance gas sensors can be fabricated using SWNTs, but the sensitivity and the number of gas molecules detected needs more enhancements. Standard chemical vapor deposition technique was used to grow large area SWNTs. The as grown

SWNT sensor was placed inside the furnace and heated up to 600 °C at 10 °C min^{-1} and held for 1 h in air. The SWNT-Fe_2O_3 composite is transferred on the plastic substrate and connected with two electrodes of silver wire as shown in Figure 4.20. It was found that at room temperature, the composite film of SWNTs-Fe_2O_3 shown clear sensing to H_2S gas and an improved response to NO_2 gas as compared with pristine SWNTs. The flexibility of the sensor was studied at room temperature for different bending angles with the exposure of 20 ppm of H_2S gas and it was found that there was no change in the response of the sensor under either with straightened or different bending angles. The gas sensor showed stable sensing response and mechanical robustness during large degree deformation cycles.

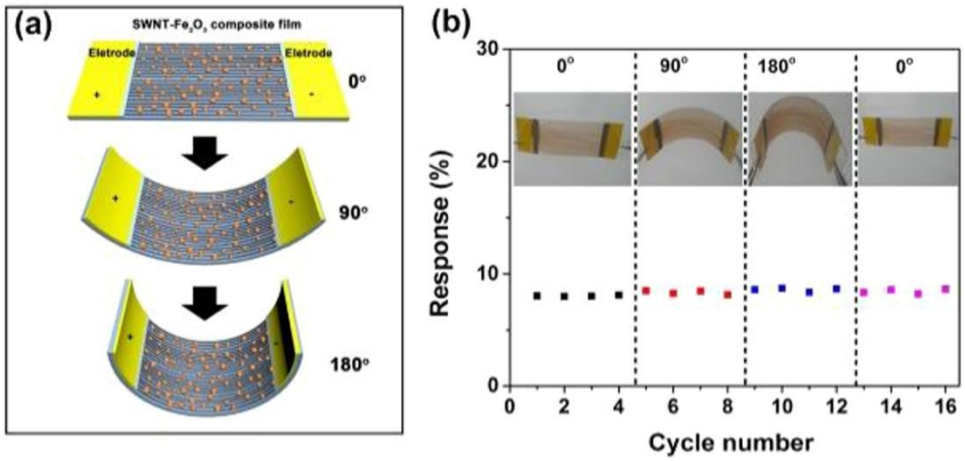

Figure 4. 20: The response of SWNTs-Fe_2O_3 composite sensor ay different bending angle under the exposure of 20 ppm H2S gas. (a) Illustration of gas sensor response at various bending angles 0°, 90 °and 180°. (b) The behavior of gas sensor when the bending angles varies from 0° to 180° and returned to 0°. Copyright permission from [318].

Xue et al. (2017) developed a polyaniline/carbon nanotube composite flexible gas sensor [319]. A sensor was fabricated for the real time detection of ammonia in anaerobic digestion. The sensor was bringing together from a packing order CNT/PANI nanocomposite network film fabricated by adding ammonium persulfate (APS) into CNT which consists of aniline solution for PANI polymerization and film deposition. It was found that at room temperature as developed flexible sensor display high sensitivity towards NH3, sensing from 200 ppb to 50 ppm. Also shows splendid selectivity to NH_3 gas as compared to other volatile gases and also shows dependable flexibility. The increase in sensitivity of the sensor is mainly attributed by the collaborative effect

of CNT and PANI, the high surface area of the nanocomposite film and functional network sensing channels. The electronic device embedded with the film having high sensitivity, strong flexibility and small size, could be suitable for NH_3 monitoring in anaerobic digestion in real time for the high efficiency and also for better stability of anaerobic digestion of renewable energy sources.

Wang et al. using wet spinning process established the fabrication of flexible organic vapor gas sensor based on carbon nanotubes/poly (styrene-butadiene-styrene) (CNT/SBS) hybrid fiber [320]. The complete fabrication and characterization of flexible pure SBS fiber and CNT/SBS hybrid composite fiber is shown in Figure 4.21. The CNTs were mixed with the commercially available SBS polymer via a two-step mixing method in order to obtain better hominization mixture, which includes melt mixing and subsequent solution mixing. After this CNT/SBS melt mixed is added to tetrahydrofuran and properly mixed at room temperature for 24 h. The spinning solution was loaded to the plastic syringe as shown in Figure 4.21. The flow rate of spinning solution was kept at 6 ml h^{-1}. The composite fiber was drawn out vertically and wound onto a spool which was stick on to the revolving drum. The sample denoted as SBS/xCNT indicates the content of CNT in weight percentage. For example, SBS/1CNT indicates the composite fiber retain 1 wt% CNT. At room temperature the SBS/1 CNT vapor sensor displays enchanting achievement, including high sensitivity, splendid mechanical reliability, fast response, good reproducibility and larger detection range. The outstanding benefits can be accredited to the higher surface area of fiber and nature of triblock SBS polymer. Capabilities of this device demonstrate their prospects of application in flexible and wearable microelectronics for Volatile organic compounds (VOC) monitoring.

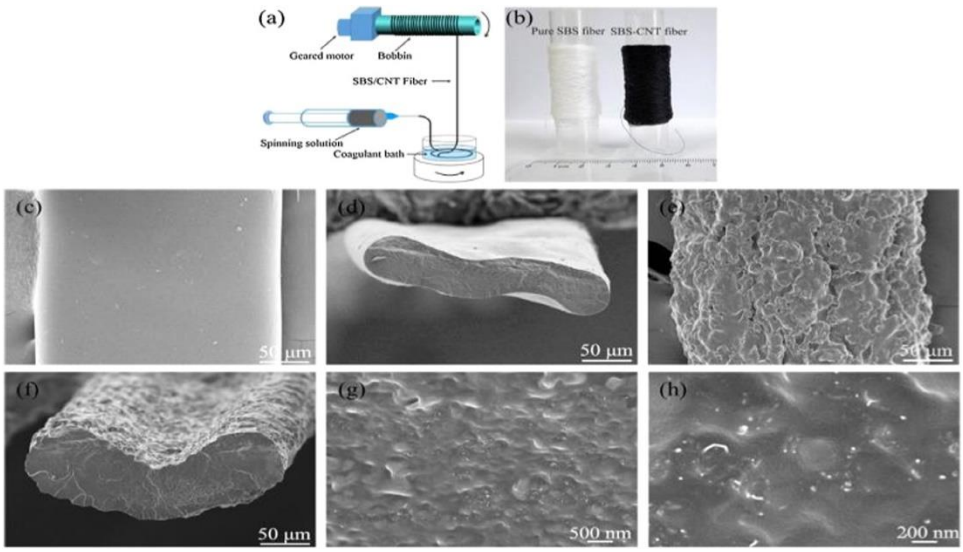

Figure 4. 21: The flexible pure SBS fiber and CNT/SBS hybrid composite fiber fabrication and characterization is shown. (a) The schematic interpretation of wet spinning method. (b) Images of pure SBS and CNT/SBS composite fiber (c) Typical FESEM image of pure SBS fiber (d) Pure SBS fiber cross section FESEM image (e), (f) Cross sectional SEM image of SBS/1 CNT composite fiber (g), (h) Enlarge Cross sectional image of SBS/1 CNT composite fiber. Copyright permission from [320].

Paul et al. (2017) developed a disposable, lightweight and flexible resistive malaria biomarker HRP2 biosensor for label free sensing based on nanofiber Zinc-oxide and multi-walled carbon nanotubes [321]. The device stepwise fabrication process is schematically depicted in Figure 4.22. The stretchable gear was concocted by drop casting of MWNT-ZnO nanofiber slurry between micro-fabricated gold electrodes. The MWNT-ZnO nanofiber suspension was prepared by sonication in DMF for 1 h. The trapped water molecules into the drop cast device were removed by annealing for 1 h at 60°. A linker solution consists of 0.1 M NHS (activator) and 0.4 M EDC coupling agent were used for processing the MWNT-ZnO nanofibers for antibody (anti-HRP2) functionalization for 4 h so as to stimulate the carboxylic (–COOH) group on nanofiber substrate. The PBS was used for washing the device and 10 μl of antibody anti-HRP2 (200 μg ml^{-1}) at 4 °C was used for overnight development of required device anti-HRP2/MWNT-ZnO. Owing to the firm amide bonds established among the activated carboxylic groups of the MWNT-ZnO nanofiber and the amine group of the antibodies, the antibodies were covalently immobilized on the nanofiber surface. The PBS with pH 7.0 was used for washing the device to remove unbound antibodies. The device was further incubating with 1 wt. % of bovine serum albumin (BSA) for 1

h at 37 °C followed by washing with PBS for blocking nonspecific binding sites. The device was incubated with various concentration of target antigen HRP2 for an enhanced span of 30 min followed by rinsing with PBS, air drying and resistance measurement for investigating the sensing performance of the device. The composite nanofiber channel has a rare property which has been utilized by the device without any further surface variation to provide novel matrix for one step covalent conjugation of the malaria HRP2 antibody. In the wider detection spectrum of 10 fg ml^{-1} − 10 ng ml^{-1} of HRP2, the fabricated chemiresistor displays excellent 8.29 kΩ g^{-1}ml of sensitivity. It was also found that for the targeted malaria antigen HRP2 the fabricated sensor demonstrated good reproducibility and specificity. The sensing mechanism can be postulated in two possible ways as the origin of change in conductance of nanofiber on biomolecular functionalization: one is owing to the alteration of electrostatic gate potential as a result of the adsorbed charged molecules and other is owing to the adsorption of ionized atoms present on the biomolecule's surface, which may modify the deletion region of the nanofiber depending on the net charge polarity.

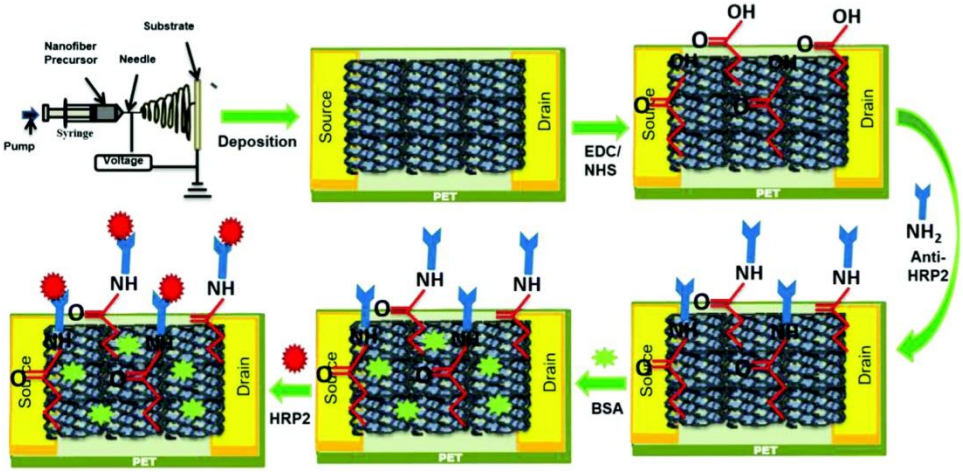

Figure 4. 22: Schematic depiction of the flexible device step wise fabrication process of resistive biosensor malaria biomarker HRP2 detection. Copyright permission from [321].

Huang et al., (2017) developed a radical view of the stretchable IR detector where CNTs were incorporated on Si/SiO_2 and polymethyl methacrylate (PMMA) substrate for realizing the detection mechanism of infrared [322]. The MWCNTs-based IR detector fabrication process flow is shown in Figure 4.23a. The anisole solution with concentration of 0.08 mg ml^{-1} was used to

dissolve PMMA so as to produce the flexible IR detector on PMMA. The PMMA was solidified on the surface of the CNTs arrays after the as prepared PMMA solution was dropped on CNTs surface and dried in an oven at 150 °C for 20 min. PMMA solution only covers the surface of the CNT only with gnomish trickling into CNT arrays because of the high surface tension. Due to the stickiness of the PMMA, after solidification the PMMA sticks onto the CNT arrays. The CNT arrays originally on SiO_2/Si was carefully pilledoff to obtain CNT arrays on PMMA substrate as shown in Figure 4.23c. The schematic diagram for testing the sensors is shown in Figure 4.23b. The semiconductor laser module with wavelength of 850 nm is used as source of infrared. The spot diameter of 3 mm was focused on one of the electrodes and other electrode acts as reference. The infrared laser with the on/off were employed to supervise the voltage across the electrodes. In conclusion, two IR detectors were developed with PMMA and SiO_2/Si substrates. In the presence of IR radiation even at IR power as low as 0.1 mW mm^{-2}, both the detectors exhibited a direct relationship with light power density and have evident feedback. Owing to the interface traps between SiO_2 and CNTs, the detector with SiO_2 substrate exhibited fast response (40 ms) and high sensitivity. The detection of human finger movements has made IR detector as a possible likely utilization of CNT based sensors for the sensing of far IR or weak thermal. A radical view of stretchable IR detector fabrication was accomplished by relocating CNT/SiO_2 structure on the PMMA substrate, which exhibited sequence of high sensitivity, flexibility and quick response (50 ms) time.

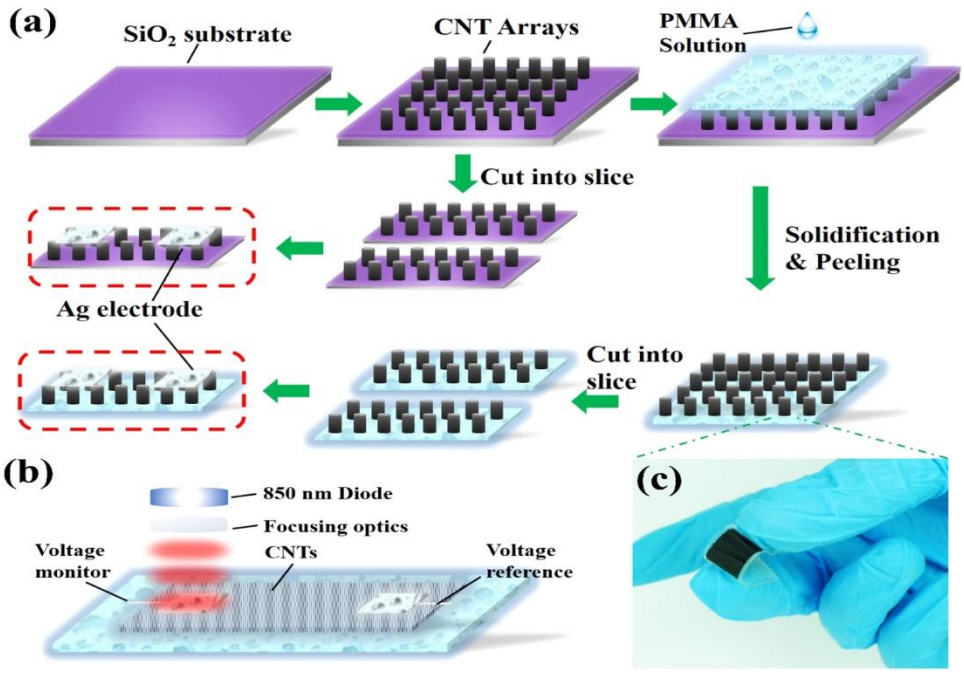

Figure 4. 23: (a) Schematic fabrication process flow of the IR detector. (b) Schematic diagram of the measurement of IR response. (c) The image of IR sensor relocated from SiO_2/Si substrate to PMMA substrate. Copyright permission from [322].

Franklin et al., (2017) developed a carbon nanotube thin film transistor (CNT-TFT) pressure sensor for measuring environmental pressure for a broad pressure spectrum [323]. The aerosol jet printer was used for printing pressure sensor on the flexible substrate polyimide. Acetone and isopropyl alcohol were used for ultrasonication of the flexible substrate polyimide followed by rinsing in DI water. To take out whatever molecular impurities and to boost ink stickiness, the glass slide was exposed to O_2 plasma at 100 W for 4 min. A backgate was printed on the substrate with silver nanoparticle (Ag NP). The single walled carbon nanotubes ink was used to print semiconducting channel. In situ electrical properties of the sensors were measured in custom-build pressure chamber. A linear variation in the transconductance of the pressure sensor over a pressure spectrum precisely correlates to common tire pressure values. The internet-of-things (IoT) capabilities of the printed sensor were demonstrated by using bluetooth communication and simple circuitry for smart tire applications. The printed smart tire sensor is capable of sensing both pressure and treads depth in real time thereby have supreme value for both the manufacturers and customers alike.

A composite of carbon nanotubes (CNT) as electrodes on gold flexible substrates were developed by Xuan et al., (2018) which are flexible and miniaturized lead and cadmium ion detector sensor supported on fully integrated electrochemical sensor integrated with micro-patterned rGO [324]. There are many advantages of this process such as decreased cost, reduced sensor size and decreased sample volume. Also, geometrically uniform, identical and well-defined electrode structures can be developed. In Figure 4.24, along with differently shaped electrodes the flexible micro-Electromechanical systems (MEMS)—based electrochemical sensor is demonstrated. The schematic illustration of the modified Au/rGO CNT/Bi composite electrode for sensing Cd and Pb ions mechanism is depicted in Figure 4.25. The surface area of electrodes was improved by mixing CNT with rGO so as to enhance the achievement of the sensor. Specific and individual stripping peaks for Cd and Pb ions were obtained in the fabricated sensor by in situ bismuth film plating. For achieving the best stripping performance, various empirical parameters, comprising electrodeposition conditions and electrolyte environment were carefully optimized. A favorable detection limit of 0.2 ppb (Pb) and 0.6 ppb (Cd) as well as high sensitivities of 926 nA/ppb cm^2 (Pb) and 262 nA/ppb cm^2 (Cd) were achieved under optimal conditions respectively. The fabricated sensor exhibited good response to both Cd and Pb ions in the concentration spectrum of 20 ppb to 200 ppb. The developed Au/rGO CNT/Bi altered electrode shows a significant improvement in the determination efficiency towards target ions because of the enlargement of electrode surface area. It was found that the developed sensor showed improved stability, sensitivity and reliability for the target heavy metal ions and also the detection of ions of heavy metal in the water was satisfactory.

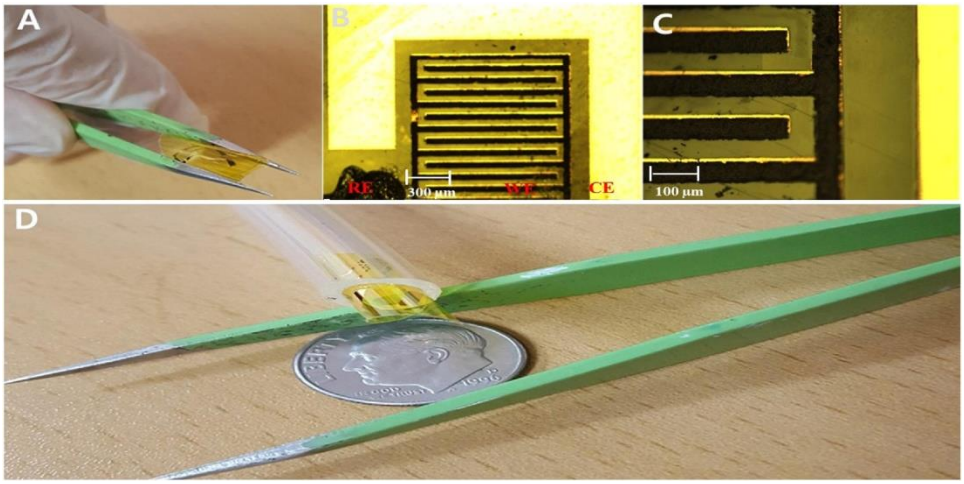

Figure 4. 24: The photograph of integrated, miniaturized and flexible heavy metal ion sensor with MEMS patterned CNT composite working electrode and reduced graphene oxide (rGO). (a), (d) Photographs of the fabricated heavy metals ion flexible sensor. (b) Microscopic images of 3 electrodes. (c) Working electrode photograph. (Working area: 1.5 mm^2, gap size: 50 μm and electrode thickness: ~1 μm). Copyright permission from [324].

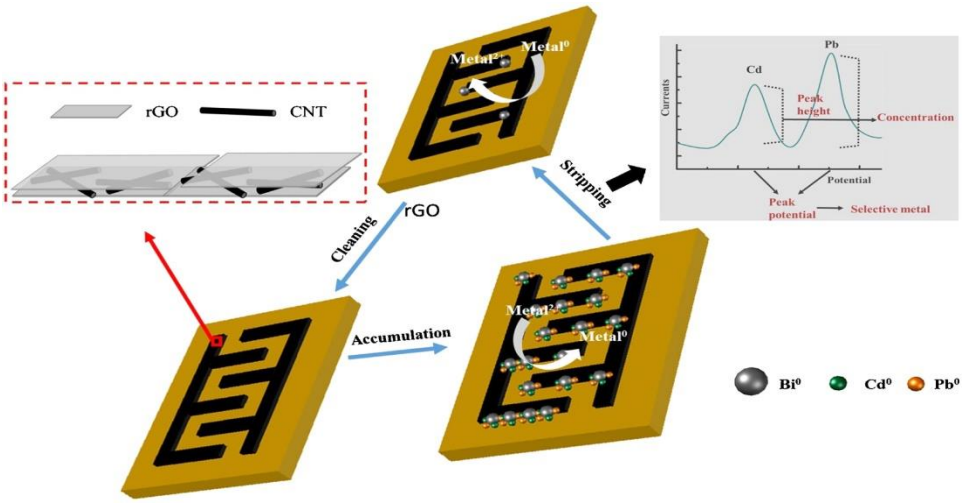

Figure 4. 25: The schematic illustration of the modified Au/rGO CNT/Bi composite electrode for sensing Cd and Pb ions mechanism is depicted. Copyright permission from [324].

A flexible and reliable chemiresistive NO_2 gas sensor was developed on Polytetrafluoroethylene (PTFE) membrane filter substrates based on SWNTs by Agarwal et al. (2018) [325]. The fabrication process of the sensor includes the development of SWNTs thin films by spray deposition technique, followed by using shadow mask for metal contact fabrication. The flexible substrate of PTFE membrane filter with diameter 47 mm, millipore omnipore, 0.2 μm were chosen for spray deposition of SWNTs. The complete spray deposition setup for the deposition of SWNT film on the flexible substrate is shown in Figure 4.26a. After spray coating, integrated metal electrodes were fabricated by sputtering the Gold metal over the SWNTs using metal shadow mask, which is cost effective patterning technique to develop chemiresistive gas sensors as shown in Figure 4.26b. The developed chemiresistive gas sensor had p-type of SWNTs. The change in the conductance responsible for sensing mechanism mainly depends upon the adsorption of analyte between the SWNT surface the oxidizing and reducing gases on the SWNT network. It was found

that for various concentrations of NO_2 extending from 0.75 to 5 ppm, the sensitivities were found to be in the range 21.6% to 167.7%. The PEI functionalization of the SWNT surface has led to the transition of p-type SWCNTs to n-type because of the presence of amine group which is rich in electron concentration. Owing to the high densities of amine group in PEI, the sticking of amine group on the side walls of SWNTs is irreversible and hence n-type behaviour of SWNTs. In presence of electron accepting nature of NO_2, the PEI functionalized SWCNT sensor resistance increases which decrease the current of n-type SWNT sensor after donating electron. To check the reproducibility and flexibility of the developed sensor, the mechanical experiments were performed by a bending sensor for various curvatures of diameters 75 mm, 12.5 mm and 6 mm. It was found that under bending conditions the resistance of the sensor remains within ±5% of resistance of the sample under horizontal position.

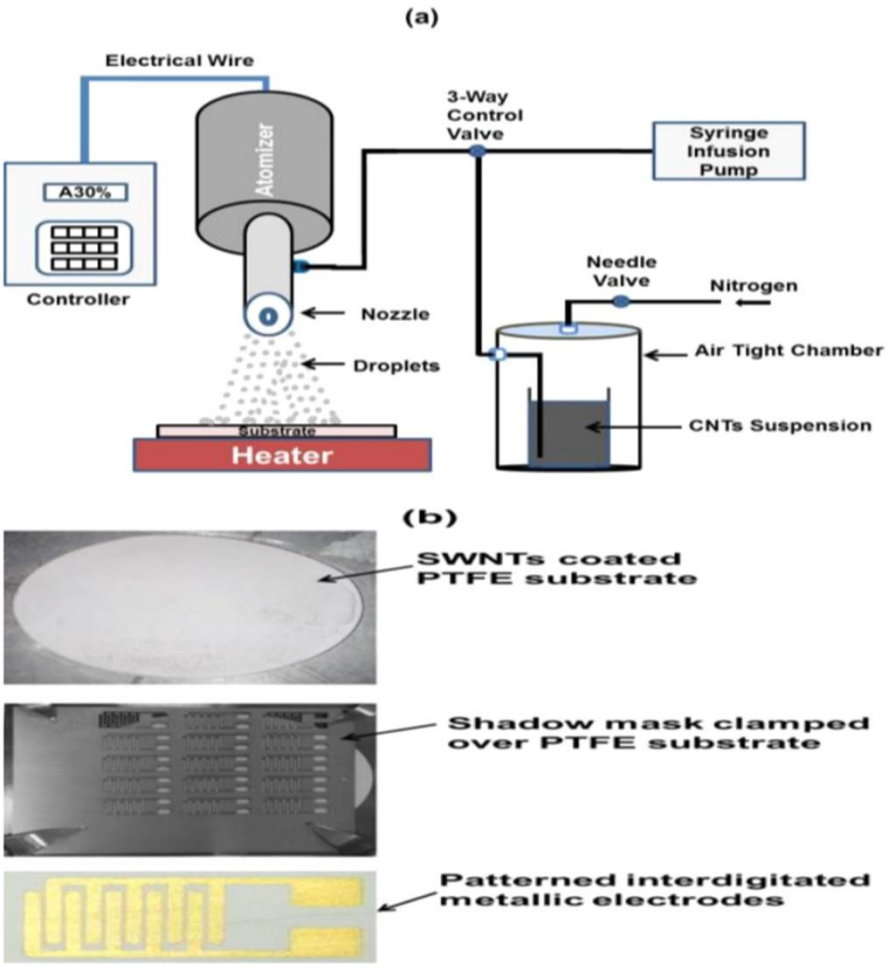

Figure 4. 26: (a) Spray deposition setup for the deposition of SWNT film on the flexible substrate. (b) Metallic shadow mask fastens with the SWCNTs covered PTFE substrate. (The integrated electrodes of single device can be viewed in image, after metal deposition through mask). Copyright permission from [325].

Jung et al., (2018) proposed a unique approach of highly sensitive flexible pressure sensor which is capable of measuring enforced pressure employing a change in the contact resistance [326]. The sensor was fabricated on the flexible substrate of poly- dimethylsiloxane (PDMS) comprising CNTs. To boost the sensitivity of the developed sensor the CNTs were made to appear on the surface of cone shaped microstructures. The sensor is fabricated by pouring a liquid PDMS precursor comprising CNTs on the silicon mold. The CNT/PDMS precursor is covered with film and a weight of 1 kg is put on it followed by applying pressure to separate air bubbles. After

solidification from silicon mold the elastomer CNT/PDMS is separated. The CNTs are exposed to the outer surface of pyramids after PDMS is selectively etched out. It was observed that the developed flexible pressure sensor had high sensitivity but not exceeding the value of 250 Pa. In addition, the developed sensor is capable of detecting very small force and fast response characteristics and good reliability.

At cellular level pH monitoring in environment is very important because minute pH change impact every living organism. Yeong et al., (2018) developed a flexible and low-cost carbon nanotubes pH sensor for live cell applications using aerosol jet technology [327]. Polyimide with a thickness of 150 μm was used as a flexible substrate. Ethanol is used for cleaning the substrate by sonication for 10 min, on the polyimide substrate the silver electrode is first printed. The sensing element sinuous CNT is then printed on the surface of silver electrode followed by drying at 200 °C for 2 h. Figure 4.27a show the bending cycles test for the flexible pH sensor. Bending and release motion of the sensor during this bending test is shown in Figure 4.27b and Figure 4.27c. The developed sensor was studied for in vitro biocompatibility. The surface of murine myoblasts was used for directly placing sensor. After 7 d of culture, it was found that a layer of cells started to grow on the edge of the top surface of the sensor. The developed flexible pH sensor showed high reliability, sensitivity, high mechanical stability, good response time, also the in vitro biocompatibility shows that the pH sensor is suitable for wearing on human skins. The Table 4.6 would give an idea about the various parameters for flexible gas sensors such as substrates, operating temperature, response time, recovery times and various other important properties which are essential for developing flexible sensors based on carbon nanotubes.

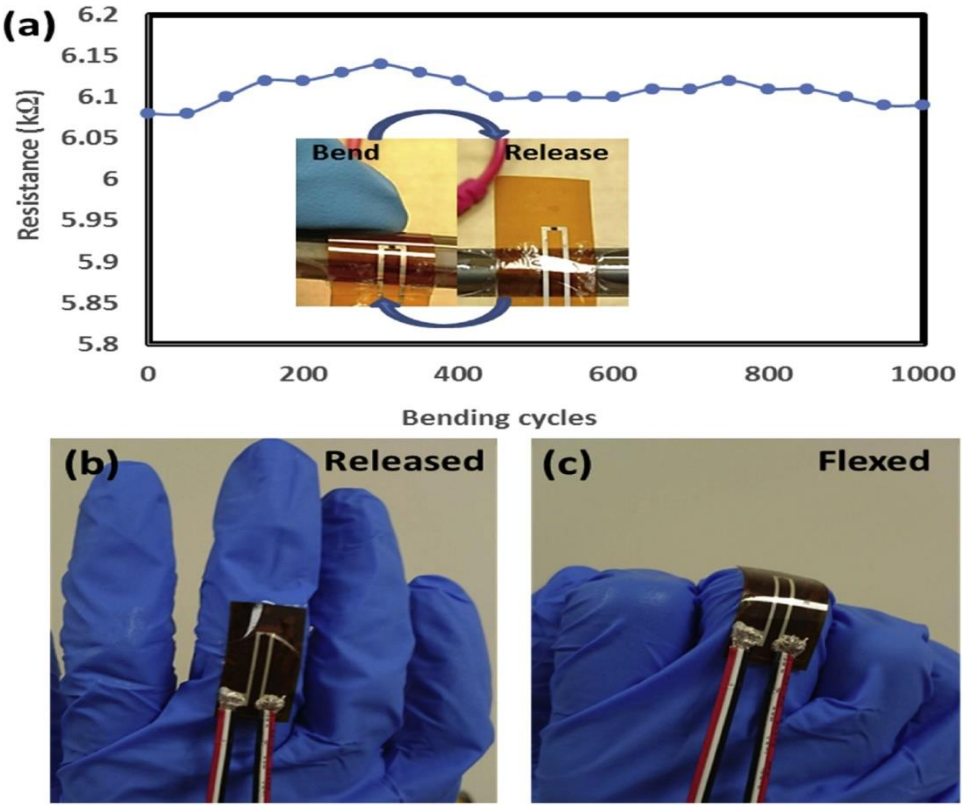

Figure 4. 27: (a) Flexibility test for the printed CNTs based pH sensor interpreting the fluctuation in measured resistance with bending cycles. Bending tests motion of bend and release is shown in inset photograph. (b) Sensor attached with gloves showing released motion. (c) Sensor attached with gloves showing bend motion during flexibility test. Copyright permission from [327].

Table 4. 6: Survey of flexible sensors based on carbon nanotubes.

Sl.no	**Agents/ gases sensors**	**Flexible Substrates**	**Flexibility/ Stability**	**Temper-ature**	**Response /Sensitivity**	**Response time**	**Recovery time**	**Ref.**
1.	H_2S	Polyethylene terephthalate (PET)	yes	RT	20 ppm	10 s	15 s	[309]
2.	NH_3	Polypyrrole/ Polyaniline (PANI)	800	RT	50 ppm	85 s	20 s	[319]
3.	H_2S	Polypyrrole/ Polyaniline (PANI)	90° to 180°	RT	20 ppm	300 s	300 s	[318]

4.	Pressure	Poly (dimethyl siloxane) (PDMS)	35000	-	19.8 kPa^{-1}	16.7 ms	-	[328]
5.	NH_3	Polyaniline (PANI)	45° to 90°	RT	25 ppm, 200 ppm, 1000 ppm	213 s, 191 s and 179 s respectively	98 s, 121 s and 229 s respectively	[329]
6.	Organic vapors	Poly(styrene-butadiene-styrene) (SBS)	1000	-	256%	≤ 40 s	-	[320]
7.	Humidity	Polyimide (PI)	yes	RT	Ultrahigh sensitivity	102 s	Several seconds	[330]
8.	NH_3	Polyaniline (PANI)	0° to 80°	RT	42% to 385%	115 s	44 s	[331]
9.	NO_2	Polyethylene terephthalate (PET)	0°, 45° and 90°	RT	14%	10 min	27 min	[307]
10.	Pressure	Poly (dimethyl siloxane) (PDMS)	>50,000	-	>1.14 kPa^{-1}	<17 ms	-	[332]
11.	NO_2	Polyimide/Polyethylene terephthalate (PI/PET)	10^6	RT	17%	7 min	15 min	[316]
12.	NO_2	Polytetrafluoroethylene (PTFE) membrane	6, 12.5, 75 mm diameter	RT	21.58% to 167.7%	4 min	13 min	[325]
13.	IR	polymethyl methacrylate (PMMA)	yes	RT	0.1 mW/mm^2	50 ms	-	[322]
14.	pH	Polyimide (PI)	yes	-	59 kΩ/pH	20 s	-	[327]
15.	NO_2	Polyimide (PI)	yes	RT	24.82% (5 ppm)	65 s	-	[333]
16.	Strain sensor	Poly (dimethyl siloxane) (PDMS)	yes	RT	1.98 MPa	-	-	[334]

17.	Strain sensor	Poly (dimethyl siloxane) (PDMS)	1000	RT	100	400-700 μs	-	[335]
18.	Humidity	Nano-fibrillated cellulose (NFC)	yes	-	69.9% (ΔI/I0)	330 s	377 s	[336]
19.	Strain sensor	polyacrylamide (PAAm)	300	RT	0.7 MPa	300 ms	-	[337]
20.	Strain sensor	Poly (dimethyl siloxane) (PDMS)	1000	RT	58.7	-	-	[338]

4.5 2D transition metal di-chalcogenides and metal oxide nanostructures based NO_2 gas sensors

Materials for NO_2 gas sensors

4.5.1 2D transition metal dichalcogenides (TMDs)

TMDs, having an ultrathin thickness and 2D morphology, present some exceptional chemical, electrical and physical properties as compared with their bulk equivalent and hence carry an immense assurance for diverse applications [149,187,188, 189,339]. There are many methods employed to prepare one or few-layered TMD nanosheets, such as chemical vapor deposition (CVD) process, liquid-phase exfoliation, wet chemical synthesis, mechanical cleavage method and electrochemical exfoliation using Li-intercalation [340-344]. The electrical and chemical properties of 2D nanostructures have made them relevant for their use in numerous applications, e.g., sensors, electronic/optoelectronic apparatus, energy storage and electrolysis [345-355]. Some structural properties of TMDs are similar to graphene. In addition to this, they exhibit some complementary properties and features which make them suitable for sensing applications. A typical example is the fabrication of electronic transistors. Although at room temperature graphene has remarkably high carrier mobility, it has poorly defined bandgap, which makes it difficult to turn off the transistors. Clearly, graphene in its pristine form is not suitable for fabricating logic

gates. On the contrary, many TMDs (such as MoS_2, $MoTe_2$ and WS_2) depict semiconducting behaviour, have a wide range of bandgap and are better suited for their use as electronic devices.

4.5.2 **MoS_2 based NO_2 gas sensors**

Among all TMDs materials, MoS_2 has got special attention for gas sensing applications. Its layered structure, high surface to volume ratio, scalability, high yield production, and cost-effectiveness make it special for gas sensing. The liquid exfoliation technique is emerging as an excellent approach for the synthesis of single or few-layered MoS_2. Furthermore, it is inherently suited for gas sensing applications owing to the introduction of a significant concentration of S vacancies in MoS_2 basal plane, which can be either functionalized via substitutional doping or behave as adsorption sites for target gases. N-Methyl Pyrrolidone (NMP) has emerged as the most suitable solvent to effectively exfoliate MoS_2. Also, MoS_2 is a natural reservoir of N atoms that can potentially dope the solute if the system is heated in the 150–200 °C temperature range and it can also play the role of doping agent, allowing to finely tune the response of MoS_2 to target gases [356,357].

MoS_2 has exceptional sensing properties but it also shows some limitations. A most serious issue with MoS_2 based sensor is its stability which is caused by fast oxidation of its top layer. MoS_2 is readily oxidized to MoO_3, which decreases the sensitively. In order to counter the oxidation problem, Lingmin et al. made hierarchical MoS_2 spheres like a 3D flower for NO_2 sensing (see Figure 4.28 (a) and (b) and (c)) [144]. They reported that MoS_2 flowers can remain stable for a long time as compared to MoS_2 films. Another advantage of using MoS_2 flowers is their porous nature which enhances the surface area and also provides additional channels for gas molecule absorption. The BET surface area of spheres like a 3D flower was found to be around 27.7 m^2/g (see Figure 4.28 (d)). The gas detection of as-developed flower-like MoS_2 for 50 ppm of NO_2 was done in variable temperature conditions (from 100 to 250 °C) to attain the optimum operating temperature. It was found that the maximum response of 78% was obtained at a temperature of 150 °C as depicted in Figure 4.29 (a). The MoS_2 sensor response curve towards NO_2 of 50 ppm is shown in Figure 4.29 (b) which shows that as-developed MoS_2 spheres act as a p-type semiconductor. The p-type behaviour is attributed to a reduction in sensor resistance on exposure to NO_2, where NO_2 behaves as the oxidizing gas. The dynamic sensing response of the sensor for

various concentrations of NO_2 (5–50 ppm) is depicted in Figure 4.29 (c), showing an increase in the sensitivity with increasing concentration of NO_2. The sensitivity and selectivity of the sensor for various gases are demonstrated in Figure 4.29 (d). Figure 4.29 (e) demonstrates good repeatability of the sensor response. The stability of the MoS_2 spheres like a 3D flower was checked for various days and the results as depicted in Figure 4.29 (f) indicate the high stability of the sensor. The adsorption of NO_2 as oxidizing gas molecules on the surface of MoS_2 led to large p-type doping of MoS_2, which significantly increases the conductance of MoS_2 [358,359].

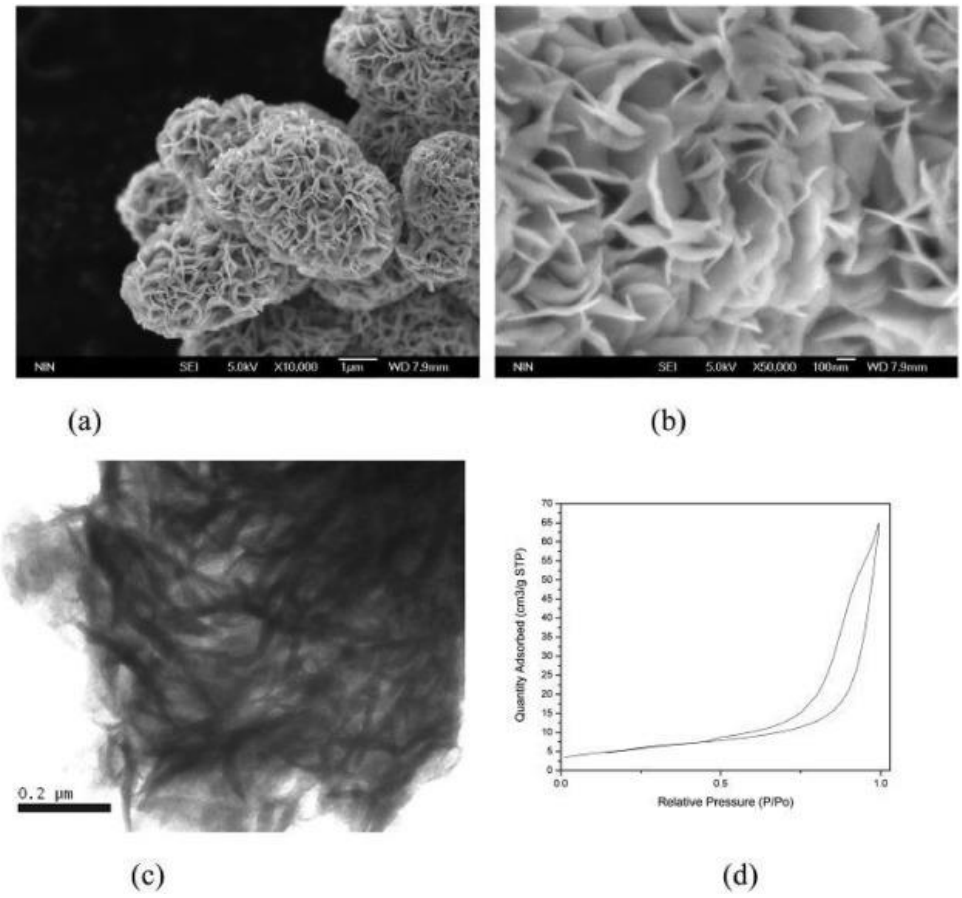

Figure 4. 28: (a) Low magnification SEM images of as-prepared MoS_2 spheres like 3D flower, (b) High magnification SEM photograph, (c) TEM photograph, (d) BET photograph. Copyright permission from Ref. [144].

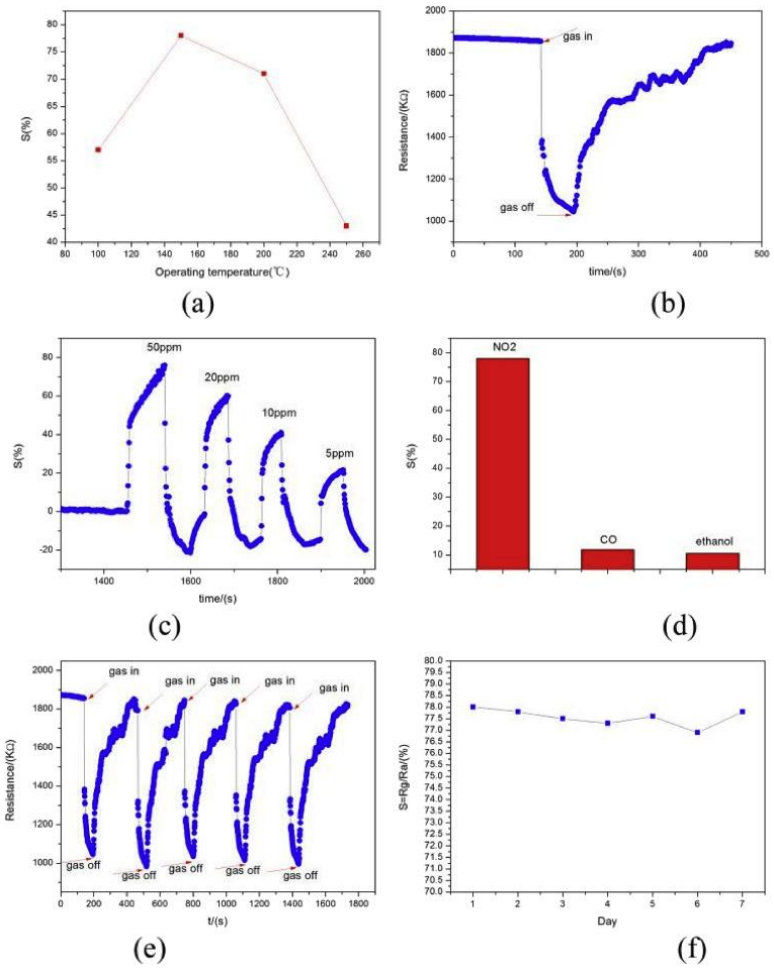

Figure 4. 29: (a) Temperature dependence study of 3D flower-like MoS_2 spheres, (b) The MoS_2 spheres like 3D flower acts like semiconductor of p-type, (c) Dynamic response for 5–50 ppm NO_2, (d) The sensitivity and selectivity analysis for various gases, (e) The repeatability analysis of MoS_2 spheres like 3D flower, (f) Stability analysis. Copyright permission from Ref. [144].

A unique technique was developed by Zeng et al., in which the surface morphology of the developed MoS_2 was tailored by changing the concentration of cetyltrimethyl ammonium bromide (CTAB) during hydrothermal treatment [146]. The hierarchical porous microspheres of MoS_2 exhibited good response and recovery properties along with high selectivity and reversibility. CTAB was found to play a very important role in deciding the morphology of resulting MoS_2. An increase in the concentration of CTAB was observed to create different shapes such as flowers, sheets and spheres. The perfect 3D spherical morphology of MoS_2 was obtained at an optimum concentration of 6 g/L. The process of adsorption and desorption of oxygen molecules on the surface of MoS_2 is responsible for gas sensing properties of the hierarchical 3D flower-like MoS_2

nanospheres. MoS_2 acts as n-type semiconductors such that in the presence of air, oxygen molecules adsorb on the surface of MoS_2 nanospheres and form ionic species (O^{2-}, O^-, O^{2-}) by capturing free electrons from the conduction band of MoS_2. This results in a decrease in the electrical conductivity or an increase in the resistance of the sensor. Oxidizing gases such as NO_2 with higher electrophilic properties capture electrons of MoS_2. Further, NO_2 also reacts with adsorbed oxygen ions to form NO_2^-. Hence the resistance of the gas sensor increases on exposure to NO_2. The authors achieved better gas sensing response in this work than some of the hybrid gas sensors as reported in Refs. [144,360,361].

The surface area can be improved in a hybrid structure. In this context, Bon-Cheol fabricated an extremely stretchable and transparent NO_2 gas detecting thin films using soft lithographic patterning on MoS_2-rGO composites [147]. A facile solution mixing process was used for preparing the MoS_2-rGO composite thin films. The composite thin film was spin-coated on the surface of the substrate followed by annealing in N_2 atmosphere for 1 h. A soft lithography technique was used for line patterning of hydrothermally reduced GO (rGO), and the MoS_2-rGO patterned composite thin films were again transferred on a PET substrate. The complete fabrication and patterning of MoS_2-rGO composite thin film are depicted in Figure 4.30. The MoS_2-rGO composite was prepared by mixing various concentrations of both MoS_2 and rGO. Sensing properties of different sensors with changing concentrations of both MoS_2 and rGO are shown in Figure 4.31. In comparison with pure rGO sensor, the sensitivity of MoS_2-rGO composite thin film towards NO_2 was 4 times higher. The electric characteristics of the MoS_2-rGO composite film sensor were maintained even when the sensor was bend about 70%. In comparison with pure rGO films, the sensitivity of the gas sensor developed on MoS_2-rGO composite film was found to be at least 300% more.

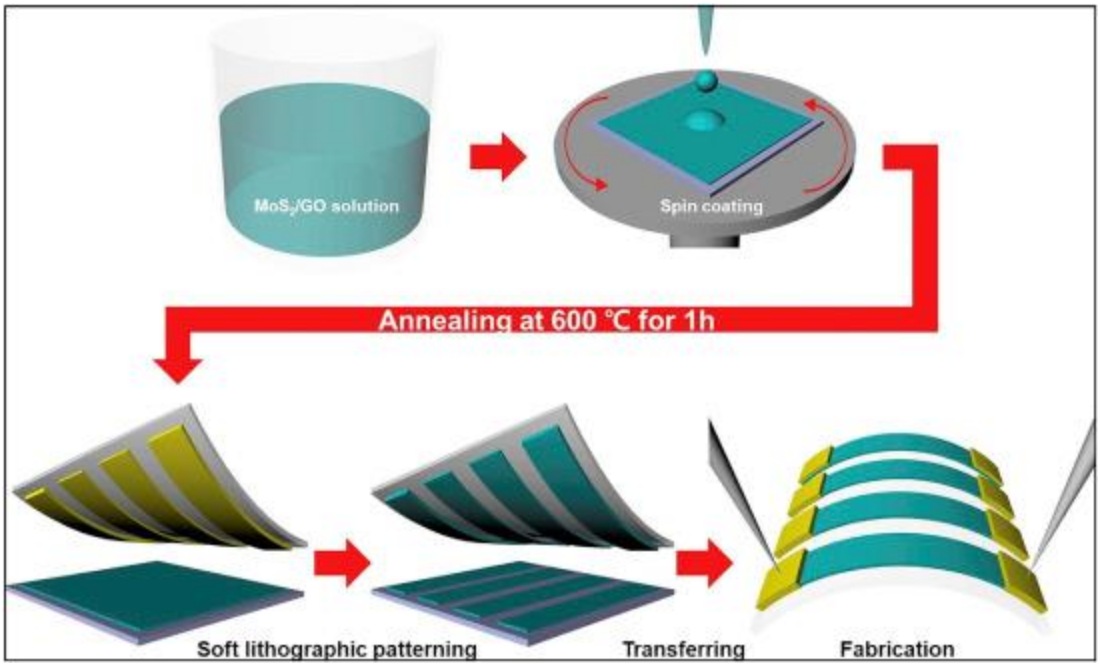

Figure 4. 30: The complete schematic diagram for the fabrication and patterning of MoS_2/rGO composites. Copyright permission from Ref. [147].

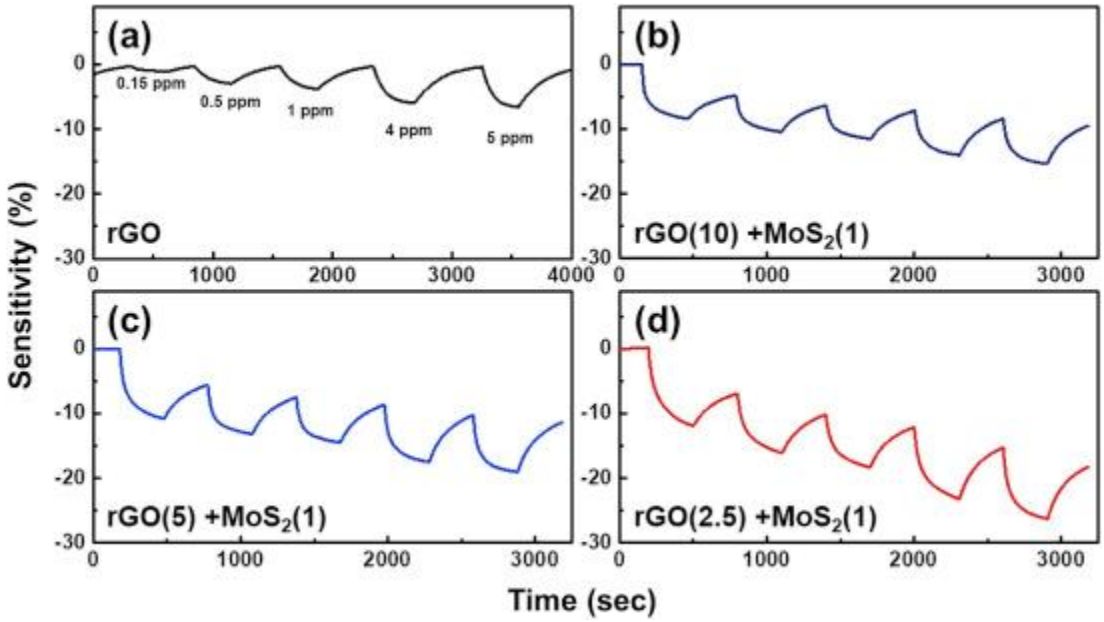

Figure 4. 31: Variations of characteristics pattern (a) rGO, (b) MoS_2/rGO (1:10), (c) MoS_2/rGO (1:5), (d) MoS_2/rGO (1:2.5) wiry film gas detector with NO_2 gas concentration. Copyright permission from Ref. [147].

Another way of obtaining a large surface area for a gas sensor is the development of vertically aligned nanostructures. Zhengcao et al. achieved highly enhanced NO_2 gas sensing performance using vertically aligned MoS_2/ZnO nanowires in the year 2018 [148]. The vertically aligned structure of MoS_2 nanosheets was produced by sulphurisation of Mo films predeposited by magnetic sputtering on hydrothermally synthesized ZnO nanowires. The dynamic response of the MoS_2–ZnO NWs sensor measured for 50 ppm of NO_2 gas with varying temperature is demonstrated in Figure 4.32 (a). It can be seen that the sensor repeatability at RT and 100 °C was zero while the sensor recovers 70–100% at 200 °C. This observation was also found for graphene-based sensors [362] and also in MoS_2 based sensors [363]. The sensing response as a function of gas concentration is depicted in Figure 4.32 (b). According to the response and recovery curves, the optimum operating temperature was found to be 200 °C. The comparative sensing response of pure MoS_2, ZnO NWs and MoS_2/ZnO nanowires at 200 °C is exhibited in Figure 4.32 (c). It was found that the sensing response of MoS_2/ZnO nanowires is superior to that of both MoS_2 and ZnO NWs. The response and repeatability of the MoS_2/ZnO nanowires sensor towards 50 ppm NO_2 are demonstrated in Figure 4.32 (d). The results show that in comparison to as-processed MoS_2 and ZnO NWs, the MoS_2/ZnO nanosheets demonstrated outstanding repeatability, recovery, selectivity, sensitivity, as a function of working temperature and also efficient to detect as low as 200 ppb of NO_2 gas.

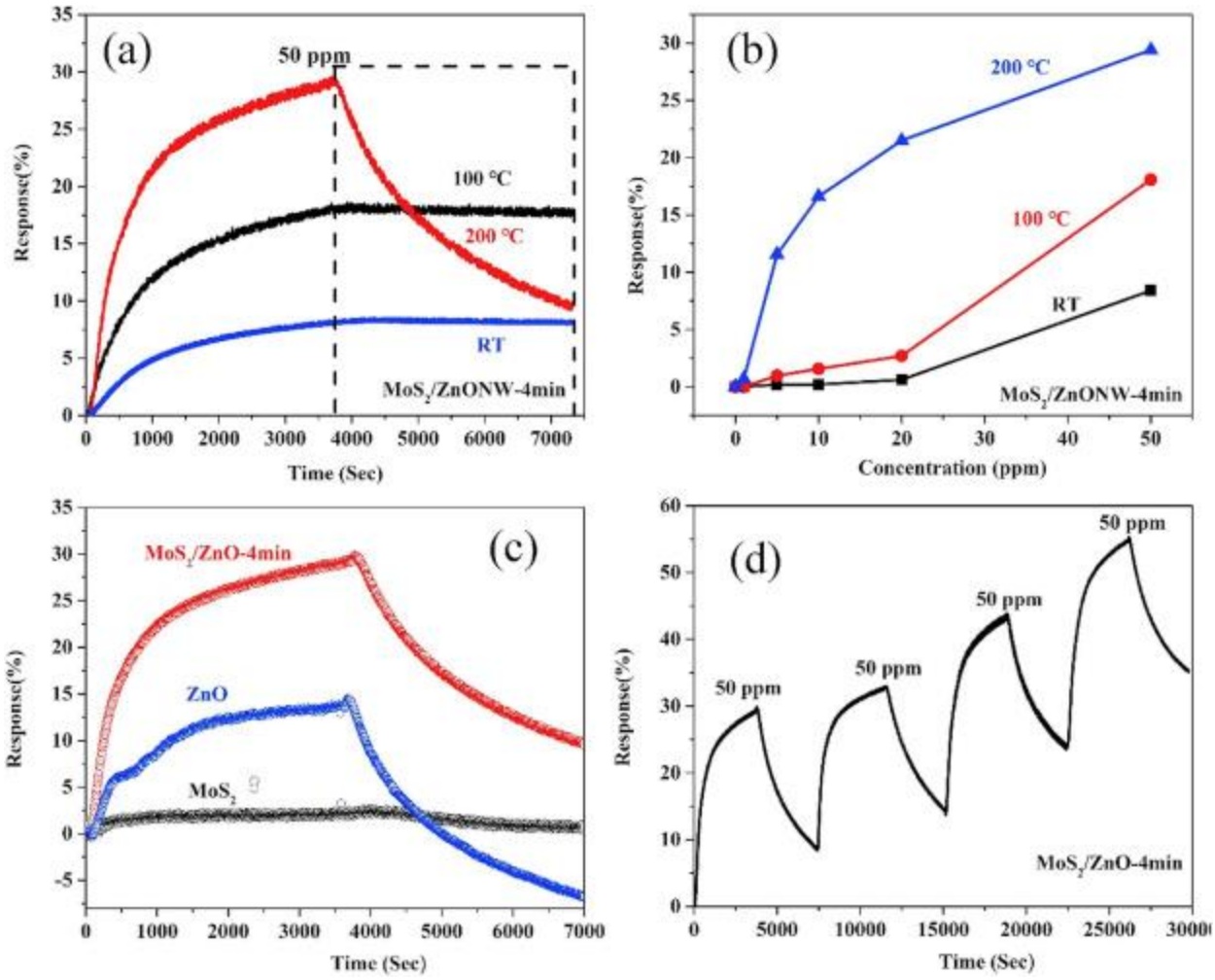

Figure 4. 32: (a) Dynamic sensing response of MoS_2/ZnO NWs nanostructures for the various temperature to 50 ppm of NO_2. (b) Sensor dynamic response as a function of gas concentration, (c) The sensing response comparison for pure MoS_2, ZnO NWs and MoS_2–ZnO nanowires at 200 °C, (d) The repeatability and response of MoS_2–ZnO nanowires sensor. Copyright permission from Ref. [148].

Donarelli et al. presented another way of changing the semiconducting behaviour of MoS_2 flakes by changing the annealing temperature. The chemically exfoliated MoS_2 based gas detector response was examined in the presence of NO_2 and other gases [149]. The chemical exfoliation of MoS_2 flakes was carried out in N-methyl pyrrolidone (NMP) followed by annealing at 150 °C or 250 °C in air. The formation of percolation paths in MoS_2 flakes as a result of interconnection between the sensing device and the electrodes is revealed by SEM analysis of the exfoliated MoS_2

flakes. The crystalline nature of the MoS_2 flakes before annealing confirmed by Raman spectroscopy while there were no appreciable bulk impurities in MoO_3 after annealing. Under the exposure of NO_2 gas, the detector processed with thermal annealing displayed a unique response of p-type. This behaviour can be attributed to nitrogen doping of "s" vacancies in MoS_2 surface, where the nitrogen atoms are possibly contributed by NMP during chemical exfoliation. The thermal annealing of sensor exhibits the n-type behaviour under exposure of NO_2. This behaviour can be attributed to significant existence of "s" vacancies in MoS_2 annealed flakes and to the surface coexistence of MoO_3 arising from the limited chemical exfoliation of the surface of the flake.

Yong's group, in 2017, developed a unique way of p-n junction tailoring and occupation modulation of sorption sites of rGO-MoS_2 nanocomposite for ultrasensitive sensing of NO_2 gas at a low operational temperature [360]. In his article, both rGO and rGO-MoS_2 hybrid thin-film sensors were fabricated for the detection of NO_2 gas at low operating temperature. The electrical response of both rGO and rGO/MoS_2 composite sensors exhibited p-type characteristic response as demonstrated in Figure 4.33 (a and b). The characteristic response of the rGO sensor is p-type because of the presence of oxygen and water doping [364]. The periodic tailoring of the p-n junction and occupation modulation of sorption sites can be attributed to the total resistance variation of the rGO-MoS_2 sensor during molecular desorption/adsorption process. When n-type MoS_2 is exposed to air, the surface adsorbed oxygen will capture electrons from its conduction band to generate oxygen anions (O_2^-), resulting in the formation of electron shell depletion region (EDR) on the surface. This results in the formation of the n-type semiconducting core region with low resistance and EDR with high resistance. Similarly, in the case of p-type semiconductors, the adsorbed oxygen anions from the hole accumulation region (HAR) with low resistance near the material surface owing to electrostatic interaction between oppositely charged species. The formation of p-n junction leads to an increase in the width of the space charge layer resulting in enhancement of sensor response and it is expected for rGO-MoS_2 junctions. The adsorption of NO_2 gas molecules creates NO_2^- through continuous recombinations from both MoS_2 and rGO. Hence both EDR and HAR would be continued, followed with both positive and negative influences on the resistance increase, respectively. The p-type response of rGO-MoS_2 is predominantly contributed by rGO. In the presence of 2 ppm of NO_2 gas, the sensing response of the rGO-MoS_2 composite sensor was found at an optimum temperature. In comparison with pure

rGO sensor, the response of the composite rGO-MoS_2 sensor is 200% higher as demonstrated in Figure 4.33 (c and d). In addition to sensitivity, other sensor parameters were also analyzed such as operating temperature, long term stability, humidity effect, selectivity, and detection limit of the rGO-MoS_2 composite sensor. The developed rGO-MoS_2 composite detector was able to detect NO_2 gas with a sensitivity of 59.8% which is 200% higher than pure rGO sensor and also the detection limit of the detector was found as 5.7 ppb.

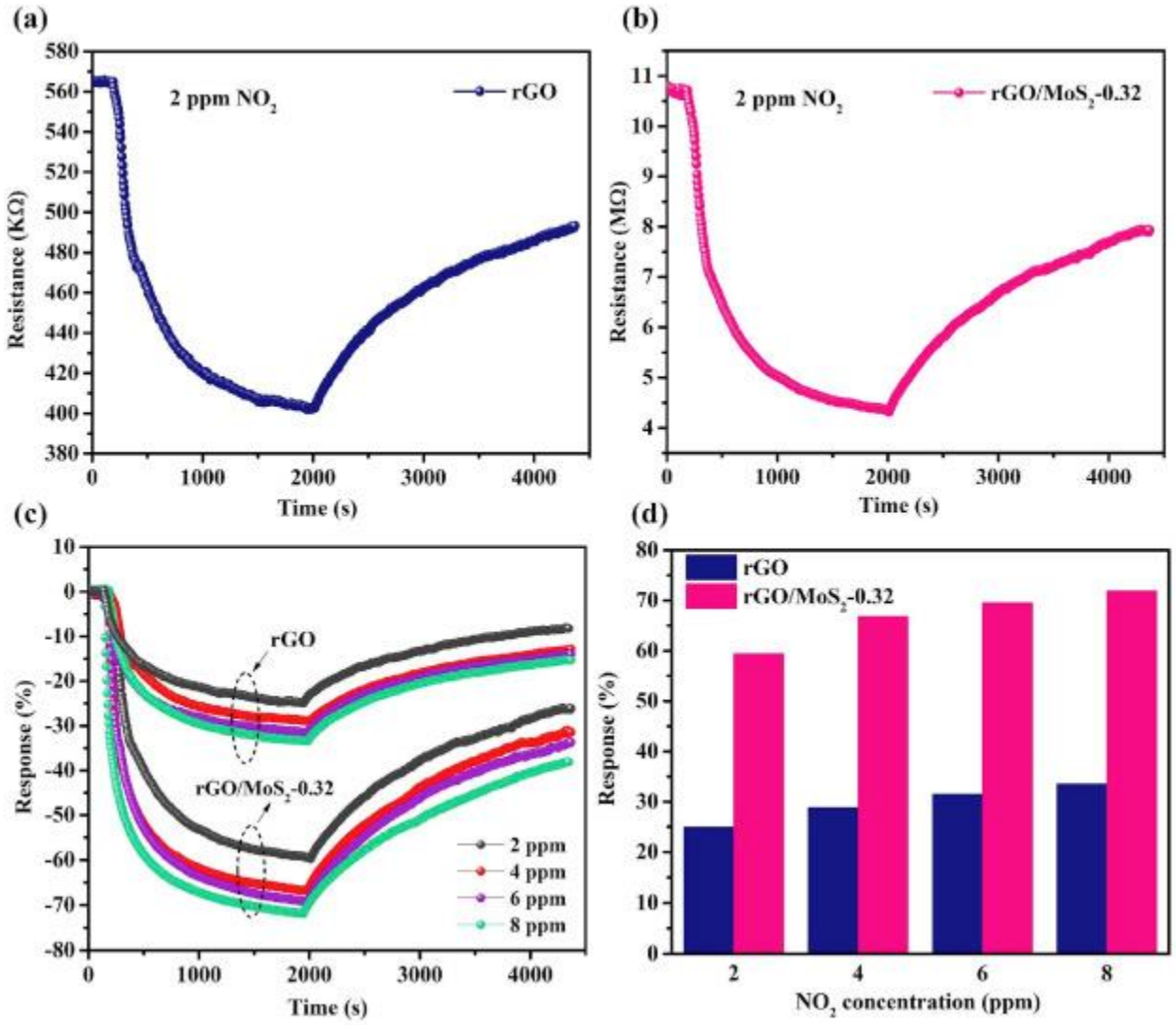

Figure 4. 33: (a) Dynamic resistance response of rGO sensor towards 2 ppm of NO_2 at 60 °C, (b) Dynamic resistance response of MoS_2 sensor towards 2 ppm of NO_2 at 60 °C, (c) Dynamic detecting response of the rGO-MoS_2 composite sensor, (d) Histogram of the sensing response of both rGO and rGO-MoS_2. Copyright permission from Ref. [360].

Sen developed another method for obtaining a high response with fast response and recovery of the sensor by increasing the operating temperature. A two-step wet-chemical method was used for fabricating NO_2 gas sensor by decorating rGO on the surface of MoS_2 NPs [188]. Firstly, a modified liquid exfoliation method was used for preparing MoS_2 NPs from the bulk MoS_2 powder. The self-assembly of MoS_2-NPs and GO sheets were employed for obtaining MoS_2-rGO hybrid sensor, followed by a hydrothermal treatment process. A certain number of functional groups still exists in rGO after the synthesis of rGO and MoS_2 using hydrothermal synthesis. Furthermore, some structural defects and vacancies can be introduced during this process, which can also act as adsorption sites for gas molecules. These sites can contribute electrons and holes to the hybrid structure of MoS_2-rGO and hence change the carrier concentration. The p-type rGO and n-type MoS_2 forms a p-n junction resulting in an increase in the sensing performance of the hybrid MoS_2-rGO sensor. The characteristics analysis revealed that the MoS_2 NPs with the size of 3–5 nm is consistently spread over rGO nanosheets. The MoS_2-rGO hybrid sensor was able to detect NO_2 gas even at RT. The typical response curve of the hybrid MoS_2-rGO sensor towards various NO_2 concentrations is shown in Figure 4.34 (a). The relationship between the NO_2 gas concentrations with the response is demonstrated in Figure 4.34 (b). The sensing response of the MoS_2-rGO hybrid detector was examined by elevating the operating temperature. It was found that with an increase in operating temperature, the MoS_2-rGO hybrid sensor shows improved response along with fast response and recovery.

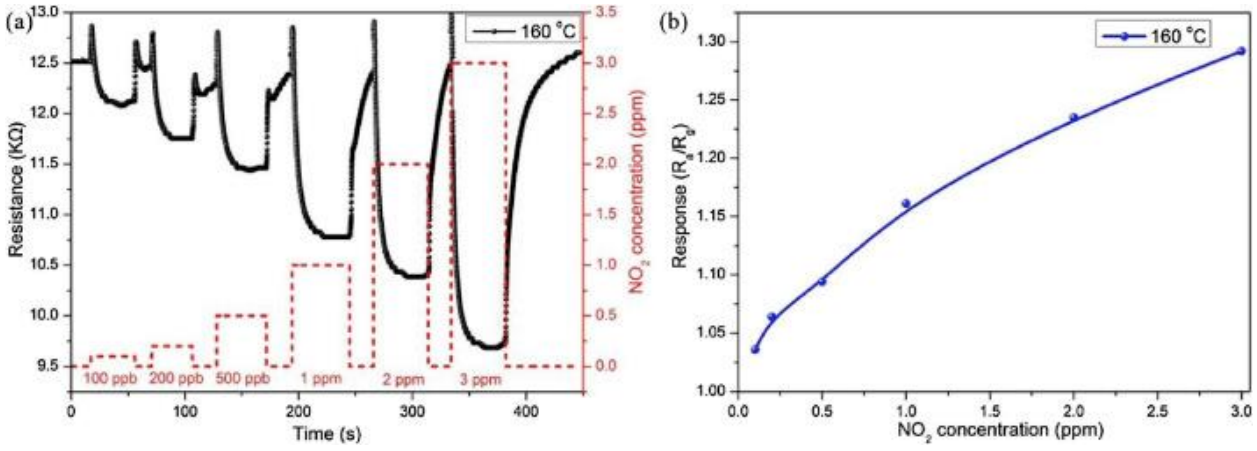

Figure 4. 34: (a) The typical response curve of the hybrid MoS_2-RGO sensor, (b) The relationship between the NO_2 gas concentrations with the response. Copyright permission from Ref. [188].

Recently in 2019, Hairong et al., developed the most efficient method of improving the performance of gas sensing by controlling the surface structure at the atomic scale. Hierarchical MoS_2 microspheres hollow structures were synthesized using a facile hydrothermal approach which offered enhanced NO_2 detection [189]. The active edge sites of MoS_2 were improved by the influx of micro-nano hierarchical design, which favours carrier exchange and increases the kinetics of gas adsorption, eventually resulting in improved sensing behaviour. In comparison to plane solid structure, the hierarchical hollow MoS_2 microspheres with added active sites exhibit outstanding detection capability with 3.1 times improvement. The formation of MoS_2 shell is followed by the nucleation on PS spheres surface facilitated by the polystyrene (PS) templates [see Figure 4.35(a)]. The hierarchical morphology is formed as the absorption continues and MoS_2 will nucleate and collect on the nanosheets shell surface [see Figure 4.35(b)]. To obtain hierarchical hollow spheres, annealing was done to vaporize the PS spheres template as shown in Figure 4.35(c). With increasing the reaction time, shell thickness, roughness of the surface and size of the sphere of spheres also increased. The nucleation of small spheres on the MoS_2 hollow spheres surface occurs and eventually with the reduction in surface energy results in the formation of solid spheres as the reaction time increases to 10 h [see Figure 4.35(d)]. The already nucleated small spheres of micrometre size start to grow and eventually separated from the hollow spheres as the time reaches 18 h [see Figure 4.35(e)]. The improvement in surface permeability, high surface area promotes gas diffusion, exchange and transportation of the hollow surface area can be associated with the nanosheets comprising the hierarchical micro-nano structure. Consequently, the sensor is capable of working at a lesser temperature with improvement in sensing response. The nanoscale and micro-level surface morphology can be controlled by the introduction of hierarchical structures thereby rendering new possibilities for improving the detection capability of MoS_2.

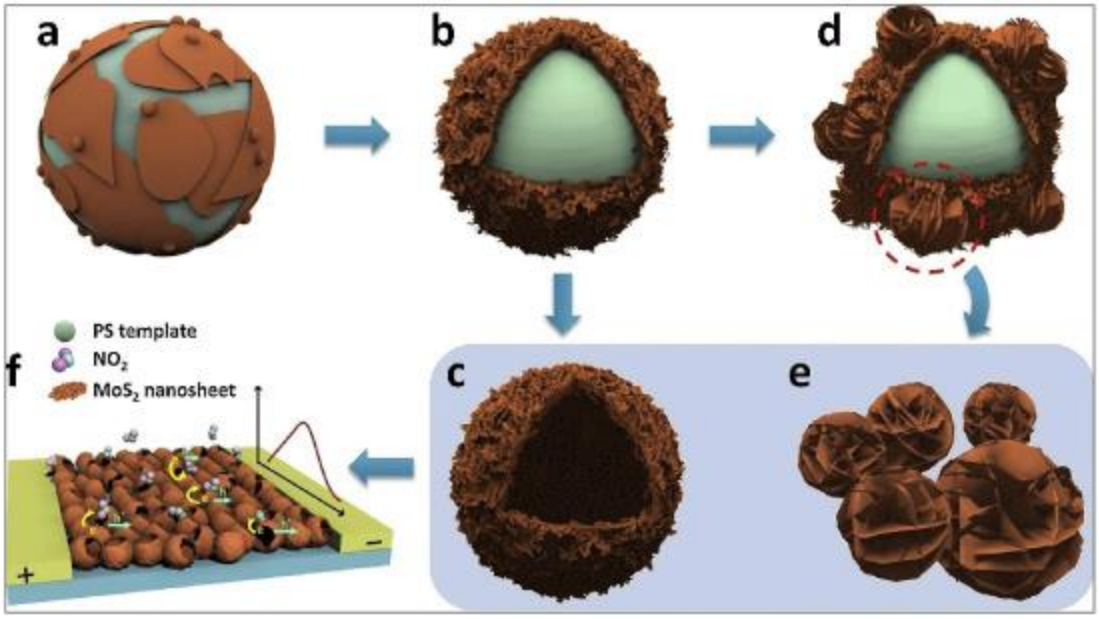

Figure 4. 35: (a) MoS_2 nanosheets nucleate on the PS template. (b) MoS_2 nanosheets nucleate and develop constantly. (c) The PS spheres template to form the hierarchical hollow spheres, (d) The surface energy reduces because small spheres start to nucleate on the MoS_2 hollow spheres surface and develop into solid spheres, (e) The small spheres grow to micrometre size and separate from the hollow spheres. Copyright permission from Ref. [189].

The change in the lateral grain size of MoS_2 is also found to improve the sensitivity of the sensor. Junmin et al. developed a high response resistive NO_2 gas sensor by employing a two-step CVD method for growing bilayer MoS_2 [190] [see Figure 4.36(a)]. The lateral grain size of the grown bilayer of MoS_2 was 50–100 μm. The response-recovery curve of the as-developed resistive MoS_2 bilayer at RT with varying adsorption of NO_2 is depicted in Figure 4.36(b). The response of as-synthesized bilayer MoS_2 resistive gas sensor as a function of NO_2 concentration is depicted in Figure 4.36(c). The response of the as-synthesized sensor to 50 ppm of NO_2, CH_4, O_2, NH_3, and H_2 at RT is demonstrated in Figure 4.36(d). The as-synthesized bilayer MoS_2 with high lateral grain size is associated with high surface mobility and increased surface evaporation. The developed resistive sensor showed p-type response and reached a super sensitivity at RT. The developed sensor has far better performance in comparison to various previous works [365,366]. The sensing mechanism of the as-developed p-type MoS_2 can be explained as follows. The initial exposure to air of p-type MoS_2 leads to the adsorption of oxygen molecules on the surface, taking away some electrons from the valence band leading to the formation of oxygen species (O_2^-, O^-).

This causes an increase in the hole concentration and a decrease in the resistance. The exposure of oxidizing NO_2 gas to the p-type MoS_2, NO_2 molecules were adsorbed on the surface as NO_2^- ions, which further extracted electrons from the valence band leading to an increase in hole concentration. The adsorption of NO_2 gas molecules leads to an accumulation of holes, resulting in the formation of the hole layer on the surface of MoS_2. The formation of the hole layer makes the p-type MoS_2 more conductive. When the supply of NO_2 gas is stopped and the p-type MoS_2 is exposed to air again, the adsorbed NO_2^-species evaporated leaving behind the captured electrons in p-type MoS_2. The following electron-hole recombination process resulted in a decrease in the hole concentration and an increase in the resistance. At the end of the electron-hole recombination process, the resistance of the p-type MoS_2 returned to the original value. Inversely, when the reducing gases NH_3, H_2, CH_4 are exposed to p-type MoS_2, the electrons chemisorbed by the oxygen species (O_2^-, O^-) were released back to the valence band of p-type MoS_2 and combined with holes in the valence band, resulting in the increase of resistance.

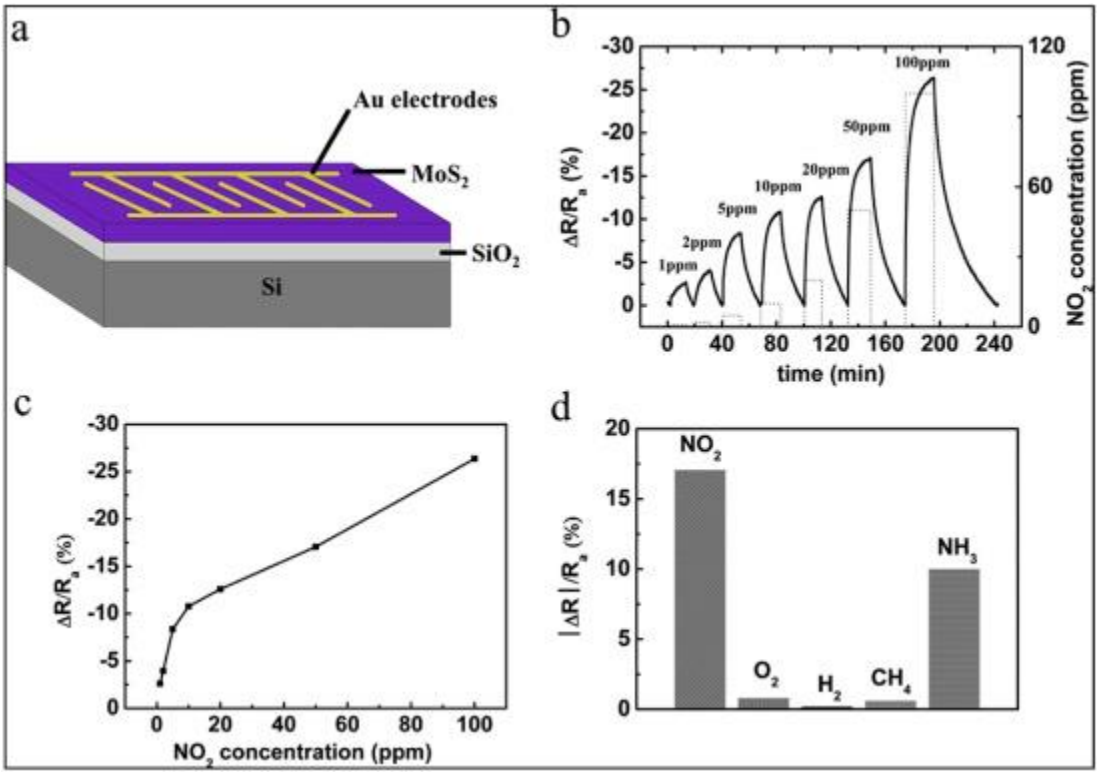

Figure 4. 36: (a) The schematic diagram of MoS_2 bilayer based resistive gas sensor, (b) The recovery-response curve of the as developed resistance MoS_2 bilayer at various concentrations of NO_2 at RT, (c) The response of as-synthesized bilayer of MoS_2 resistive gas sensor as a function

of NO_2 concentration, (d) The response of the as-synthesized sensor to 50 ppm of NO_2, CH_4, O2, NH_3, H_2 at RT. Copyright permission from Ref. [190]

Recently in 2019, Shaofeng et al., synthesized an extremely selective NO_2 gas sensor based on a novel rGO-MoS_2-CdS nanocomposite film by facile solvothermal treatment [191]. A new heterostructure is formed where CdS nanocones were grown on the 2D layered rGO-MoS_2 substrate by employing a facile solvothermal treatment. The developed hybrid nanocomposite of rGO-MoS_2-CdS displayed an exquisite selectivity towards NO_2 gas and this can be associated with the structural combination of MoS_2/CdS heterostructure on rGO layer. The detecting capability of the synthesized heterostructure rGO-MoS_2-CdS nanocomposite towards numerous concentrations of NO_2 gas has been analyzed. The three different nanocomposites response towards various concentrations, i.e., 0.1–11 ppm of NO_2 is depicted in Figure 4.37(b). In all concentration ranges, the repeatability of the sensor was very good. Three different nanocomposite rGO-MoS_2-CdS-a, rGO-MoS_2-CdS-b, rGO-MoS_2-CdS-c sensors with different concentrations of CdS were obtained by solvothermal treatment at 120 °C for 6 h, 12 h and 24 h, respectively. In the solvothermal treatment, increase in time from 6 h to 12 h leads to the homogeneous dispersion of CdS nanocones on the surface of rGO-MoS_2 and hence the formation of more p-n junctions. The sensing response of nanocomposite rGO-MoS_2-CdS-b increased from 10.3% to 25.7% for the same concentrations of NO_2 gas as depicted in Figure 4.37(c). However, the increase in time of solvothermal treatment results in the formation of many hemispheres composed of nanocones and the sensitivity decreases from 25.7% to 16.1%. The nanocomposite sensor before and after NO_2 exposure is depicted in Figure 4.37(a). In comparison with other rGO based sensor, the nanocomposite rGO-MoS_2-CdS with lots of heterojunctions, higher specific surface area and more adsorption sites showed an excellent response of 25.7% in the presence of 0.2 ppm of NO_2. Moreover, the hybrid detector depicted an outstanding gas detecting constancy at the operating temperature of 75 °C. This enhanced gas sensing has been explained on the basis of an assumption that O_2^- and NO_2^- formation takes place on the surface of nanocomposite films. The electron shell depletion region is formed on the surface when nanocomposite film is exposed to air, as surface adsorbed oxygen will capture electrons from the conduction band of CdS and MoS_2, forming oxygen anions (O_2^-). This process is responsible for the formation of n-type MoS_2/CdS electron shell depletion region. In the case of rGO, adsorbed oxygen anions cause hole accumulation near the surface of sensing material owing to the electrostatic interaction between opposite charge species. The interaction of

NO_2 to rGO is weak and hence NO_2 would be preferentially adsorbed onto the rGO/MoS_2/CdS heterojunctions. The NO_2 molecules adsorption takes place in the form of NO_2^-, and electrons are continuously withdrawn from rGO/MoS_2/CdS heterojunctions.

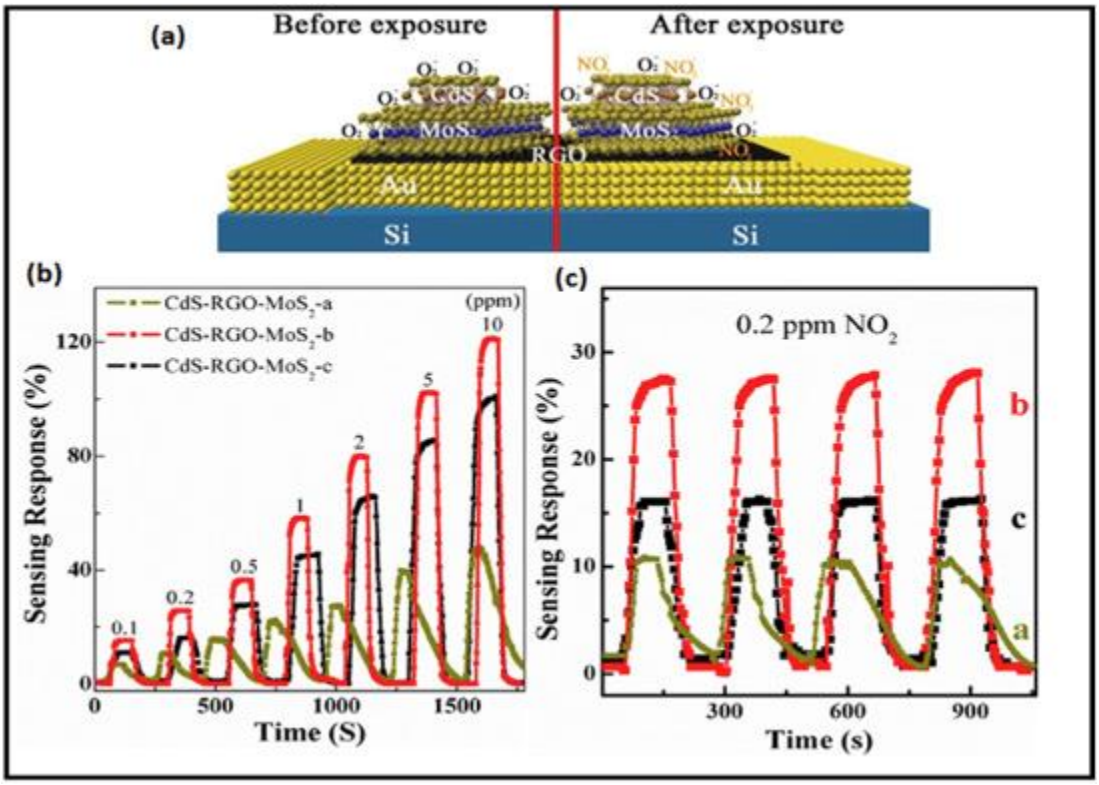

Figure 4. 37: (a) The nanocomposite sensor before and after NO_2 exposure, (b) The three different nanocomposites response towards various concentrations 0.1–11 ppm of NO_2, (c) The sensing response of the three-nanocomposite sensor for same 0.2 ppm of NO_2 gas. Copyright permission from Ref. [191].

In the same year 2019, Zhong et al., employed piezo-phototronic effects and photogating for obtaining single-layer MoS_2 for an enhanced NO_2 gas sensing [192]. The authors irradiated the sensor with a red light-emitting diode (LED) and compared the sensor response in light and dark conditions. The sensor response was also compared by in tensile strain and no strain conditions. In this article [364], an individual layer MoS_2 based NO_2 gas detector with simple and reliable flexibility is presented. The 2D semiconductor characteristics and the ultra-high specific surface area are attributed to the high sensitivity of flexible sensor towards NO_2 gas. The as-developed single-layer MoS_2 sensor showed better performance in terms of sensitivity, recovery and response towards NO_2 as compared to different works done on single-layer MoS_2 [359, 367]. The surface charge transfer in the direct bandgap of ultrathin Schottky contacts of MoS_2, photo electricity and

also coupling among piezoelectricity can be associated with the sensitivity modulation of the flexible NO_2 sensor.

The enhanced sensitivity and selectivity of the sensor can be achieved by a suitable combination of large active edge sites with a large surface area. Kumar et al. have developed a one-dimensional MoS_2 nanowire network (NW) for enhanced NO_2 gas sensing [193]. The one-dimensional MoS_2 NW network was obtained by using controlled turbulent vapor flow from the chemical transport reaction. At different temperatures, the sensing behaviours of the developed MoS_2 NW network were investigated in the presence of discrete molarity of NO_2. The MoS_2 NW network sensor demonstrated 2-fold enhanced sensitivity for NO_2 at 60 °C in comparison with sensitivity at RT and also a very low detection limit. The recovery and response time for the MoS_2 NW network sensor was 172 s and 16 s, respectively at 60 °C while the sensitivity of the sensor deteriorated at 120 °C. The enhanced sensitivity and selectivity towards NO_2 gas can be associated to a combination of the large surface area along with sufficient active edge sites and calibration of the high voltage barrier at the junction of nanowires during adsorption and desorption of gas molecules. The sensing mechanism of the developed MoS_2 nanowire sensor can be attributed to a change in carrier concentration of MoS_2 owing to chemisorption or physisorption or both, of gaseous molecules. The two factors which are responsible for the variation in the carrier concentrations are the active site density at the surface of MoS_2 and the behaviour (reducing or oxidizing) of gases. At RT both humidity and oxygen occupy a large number of active sites, thereby extracting electrons from the exposed sites of S edge ($\bar{1}010$) and Mo edge ($10\bar{1}0$) of the MoS_2 nanowires. Also, due to high vacancy density of the MoS_2 nanowires oxygen is chemisorbed on the sulfur vacancy. This results in a decrease in the concentration of electrons and the creation of the depletion layer. Thus, due to the presence of oxygen and humidity on the surface of MoS_2 nanowires, a smaller number of active sites are available for NO_2 gas molecules adsorption, resulting in a reduction in the response of sensor at RT. Annealing of the device at 60 °C leads to desorption of both humidity and oxygen gas molecules, resulting in the availability of a large number of active sites and electron concentration in MoS_2 nanowires.

Furthermore, Yong et al. developed a unique UV light stimulated room temperature NO_2 gas sensor based on few-layered MoS_2 film decorated with Au nanoparticles [194]. Under dark conditions, MoS_2 sensor in comparison to the as-processed MoS_2–Au depicted a response of 10%

in the presence of 2.5 ppm NO_2 which is two times more. The increase in the sensitivity of MoS_2–Au can be attributed to the increase in the reaction sites because of the interfaces and spillover effect and smaller baseline effect due to Au decoration. Incomplete recovery was obtained for all the sensors. The MoS_2–Au based NO_2 sensor under the illumination of UV light depicted three times better response, favourable repeatability and full recovery was accomplished in contrast with the absence of UV light conditions. Two conditions cause the above event. One of the conditions is the effective charge separation at MoS_2–Au interface resulting in repeatable and reversible reactions. The second condition is the additional photo introduced charge carriers which ensure adequate solid-gas interaction between target gas molecules and sensing layer. The author was able to achieve room temperature, UV light assisted, sensitive, reversible and highly selective NO_2 gas sensing based on a few layers of MoS_2–Au nanocomposites serving as sensing layer.

The major challenge regarding sensors based on MoS_2 is that the sensor suffers from long recovery and response time, specifically at room temperature. Kumar et al. developed the photo-activated extremely reversible and quick sensing of NO_2 at RT by employing improved p-MoS_2 flakes with blend in edge and plane [368]. The detector depicted a fast response with a sensitivity of about 10.6% for 10 ppm NO_2 without complete recovery. However, full recovery was achieved by UV light illumination at RT. The UV aided NO_2 sensing showed enhanced sensing in terms of fast recovery and response with increased sensitivity towards 10 ppm NO_2 at room temperature.

In the year 2018, Yang et al. fabricated a hetero-nanostructure of MoS_2/ZnO for enhanced NO_2 gas detection at room temperature (RT) [198]. Hetero-structure fabrication is an impressive approach to alter the electronic behaviour of intrinsic MoS_2 nanosheets, thereby accomplishing high sensitivity and outstanding recovery properties. A simple wet chemical method was employed to fabricate a novel p-n hetero-nanostructure on MoS_2 nanosheets using surface modification. The surface modification of MoS_2 with nanoparticles of zinc oxide (ZnO NPs) results in the formation of hetero-nanostructure of MoS_2/ZnO which is capable of outstanding performance of 3050% to 5 ppm NO_2, which is eleven-fold more than that for pure MoS_2 NPs sensor. The hetero-nanostructures of MoS_2/ZnO exhibit p-type characteristics, which shows that the major charge carriers are MoS_2 NSs and ZnO NPs act as active decorations. In case of pristine p-type MoS_2 NSs, the defects on the surface of MoS_2 act as active sites for NO_2 gas molecules. The response and recovery are slow due to the defect dominated process owing to high adsorption energy. During

the sensing process, the electrophilic NO_2 molecules capture electrons from the conduction band of MoS_2, leading to an increase in the conductivity of the sensor. The as-developed hetero-nanostructure is capable of more than 90% recovery at RT. Also, the sensor possesses a very fast response time of the 40 s, great stability, outstanding selectivity and lower detection limit of 50 ppb. The as-developed MoS_2/ZnO hetero-nanostructure showed better performance in comparison with many previously reported articles [144,149,369].

In the same year, Kumar et al. employed a controlled vapor transport process for obtaining hybrid microflower of MoS_2–MoO_3 for an efficient gas sensing at RT [199]. Various characterization techniques were used for studying crystal structure and morphology of the developed hybrid micro flower. The hybrid micro flower analysis with a cathodoluminescence mapping revealed that the flower petals, as well as nanosheets, are composed of MoS_2 while the core of micro flower comprises of MoO_3. Without any external stimulus (like thermal or optical), the hybrid MoS_2–MoO_3 sensor exhibited a sensitivity of 33.6% towards 10 ppm NO_2 gas with complete recovery at RT. In comparison with various earlier reports on MoS_2, the as-developed MoS_2–MoO_3 sensor showed a low response time of 19 s with total recovery and an outstanding selectivity towards NO_2 against different other gases at room temperature. The sensing mechanism is associated with a build-up of modulation of a potential barrier at the interface of MoS_2–MoO_3 during desorption/adsorption of NO_2 and high hole injection from MoO_3 to MoS_2. Also, this article demonstrates that by controlling the micro and nanostructures the properties of 2D materials can be altered toward utilization in modern electronics. Energy band diagram is used to explain the sensing mechanism of MoS_2–MoO_3 hybrid. The work function of MoO_3 and MoS_2 are 5.3 and 4.7 eV, respectively. This energy offset band of 0.6 eV forms a potential barrier and leads to efficient electron-hole separation at the n-MoS_2/n-MoO_3 junction. The potential barrier at the n-n heterojunction plays an important role in the modulation of the conduction channel width that is essentially responsible for the fluctuation of the device resistance.

It was found that at room temperature, in comparison to horizontally aligned MoS_2 flakes, the vertically aligned (VA) MoS_2 flakes exhibited two times higher response to NO_2. Kumar et al., developed the VA-MoS_2 flakes network-based highly sensitive and reversible NO_2 resistive gas sensor [200]. A kinetically restrained fast growth approach of CVD process was used for synthesizing vertically and horizontally aligned MoS_2 flakes on SiO_2/Si substrate. At an optimized

operating temperature (100 °C), the detector depicted complete recovery upon NO_2 exposure. The sensing behaviour of VA-MoS_2 sensor was studied for various gases such as CO_2, H_2S, NH_3, CH_4 and H_2. The VA-MoS_2 sensor exhibited great selectivity towards NO_2 gas with a high response as well as good reversibility. These responses can be associated with the large aspect ratio, high adsorption energy on exposed edge sites, strong interaction between gas molecules and the exposed edge sites at the interface.

4.5.3 **Miscellaneous TMDs based NO_2 gas sensors**

Tingting et al. introduced a new material for NO_2 gas sensing, i.e. WS_2 nanosheets. The developed resistive gas sensor based on WS_2 demonstrated a p-type behaviour and the sensor was able to achieve a superior response of about 9.3% for 0.1 ppm NO_2 at room temperature. The detector showed superb stability in low and moderate humidity. The increase in the sensitivity of WS_2 gas sensor towards NO_2 gas can be attributed to the rough surface and ultrathin nanostructure of WS_2 nanosheets. Hydrothermal and calcination processes were employed for developing ultra-thin WS_2 nanosheets for ultra-high sensing response of NO_2 gas [187]. A thickness of about 5 nm of ultra-thin WS_2 nanosheets was achieved by employing cost-effective hydrothermal approach followed by calcination technique. The interconnection of WS_2 nanosheets led to the formation of a three-dimensional wall like the design. The typical response-recovery characteristics demonstrated that in the presence of NO_2, the resistance decreases rapidly, and the response of the gas detector elevated with NO_2 concentration as depicted in Figure 4.38(a). With varying the concentration of NO_2, the corresponding responses also changed significantly. The relationship between the gas sensing response and concentration of NO_2 gas is depicted in Figure 4.38(b). The repeatability of the gas sensor towards 5 ppm NO_2 gas is demonstrated in Figure 4.38(c). The response of WS_2 sensor in this work is better as compared to the previous works [190,370]. The cycling response for 5 ppm NO_2 shows no decline in sensor response for five cycles, thus, substantiating good repeatability of WS_2 detector.

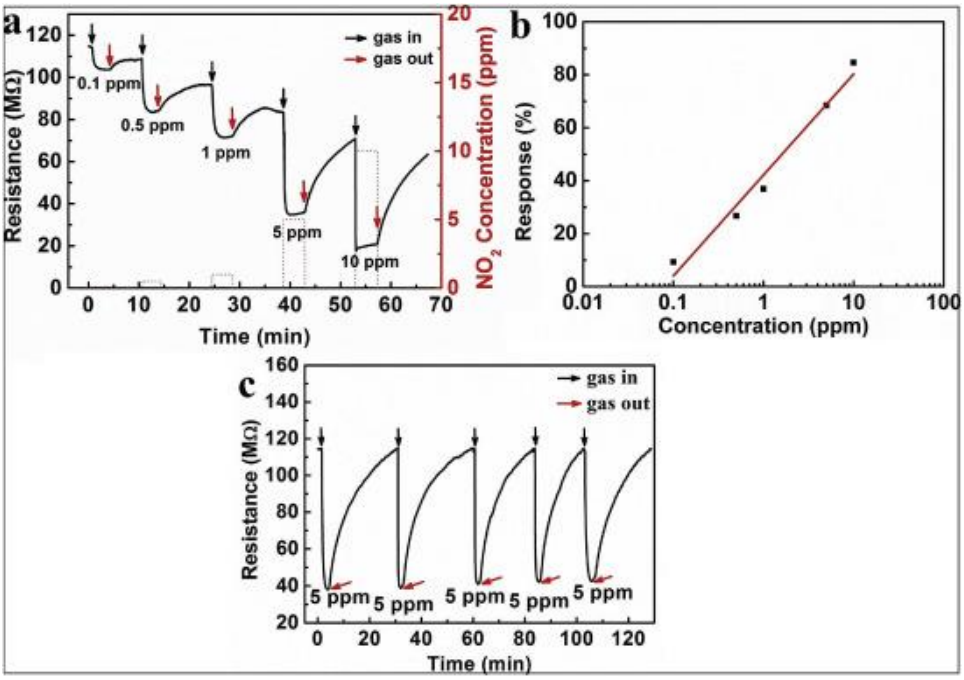

Figure 4. 38: (a) The typical response-recovery curve with various concentration of NO_2, (b) The relation between response and concentration of NO_2, (c) The repeatability of the WS_2 gas sensor in the presence of 5 ppm of NO_2. Copyright permission from Ref. [187].

In the year 2018, Roya et al. proposed unique structures of WS_2/graphene aerogel hybrid to enhance the selectivity of NO_2 gas detection. They investigated the influence of temperature and ambient humidity on the NO_2 detecting tendency of WS_2/graphene sensor [145]. Two electrodes were microfabricated on the surface of WS_2/graphene hybrid aerogel in order to probe its gas detecting performance. The characterization of hybrid WS_2/graphene aerogel composite establishes the existence of both graphene and WS_2. The continuous 3D nanostructure material deposited on sensor material is established. Also, it has been confirmed that in hybrid aerogel composite, WS_2 and graphene are distinguished by lattice spacing indicating WS_2 is one to five-layered and graphene being one to six-layered. At room temperature, with an increase in humidity, sensing response and recovery towards NO_2 gas also increase. In a dry atmosphere, with an increase in temperature till 180 °C, recovery and response rates also increase, and signal recovery is enhanced, however, signal feedback is decreased. The hybrid WS_2/graphene aerogel composite sensor showed excellent selectivity towards NO_2.

Alexander et al. fabricated gold decorated WS_2 nanotube photoresistive sensor for NO_2 gas detection [371]. An aqueous solution of $HAuCl_4$ was used to prepare a composite of gold nanoparticles (AuNPs) and WS_2 nanotubes. Plasmonic features of the obtained nanocomposites were confirmed with the help of electron energy loss spectroscopy in scanning transmission electron microscopy regime (STEM-EELS) and Optical extinction spectroscopy. It was found that at room temperature the NT-WS_2 and Au-NT-WS_2 depicted a remarkable sensitivity towards NO_2 under illumination from 530 nm light-emitting diode. In the range of 0.25–2.0 ppm of NO_2, the Au-NT-WS_2 nanocomposites sensor exhibited an enhanced sensitivity and higher photo-response as compared to pristine NT-WS_2.

Yongxiang et al. developed SnS_2 based wireless gas sensor which demonstrates extreme selectivity towards NO_2 gas. For fabricating sensor, they used a low temperature co-fired ceramic technique (LTCC) and a resonant antenna circuit [372]. The sensor structure designed as LC were both IDC (C_s) and a planar square spiral inductor (L_s) integrated on LTCC structure. A resonant circuit was obtained by connecting both capacitor and inductor into LTCC body. In order to determine the resistance of the LC sensor through physisorption-based charge transfer and polarization effect after NO_2 adsorption, a sensitive film of 2D SnS_2 was laminated on the IDC electrodes. The highly selective and sensitive behaviour of 2D material SnS_2 towards NO_2 gas makes it a suitable material for sensing film. A comprehensive analysis of the developed wireless sensing mechanism was done for NO_2 gas. The variation in the resistance and dielectric properties of the sensing film is attributed to the physisorption based interaction between 2D SnS_2 surface and NO_2 gas, influencing the physical response of the LC antenna sensor which is in complete agreement with previous work [373]. Investigations under the influence of various concentrations of NO_2 at different temperatures found the wireless gas sensor to exhibit the highest response at 120 °C with a low detection limit of 0.6 ppm. In the wireless gas sensing and analysis, the developed sensor could be very useful as it has good response and response profiles. Moreover, this work also demonstrated the feasibility of integrating various other sensitive materials on LTCC platform for various gas species.

Khan et al. developed an extremely selective and ultra-sensitive NO_2 gas detector employing quasi physisorption 2D tungsten oxide (WO_3) [374]. The first step of the analysis was to find out an optimum temperature which gives a maximum response with fast response and

recovery. It was found that the rise in temperature boosted the sensor response, but recovery and response times decreased. The optimum temperature for the developed sensor was found to be 150 °C as with the further increase in temperature the response decreases. The reason for this behaviour can be interpreted by the fact that at higher temperatures, the rate of adsorption becomes less than the rate of desorption and consequently the response decreases [375]. Two samples heated at 450 °C and 225 °C give a response factor of ~4 and ~15, respectively at 20 ppb of NO_2 gas concentration. The reversibility of both sensors was excellent as both sensors recovered their baselines fully. However, recovery of the sensor heated at 225 °C was faster in comparison to the sensor heated at 450 °C. The NO_2 gas molecules adsorbed on surface act as an electron acceptor and accept electrons from WO_3 [373]. Owing to the charge transfer mechanism, the number of free electrons is reduced and the resistance increases, which is the n-type behaviour. The increase in sensitivity of the sensor annealed at 225 °C can be accredited to the better synergy between NO_2 gas molecules and stronger dipole material WO_3. The semiconducting nature of 2D sheets of WO_3 annealed at 225 °C have been established by XPS analysis. However, the sample annealed at 450 °C and the unannealed sample showed metallic behaviour and hence require more electrons for full-on/off switching. The other reason in case of unannealed is sample hydration while in case of the sample heated at 450 °C is not a fully monoclinic structure of the sample. In the case of the sample heated at 225 °C, a combination of semiconducting nature, hydration, degraded oxygen vacancies and monoclinic crystal structure is responsible for higher selectivity and sensitivity towards NO_2 gas.

The 2D transition metal dichalcogenides (TMDs) based sensor performance for sensing NO_2 gas has been discussed. These sensors are more durable and convenient in terms of methods of preparation, structure, materials used, the concentration of NO_2 gas, response and recovery times, and operating temperature. Numerous samples and progress in the development of NO_2 based gas sensors using TMD nanostructures and its hybrid have been enumerated in Table 4.2.

4.6 Metal-oxide based nanostructures

A detailed research on sensing applications based on metal oxides have shown that the sensing phenomenon is very complicated and it depends on many parameters of metal oxides such as thickness, porosity, grain size, catalytic reactivity, grain network, agglomerations, bulk

conductivity, surface stoichiometry, surface architecture, bandgap and so on [143,376,377,378,379]. Analysis of gas sensors based on metal oxides has shown that there is a great influence of above-mentioned factors on gas sensing behaviour of the developed sensors. With respect to the above-mentioned parameters, the optimization of gas sensors has been achieved by applying many technological approaches [195]. It has been shown that all the important properties of metal oxides for gas sensing applications can be really influenced by the control of the deposition parameters, doping during synthesis or deposition and post-deposition treatments.

4.6.1 **ZnO nanowire based NO_2 gas sensors**

ZnO has may shape and structural forms under various growth conditions. Wurtzite is thermodynamically the most favoured form of ZnO under ambient conditions. Oxides of Zinc, Tin, Titanium, etc., are usually used in metal oxide-based semiconductor sensors as sensing element. Moreover, nanostructured metal oxides are promising candidates as a gas sensor due to their large surface-to-volume ratio which is more desirable for the diffusion of target gases in sensor material.

A highly selective NO_2 gas sensor with fast response and recovery and high sensitivity was developed using ZnO nanowires (ZNW) array [204]. A seed layer deposition technique was used for preparing arrays of ZNW on the surface of the detection electrode. A facile hydrothermal route was followed by Shen et al. for developing arrays of ZNW in-situ grown on detecting electrode for NO_2 gas detection [204]. In seed growth system, a Zn $(CH_3COO)_2 \cdot 2H_2O$ ethanol solution was used with Zn $(NO_3)_2 \cdot 6H_2O$-HMTA ($C_6H_{12}N_4$) as a hydrothermal route in a dipping process. The gas detecting response of the ZNW arrays revealed that the detector had good selectivity and reproducibility, as well as the response of the sensor, showed a linear dependence on NO_2 concentration in 1–30 ppm range. The ZNW array sensor was highly selective to NO_2 with fast recovery time, fast response and high sensitivity. At the optimum temperature of 200 °C, the ZNW array sensor showed a maximum response towards 3.3–5 ppm of NO_2 gas with fast recovery and response times of 21 s and 25 s, respectively. The developed ZNW array by facile hydrothermal route is favourable for commercial applications. The electron depletion theory is used for explaining the sensing mechanism of ZNW arrays to NO_2. The oxygen molecules are adsorbed on the surface of ZNW arrays when exposed to air. These oxygen molecules then capture electrons from the conduction band of ZNW and transform into ionic species (O^{2-}, O^-, O_2^-). This electron

transfer forms an electron depletion region on the surface of ZNW arrays. Hence the resistance of the ZNW arrays is increased as major charge carriers in n-type ZnO semiconductor are electrons. When NO_2 molecules adsorb on ZnO nanowires surface, they continuously capture electrons from the conduction band. This is because the electron affinity of the NO_2 gas is higher than oxygen. In this way, the concentration of electrons in the conduction band decreases drastically, resulting in the larger electron depletion region and higher resistance. Upon NO_2 desorption, the resistance of ZNW arrays returns to its initial value.

In the following year 2018, Cui et al. developed a unique and path-breaking technique to reduce the operating temperature of metal oxide-based NO_2 gas sensors [205]. A three-step facile process was used for preparing two different structures, i.e., ZnO–CuO NWs (ZnO nanowires decorated with CuO nanoparticles) and nanowires of ZnO–CuO core-shell (C–S NWs). The response for both reducing gas benzene and oxidizing gas NO_2 were analyzed. Heterostructures of ZnO–CuO were obtained by a thermal oxidation process from heterostructure of ZnO–Cu C–S NWs in the temperature ranges from 300 to 600 °C for 1 h. The heterostructures of ZnO–CuO were investigated by FESEM in the presence of various oxidizing conditions. The top layer is the ZnO–CuO heterostructures; the middle layer is the ITO film, and the bottom layer is the glass substrate. Thermal oxidation at a relatively low temperature of around 300 and 400 °C maintains the C–S structures of NWs while thermal oxidation at higher temperatures of around 500 and 600 °C reduces the roughness of the sample which is mainly attributed to the increase in the crystallinity of CuO at higher temperatures. At higher temperatures (500 °C & 600 °C), the C–S composition changed to nanoparticles named as ZnO–CuO NWs. The optimum operating temperature in the presence of benzene for ZnO–CuO C–S NWs was 250 °C while for an oxidizing gas like NO_2, it was around 300 °C for ZnO–CuO NWs and 350 °C for ZnO NWs. The p-type response of ZnO–CuO NWs indicates that ZnO NWs influence carrier transportation within the sensing layer. On the other hand, ZnO–CuO C–S NWs demonstrate n-type behaviour indicating the dominance of CuO shell in sensing performance. In conclusion, it was found that ZnO–CuO NWs and pure ZnO NWs show increased sensing performance while ZnO–CuO C–S NWs exhibit poor sensing behaviour.

For increasing the response of NO_2 sensor at low operating temperature, Shen et al. proposed Pd doping in ZNWs. They observed that the response of sensor increased with increment

in Pd doping. They made Pd-functionalized ZnO nanowires (Pd-ZNWs) by exploiting a facile hydrothermal one-pot approach [157]. Post hydrothermal process, the Pd was self-configured on ZnO nanowires surface (ZNWs). The characteristics analysis of the developed Pd-ZNWs demonstrates that the Pd functionalization has not influenced the morphology and size of ZNWs. In comparison to pure ZNWs, the functionalized Pd-ZNWs sample showed lower operating temperature, higher response, faster recovery and response towards NO_2. A combination of chemical and electronic sensitization of Pd is responsible for the sensing mechanism of Pd-ZNWs. The dissociation of NO_2 into ionized or nonionized species such as NO, NO^+ and O on the surface of ZNWs can be facilitated by the chemical sensitization of Pd/PdO nanoparticles. The dissociated species are transferred on the surface of ZNWs by means of a spillover effect. Hence, the electrons from the conduction band of ZNWs can be readily captured by the dissociated species, resulting in wider electron depletion layer and large resistance variation.

Lingmin et al. developed a 3D hybrid optoelectronic NO_2 gas sensor with enhanced sensing capabilities in 2018 [211]. In this work, the facile solution method, thermal reduction and spray deposition techniques were employed for obtaining ZnO nanowalls grown in-situ on the surface of porous rGO (PG). The result showed that 3D ZnO-PG hybrid nanocomposites composed homogeneously interconnected 3D ZnO nanowalls network on the surface of PG films. The developed 3D hybrid is responsible for providing channels for gas diffusion. The ZnO-PG hybrid nanocomposite sensor exhibited good photodetecting response of 7.4 under 365 nm UV irradiation. The sensitivity of the sensor towards 50 ppm NO_2 was found to be 35.31 at RT under the UV illumination of 1.2 mW/cm^2. In comparison with pure ZnO sensor, the sensitivity of 3D ZnO-PG hybrid sensor was 2.24 folds higher [380,381]. For 50 ppm of NO_2, the recovery and response times for the hybrid sensor were ~2 s and ~37 s, respectively. In the ambient atmosphere, oxygen molecules adsorb on the surface of ZnO nanowalls and ionize to O_2^- by capturing free electrons from the surface of ZnO to generate a high depletion region with high resistance at the surface. The energy bandgap of ZnO is 3.2 eV which is lower than photo energy of UV irradiation (3.4 eV). Electron-hole pairs are photo-generated when UV light is irradiated on ZnO nanowalls, followed by migration of holes to the surface and the O_2^- species are photo-desorbed. As a result, the remaining unpaired electrons will contribute to the decrease in electrical resistance and the depletion layer is diminished. In the presence of NO_2 gas, the adsorbed NO_2 gas molecules capture the photo-generated electrons and react with adsorbed oxygen ions thereby, increasing the

resistance of the sensing material. In the case of hybrid structure, the Fermi energy level of ZnO is lower than rGO owing to the difference in work functions of n-ZnO (5.20 eV) and PG (4.75 eV). This facilitates the charge transfer from PG to the conduction band of ZnO and further increases the adsorption of NO_2.

In the same year, Nguyen et al. proposed another technique for developing metal oxide-based gas sensor [382]. Thermal evaporation process was used for on-chip growth of Zn_2SnO_4 and ZNW. In this report, the effects of distance between the microelectronic chip and the source on the gas on sensing behaviour of the developed sensors Zn_2SnO_4 and ZNW were investigated. It was found that the alignment of microelectrode chips of 2–6 cm size results in the identical consequence for ZnO nanowire detectors but an order of degree change in response for Zn_2SnO_4 as deliberated at 10 ppm of NO_2 gas. The response of Zn_2SnO_4 nanowire sensor towards 10 ppm of NO_2 in comparison with ZNW sensor is significantly higher. The comparative gas sensing studies of both Zn_2SnO_4 and ZNW sensors revealed that the former exhibits better sensitivity and selectivity towards NO_2 gas. With an increase in the growth time duration of Zn_2SnO_4, the sensitivity towards NO_2 gas increases. However, the sensitivity decreases if the growth time is prolonged beyond. The sensing mechanism can be explained on the basis of reaction of reduced gases with adsorbed oxygen on the surface of NWs.

In the following year, Yanbai et al. demonstrated a unique technique for obtaining better selectivity towards NO_2 gas as well as the sensing response approaching the theory of power laws. They used a hybrid structure of ZNW and Au nanoparticles for enhancing the sensing of NO_2 gas [383]. A facile one-pot hydrothermal approach was used for the synthesis of ZNWs with various concentrations of Au nanoparticles to obtain hybrid Au-ZNWs and ZNWs. The structural analysis of Au-ZNWs revealed that Au nanoparticles self-assembled on the surface of ZNWs and addition of $HAuCl_4$ have suppressed the c-axis growth of ZNWs in the synthesis of Au-ZNWs. The gas detecting performance of the hybrid sensor was analyzed and it was found that in comparison with pure ZNWs sensors, the Au-ZNWs sensors showed better sensitivities [384,385]. The maximum response for 1 mol% Au-ZNWs hybrid sensor at 150 °C was 31.4 which is 4 times higher in comparison with the pure ZNWs sensor response of 8.2. Also, it was found that 1 mol% Au-ZNWs hybrid sensor has the shortest recovery and response time of 18 s and 29 s for an extended spectrum of performing temperature. A hybrid sensor of Au-ZNWs sensor with various concentrations of

Au has shown better selectivity towards NO_2 gas in comparison to pure ZNWs sensors. The relationship between the concentration of Au in the hybrid Au-ZNWs sensor and the sensing response follows the theory of power laws. The modulation of the electron depletion layer is responsible for the NO_2 gas sensing mechanism of pure ZNWs. In the ambient air, oxygen molecules will be adsorbed on the surface of ZNWs by trapping the free electrons in the conduction band of ZnO semiconductor. This results in the formation of an electron depletion region. In the presence of strong oxidizing gas, e.g. NO_2, NO_2 gas molecules adsorb on the surface of ZnO and O_2 gas molecules are removed from the surface with the release of free electrons. In comparison to oxygen, NO_2 gas molecules have higher electron affinity. Therefore, the NO_2 gas molecules will trap more electrons and convert to NO_2^-, thereby facilitating the formation of a larger electron depletion region with higher resistance. Self-assembly of Au nanoparticles on the surface of ZNWs creates more active sites for NO_2 molecules adsorption, which is known as a spillover effect. Besides, Au nanoparticles also facilitate the dissociation of NO_2 gas molecules into ionized or neutral species, possibly including O, NO, NO^+. These disassociated species are transported to the surface of ZNWs by spillover effect, which is the main reason for faster recovery and response after Au functionalization.

Another group led by Tai et al., in 2017 developed a light aided NO_2 gas sensor based on ZnO–Ag nanoparticles for enhanced gas sensing response at room temperature [202]. A modified polymer structure gel technique was used for preparing hybrid ZnO–Ag nanoparticles. They observed an enhancement in surface oxygen vacancies, which was attributed to the formation of heterojunction between the two materials. In comparison with pure ZnO, the sensitivity of ZnO–Ag to NO_2 gas (0.5–5 ppm) is increased under the influence of different irradiations (λ = 365–520 nm). The room temperature resistive response under the illumination of 430 nm light of ZnO–Ag heterostructured nanoparticles to NO_2 gas from 0.5 to 5 ppm is displayed in Figure 4.39(a). Similarly, the response curve for the ZnO–Ag hybrid structures is displayed in Figure 4.39(b). Figure 4.39(c) demonstrates the responses of ZnO and ZnO–Ag nanoparticles for the concentration variation from 500 ppb to 5 ppm under the influence of 430 nm of light at RT. The various sensor responses to NO_2 under the influence of various wavelengths of light is described in Figure 4.39(d). These analyses revealed an excellent heterojunction between AG-NPs and ZnO particles. The enhanced gas sensing is mainly because of the synergism developed due to the Ag deposition and oxygen vacancies. The SPR effect of Ag-NPs produced on the surface of ZnO under the influence

of UV illumination holds great potential for ZnO–Ag nanoparticles as an application for gas detection. Enhancement of charge separation is mainly done due to the formation of electron sink of surface oxygen vacancies and AgNPs. The positive impacts of moisture on the sensing performance of NO_2 of the as developed heterostructures can be associated with the photocatalytic reception associated with water molecules.

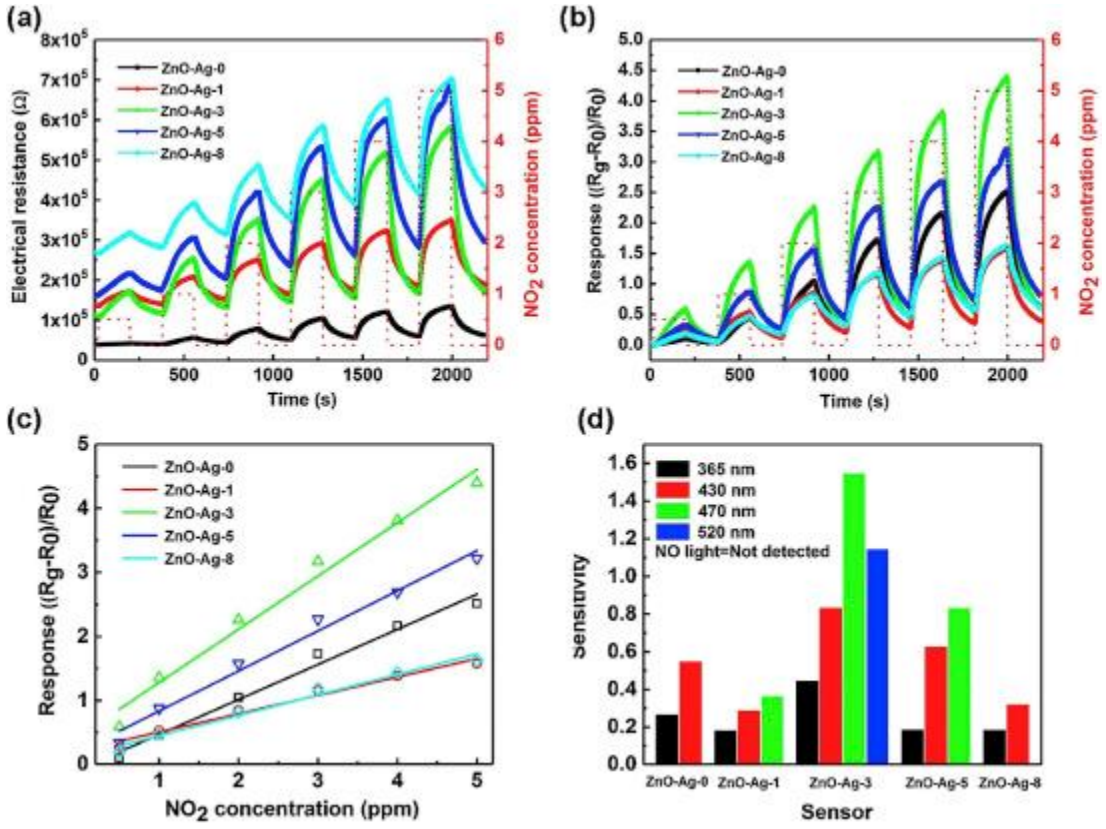

Figure 4. 39: (a) Resistance plots, (b) Response plots, (c) Response curves for ZnO–Ag in the range of 500 ppb to 5 ppm under the illumination of 430 nm light at RT, (d) The sensitivities of various sensors to NO_2 gas under the illumination of various wavelengths of light. Copyright permission from Ref. [202].

Chongmu et al. also developed a highly sensitive gas sensor by adopting a unique method of increasing the surface area. A composite structure of Pd–ZnO co-decorated SnO_2 nanorod sensor was fabricated for enhanced NO_2 gas sensing performance [218]. A three-step process was used for synthesizing SnO_2 nanorod co-decorated with Pd–ZnO: the thermal evaporation of Sn powder was used for SnO_2 nanorod synthesis persuaded by a sol-gel accumulation of Pd and ZnO NPs. The response of the developed nanorod sensor is examined in the presence of NO_2 gas. The

Pd and ZnO NPs were composed of face centred cubic structured Pd single crystal and wurtzite-structured ZnO single crystal, while the nanorods comprised primitive tetragonal structured single-crystal SnO_2. TEM and corresponding electron diffraction of co-decorated ZnO–Pd on SnO_2 surface are shown in Figure 4.40(a–d). The temperature dependence of the sensor response in the case of both pristine SnO_2 and Pd–ZnO–SnO_2 is shown in Figure 4.40(e). The dynamic sensing response of different detectors for NO_2 gas at 300 °C is shown in Figure 4.41(a–d). The comparison of dynamic sensing response of pristine SnO_2 nanorods, the response of ZnO decorated SnO_2, Pd decorated SnO_2 nanorods and Pd–ZnO co-decorated SnO_2 nanorod is shown in Figure 4.41(a–d). It was found that in comparison with ZnO or Pd decorated SnO_2 nanorods, the Pd/ZnO co-decorated SnO_2 nanorods showed a remarkably improved sensing response towards NO_2 gas. Also, Pd–ZnO co-decorated sensor has a fast response and higher selectivity in comparison to pristine sensors. The SEM morphology analysis displayed that both ZnO and Pd touched each other in Pd–ZnO co-decorated SnO_2 nanorods. The main reason for the difference in the sensing response between pristine and co-decorated SnO_2 sensor is the formation of ZnO–SnO_2 and Pd–SnO_2 interface. The gas sensing mechanism of the Pd/ZnO co-decorated SnO_2 nanorod is based on ZnO–SnO_2 and Pd–SnO_2 interface. Electrons transfer from SnO_2 to ZnO in a vacuum after contact, owing to higher fermi level of SnO_2 than that of ZnO resulting in the formation of accumulation and depletion on the SnO_2 and ZnO sides, respectively near the ZnO–SnO_2 interface. In ambient air, the adsorbed oxygen molecules capture electrons from the conduction band of SnO_2 and ZnO and transform into oxygen ions, depending on the operating temperature. This results in the formation of the depletion layer on both SnO_2 and ZnO sides of ZnO–SnO_2 interface. In addition to the formation of a depletion layer, a potential barrier with a height of E_1 is also formed at the interface. In the presence of NO_2 gas molecules, more transfer of electrons from the conduction band of SnO_2 and ZnO to the adsorbed oxygen takes place, leading to the formation of wider depletion layer on both sides of SnO_2 and ZnO. This results in the formation of smaller channel width (W2) and hence increase in the resistance. Therefore, the enhanced electrical response of the nanorod sensor to NO_2 gas was found. In addition to the depletion layer, a potential barrier with height E_2 also forms at both sides of the interface. The potential barrier E_2 is higher than E_1, a larger potential modulation takes place in the presence of gas and hence an enhanced electrical response of the nanorod sensor to NO_2 gas was reported.

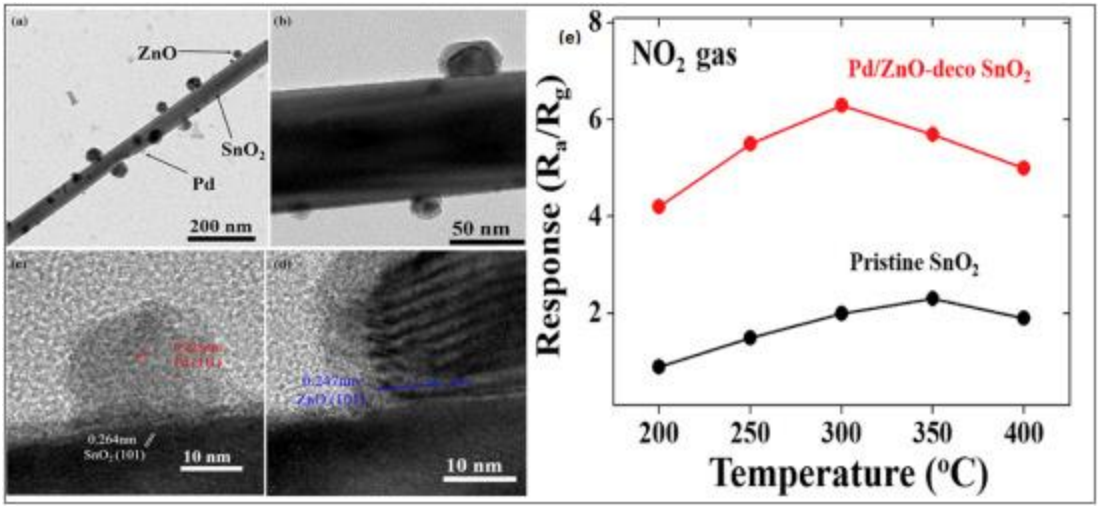

Figure 4. 40: (a) Low magnification TEM images of Pd/ZnO–SnO_2, (b) Medium resolution TEM of Pd/ZnO–SnO_2, (c) High-resolution TEM of Pd/ZnO decorated SnO_2, (d) corresponding electron diffraction of co-decorated ZnO/Pd on SnO_2 surface, (e) The temperature dependence on the sensor in case of both pristine SnO_2 and Pd/ZnO–SnO_2. Copyright permission from Ref. [218].

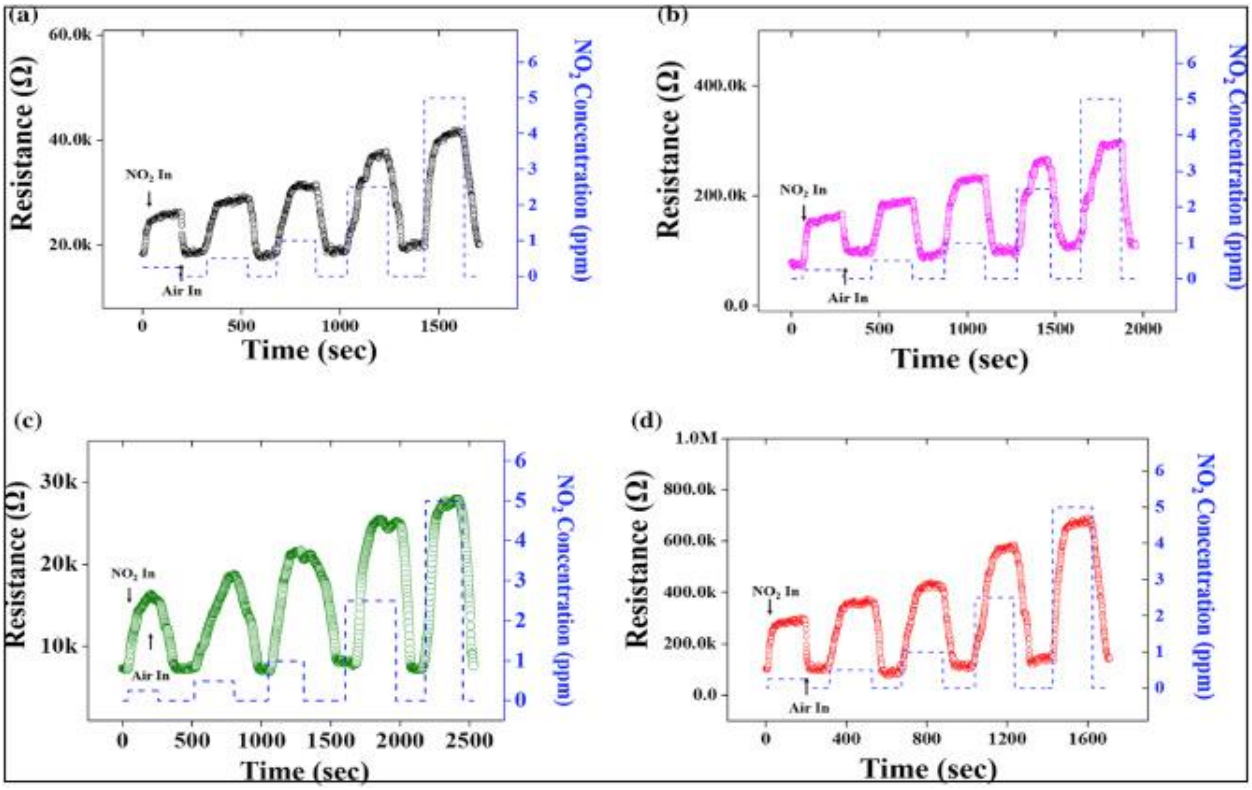

Figure 4. 41: The dynamic sensing response of different sensor in the existence of NO_2 gas at 300 °C. (a) the response of pure SnO_2 nanorods, (b) the response of ZnO decorated SnO_2 nanorods, (c) the response of Pd decorated SnO_2 nanorods, (d) and the response of Pd/ZnO co-decorated SnO_2 nanorods. Copyright permission from Ref. [218].

In 2017, Qin et al. developed a unique surface etching method of ZnO micro/nanowire which had led to an increase in the sensitivity, response and recovery time [162]. The etching of the microwire surface area leads to an increase in the surface density of single ionized oxygen vacancies and specific surface area and hence the increase in the adsorption sites for gas molecules. This surface etching ultimately results in an increase in sensitivity by about ~20%. Under the influence of UV light of 148.8 mW/cm^2, the sensitivity of the sensor further increased to 411% and recovery and response time decreased to ~2% and ~20% under dark and light conditions, respectively. The surface etching method of microwire of ZnO leads to an increase in the sensitivity from 3.6% to 71.8% in the presence of 20 ppm of NO_2. By controlling the etching time, the sensitivity of the sensor can be controlled. The ZnO MW based sensor showed an increase in the sensitivity and reduction in response and recovery time under UV illumination at room temperature.

In the following year 2018, Betty et al. proposed a highly selective gas sensor based on a hybrid structure of porous silicon and ZnO [165]. The chemically processed ZnO nanoparticles were drop casted upon single crystalline silicon (p-type) substrate (Si) and also on electrochemically processed p-type porous silicon (PS). At room temperature, the PS-ZnO sensor showed an increase in the current for NO_2 gas while there was no significant change in the presence of other oxidizing and reducing gases. The sensor displayed a response time of 50 s while the sensitivity of 35% in the presence of 200 ppb of NO_2 at 25 °C. The temperature dependence was also studied, and it was found that the suitability of the sensor is up to 60 °C only. The PS-ZnO sensor showed a maximum response to NO_2 gas while very less response to NH_3 and SO_2. Two different heterostructures, i.e., planar silicon-ZnO (Si–ZnO) and ZnO on electrochemically processed porous silicon (PS–ZnO) were prepared. The gas sensitivity of PS-ZnO sensor is extremely high to NO_2 in ppb range with high specificity while Si–ZnO sensor has higher sensitivity with precise responses to NH_3 and SO_2.

In the same year, Yu et al. proposed a highly sensitive NO_2 gas sensor based on the heterostructures of ZnO-rGO [203]. The soft solution and thermal reduction processes were used

for fabricating ZnO nano-walls modified with rGO nano-sheets. The ZnO layer was homogeneously deposited on the surface of rGO. The sensing performance of the developed sensor was studied. At room temperature, the authors observed an increase in the electrical carrier concentration from 0.04×10^{15} cm^3 to 3.148×10^{15} cm^3 and decrease in the electrical resistances from 998.8.cm^{-1} to 16.01.cm^{-1} for the ZnO-rGO heterojunction. It was also found that the ZnO-rGO heterojunction exhibited good sensitivity, selectivity and response to NO_2 gas. The remarkable connection between a 3D planar network of ZnO nanowalls with porous nature and rGO is responsible for the enhancement in the performance of ZnO-rGO heterostructures at room temperature in comparison with ZnO nanowalls or rGO. Also, the as-developed ZnO-rGO heterostructures at room temperature have good repeatability and stability. In the ambient atmosphere, the oxygen molecules adsorbed on the surface of ZnO and ionized to O^- by capturing free electrons from the ZnO, result in the variation of sensor resistance. When exposed to NO_2 gas, the adsorbed NO_2 gas molecules will capture the electrons from ZnO surface as it has higher electron affinity then pre-adsorbed oxygen. Hence, the overall resistance increases when exposed to NO_2 gas. In case of heterostructures of ZnO-rGO, the fermi level of n-ZnO (5.20 eV) being higher than rGO (4.75 eV), allows charge transfer from rGO to the conduction band of ZnO, further increasing the adsorption of NO_2. Hence, the increase in the sensitivity can be attributed to the electron transfer between rGO and ZnO.

Another group in 2018, developed a visible ultraviolet (UV) photodetector based on ZnO nanorod which is highly sensitive and selective towards NO_2 gas [386]. The sensing material ZnO nanorod was obtained by using a two-step chemical method. The large surface area for sensing mechanism was provided by well-aligned one-dimensional (1D) network of ZnO nanorods. The UV photodetector in A region (364.81 A/W) possess fast photo-switching analysis at 5 V bias voltage and high responsivity. It shows the junction formed between metal and semiconductor is good ohmic contact. The sensing performance of ZnO nanorods was monitored at a temperature of about 175 °C. The maximum sensing response at 40 ppm of NO_2 was found to be 35. The ZnO nanorod detector also shows high selectivity for NO_2 gas. Good repeatable characteristics of the as-developed sensor can be seen at the lower concentration of 2 ppm of NO_2. Simple and cost-effective sensor technology was employed for developing extremely ordered ZnO nanorod as highly sensitive NO_2 sensor and highly sensitive UV photodetector.

The recent advancement in the material refining methods has allowed scientists to explore research and record the properties of nanostructured metal oxides. One of the better options is the multitude application of ZnO. In this regard, Vanalakar et al. employed a hydrothermal route for synthesizing ZnO nanorods for an enhanced sensing response towards NO_2 gas at low temperature [387]. In this paper, the hydrothermal method is used for developing ZnO on the silicon substrate and both chemical and physical properties were thoroughly characterized. Different samples were obtained with different concentrations of zinc nitrate. FESEM images revealed the formation of vertically aligned ZnO nanorods by hydrothermal method. Also, with increasing concentration of zinc nitrate, nanorods become denser and grow larger in size. However, as compared with other samples, the ZnO-d becomes slightly shorter. They observed that the prepared ZnO nanorods are vertically aligned and show the wurtzite type structure. The PL analysis of as-prepared sample confirms the presence of defects. These defects come into picture due to the oxygen vacancy concentration. These defects in conjunction with a high surface area of the nanorods and optical inter rod spacing create conditions for high adsorption and diffusion. The developed ZnO gas detector exhibited a superior response of about 570 for 100 ppm NO_2 at 150 °C. Along with high sensing response, the ZnO sensor also exhibits high selectivity at a lower temperature.

Recently, V.B. Patil et al. developed an outstanding sensor with a high response, fast response and recovery, high stability and reproducibility based on heterostructure of ZnO NWs-CuO nanoparticles [206]. The design of the device technology working at low temperature with highly sensitive performance using heterostructure materials is very crucial. The sensors were named as NWA and NWG after thermal evaporation process via annealing in air and argon, respectively. The topology at various magnifications of ZnO–CuO heterostructure clearly shows the creation of ZnO–CuO heterostructure between n-type ZnO and p-type CuO NPs. Also, surface morphology study revealed well-aligned porous nature of NWG-type ZnO–CuO heterostructures in contrast to NWA heterostructures. The high surface-to-volume ratio of the NWs type morphology is beneficial for gas detection. The developed heterostructures of ZnO–CuO showed remarkable response to NO_2 gas having fast response and recovery, high stability, high response, and outstanding reproducibility. The general gas sensing mechanism of metal oxides semiconductor is well understood. In the case of heterostructures of ZnO–CuO, the sensing comes from the top of the ZnO layer and depletion layer formed between ZnO and CuO. In an ambient atmosphere, oxygen gets adsorbed on the surface of the depletion layer in the forms of O, O^{2-}, O_2^-

by accepting electrons from the surface matrix. Also, the positioning of the ZnO NWs on the top of CuO NPs is advantageous to enhance the response towards NO_2 due not only to increased surface-to-volume ratios but also to a spatially heterogeneous surface matrix, as such type of matrix is appropriate for improved adsorption/desorption of NO_2 gas molecules.

4.6.2 **Miscellaneous metal oxide-based NO_2 gas sensors**

In 2018, Fu et al. adopted a facile two-step synthesis approach was used to synthesize actinomorphic flower-shaped core-shell structured ZnO–$ZnFe_2O_4$ composites for an enhanced gas sensing response [163]. In analogy with pure ZnO, the flower-shaped ZnO–$ZnFe_2O_4$ composite was found to be highly sensitive, with shorter recovery and response times and more selective to a low concentration of NO_2 at an operating temperature of 200 °C. The XRD analysis of the composite confirmed the wurtzite ZnO structure and also the residual peak attributed to the spinel $ZnFe_2O_4$ structure. The highly crystalline nature of ZnO–$ZnFe_2O_4$ composites was indicated by the sharp and narrow diffraction peaks. The deficiency of any other peak confirms the purity of ZnO–$ZnFe_2O_4$ composites. The sensing mechanism of ZnO–$ZnFe_2O_4$ based sensor can be attributed to the flower-like core-shell structure and the formation of p-n heterojunction at the interface of ZnO and $ZnFe_2O_4$ composite. In the presence of ambient air, oxygen adsorbs on the surface and two conjugated electron depletion layers are formed on the surface of $ZnFe_2O_4$ nanoparticles and the interface between ZnO and $ZnFe_2O_4$. The adsorbed oxygen molecules (O, O_2^-, O^{2-}) not only capture electrons from the $ZnFe_2O_4$ shell but also capture electrons from ZnO core, making ZnO–$ZnFe_2O_4$ based sensor highly resistive in comparison to pure ZnO. When a highly oxidizing NO_2 gas is exposed to the heterostructures of ZnO–$ZnFe_2O_4$, the NO_2 gas acts as an electron acceptor to capture more electrons due to their high electron affinity than that of oxygen, leading to the remarkable increase of the sensor resistance and electron depletion width. This result makes the actinomorphic flower-shaped ZnO–$ZnFe_2O_4$ composites a perfect contender for NO_2 gas sensing.

In the same year, Sheng et al. developed a gas sensor for room temperature NO_2 detection under UV light based on ZnO-silk fibroin (ZnO/SF) using hydrothermal method [164]. The UV light-activated sensor was efficient and able to trace NO_2 gas very fast at RT. Under the influence of UV light of 365 nm, the ZnO-SF detector demonstrated the response of 85 and average recovery

and response time of 16 s and 26 s, respectively towards 20 ppm of NO_2 at RT. Also, the as-developed ZnO-SF sensor showed excellent linearity in response toward NO_2 at RT under UV illumination. The SEM investigation validated the existence of small block-shaped and small particles while XRD investigations indicated the existence of wurtzite ZnO structure and the absence of any impurities.

Gosavi et al., in 2017 provided a breakthrough in the field of ZnO metal oxide-based gas sensors with high sensitivity towards NO_2 gas. They developed flower-shaped ZnO thin films for resistive sensing of NO_2 gas [161]. A cost-effective, soft chemical solution synthesis technique was employed for uniform deposition of jasmine flower-shaped thin films. X-ray diffraction study of the ZnO revealed the hexagonal wurtzite structure. It was also found that at all deposition temperatures, a large jasmine flower-shaped structure of ZnO is uniformly maintained. The elemental investigation of the sample confirms the presence of Zn and O with no impurities. The combined analyses of Raman spectroscopy, resistivity analysis and elemental analysis confirmed the presence of oxygen vacancies and wurtzite structure of ZnO. The as-grown jasmine flower-shaped ZnO thin film-based detector exhibits a high sensitivity towards 10 ppm of NO_2 with rapid recovery and fast response time of 54 s and 65 s, respectively.

A sol-gel method was used for developing ZnMgO thin films for studying structural, NO_2 gas sensing and optical properties [388]. The sol-gel processed thin films of ZnO and ZnMgO was spin-coated on a glass substrate. The thin film ZnMgO absorption spectra analysis shows a bandgap variation from 3.19 to 3.36 eV which agrees well with PL emission measured at low temperatures. The gas sensing measurements of the ZnMgO samples were performed in air containing 100 ppm of NO_2. The incorporation of magnesium into ZnO leads to decreased sensor response towards NO_2. However, on increasing the concentration of magnesium in the sample, the response and recovery times drop significantly.

In another approach, Patil et al. prepared a highly selective NO_2 gas sensor with a low detection limit. Thin films of ZnO were synthesized using sol-gel and spin coating procedures for detecting NO_2 gas [207]. The sensing performance of as-prepared ZnO thin films towards different gases, e.g., H_2S, CH_3OH, NO_2, Cl_2 and NH_3 were studied at various operating temperatures. At a temperature of 200 °C and 100 ppm of NO_2, the as-developed ZnO thin film sensor exhibited a response of 12.3. The as-processed ZnO thin film sensor depicted a highly selective response to

NO_2 gas besides the detector is capable of detecting NO_2 concentration as low as 5 ppm with a response of 4.1. Most of the metal oxide-based gas sensors detect gas at high operating temperatures. This requires an additional requirement of heating the sample in order to attain the detection temperature. The thermal treatment of the sensor produces oxygen which plays a vital role in gas sensing mechanism. The oxygen molecules adsorb on the surface and grain boundary of the metal oxide sensor to create a depletion region. The adsorbed oxygen changes into O^- ions by capturing electrons from the metal surface. This increases the number of electrons in the sensing layer.

Katz et al. fabricated a hybrid structure combining a polymer with metal oxide which provides high sensing response to NO_2 gas. The hybrid structure, i.e., P3HT-ZnO@GO composite, was obtained from zinc oxide-graphene oxide (ZnO@GO) and (P3HT) poly (3-hexylthiophene) nanoparticles [215]. The ionic aggregation was used to prepare core-shell nanostructure particles of zinc oxide (ZnO) and graphene oxide (GO). The organic field-effect transistors (OFETs) for gas sensing were fabricated by spin coating the prepared mixtures of ZnO@GO and P3HT on the oxide deposited silicon substrate. The gas sensing properties of the developed composite structures of ZnO@GO and P3HT composite as semiconducting material for OFETs were investigated in the presence of nitrogen dioxide (NO_2) gas. In comparison with pure P3HT, the developed hybrid P3HT-ZnO@GO composite has sensing response up to 210% under the exposure of 5 ppm of NO_2 gas. As the amount of weight fraction of ZnO@GO rises, the sensing response of the sensor also increases accordingly at RT. The sensor response was also found to increase with the increase in exposure time and NO_2 concentration.

In 2018, Tian et al. proposed another approach in which multilayered black phosphorus (m-BP) was incorporated in ZnO, forming composite structures of ZnO-BP which exhibit outstanding selectivity, higher response as well as rapid response behaviour [216]. In hollow spheres of zinc oxide (ZnO) the multilayers of black phosphorus (m-BP) were effectively incorporated and the resultant composite structure was named as ZnO-BP. The incorporation of BP into ZnO-BP composite leads to the large surface area, enhanced charge transfer and excellent carrier mobility in comparison with BP, graphene and ZnO based sensors. The developed ZnO-BP composite sensor exhibits the ultra-high sensing limit, i.e., 1 ppb of NO_2 gas.

Recently, Aziz et al. developed an advanced approach for synthesizing polycrystalline, self-supporting ZnO nanofibers, which are capable of detecting very low levels of NO_2 [389]. The developed polycrystalline ZnO is able to detect 1 part per billion (ppb) of NO_2 gas. The core-shell electro-spinning of the inorganic metal precursor such as zinc neodecanoate is used for creating ZnO nanofibers for NO_2 detection. The use of this new and innovative method resulted in the formation of self-supporting, contamination-free, polycrystalline ZnO nanofibers with average grain size and diameter of 8 and 50 nm, respectively. These properties are ideal for gas sensing purposes. The core-shell electrospinning method used in this paper is very cost-effective and can be easily scaled. The sensitivity of the device can be enhanced by employing interdigitated electrodes and aligned electrospun fibres. This simple technique can be easily used for various metal precursor solutions, thereby assisting the formation of other metal oxides. The functionalities and properties of these materials could be very useful in many fields including energy generation and storage, sensing and wearable technologies. The polycrystalline nature of synthesized ZnO and the presence of nanograins may be suitable for application in spintronics where ferromagnetism in ZnO has been associated with the ZnO grain boundaries; other uses may comprise syngas cleansing water and air.

In a unique approach, the assembly of the smallest nanoparticles with mesoporous ZnO sheets was obtained which depicted a high response at room temperature towards NO_2 gas. Wang et al. constructed small nanoparticles to develop mesoporous ZnO sheets using facile synthesis for increased NO_2 gas detection at RT [210]. At low temperature such as 100 °C, calcination of δ-Zn $(OH)_2$ precursor was performed for facile synthesis of nanoparticles assembled mesoporous ZnO sheets. Ultrasmall ZnO nanoparticles with a high surface area of 87.63 $m^2\ g^{-1}$ and an average crystal size less than 10 nm were assembled for developing mesoporous ZnO sheets. The enhancement in the sensitivity response of the sensor towards NO_2 gas can be accredited to the high surface area, oxygen vacancies and rich mesopores which facilitate the diffusion and adsorption of NO_2 molecules. The assembly of nanoparticles to obtain mesoporous ZnO sheets depicted a high response of about 135% at room temperature towards 1 ppm NO_2. Also, the developed sensors exhibited full reversibility, good selectivity towards NO_2 and superior recovery/response times. The nanoparticles of ZnO with small crystal size increases radical modulation in the conduction channel for NO_2 gas sensing operations.

In 2018, Yi et al. developed a method for increasing the sensing area to enhance sensitivity. Synthesis of ZnO–SnO_2 composite was done by a facile solvothermal method in order to decorate ZnO onto SnO_2 microspheres [160]. The study displayed that the developed sensor was highly sensitive to NO_2 gas molecules. It was found that in comparison with pure SnO_2 microspheres, ZnO–SnO_2 microspheres-based sensor response was 3 times higher at optimum temperature towards 100 ppm of NO_2. The recovery and response time were also reduced remarkably. The increase in the sensitivity is attributed to the extra area available for adsorption of NO_2 molecules provided by ZnO decoration. The SEM images obtained clearly show the porous structure of SnO_2 microspheres (see Figure 4.42). The deposition of ZnO on SnO_2 completely retains the porous structure of pristine SnO_2 without any disturbance on the structure. They observed the coexistence of both ZnO and SnO_2 particles and the tetragonal structure of SnO_2 (See Figure 4.42).

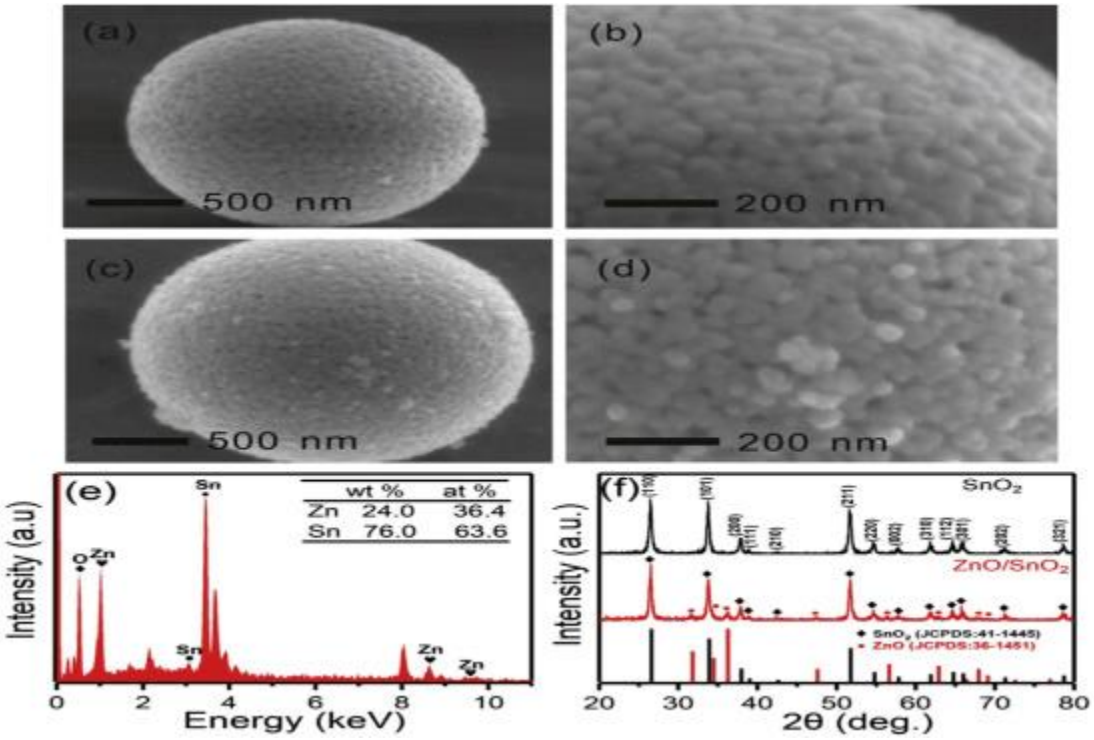

Figure 4. 42: (a) & (b) Typical SEM photographs of pure SnO_2 microspheres. (c) & (d) SEM photographs of ZnO–SnO_2 hybrid material microspheres. (e) ZnO–SnO_2 composites EDX spectrum. (f) Pristine SnO_2 and ZnO–SnO_2 composite XRD pattern comparison. Copyright permission from Ref. [160].

Verma et al. developed a highly selective NO_2 gas sensor by synthesizing a ternary complex of CuO–ZnO/rGO from ZnO nanosheets and CuO 1D nano chains, which were synthesized via reflecting and wet chemical method, respectively [219]. The influence of individual ZnO and CuO material composition on the sensing behaviour of the composites of CuO–ZnO/rGO towards NO_2 gas have been investigated. The drop-casting method is used for synthesizing composites of CuO–ZnO/rGO with different concentrations of both ZnO and CuO on glass substrates. It was found that at room temperature (RT), the developed hybrid CuO–ZnO/rGO with a composition (CuO: ZnO = 1:1) have a sensitivity of ~62.9 towards NO_2 of 40 ppm concentration. In comparison with ZnO/rGO and CuO/rGO sensors, the composite sensor CuO–ZnO/rGO sensitivity towards NO_2 gas is 1.3 and 3.1 times higher respectively. The developed composite sensor is highly selective towards NO_2 gas and moreover, this sensor shows good stability for a period of 5 weeks.

Wang et al. developed a unique approach for enhancing the sensitivity, response and recovery speed of the sensor to many folds. For achieving a mentioned enhancement in sensor characteristics, they simply annealed the sensor at high temperature. The highly sensitive gas sensor for detecting ppb levels of NO_2 at low operating temperature was made by In_2O_3 nanobricks [209]. Oil bath storm and consequent calcination process without any surfactants or templates were used for synthesizing brick-like In_2O_3 nanomaterials. Internal defect structures and surface states of the material can be influenced by the different temperatures of calcination process. The influence of internal defects and material surface states on gas sensing is illustrated by XPS and photoluminescence spectra (PL). It was found that the 400 °C annealed In_2O_3 nanomaterial sample has a high sensing response of 402 towards 500 ppb NO_2 gas with fast recovery and response time at relatively low performing temperature of 50 °C. Also, the sensor has a great stability period of over 30 days and a good linear response. The reasons for such superior gas sensing properties can be accredited to good electrical properties, large surface area and sufficient chemically adsorbed oxygen. The developed In_2O_3 sensor outperforms many other works on NO_2 gas sensing based on hybrids of In_2O_3 [390,391,392,393].

Table 4.3 enlists the performance parameters such as preparation method, structure, materials used, the concentration of NO_2 gas, response and recovery times, and operating temperature for NO_2 gas sensors based on various oxide nanostructures and their hybrids.

4.6.3 **Graphene-based nanostructures**

The addition of reduced graphene oxide (rGO) into SnO_2 not only improved the response and recovery speeds but the response of the sensor also increases with temperature. Wang et al. developed a composite of rGO and SnO_2 nanoparticles for enhanced NO_2 gas sensing [394]. A hydrothermal method with facile one-pot microwave assistance was used for obtaining rGO/SnO_2 composites. The optimal operating temperature for both rGO/SnO_2 composite and pure SnO_2 were found to be 75 and 65 °C, respectively. The peak response for the rGO/SnO_2 composite sensor was found to be 227.6 while in case of pure SnO_2 sensor response was 34.6 for 350 ppb of NO_2 gas. Temperature greatly affects the surface reactions and thus, can be responsible for the temperature-dependent property of the sensor. The sensing gas particles (e.g., NO_2) fail to interact with oxygen species pre-adsorbed on sensor surface at lower temperatures owing to inadequate thermal energy. The sensor responses considerably increase with increase in temperature as the gas particles attain sufficient thermal energy to overcome the activation energy boundary of surface reactions. However, with further increase in temperature, the response is limited by difficulties in gas adsorption and low utilization rate of the sensing layer [395]. The utilization rate and the gas adsorption were found to be in balance at 75 °C, resulting in a maximum response of the composite sensor at this temperature. The addition of rGO helps in improving both recovery and response speeds. In case of pure SnO_2 sensor, the recovery and response time were 54.7 and 39.2 min, respectively; which in case of rGO/SnO_2 composites were 1 and 6.5 min, respectively. The increase in surface area of rGO/SnO_2 composites due to the addition of rGO leads to the increase in sensitivity of the sensor.

Flexible sensors hold great promise for various innovative applications in fields such as environment, medicine, biology and most importantly, healthcare. Considering the fact that most of the healthcare electronics, wearable systems and laboratory on-chip testing tools can be expected to come in contact with arbitrarily curved interfaces, the flexibility of the sensor is essential for improving the interactions. Zhang et al. reported a flexible sensor based on direct laser writing technology (DLW) for the fabrication of composite films of graphene oxide (GO) and In_2O_3 for NO_2 sensing flexible arrays working at RT [396]. The photoreduction of GO is achieved by laser treatment which led to the creation of porous structure allowing the removal of oxygen

groups. The laser treatment also enables mask free patterning in a programmable manner, resulting in the assimilation of flexible sensor arrays on any substrates. In general, both In_2O_3 and GO are not conductive and hence the composite In_2O_3@GO is insulating in nature with resistance found to be ~$7.6*10^8$ Ω. Laser treatment of the In_2O_3@GO composites decreases the resistance to ~230 Ω. Under the controlled environment, the sensitivity of rGO based sensor is low in comparison to the sensitivity of In_2O_3@GO composites. The developed In_2O_3@GO composite sensor showed an admirable selectivity toward NO_2 gas and offers a linear dependence to the NO_2 concentration [397].

Ching-Ting et al. developed a membrane-based gas sensor. One advantage of membrane-based gas sensors is their applicability for differing gas components. A highly sensitive NO_2 gas sensor using rGO and ZnO membrane was developed [398]. In addition, an installed sensor cell can be calibrated without dismounting under an unknown background concentration. The GO-ZnO complex films were processed by coating the GO-ZnO solution on glass substrates. The rGO-ZnO composite films were obtained by removing the oxygen-containing functional groups residing on GO-ZnO composite by employing a thermal annealing method. In comparison to rGO and ZnO sensing membrane, the sensitivity of the rGO-ZnO film is better and the reason for this increase in composite sensor response can be accredited to the elimination of oxygen-containing functional groups. The increase in sensitivity of rGO-ZnO composite films can be accredited to the structure of C–O–Zn bonds and supply of electrons from the oxygen vacancies of ZnO material. The effect of GO/ZnO ratio on the sensing performance was also studied where 0.08 was found to be the optimized ratio. The various parameters for the rGO-ZnO composite sensor such as response time, sensing responsivity and recovery time were found to be 6.2 min, 47.4% and 15.5 min, respectively for 100 ppm NO_2 environment at RT. In the case of rGO sensor, the response time, sensor responsivity and recovery time were 10.3 min, 19.0% and 75.9 min, respectively. The detection limit for the composite sensor was found to be 5 ppm with linear sensing responsivity from 10 ppm to 100 ppm.

Zhang et al. reported the impact of oxygen-containing groups on the rGO based NO_2 gas sensor at room temperature [399]. The modified hummers method was employed to obtain graphene oxide (GO). Hydrothermal reduction method was used to obtain a series of rGO from the graphene oxide at oxidation temperatures of 65–95 °C. The sensitivity of the sensor first

increases with a rise in the oxidation temperature of GO and then decreases with the further increase in the temperature. The rGO sample obtained by the oxidation of GO at 85 °C exhibited the highest sensitivity of 36.7% at 5 ppm of NO_2 at RT. This increase in sensitivity of the sample oxidized at 85 °C can be accredited to the presence of C–O bonds in large number in the sample. It has already been reported that the sheet edges of rGO are occupied by carboxyl and carbonyl groups, while the basal plane is occupied by epoxy and hydroxyl groups at both sites [400, 401]. The rGO edges occupied by carbonyl group and vertical to the basal plane is occupied by hydroxyl group which possess higher adsorption energies −0.504 eV and −0.238 eV than the other functional groups and it is more important for adsorption of NO_2 gas molecules. Hence the sensitivity of the rGO sensor depends on the presence of several C–O bonds.

Richard et al. proposed a unique material to enhance the sensitivity of NO_2 gas sensors, i.e., TiO_2. A sol-gel technique was employed to synthesize both pure TiO_2 and graphene/TiO_2 hybrid to monitor and neutralize the effects of NO_2 gas [402]. The hybrid structure of graphene/TiO_2 was obtained by the addition of graphene in the reaction vessel before the beginning of the sol-gel reaction followed by annealing ($GTiO_2S$). In another method, the graphene was added to already annealed TiO_2 nanoparticles ($GTiO_2M$). $GTiO_2S$ derived sensor exhibited more sensing response than the sensor fabricated from $GTiO_2M$. In the presence of low power UV illumination, the sensor showed strengthened response to 1750 ppb of NO_2 which is two-fold the response in dark. The detection limit of the sensor was found to be 50 ppb of NO_2. In comparison to other NO_2 sensors based on TiO_2 which work at high temperatures, the gas sensor based on $GTiO_2S$ works at RT. Also, the detection limit for $GTiO_2S$ is lower (in ppb level) with a short response and recovery times.

4.7 Conclusion

Investigation attempts in the field associated with CNTs have shown tremendous improvement in the last two decades. In this chapter, an effort has been made to furnish the latest analysis of CNT-based sensors and their possible utilization. In this review, the extraordinary unique features of CNTs have been emphasized which can be used for numerous possible utilizations of CNT-supported gas sensors. In addition, various stages have been established to detect several gases for instance NO_2, CO_2, NH_3, H_2, CO, H_2S and Ethanol. Every single method which are compiled above have their own imperfection and benefits. The bare CNTs can be functionalized with different metal nanoparticles or polymers which can be helpful for the production of various gas sensors with better selectivity and sensitivity. Even though in the last two decades CNTs gas sensors have revealed considerable prospects experimentally, there are still numerous challenges and limitations which needs to be looked upon in the time ahead for pragmatic implementation

Also, I have highlighted the state of the art of emerging wearable and flexible physical sensing platforms. Among all the emerging technologies, the development of flexible and wearable devices is vital for healthcare and medicine fields. Over the past decade, there was a rapid advance in the processing methods, materials and platforms which has led to the increase in the development of stretchable and flexible sensors for different functions.

The well-known CMOS silicon-based devices are manufactured using a complicated fabrication process which are expensive, time consuming, and involves several steps. Also, these devices are brittle, rigid with thick layers and limited to small areas. Printing technology appears to be a solution to these technological disadvantages, offering several advantages such as low cost, high seed, possibility of room temperature processing and most importantly applicability to flexible substrates. Printing technology also provides direct patterning on substrate eliminating the need for expensive masks and opening the door to complex patterns and choice of materials. In spite of having lots of advantages of printed photodetectors, the vast majority of the current commercially available optical devices are not based on printed technologies. Photodetectors can be easily integrated into polymer films solutions which can be applied to flexible surfaces.

The novel properties of the thin film flexible and wearable technologies such as economical, less power consuming, biocompatible, multifunctional, mechanical flexibility and simple device integration allow them to be utilized in a wide range of applications from water purification to

space exploration and many more. In future, there are diverse challenges and opportunities for the researchers in the area of development of stretchable and flexible sensors. Biocompatibility analysis of the stretchable and flexible sensors which are attached to the human body in terms of its toxicity is of great importance. Innovative approaches such as design of devices, surface manipulation, material selection, methods of assembly and also surface engineering can play a crucial role in solving the above-mentioned challenges.

The gas sensor fabrication has experienced a radical transformation into a thin film from powder-based thick films formed by chemical and physical vapor deposition techniques. Both deposition techniques facilitate the use of porous structures which are relevant for gas sensing and also help in controlling the material microstructures such as grain boundary and size. Literature survey on materials for gas sensor helps us in identifying the major three different classes of materials which are essential for gas sensing. The three classes of materials are 2D transition metal dichalcogenides (TMDs), oxide nanostructures, and graphene composites which have undoubtedly proven their potential for spontaneous sensing of toxic and dangerous gases and under controlled condition, the real-time gas observation. In spite of all this, there are some relevant disadvantages to these materials, which leave room for further improvements to enhance stability and selectivity. Moreover, in the case of both graphene and TMDs, the gas detection mechanism is still not well settled. The design of heterostructures and surface functionalization with a variety of nanomaterials can overcome these disadvantages in the near future. In summary, the TMDs nanosheets with their rare attributes coupled with substantial production have excited tremendous research efforts to exploit them as building blocks for structurally important functional composite nanomaterials. The formation of innovative functional hybrids of TMDs has been accomplished by conjugation of transition metals and chalcogen atoms. In this survey, I have studied the latest development in the TMDs and metal oxide nanostructures based NO_2 gas sensors and the summary is given in two tables. Along with the advancement of modern approaches, one of the utmost encouraging chances in this area is the hybridization of other kinds of TMDs nanostructures such as ZrS_2, WS_2, HfS_2, and WSe_2 with a range of materials to achieve innovative functional composites for numerous operations.

4.8 References:

[1] P. Mehrotra, Biosensors and their applications - a review, J. Oral Biol. Craniofac. Res. (2016).

[2] C.C. Conrad, K.G. Hilchey, A review of citizen science and community-based environmental monitoring: issues and opportunities, Environ. Monit. Assess. (2011).

[3] Y. Bar-Cohen, Biomimetics—using nature to inspire human innovation, Bioinspir. Biomim. 1 (March (1)) (2006) P1–P12.

[4] Jing Kong, Nathan R. Franklin, Chongwu Zhou, Michael G. Chapline, Shu Peng, Kyeongjae Cho, Hongjie Dai, Nanotube Molecular Wires as Chemical Sensors, 2000.

[5] R.J. Chen, N.R. Franklin, J. Kong, J. Cao, T.W. Tombler, Y. Zhang, H. Dai, Molecular photodesorption from single-walled carbon nanotubes, Appl. Phys. Lett. (2001).

[6] S. Seager, W. Bains, The search for signs of life on exoplanets at the interface of chemistry and planetary science, Sci. Adv. (2015).

[7] O. Lupan, V.V. Ursaki, G. Chai, L. Chow, G.A. Emelchenko, I.M. Tiginyanu, A.N. Gruzintsev, A.N. Redkin, Selective hydrogen gas nanosensor using individual ZnO nanowire with fast response at room temperature, Sens. Actuators B Chem. 144 (January (1)) (2010) 56–66.

[8] H. Chang, J. Do Lee, S.M. Lee, Y.H. Lee, Adsorption of NH 3 and NO 2 molecules on carbon nanotubes, Appl. Phys. Lett. 79 (96) (2001), 123112–2773.

[9] K. Indira, U.K. Mudali, T. Nishimura, N. Rajendran, A review on TiO_2 nanotubes: influence of anodization parameters, formation mechanism, properties, corrosion behavior, and biomedical applications, J. BioTribo-Corros. (2015).

[10] M.C. Kaur, Amandeep Singh, Inderpreet Kumar, Jitender Madhwal, Devinder Bhatnagar, P.K. Mathur, P.C. Bernardo, C.A. Paiva, An environment friendly highly sensitive ethanol vapor sensor based on polymethylethacrylate: functionalized-multiwalled carbon nanotubes composite, Adv. Sci. Eng. Med. 5 (10) (2013) 1062–1066.

[11] A. Kumari, N. Prasad, A. Kaur, S.K. Dixit, P.K. Bhatnagar, P.C. Mathur, "Effect of surfactant assisted dispersed graphene on sensitivity of MWCNT-alcohol sensor", AIP Conference Proc. 568 (2014) 568–570.

[12] A. Kaur, I. Singh, J. Kumar, C. Bhatnagar, S.K. Dixit, P.K. Bhatnagar, P.C.Mathur, J.A. Covas, M. Da Conceicao, Paiva, "Enhancement in the performance of multi-walled carbon nanotube: poly(methylmethacrylate) composite thin film ethanol sensors through appropriate nanotube functionalization, Mater. Sci. Semicond. Process. 31 (2015) 166–174.

[13] S.S. Varghese, S. Lonkar, K.K. Singh, S. Swaminathan, A. Abdala, Recent advances in graphene-based gas sensors, Sens. Actuators B Chem. 218(October) (2015) 160–183.

[14] S.V.N.T. Kuchibhatla, A.S. Karakoti, D. Bera, S. Seal, One dimensional nanostructured materials, Prog. Mater. Sci. 52 (July (5)) (2007) 699–913.

[15] B. Kumar, M. Castro, J.F. Feller, Poly(lactic acid)–multi-wall carbon nanotube conductive biopolymer nanocomposite vapour sensors, Sens. Actuators B Chem. 161 (January (1)) (2012) 621–628.

[16] M. Trojanowicz, Analytical applications of carbon nanotubes: a review, TrAC Trends Anal. Chem. 25 (May (5)) (2006) 480–489.

[17] S. Kumar, V. Pavelyev, P. Mishra, N. Tripathi, Sensitive detection of nitrogen dioxide using gold nanoparticles decorated single walled carbon nanotubes, CEUR Workshop Proc. 1900 (September) (2017).

[18] L. Bai, Z. Zhou, Computational study of B- or N-doped single-walled carbon nanotubes as NH3 and NO_2 sensors, Carbon N. Y. 45 (September (10)) (2007) 2105–2110.

[19] K. Varshney, Carbon nanotubes: a review on synthesis, properties and applications, Int. J. Eng. Res. Gen. Sci. 2 (4) (2014).

[20] B. Zhan, C. Li, J. Yang, G. Jenkins, W. Huang, X. Dong, Graphene Field-Effect Transistor and Its Application for Electronic Sensing, 2014.

[21] K. Hata, D.N. Futaba, K. Mizuno, T. Namai, Water-Assisted Highly Efficient Synthesis of Impurity-Free Single-Walled Carbon Nanotubes, 2004.

[22] E. Pop, D. Mann, Q. Wang, K. Goodson, H. Dai, Thermal conductance of an individual single-wall carbon nanotube above room temperature, Nano Lett. (2006).

[23] X. Guo, J.B. Wang, H.W. Zhang, Mechanical properties of single-walled carbon nanotubes based on higher order Cauchy–born rule, Int. J. Solids Struct. 43 (March (5)) (2006) 1276–1290.

[24] H.-B. Chen, J.-D. Lin, Y. Cai, X.-Y. Wang, J. Yi, J. Wang, G. Wei, Y.-Z. Lin, D.-W. Liao, Novel multi-walled nanotubes-supported and alkali-promoted Ru catalysts for ammonia synthesis under atmospheric pressure, Appl. Surf. Sci. 180 (August (3–4)) (2001) 328–335.

[25] H. F. G, T.T.T.W. Ebbesen, H.J. Lezec, H. Hiura, J.W. Bennett, Electrical Conductivity of Individual Carbon Nanotubes, 1996.

[26] M.-F. Yu, B.S. Files, S. Arepalli, R.S. Ruoff, Tensile Loading of Ropes of Single Wall Carbon Nanotubes and Their Mechanical Properties, 2000.

[27] T. Dürkop, B.M. Kim, M.S. Fuhrer, Properties and applications of high-mobility semiconducting nanotubes, J. Phys. Condens. Matter (2004).

[28] M. W. Rowell, M. A. Topinka, M. D. McGehee, H. J. Prall, G. Dennler, N. S. Sariciftci, L. Hu, and G. Gruner, "Organic solar cells with carbon nanotube network electrodes." Appl. Phys. Lett., 88 (2006).

[29] G. Gruner, "Carbon nanotube films for transparent and plastic electronics." J. Mater. Chem., 16, 3533 (2006).

[30] K. Ellmer, "Past achievements and future challenges in the development of optically transparent electrodes." Nat. Photonics, 6, 809 (2012).

[31] S. N. Habisreutinger, T. Leijtens, G. E. Eperon, S. D. Stranks, R. J. Nicholas, and H. J. Snaith, "Carbon nanotube/polymer composites as a highly stable hole collection layer in perovskite solar cells." Nano Lett., 14, 5561 (2014).

[32] Y. Liu, X. Y. Yu, Y. Fang, X. Zhu, J. Bao, X. Zhou, and X. W. (David) Lou, "Confining SnS2Ultrathin nanosheets in hollow carbon nanostructures for efficient capacitive sodium storage." Joule, 2, 725 (2018).

[33] H. Li et al., "An extremely safe and wearable solid-state zinc ion battery based on a hierarchical structured polymer electrolyte." Energy Environ. Sci., 11, 941(2018).

[34] H. He, Q. Gan, H. Wang, G. L. Xu, X. Zhang, D. Huang, F. Fu, Y. Tang, K. Amine, and M. Shao, "Structure-dependent performance of TiO_2/C as anode material for Na-ion batteries." Nano Energy, 44, 217 (2018).

[35] E. A. Mwafy and A. M. Mostafa, "Multi walled carbon nanotube decorated cadmium oxide nanoparticles via pulsed laser ablation in liquid media." Opt. Laser Technol., 111, 249 (2019).

[36] J. O. Thostenson, Z. Li, C. H. J. Kim, A. Ajnsztajn, C. B. Parker, J. Liu, A. V. Peterchev, J. T. Glass, and S. M. Goetz, "Integrated flexible conversion circuit between a flexible photovoltaic and supercapacitors for powering wearable sensors." J. Electrochem. Soc., 165, B3122 (2018).

[37] B. Pohl and H. D. Wiemhöfer, "Highly thermal and electrochemical stable dinitrile disiloxane as co-solvent for use in lithium-ion batteries." J. Electrochem. Soc.,162, A460 (2015).

[38] V. Müller, R.-G. Scurtu, K. Richter, T. Waldmann, M. Memm, M. A. Danzer, and M. Wohlfahrt-Mehrens, "Effects of mechanical compression on the aging and the expansion behavior of Si/C-Composite|NMC811 in different lithium-ion battery cell formats." J. Electrochem. Soc., 166, A3796 (2019).

[39] D. Bresser, B. Oschmann, M. N. Tahir, F. Mueller, I. Lieberwirth, W. Tremel, R. Zentel, and S. Passerini, "Carbon-coated anatase TiO_2 nanotubes for liand naion anodes." J. Electrochem. Soc., 162, A3013 (2015).

[40] J. Homann, F. Kratz, and H. Laube, "Galactosamine (Galam) liver damage: dissociation of effects of diethyldithiocarbamate (DTC) on sGOT, insulin, liver 7- ethoxycoumarine hydroxylase (7-EtCH) and on liver histology in fed and fasted rats." Naunyn. Schmiedebergs. Arch. Pharmacol., 313, 6252 (1980).

[41] Y. He, W. Chen, C. Gao, J. Zhou, X. Li, and E. Xie, "An overview of carbon materials for flexible electrochemical capacitors." Nanoscale, 5, 8799 (2013).

[42] Z. Zhang et al., "A colour-tunable, weavable fibre-shaped polymer light-emitting electrochemical cell." Nat. Photonics, 9, 233 (2015).

[43] Y. Lin, S. Taylor, H. Li, K. A. S. Fernando, L. Qu, W. Wang, L. Gu, B. Zhou, and Y. P. Sun, "Advances toward bioapplications of carbon nanotubes." J. Mater. Chem., 14, 527 (2004).

[44] S. K. Smart, A. I. Cassady, G. Q. Lu, and D. J. Martin, "The biocompatibility of carbon nanotubes." Carbon N. Y., 44, 1034 (2006).

[45] R. Vankayala and K. C. Hwang, "Near-infrared-light-activatable nanomaterial mediated phototheranostic nanomedicines: an emerging paradigm for cancer treatment." Adv. Mater., 301706320 (2018).

[46] L. Nela, J. Tang, Q. Cao, G. Tulevski, and S. J. Han, "Large-area highperformance flexible pressure sensor with carbon nanotube active matrix for electronic skin." Nano Lett., 18, 2054 (2018).

[47] C. Mu, Y. Song, W. Huang, A. Ran, R. Sun, W. Xie, and H. Zhang, "Flexible normal-tangential force sensor with opposite resistance responding for highly sensitive artificial skin." Adv. Funct. Mater., 28, 1707503 (2018).

[48] W. Bai, T. Kuang, C. Chitrakar, R. Yang, S. Li, D. Zhu, and L. Chang, "Patchable micro/nanodevices interacting with skin." Biosens. Bioelectron., 122, 189 (2018).

[49] L. Hu, M. Pasta, F. La Mantia, L. Cui, S. Jeong, H. D. Deshazer, J. W. Choi, S. M. Han, and Y. Cui, "Stretchable, porous, and conductive energy textiles." Nano Lett., 10, 708 (2010).

[50] G. Zhou, F. Li, and H. M. Cheng, "Progress in flexible lithium batteries and future prospects." Energy Environ. Sci., 7, 1307 (2014).

[51] N. T. S. S. Islam, "A new approach for orientation-controlled growth of CNTs: an in- depth analysis on the role of oxygen plasma treatment to catalyst." Appl. Nanosci., 7, 125 (2017).

[52] M. Eslamian, "Inorganic and organic solution-processed thin film devices." NanoMicro Letters, 9, 1 (2017).

[53] S. Kumar, R. Rani, N. Dilbaghi, K. Tankeshwar, and K. H. Kim, "Carbon nanotubes: a novel material for multifaceted applications in human healthcare." Chem. Soc. Rev., 46, 158 (2017).

[54] K. Fu, Y. Yao, J. Dai, and L. Hu, "Progress in 3D printing of carbon materials for energy-related applications." Adv. Mater., 29 (2017).

[55] N. Tripathi, V. Pavelyev, and S. S. Islam, "Synthesis of carbon nanotubes using green plant extract as catalyst: unconventional concept and its realization." Appl. Nanosci., 7, 557 (2017).

[56] S. Yao and Y. Zhu, "Nanomaterial-enabled stretchable conductors: strategies, materials and devices." Adv. Mater., 27, 1480 (2015).

[57] J. Kim et al., "Stretchable silicon nanoribbon electronics for skin prosthesis." Nat. Commun., 5, 1 (2014).

[58] T. Sekitani, H. Nakajima, H. Maeda, T. Fukushima, T. Aida, K. Hata, and T. Someya, "Stretchable active-matrix organic light-emitting diode display using printable elastic conductors." Nat. Mater., 8, 494 (2009).

[59] S. Beg, M. Rizwan, A. M. Sheikh, M. S. Hasnain, K. Anwer, and K. Kohli, "Advancement in carbon nanotubes: basics, biomedical applications and toxicity." J. Pharm. Pharmacol., 63, 141 (2011).

[60] M. Ajayan Pulickel, M. Endo, and M. S. Strano, "Potential applications of carbon nanotubes." Carbon Nanotub. Adv. Top. Synth. Struct. Prop. Appl. Top. Appl. Physics., 111, 13 (2008).

[61] C. Hierold, A. Jungen, C. Stampfer, and T. Helbling, "Nano electromechanical sensors based on carbon nanotubes." Sensors and Actuators, A: Physical, 136, 51(2007).

[62] S. Kumar, V. Pavelyev, P. Mishra, and N. Tripathi, "Sensitive detection of nitrogen dioxide using gold nanoparticles decorated single walled carbon nanotubes." in CEUR Workshop Proceedings, 1900, p. 74 (2017).

[63] M. A. Monne, X. Lan, and M. Y. Chen, "Review article material selection and fabrication processes for flexible conformal antennas." Int. J. Antennas Propag., 2018, 14 (2018).

[64] S. W. Hwang et al., "Biodegradable elastomers and silicon nanomembranes/ nanoribbons for stretchable, transient electronics, and biosensors." Nano Lett., 15, 2801 (2015).

[65] J. A. Rogers, M. G. Lagally, and R. G. Nuzzo, "Synthesis, assembly and applications of semiconductor nanomembranes." Nature, 477, 45 (2011).

[66] Y. Meng, Y. Zhao, C. Hu, H. Cheng, Y. Hu, Z. Zhang, G. Shi, and L. Qu, "Allgraphene core-sheath microfibers for all-solid-state, stretchable fibriform supercapacitors and wearable electronic textiles." Adv. Mater., 25, 2326 (2013).

[67] K. S. Kim, Y. Zhao, H. Jang, S. Y. Lee, J. M. Kim, K. S. Kim, J. H. Ahn, P. Kim, J. Y. Choi, and B. H. Hong, "Large-scale pattern growth of graphene films for stretchable transparent electrodes." Nature, 457, 706 (2009).

[68] S. Kumar, V. Pavelyev, P. Mishra, and N. Tripathi, "A review on chemiresistive gas sensors based on carbon nanotubes: device and technology transformation." Sensors Actuators A Phys., 283, 174 (2018).

[69] Z. Lv et al., "Honeycomb-lantern-inspired 3D stretchable supercapacitors with enhanced specific areal capacitance." Adv. Mater., 30, 1805468 (2018).

[70] M. E. McConney et al., "Direct synthesis of ultra-thin large area transition metal dichalcogenides and their heterostructures on stretchable polymer surfaces." J. Mater. Res., 31, 967 (2016).

[71] W. Zhao, R. M. Ribeiro, and G. Eda, "Electronic structure and optical signatures of semiconducting transition metal dichalcogenide nanosheets." Acc. Chem. Res., 48, 91 (2015).

[72] C. Clement Raj and R. Prasanth, "Review—advent of TiO_2 nanotubes as supercapacitor electrode." J. Electrochem. Soc., 165, E345 (2018).

[73] M. Amjadi, A. Pichitpajongkit, S. Lee, S. Ryu, and I. Park, "Highly stretchable and sensitive strain sensor based on silver nanowire-elastomer nanocomposite." ACS Nano, 8, 5154 (2014).

[74] P. Lee, J. Lee, H. Lee, J. Yeo, S. Hong, K. H. Nam, D. Lee, S. S. Lee, and S. H. Ko, "Highly stretchable and highly conductive metal electrode by very long metal nanowire percolation network." Adv. Mater., 24, 3326 (2012).

[75] J. Y. Oh et al., "Intrinsically stretchable and healable semiconducting polymer for organic transistors." Nature, 539, 411 (2016).

[76] J. Song, J. Li, J. Xu, and H. Zeng, "Superstable transparent conductive Cu@Cu4 Ni nanowire elastomer composites against oxidation, bending, stretching, and twisting for flexible and stretchable optoelectronics." Nano Lett., 14, 6298 (2014).

[77] N. Tripathi, P. Mishra, B. Joshi, and S. S. Islam, "Precise control over physical characteristics of carbon nanotubes by differential variation of Argon flow rate during chemical vapor deposition processing: A systematic study on growth kinetics." Mater. Sci. Semicond. Process., 35, 207 (2015).

[78] B. Vigolo, A. Penicaud, C. Coulon, C. Sauder, R. Pailler, C. Journet, P. Bernier, and P. Poulin, "Macroscopic fibers and ribbons of oriented carbon nanotubes." Science, 290, 1331 (2000).

[79] K. Jiang, Q. Li, and S. Fan, "Nanotechnology: spinning continuous carbon nanotube yarns." Nature, 419, 801 (2002).

[80] B. A. Kakade, V. K. Pillai, D. J. Late, P. G. Chavan, F. J. Sheini, M. A. More, and D. S. Joag, "High current density, low threshold field emission from functionalized carbon nanotube bucky paper." Appl. Phys. Lett., 97, 073102 (2010).

[81] R. B. Sharma, D. J. Late, D. S. Joag, A. Govindaraj, and C. N. R. Rao, "Field emission properties of boron and nitrogen doped carbon nanotubes." Chem. Phys. Lett., 428, 102 (2006).

[82] S. Kumar, V. Pavelyev, P. Mishra, N. Tripathi, P. Sharma, and F. Calle, "A review on 2D transition metal di-chalcogenides and metal oxide nanostructures based NO_2 gas sensors." Mater. Sci. Semicond. Process., 107, 104865 (2020).

[83] N. Joshi, T. Hayasaka, Y. Liu, H. Liu, O. N. Oliveira, and L. Lin, "A review on chemiresistive room temperature gas sensors based on metal oxide nanostructures, graphene and 2D transition metal dichalcogenides." Microchim. Acta, 185, 213 (2018).

[84] N. Joshi et al., "One-step approach for preparing ozone gas sensors based on hierarchical NiCo2O4 structures." RSC Adv., 6, 92655 (2016).

[85] N. Joshi et al., "Yolk-shelled ZnCo2O4 microspheres: surface properties and gas sensing application." Sensors Actuators, B Chem., 257, 906 (2018).

[86] X. Liu, T. Ma, N. Pinna, and J. Zhang, "Two-dimensional nanostructured materials for gas sensing." Adv. Funct. Mater., 27, 1 (2017).

[87] E. Comini, C. Baratto, G. Faglia, M. Ferroni, A. Vomiero, and G. Sberveglieri, "Quasi-one dimensional metal oxide semiconductors: preparation, characterization and application as chemical sensors." Prog. Mater Sci., 54, 1 (2009).

[88] D. Zappa, A. Bertuna, E. Comini, N. Kaur, N. Poli, V. Sberveglieri, and G. Sberveglieri, "Metal oxide nanostructures: preparation, characterization and functional applications as chemical sensors." Beilstein J. Nanotechnol., 8, 1205 (2017).

[89] N. Barsan, C. Simion, T. Heine, S. Pokhrel, and U. Weimar, "Modeling of sensing and transduction for p-type semiconducting metal oxide based gas sensors." J. Electroceramics., 25, 11 (2010).

[90] P. T. Moseley, "Progress in the development of semiconducting metal oxide gas sensors: a review." Meas. Sci. Technol., 082001, 082001 (2017).

[91] Y. Wang et al., "Low-temperature H2S detection with hierarchical Cr-Doped WO3 microspheres." ACS Appl. Mater. Interfaces, 8, 9674 (2016).

[92] Z. Li et al., "Advances in designs and mechanisms of semiconducting metal oxide nanostructures for high-precision gas sensors operated at room temperature." Mater. Horizons, 6, 470 (2019).

[93] A. Bag and N. E. Lee, "Gas sensing with heterostructures based on twodimensional nanostructured materials: a review." J. Mater. Chem. C, 7, 13367 (2019).

[94] D. Barreca, E. Comini, A. P. Ferrucci, A. Gasparotto, C. Maccato, C. Maragno, G. Sberveglieri, and E. Tondello, "First example of ZnO−TiO_2 nanocomposites by chemical vapor deposition: structure, morphology, composition, and gas sensing performances." Chem. Mater., 19, 5642 (2007).

[95] W. J. Moon, J. H. Yu, and G. M. Choi, "The CO and H2 gas selectivity of CuOdoped SnO_2–ZnO composite gas sensor." Sensors Actuators B Chem., 87, 464 (2002).

[96] C. R. Newman, C. D. Frisbie, D. A. Da Silva Filho, J.-L. Brédas, P. C. Ewbank, and K. R. Mann, "Introduction to organic thin film transistors and design of nchannel organic semiconductors." Chem. Mater., 16, 4436 (2004).

[97] X. Duan, C. Niu, V. Sahi, J. Chen, J. W. Parce, S. Empedocles, and J. L. Goldman, "High-performance thin-film transistors using semiconductor nanowires and nanoribbons." Nature, 425, 274 (2003).

[98] P. Sharma and N. Gupta, "Two dimensional simulation and analysis of density-ofstates (Dos) in top-gated Nanocrystalline Silicon thin film transistor (nc-Si TFT)." Int. J. Nanoelectron. Mater., 10, 101 (2017).

[99] P. Sharma and N. Gupta, "Model for threshold voltage instability in top-gated nanocrystalline silicon thin film transistor." J. Comput. Electron., 15, 666 (2016).

[100] S. Zhang, S. Chen, F. Hu, L. Ding, Y. Gu, B. Yan, F. Yang, M. Jiang, and Y. Cao, "Patterned flexible electrochromic device based on monodisperse silica/polyaniline core/shell nanospheres." J. Electrochem. Soc., 166, H343 (2019).

[101] J. Yoneda et al., "A quantum-dot spin qubit with coherence limited by charge noise and fidelity higher than 99.9%." Nat. Nanotechnol., 13, 102 (2018).

[102] G. Wu, Y. Cheng, Z. Yang, Z. Jia, H. Wu, L. Yang, H. Li, P. Guo, and H. Lv, "Design of carbon sphere/magnetic quantum dots with tunable phase compositions and boost dielectric loss behavior." Chem. Eng. J., 333, 519 (2018).

[103] P. Sharma and N. Gupta, “Electronic behavior of nanocrystalline silicon thin film transistor.” Nanomater. Their Appl., 84, 209 (2017).

[104] P. Sharma, “Threshold voltage modeling on nanocrystalline silicon thin film transistors.” J. Electron Devices, 19, 1608 (2014).

[105] K. Y. Wang, Y. K. Chiu, and H. C. Cheng, “Electrochemical capacitors of horizontally aligned carbon nanotube electrodes with oxygen plasma treatment.” J. Electrochem. Soc., 164, A1587 (2017).

[106] R. P. Tortorich, E. Song, and J.-W. Choi, “Inkjet-printed carbon nanotube electrodes with low sheet resistance for electrochemical sensor applications.” J. Electrochem. Soc., 161, B3044 (2014).

[107] C. C. Raj and R. Prasanth, “Transverse tuning of TiO_2 nanotube array by controlling the electrochemical charge transfer resistance with potassium carbonate and sodium carbonate composition in ammonium fluoride electrolyte.” J. Electrochem. Soc., 162, E23 (2015).

[108] T. H. V. Kumar and A. K. Sundramoorthy, “Non-enzymatic electrochemical detection of urea on silver nanoparticles anchored nitrogen-doped single-walled carbon nanotube modified electrode.” J. Electrochem. Soc., 165, B3006 (2018).

[109] M. Arefin, “Empirical equation based chirality (n, m) assignment of semiconducting single wall carbon nanotubes from resonant raman scattering data.” Nanomaterials, 3, 1 (2012).

[110] L. Ding, A. Tselev, J. Wang, D. Yuan, H. Chu, T. P. McNicholas, Y. Li, and J. Liu, “Selective growth of well-aligned semiconducting single-walled carbon nanotubes.” Nano Lett., 9, 800 (2009).

[111] N. Izard, S. Kazaoui, K. Hata, T. Okazaki, T. Saito, S. Iijima, and N. Minami, “Semiconductor-enriched single wall carbon nanotube networks applied to field effect transistors.” Appl. Phys. Lett., 92, 243112 (2008).

[112] A. Star, T.-R. Han, J.-C. P. Gabriel, K. Bradley, and G. Grüner, “Interaction of aromatic compounds with carbon nanotubes: correlation to the hammett parameter of the substituent and measured carbon nanotube FET response.” Nano Lett., 3, 1421 (2003).

[113] S. J. Kang, C. Kocabas, T. Ozel, M. Shim, N. Pimparkar, M. A. Alam, S. V. Rotkin, and J. A. Rogers, “High-performance electronics using dense, perfectly aligned arrays of single-walled carbon nanotubes.” Nat. Nanotechnol., 2, 230 (2007).

[114] S. Park, M. Vosguerichian, and Z. Bao, “A review of fabrication and applications of carbon nanotube film-based flexible electronics.” Nanoscale, 5, 1727 (2013).

[115] Q. Zhang, S. Rastogi, D. Chen, D. Lippits, and P. J. Lemstra, “Low percolation threshold in single-walled carbon nanotube/high density polyethylene composites prepared by melt processing technique.” Carbon N. Y., 44, 778 (2006).

[116] N. Tripathi, V. Pavelyev, and S. S. Islam, “Tunable growth of single-wall CNTs by monitoring temperature increasing rate.” Int. Nano Lett., 8, 101 (2018).

[117] P. Sharma, N. Tripathi, and N. Gupta, “Nanocrystalline silicon thin film prepared by e-beam evaporation for display application.” J. Mater. Sci., Mater. Electron., 28, 3891 (2017).

[118] M. Vosgueritchian, D. J. Lipomi, and Z. Bao, “Highly conductive and transparent PEDOT:PSS films with a fluorosurfactant for stretchable and flexible transparent electrodes.” Adv. Funct. Mater., 22, 421 (2012).

[119] Y. Wang, R. Yang, Z. Shi, L. Zhang, D. Shi, E. Wang, and G. Zhang, “Superelastic graphene ripples for flexible strain sensors.” ACS Nano, 5, 3645 (2011).

[120] B.-H. Jo, L. M. Van Lerberghe, K. M. Motsegood, and D. J. Beebe, “Threedimensional micro-channel fabrication in polydimethylsiloxane (PDMS) elastomer.” J. Microelectromechanical Syst., 9, 76 (2000).

[121] M.-Y. Choi, D. Choi, M.-J. Jin, I. Kim, S.-H. Kim, J.-Y. Choi, S. Y. Lee, J. M. Kim, and S.-W. Kim, “Mechanically powered transparent flexible chargegenerating nanodevices with piezoelectric ZnO nanorods.” Adv. Mater., 21, 2185 (2009).

[122] S. Ito, N. L. C. Ha, G. Rothenberger, P. Liska, P. Comte, S. M. Zakeeruddin, P. Péchy, M. K. Nazeeruddin, and M Grätzel, "High-efficiency (7.2%) flexible dye-sensitized solar cells with Ti-metal substrate for nanocrystalline-TiO_2 photoanode." Chem. Commun., 38, 4004 (2006).

[123] F. C. Krebs, "All solution roll-to-roll processed polymer solar cells free from indium-tin-oxide and vacuum coating steps." Org. Electron. physics, Mater. Appl., 10, 761 (2009).

[124] P. Hu et al., "Highly responsive ultrathin GaS nanosheet photodetectors on rigid and flexible substrates." Nano Lett., 13, 1649 (2013).

[125] A. R. Madaria, A. Kumar, F. N. Ishikawa, and C. Zhou, "Uniform, highly conductive, and patterned transparent films of a percolating silver nanowire network on rigid and flexible substrates using a dry transfer technique." Nano Res., 3, 564 (2010).

[126] K. Dong et al., "Versatile core–sheath yarn for sustainable biomechanical energy harvesting and real-time human-interactive sensing." Adv. Energy Mater., 8, 1801114 (2018).

[127] J. Lewis, "Material challenge for flexible organic devices." Mater. Today, 9, 38 (2006).

[128] S. K. Lee, M. J. Song, J. H. Kim, T. S. Kan, Y. K. Lim, J. P. Ahn, and D. S. Lim, "3D-networked carbon nanotube/diamond core–shell nanowires for enhanced electrochemical performance." NPG Asia Mater., 6 (2014).

[129] T. H. Le, Y. Kim, and H. Yoon, "Electrical and electrochemical properties of conducting polymers." Polymers, 9, 150 (2017).

[130] W.H. Organization, World Health Statistics, 2018: Monitoring Health for the SDGs Sustainable Development Goals, World Health Organization, 2018.

[131] T.W. Hesterberg, W.B. Bunn, R.O. McClellan, A.K. Hamade, C.M. Long, P. A. Valberg, Critical review of the human data on short-term nitrogen dioxide (NO_2) exposures: evidence for NO_2 no-effect levels, Crit. Rev. Toxicol. 39 (9) (2009) 743–781.

[132] B. Bhangare, N.S. Ramgir, S. Jagtap, A.K. Debnath, K.P. Muthe, C. Terashima, D. K. Aswal, S.W. Gosavi, A. Fujishima, XPS and Kelvin probe studies of SnO_2/RGO nanohybrids based NO_2 sensors, Appl. Surf. Sci. 487 (March) (2019) 918–929.

[133] M.L. Wong, B.D. Charnay, P. Gao, Y.L. Yung, M.J. Russell, Nitrogen oxides in early earth's atmosphere as electron acceptors for life's emergence, Astrobiology 17 (10) (2017) 975–983.

[134] D.S. Jyethi, in: U. Kulshrestha, P. Saxena (Eds.), Plant Responses to Air Pollution, Springer Singapore, Singapore, 2016, pp. 5–19, https://doi.org/10.1007/978- 981-10-1201-3_2.

[135] S.M. Bernard, J.M. Samet, A. Grambsch, K.L. Ebi, I. Romieu, Environ. Health Perspect. 109 (2001) 199–209.

[136] B.J. Finlayson-Pitts, J.N. Pitts Jr., Chemistry of the Upper and Lower Atmosphere: Theory, Experiments, and Applications, Academic press, 1999.

[137] G. Korotcenkov, The role of morphology and crystallographic structure of metal oxides in response of conductometric-type gas sensors, Mater. Sci. Eng. R Rep. 61 (2008) 1–39.

[138] P.G. Han, H. Wong, M.C. Poon, Sensitivity and stability of porous polycrystalline silicon gas sensor, Colloid. Surf. A Physicochem. Eng. Asp. 179 (2001) 171–175.

[139] A. Zandi, A. Gilani, H. Ghafoori fard, J. Koohsorkhi, An optimized resistive CNTbased gas sensor with a novel configuration by top electrical contact, Diam. Relat. Mater. 93 (January) (2019) 224–232.

[140] H. Jeong, Y. Noh, D. Lee, Highly stable and sensitive resistive flexible humidity sensors by means of roll-to-roll printed electrodes and flower-like TiO_2 nanostructures, Ceram. Int. 45 (1) (2019) 985–992.

[141] A. Mirzaei, et al., An overview on how Pd on resistive-based nanomaterial gas sensors can enhance response toward hydrogen gas, Int. J. Hydrogen Energy 44 (36) (2019) 20552–20571.

[142] J.M. Walker, S.A. Akbar, P.A. Morris, Synergistic effects in gas sensing semiconducting oxide nano-heterostructures: a review, Sens. Actuators B Chem. 286 (December 2018) (2019) 624–640.

[143] G. Korotcenkov, V. Brinzari, B.K. Cho, In2O3- and SnO_2-based ozone sensors: design and characterization, Crit. Rev. Solid State Mater. Sci. 43 (2) (2018) 83–132.

[144] L. Yu, et al., Hierarchical 3D flower-like MoS 2 spheres : post-thermal treatment in vacuum and their NO 2 sensing properties, Mater. Lett. 183 (2016) 122–126

[145] W. Yan, M.A. Worsley, T. Pham, A. Zettl, C. Carraro, R. Maboudian, Effects of ambient humidity and temperature on the NO 2 sensing characteristics of WS 2/ graphene aerogel, Appl. Surf. Sci. 450 (2018) 372–379.

[146] Y. Zhang, W. Zeng, Y. Li, Hydrothermal synthesis and controlled growth of hierarchical 3D flower-like MoS2 nanospheres assisted with CTAB and their NO_2 gas sensing properties, Appl. Surf. Sci. 455 (May) (2018) 276–282.

[147] M. Wook, S. Myeoung, K. Nam, K. An, B. Ku, Highly transparent and flexible NO 2 gas sensor film based on MoS 2/rGO composites using soft lithographic patterning, Appl. Surf. Sci. 456 (June) (2018) 7–12.

[148] S. Zhao, G. Wang, J. Liao, S. Lv, Z. Zhu, Z. Li, Vertically aligned MoS 2/ZnO nanowires nanostructures with highly enhanced NO 2 sensing activities, Appl. Surf. Sci. 456 (June) (2018) 808–816.

[149] M. Donarelli, et al., Response to NO 2 and other gases of resistive chemically exfoliated MoS 2 -based gas sensors, Sens. Actuators B Chem. 207 (2) (2015) 602–613.

[150] A. Kumar, S. Kumar, A convenient and efficient copper-catalyzed synthesis of unsymmetrical and symmetrical diaryl chalcogenides from arylboronic acids in ethanol at room temperature, Tetrahedron 70 (9) (2014) 1763–1772.

[151] Y.S. Shim, et al., Synthesis of numerous edge sites in MoS2via SiO_2Nanorods platform for highly sensitive gas sensor, ACS Appl. Mater. Interfaces 10 (37) (2018) 31594–31602.

[152] E. Lee, Y.S. Yoon, D.J. Kim, Two-dimensional transition metal dichalcogenides and metal oxide hybrids for gas sensing, ACS Sens. 3 (10) (2018) 2045–2060.

[153] H. Medina, et al., Wafer-scale growth of WSe2 monolayers toward phaseengineered hybrid WOx/WSe2 films with sub-ppb NOx gas sensing by a lowtemperature plasma-assisted selenization process, Chem. Mater. 29 (4) (2017) 1587–1598.

[154] E. Núnez ~ Carmona, et al., Detection of food and skin pathogen microbiota by means of an electronic nose based on metal oxide chemiresistors, Sens. Actuators B Chem. 238 (2017) 1224–1230.

[155] H.K. Hong, C.H. Kwon, S.R. Kim, D.H. Yun, K. Lee, Y.K. Sung, Portable electronic nose system with gas sensor array and artificial neural network, Sens. Actuators B Chem. 66 (1) (2000) 49–52.

[156] S. Chen, Y. Tang, K. Zhan, D. Sun, X. Hou, Chemiresistive nanosensors with convex/concave structures, Nano Today 20 (2018) 84–100.

[157] X. Chen, et al., NO_2 sensing properties of one-pot-synthesized ZnO nanowires with Pd functionalization, Sens. Actuators B Chem. 280 (2) (2019) 151–161.

[158] Y. Chen, et al., Two-dimensional metal nanomaterials: synthesis, properties, and applications, Chem. Rev. 118 (13) (2018) 6409–6455.

[159] O. Lupan, V. Postica, F. Labat, I. Ciofini, T. Pauport&#xfffd;e, R. Adelung, Ultra-sensitive and selective hydrogen nanosensor with fast response at room temperature based on a single Pd/ZnO nanowire, Sens. Actuators B Chem. 254 (2018) 1259–1270.

[160] Z. Li, J. Yi, Synthesis and enhanced NO_2-sensing properties of ZnO-decorated SnO_2 microspheres, Mater. Lett. 236 (2) (2019) 570–573.

[161] Y.N. Rane, et al., Synthesis of flower shaped ZnO thin films for resistive sensing of NO_2 gas, Microchim. Acta 184 (7) (2017) 2455–2463.

[162] L. Meng, et al., Enhancing the performance of room temperature ZnO microwire gas sensor through a combined technology of surface etching and UV illumination, Mater. Lett. 212 (2) (2018) 296–298.

[163] A. Runa, X. Zhang, G. Wen, B. Zhang, W. Fu, H. Yang, Actinomorphic flower-like n-ZnO/p-$ZnFe_2O_4$ composite and its improved NO_2 gas-sensing property, Mater. Lett. 225 (2018) 73–76.

[164] R. Gao, Z. Ying, W. Sheng, P. Zheng, Gas sensors based on ZnO/silk fibroin film for nitrogen dioxide detection under UV light at room temperature, Mater. Lett. 229 (2018) 210–212.

[165] C.A. Betty, K. Sehra, K.C. Barick, S. Choudhury, Facile preparation of Silicon/ZnO thin film heterostructures and ultrasensitive toxic gas sensing at room temperature: substrate dependence on specificity, Anal. Chim. Acta 1039 (2018) 82–90.

[166] R. Kumar, N. Goel, A.V. Agrawal, R. Raliya, S. Rajamani, G. Gupta, P. Biswas, M. Kumar, M. Kumar, Boosting sensing performance of vacancy-containing vertically aligned MoS_2 using rGO particles, IEEE Sens. J. 1748 (c) (2019), pp. 1–1.

[167] H. Long, A. Harley-Trochimczyk, T. Pham, Z. Tang, T. Shi, A. Zettl, C. Carraro, M. A. Worsley, R. Maboudian, High surface area MoS2/graphene hybrid aerogel for ultrasensitive NO_2 detection, Adv. Funct. Mater. 26 (28) (2016) 5158–5165.

[168] P.V. Sarma, C.S. Tiwary, S. Radhakrishnan, P.M. Ajayan, M.M. Shaijumon, Oxygen incorporated WS2 nanoclusters with superior electrocatalytic properties for hydrogen evolution reaction, Nanoscale 10 (20) (2018) 9516–9524.

[169] J. Mei, Y. Zhang, T. Liao, Z. Sun, S.X. Dou, Strategies for improving the lithiumstorage performance of 2D nanomaterials, Natl. Sci. Rev. 5 (3) (2018) 389–416.

[170] H. Schmidt, F. Giustiniano, G. Eda, Electronic transport properties of transition metal dichalcogenide field-effect devices: surface and interface effects, Chem. Soc. Rev. 44 (21) (2015) 7715–7736.

[171] H. Jin, C. Zhao, R. Gui, X. Gao, Z. Wang, Reduced graphene oxide/nile blue/gold nanoparticles complex-modified glassy carbon electrode used as a sensitive and label-free aptasensor for ratiometric electrochemical sensing of dopamine, Anal. Chim. Acta 1025 (2018) 154–162.

[172] P. Wiench, Z. Gonzalez, R. Men endez, B. Grzyb, G. Gryglewicz, Beneficial impact of oxygen on the electrochemical performance of dopamine sensors based on Ndoped reduced graphene oxides, Sens. Actuators B Chem. 257 (2018) 143–153.

[173] C. Zhao, et al., Facile synthesis of SnO_2hierarchical porous nanosheets from graphene oxide sacrificial scaffolds for high-performance gas sensors, Sens. Actuators B Chem. 258 (2018) 492–500.

[174] H. Mahmood, L. Vanzetti, M. Bersani, A. Pegoretti, Mechanical properties and strain monitoring of glass-epoxy composites with graphene-coated fibers, Compos. Part A Appl. Sci. Manuf. 107 (2018) 112–123.

[175] J. Hao, L. Ji, K. Wu, N. Yang, Electrochemistry of ZnO@reduced graphene oxides, Carbon N. Y. 130 (2018) 480–486.

[176] X. Yan, et al., Morphology-controlled synthesis of Bi2S3 nanorods-reduced graphene oxide composites with high-performance for electrochemical detection of dopamine, Sens. Actuators B Chem. 257 (2018) 936–943.

[177] J. Kong, Nanotube molecular wires as chemical sensors, Science 287 (5453) (2000) 622–625 (80-.).

[178] D. Kumar, et al., Effect of single wall carbon nanotube networks on gas sensor response and detection limit, Sens. Actuators B Chem. 240 (2017) 1134–1140.

[179] S.W. Lee, W. Lee, Y. Hong, G. Lee, D.S. Yoon, Recent advances in carbon materialbased NO_2 gas sensors, Sens. Actuators B Chem. 255 (2) (2018) 1788–1804.

[180] S.-W. Choi, J. Kim, Y.T. Byun, Highly sensitive and selective NO_2 detection by Pt nanoparticles-decorated single-walled carbon nanotubes and the underlying sensing mechanism, Sens. Actuators B Chem. 238 (Jan. 2017) 1032–1042.

[181] Q.T. Minh Nguyet, et al., Superior enhancement of NO_2gas response using n-p-n transition of carbon nanotubes/SnO_2nanowires heterojunctions, Sens. Actuators B Chem. 238 (2) (2017) 1120–1127.

[182] S. Kumar, V. Pavelyev, P. Mishra, N. Tripathi, A review on chemiresistive gas sensors based on carbon nanotubes: device and technology transformation, Sens. Actuators A Phys. 283 (2018) 174–186.

[183] Y.H. Navale, et al., Zinc oxide hierarchical nanostructures as potential NO_2 sensors, Sens. Actuators B Chem. 251 (2) (2017) 551–563.

[184] Z. Zhang, et al., Novel SnO_2@ZnO hierarchical nanostructures for highly sensitive and selective NO_2 gas sensing, Sens. Actuators B Chem. 257 (2018) 714–727.

[185] X. Sui, C. Hong, W. Pang, C. Chen, Unsymmetrical α-diimine palladium catalysts and their properties in olefin (co)polymerization, Mater. Chem. Front. 1 (5) (2017) 967–972.

[186] N. Karmakar, et al., Room temperature NO_2 gas sensing properties of ptoluenesulfonic acid doped silver-polypyrrole nanocomposite, Sens. Actuators B Chem. 242 (2) (2017) 118–126.

[187] T. Xu, et al., The ultra-high NO 2 response of ultra-thin WS 2 nanosheets synthesized by hydrothermal and calcination processes, Sens. Actuators B Chem. 259 (2) (2018) 789–796.

[188] Z. Wang, et al., Rational synthesis of molybdenum disulfide nanoparticles decorated reduced graphene oxide hybrids and their application for highperformance NO_2 sensing, Sens. Actuators B Chem. 260 (2) (2018) 508–518.

[189] Y. Li, et al., Hierarchical hollow MoS 2 microspheres as materials for conductometric NO_2 gas sensors, Sens. Actuators B Chem. 282 (November 2018) (2019) 259–267.

[190] T. Xu, et al., High-response NO 2 resistive gas sensor based on bilayer MoS 2 grown by a new two-step chemical vapor deposition method, J. Alloy. Comp. 725 (2) (2017) 253–259.

[191] S. Shao, L. Che, Y. Chen, M. Lai, S. Huang, R. Koehn, A novel RGO-MoS_2 -CdS nanocomposite film for application in the ultrasensitive NO 2 detection, J. Alloy. Comp. 774 (2) (2019) 1–10.

[192] J. Guo, R. Wen, J. Zhai, Z. Lin, Enhanced NO 2 gas sensing of a single-layer MoS_2 by photogating and piezo-phototronic effects, Sci. Bull. 64 (2019) 128–135.

[193] M. Kumar, Rahul Kumar, Neeraj Goel, High performance NO_2 sensor using MoS_2 nanowires network, Appl. Phys. Lett. 112 (5) (2018), 053502.

[194] Y.G. Yong Zhou, Cheng Zou, Xiaogang Lin, UV light activated NO_2 gas sensing based on Au nanoparticles decorated few-layer MoS2 thin film at room temperature, Appl. Phys. Lett. 113 (8) (2018), 082103.

[195] M. Bao, et al., "Plate-like p–n heterogeneous NiO/WO3 nanocomposites for high performance room temperature NO_2 sensors, Nanoscale 6 (2014) 4063–4066.

[196] J. Cha, S. Choi, I. Kim, 2D WS2-edge functionalized multi-channel carbon nanofibers: effect of WS_2 edge-abundant structure on room temperature NO_2 sensing, J. Mater. Chem. 5 (18) (2017) 8725–8732.

[197] S. Zhao, Z. Li, G. Wang, J. Liao, S. Lv, Z. Zhu, Highly enhanced response of MoS $_2$/ porous silicon nanowire heterojunctions to NO 2 at room, RSC Adv. 8 (2018) 11070–11077.

[198] Y. Han, et al., Design of hetero-nanostructures on MoS 2 nanosheets to boost NO_2 room-temperature sensing, ACS Appl. Mater. Interfaces 10 (26) (2018) 22640–22649.

[199] R. Kumar, N. Goel, M. Mishra, G. Gupta, M. Fanetti, M. Valant, "Growth of MoS 2 – MoO_3 hybrid microflowers via controlled vapor transport process for efficient gas sensing at room temperature, Adv. Mater. Interfaces 5 (10) (2018) 1800071.

[200] R. Kumar, P. Kulriya, M. Mishra, F. Singh, G. Gupta, M. Kumar, Highly selective and reversible NO_2 gas sensor using vertically aligned MoS2 flake networks, Nanotechnology 29 (46) (2018) 464001.

[201] X. Li, J. Wang, D. Xie, J. Xu, Y. Xia, L. Xiang, Enhanced p-type NO_2-sensing properties of ZnO nanowires utilizing CNTs electrode 206 (Nov. 2017) 18–21.

[202] Q. Zhang, et al., Visible light-assisted room temperature gas sensing with ZnO-Ag heterostructure nanoparticles, Sens. Actuators B Chem. 259 (2018) 269–281.

[203] Z. Liu, et al., Facial development of high performance room temperature NO_2gas sensors based on ZnO nanowalls decorated rGO nanosheets, Appl. Surf. Sci. 423 (2017) 721–727.

[204] X. Chen, et al., In-situ growth of ZnO nanowire arrays on the sensing electrode via a facile hydrothermal route for high-performance NO_2sensor, Appl. Surf. Sci. 435 (2) (2018) 1096–1104.

[205] K. Diao, J. Xiao, Z. Zheng, X. Cui, Enhanced sensing performance and mechanism of CuO nanoparticle-loaded ZnO nanowires: comparison with ZnO-CuO core-shell nanowires, Appl. Surf. Sci. 459 (July) (2018) 630–638.

[206] Y.H. Navale, S.T. Navale, F.J. Stadler, N.S. Ramgir, V.B. Patil, Enhanced NO 2 sensing aptness of ZnO nanowire/CuO nanoparticle heterostructure-based gas sensors, Ceram. Int. 45 (2) (2019) 1513–1522.

[207] N.B. Patil, A.R. Nimbalkar, M.G. Patil, ZnO thin film prepared by a sol-gel spin coating technique for NO 2 detection, Mater. Sci. Eng. B 227 (2) (2018) 53–60.

[208] J. Kim, J. Lee, A. Mirzaei, H. Woo, S. Sub, SnO 2 (n) -NiO (p) composite nanowebs : gas sensing properties and sensing mechanisms, Sens. Actuators B Chem. 258 (2018) 204–214.

[209] D. Han, L. Zhai, F. Gu, Z. Wang, Highly sensitive NO 2 gas sensor of ppb-level detection based on in 2 O 3 nanobricks at low temperature, Sens. Actuators B Chem. 262 (2) (2018) 655–663.

[210] R. Chen, J. Wang, L. Xiang, Facile synthesis of mesoporous ZnO sheets assembled by small nanoparticles for enhanced NO_2 sensing performance at room temperature, Sens. Actuators B Chem. 270 (2018) 207–215.

[211] L. Qi, L. Yu, Z. Liu, F. Guo, X. Fan, An enhanced optoelectronic NO 2 gas sensors based on direct growth ZnO nanowalls in situ on porous rGO, J. Alloy. Comp. 749 (2) (2018) 244–249.

[212] H. Lee, Y. Heish, C. Lee, High sensitivity detection of nitrogen oxide gas at room temperature using zinc oxide-reduced graphene oxide sensing membrane, J. Alloy. Comp. 773 (2019) 950–954.

[213] A.R. Nimbalkar, N.B. Patil, V.V. Ganbavle, S.V. Mohite, K.V. Madhale, M.G. Patil, Sol-gel derived aluminium doped zinc oxide thin films : a view of aluminium doping effect on physicochemical and NO 2 sensing properties, J. Alloy. Comp. 775 (2) (2019) 466–473.

[214] A. You, M.A.Y. Be, I. In, Multi-layered zinc oxide-graphene composite thin films for selective nitrogen dioxide sensing, J. Appl. Phys. 084501 (November 2017) (2018).

[215] Y. Yang, H.E. Katz, "Hybrid of P3HT and ZnO @ GO nanostructured particles for increased NO 2 sensing response y, J. Mater. Chem. C 5 (2017) 2160–2166.

[216] Q. Li, Y. Cen, J. Huang, X. Li, H. Zhang, Y. Geng, Zinc oxide – black phosphorus composites for ultrasensitive nitrogen dioxide sensing y, Nanoscale Horiz. 3 (2018) 525–531.

[217] Lalit Chandra, R. Dwivedi, V.N. Mishra, Highly sensitive NO_2 sensor using brushcoated ZnO nanoparticles, Mater. Res. Express 4 (2017) 105030.

[218] S. Bok, C. Woo, S. Lee, C. Lee, S. Lee, Enhanced NO 2 gas-sensing performance of Pd/ZnO-codecorated SnO 2 nanorod sensors, Appl. Phys. A 124 (12) (2018) 1–9.

[219] Jyoti, G.D. Varma, Synthesis of CuO-ZnO/rGO ternary composites for superior NO_2 gas sensor at room temperature, Mater. Res. Express 6 (3) (2018), 035011.

[220] M. Kumar, Y. Ando, Chemical vapor deposition of carbon nanotubes: a review on growth mechanism and mass production, J. Nanosci. Nanotechnol. (2010).

[221] J. Prasek, J. Drbohlavova, J. Chomoucka, J. Hubalek, O. Jasek, V. Adam, R. Kizek, Methods for carbon nanotubes synthesis—review, J. Mater. Chem. (2011).

[222] N. Tripathi, P. Mishra, H. Harsh, S.S. Islam, Fine-tuning control on CNT diameter distribution, length and density using thermal CVD growth at atmospheric pressure: an in-depth analysis on the role of flow rate and flow duration of acetylene (C2H2) gas, Appl. Nanosci. 5 (1) (2015) 19–28.

[223] K. Liu, K. Jiang, C. Feng, Z. Chen, S. Fan, A growth mark method for studying growth mechanism of carbon nanotube arrays, Carbon N. Y. 43 (November (14)) (2005) 2850–2856.

[224] M. Paradise, T. Goswami, Carbon nanotubes – production and industrial applications, Mater. Des. 28 (January (5)) (2007) 1477–1489.

[225] N. Tripathi, S.S. Islam, A new approach for orientation-controlled growth of CNTs : an in- depth analysis on the role of oxygen plasma treatment to catalyst, Appl. Nanosci. 7 (3) (2017) 125–129.

[226] N. Tripathi, V. Pavelyev, S.S. Islam, Synthesis of carbon nanotubes using green plant extract as catalyst: unconventional concept and its realization, Appl. Nanosci. 7 (8) (2017) 557–566.

[227] N. Yan, C. Xiao, Y. Kou, Transition metal nanoparticle catalysis in green solvents, Coord. Chem. Rev. 254 (May (9–10)) (2010) 1179–1218.

[228] S. Huang, Q. Cai, J. Chen, Y. Qian, L. Zhang, Metal-catalyst-free growth of single-walled carbon nanotubes on substrates, J. Am. Chem. Soc. (2009).

[229] M.M.A. Rafique, J. Iqbal, Production of carbon nanotubes by different routes — a review, J. Encapsulation Adsorpt. Sci. 1 (June) (2011) 29–34.

[230] W.Z. Li, S.S. Xie, L.X. Qian, B.H. Chang, B.S. Zou, W.Y. Zhou, R.A. Zhao, G. Wang, Large-scale synthesis of aligned carbon nanotubes, Science (80-.) 274 (5293) (1996) 1701–1703.

[231] N. Tripathi, P. Mishra, B. Joshi, Harsh, S.S. Islam, Catalyst free, excellent quality and narrow diameter of CNT growth on Al2O3 by a thermal CVD technique, Phys. E Low-Dimension. Syst. Nanostruct. 62 (August) (2014) 43–47.

[232] T. Guo, P. Nikolaev, A. Thess, D.T. Colbert, R.E. Smalley, Catalytic growth of single-walled manotubes by laser vaporization, Chem. Phys. Lett. 243 (1–2) (1995) 49–54.

[233] V. Datsyuk, M. Kalyva, K. Papagelis, J. Parthenios, D. Tasis, A. Siokou, I. Kallitsis, C. Galiotis, Chemical oxidation of multiwalled carbon nanotubes, Carbon N. Y. 46 (May (6)) (2008) 833–840.

[234] P.-X. Hou, C. Liu, H.-M. Cheng, Purification of carbon nanotubes, Carbon N. Y. 46 (December (15)) (2008) 2003–2025.

[235] S. Scaccia, M. Carewska, P.P. Prosini, Study of purification process of single-walled carbon nanotubes by thermoanalytical techniques, Thermochim. Acta 435 (September (2)) (2005) 209–212.

[236] J. Li, Y. Lu, Q. Ye, M. Cinke, J. Han, M. Meyyappan, Carbon nanotube sensors for gas and organic vapor detection, Nano Lett. (2003).

[237] J. Suehiro, G. Zhou, M. Hara, Fabrication of a carbon nanotube-based gas sensor using dielectrophoresis and its application for ammonia detection by impedance spectroscopy, J. Phys. D Appl. Phys. 36 (3603) (2003) 109–114.

[238] A. Abdelhalim, A. Abdellah, G. Scarpa, P. Lugli, Fabrication of carbon nanotube thin films on flexible substrates by spray deposition and transfer printing, Carbon (2013).

[239] R.C. Tenent, T.M. Barnes, J.D. Bergeson, A.J. Ferguson, B. To, L.M. Gedvilas, M.J. Heben, J.L. Blackburn, UItrasmooth, large-area, high-uniformity, conductive transparent single-walled-carbon-nanotube films for photovoltaics produced by ultrasonic spraying, Adv. Mater. (2009).

[240] A. Abdellah, B. Fabel, P. Lugli, G. Scarpa, Spray deposition of organic semiconducting thin-films: towards the fabrication of arbitrary shaped organic electronic devices, Org. Electron. physics, Mater. Appl. (2010).

[241] X. Zhao, B.T.T. Chu, B. Ballesteros, W. Wang, C. Johnston, J.M. Sykes, P.S. Grant, Spray deposition of steam treated and functionalized single-walled and multi-walled carbon nanotube films for supercapacitors, Nanotechnology 20 (6) (2009).

[242] S. Huang, A.W.H. Mau, T.W. Turney, P.A. White, L. Dai, Patterned growth of well-aligned carbon nanotubes: a soft-lithographic approach, J. Phys. Chem. B 104 (10) (2000) 2195–2196.

[243] J. Chang, C.K. Najeeb, J.-H. Lee, J.-H. Kim, Single-walled carbon nanotubes/polymer composite electrodes patterned directly from solution, Langmuir 27 (11) (2011) 7330–7336.

[244] T.H. da Costa, J.-W. Choi, A flexible two-dimensional force sensor using PDMS nanocomposite, Microelectron. Eng. 174 (2017) 64–69.

[245] L. Valentini, I. Armentano, J.M. Kenny, C. Cantalini, L. Lozzi, S. Santucci, Sensors for sub-ppm NO_2 gas detection based on carbon nanotube thin films Sensors for sub-ppm NO_2 gas detection based on carbon nanotube thin films, Appl. Phys. Lett. Addit. Inf. Appl. Phys. Lett. J. Homepage 82 (961) (2003).

[246] X. Li, J. Wang, D. Xie, J. Xu, Y. Xia, L. Xiang, Enhanced p-type NO_2-sensing properties of ZnO nanowires utilizing CNTs electrode, Mater. Lett. 206 (2017).

[247] S.-W. Choi, J. Kim, Y.T. Byun, Highly sensitive and selective NO_2 detection by Pt nanoparticles-decorated single-walled carbon nanotubes and the underlying sensing mechanism, Sens. Actuators B Chem. 238 (January) (2017) 1032–1042.

[248] Y.J. Kwon, A. Mirzaei, S.Y. Kang, M.S. Choi, J.H. Bang, S.S. Kim, H.W. Kim, Synthesis, characterization and gas sensing properties of ZnO-decorated MWCNTs, Appl. Surf. Sci. 413 (August) (2017) 242–252.

[249] A. Sharma, M. Tomar, V. Gupta, Room temperature trace level detection of NO_2 gas using SnO_2 modified carbon nanotubes-based sensor, J. Mater. Chem. 22 (November (44)) (2012) 23608–23616.

[250] Q.T. Minh Nguyet, N. Van Duy, N.T. Phuong, N.N. Trung, C.M. Hung, N.D. Hoa, N. Van Hieu, Superior enhancement of NO_2gas response using n-p-n transition of carbon nanotubes/SnO_2nanowires heterojunctions, Sens. Actuators B Chem. (2017).

[251] J. Lee, H. Kim, S.J. Kahng, G. Kim, Y.W. Son, J. Ihm, H. Kato, Z.W. Wang, T. Okazaki, H. Shinohara, Y. Kuk, Bandgap modulation of carbon nanotubes by encapsulated metallofullerenes, Nature 415 (6875) (2002) 1005–1008.

[252] J.H. Lee, A. Katoch, S.W. Choi, J.H. Kim, H.W. Kim, S.S. Kim, Extraordinary improvement of gas-sensing performances in sno$_2$nanofibers due to creation of local p - N heterojunctions by loading reduced graphene oxide nanosheets, ACS Appl. Mater. Interfaces 7 (5) (2015) 3101–3109.

[253] P.B. Agarwal, B. Alam, D.S. Sharma, S. Sharma, S. Mandal, A. Agarwal, Flexible and Printed Electronics Flexible NO 2 Gas Sensor Based on Single-walled Carbon Nanotubes on Polytetrafluoroethylene Substrates, 2018.

[254] J. Li, Y. Lu, M. Meyyappan, Nano chemical sensors with polymer-coated carbon nanotubes, IEEE Sens. J. (2006).

[255] A.K. Sharma, A. Mahajan, R.K. Bedi, S. Kumar, A.K. Debnath, D.K. Aswal, CNTs based improved chlorine sensor from non-covalently anchored multi-walled carbon nanotubes with hexa-decafluorinated cobalt phthalocyanines, RSC Adv. (2017).

[256] D. Jung, K.H. Lee, D. Kim, L.J. Overzet, G.S. Lee, A gas sensor using a multi-walled carbon nanotube sheet to detect oxygen molecules, J. Nanosci. Nanotechnol. 13 (December (12)) (2013) 8275–8279.

[257] F. Schütt, V. Postica, R. Adelung, O. Lupan, Single and networked ZnO-CNT hybrid tetrapods for selective room-temperature high-performance Ammonia sensors, ACS Appl. Mater. Interfaces (2017).

[258] A.G. Bannov, O. Jasek, A. Manakhov, M. Marik, D. Necas, L. Zajickova, High-performance Ammonia gas sensors based on plasma treated carbon nanostructures, IEEE Sens. J. (2017).

[259] H.H. Choi, J. Lee, K.Y. Dong, B.K. Ju, W. Lee, Noxious gas detection using carbon nanotubes with Pd nanoparticles, Nanoscale Res. Lett. 6 (2011) 1–6.

[260] Y. Lin, K. Kan, W. Song, G. Zhang, L. Dang, Y. Xie, P. Shen, L. Li, K. Shi, Controllable Synthesis of Co3O4/polyethyleneimine-Carbon Nanotubes Nanocomposites for CO and NH3 Gas Sensing at Room Temperature, 639, Elsevier Ltd, 2015, pp. 187–196, 05-Aug.

[261] S. Kim, H.R. Lee, Y.J. Yun, S. Ji, K. Yoo, W.S. Yun, J.-Y. Koo, D.H. Ha, Effects of polymer coating on the adsorption of gas molecules on carbon nanotube networks, Appl. Phys. Lett. 91 (August (9)) (2007) 093126.

[262] C.S. Huang, B.R. Huang, Y.H. Jang, M.S. Tsai, C.Y. Yeh, Three-terminal CNTs gas sensor for N2 detection, in: Diamond and Related Materials, 2005.

[263] W. Lu, P. Xie, C.M. Lieber, Nanowire transistor performance limits and applications, IEEE Trans. Electron Devices 55 (11) (2008) 2859–2876.

[264] I. Sayago, E. Terrado, E. Lafuente, M.C. Horrillo, W.K. Maser, A.M. Benito, R. Navarro, E.P. Urriolabeitia, M.T. Martinez, J. Gutierrez, Hydrogen sensors based on carbon nanotubes thin films, in: Synthetic Metals, 2005.

[265] A.S. Alshammari, M.R. Alenezi, K.T. Lai, S.R.P. Silva, Inkjet printing of polymer functionalized CNT gas sensor with enhanced sensing properties, Mater. Lett. 189 (February) (2017) 299–302.

[266] D.W.H. Fam, A.I.Y. Tok, A. Palaniappan, P. Nopphawan, A. Lohani, S.G. Mhaisalkar, Selective sensing of hydrogen sulphide using silver nanoparticle decorated carbon nanotubes, Sens. Actuators B: Chem. 138 (April (1)) (2009) 189–192.

[267] D. Jung, M. Han, G.S. Lee, Room-temperature gas sensor using carbon nanotube with cobalt oxides, Sens. Actuators B: Chem. 204 (2014) 596–601.

[268] D. Kim, P.V. Pikhitsa, H. Yang, M. Choi, Room Temperature CO and H2 Sensing With Carbon Nanoparticles, Nanotechnology (2011).

[269] C.S. Huang, B.R. Huang, C.H. Hsiao, C.Y. Yeh, C.C. Huang, Y.H. Jang, Effects of the catalyst pretreatment on CO_2 sensors made by carbon nanotubes, Diam. Relat. Mater. 17 (April (4–5)) (2008) 624–627.

[270] O. Sidek, S.A. Quadri, S. Kabir, M.H. Bin Afzal, Application of carbon nanotube in wireless sensor network to monitor carbon dioxide, J. Exp. Nanosci. 8 (February (2)) (2013) 154–161.

[271] M.T. Humayun, R. Divan, Y. Liu, L. Gundel, P.A. Solomon, I. Paprotny, Novel chemoresistive C sensor with 10ppm sensitivity based on multiwalled carbon nanotubes functionalized with SnO_2 nanocrystals, J. Vac. Sci. Technol. A 34 (January (1)) (2016).

[272] A. Firouzi, S. Sobri, F.M. Yasin, F.R. Ahmadun, CH4 and CO_2 detection by using carbon nanotube-based sensors, Adv. Mater. Res. 214 (2011) 482–489.

[273] C.S. Huang, B.R. Huang, Y.H. Jang, M.S. Tsai, C.Y. Yeh, Three-terminal CNTs gas sensor for N2 detection, Diam. Related Mater. 14 (11-12) (2005) 1872–1875.

[274] A.S. Ghasemi, A DFT computation for comparison of NQR of O_2, N_2 and CO over the surface of Single-Walled Carbon Nanotubes, Research Journal of Applied Sciences, Eng. Technol. 5 (6) (2013) 1892–1898.

[275] S. Abdel Aal, Reactivity of boron- and nitrogen-doped carbon nanotubes functionalized by (Pt, Eu) atoms toward and CO: A density functional study, Int. J. Mod. Phys. C 7 (July (27)) (2016).

[276] Z.H. Khan, N.A. Salah, S.S. Habib, A. Azam, M.S. El-Shahawi, Multi-walled carbon nanotubes film sensor for carbon mono-oxide gas, Curr. Nanosci. 8 (April (2)) (2012) 274–279.

[277] Z. Hou, J. Wu, W. Zhou, X. Wei, D. Xu, Y. Zhang, B. Cai, A MEMS-based ionization gas sensor using carbon nanotubes, IEEE Trans. Electr. Dev. 54 (June (60)) (2007) 1545–1548.

[278] H.R. Ali-Akbari, M. Shaat, A. Abdelkefi, Bridged single-walled carbon nanotube-based atomic-scale mass sensors, Appl. Phys. A 122 (August (8)) (2016).

[279] S. Shadmehr, M. Coleman, B. Liu, J. Liu, X.(Shirley) Tang, Reversible gating of ion transport through DNA-functionalized carbon nanotube membranes, RSC Adv. 7 (2) (2017) 611–616.

[280] A. Paul, B. Bhattacharya, T.K. Bhattacharyya, Fabrication and performance of solution-based micropatterned DNA functionalized carbon nanotube network as humidity sensors, IEEE Trans. Nanotechnol. 13 (March (2)) (2014) 335–342.

[281] B. Kim, H. Chung, W. Kim, High-performance supercapacitors based on vertically aligned carbon nanotubes and nonaqueous electrolytes, Nanotechnology 23 (April (15)) (2012) 155401.

[282] A. Gohier, J. Chancolon, P. Chenevier, D. Porterat, M. Mayne-L'Hermite, C. Reynaud, Optimized network of multi-walled carbon nanotubes for chemical sensing, Nanotechnology 22 (March (10)) (2011).

[283] N. Van Hieu, L.T.B. Thuy, N.D. Chien, Highly sensitive thin film N gas sensor operating at room temperature based on SnO_2/MWCNTs composite, Sens. Actuators B: Chem. 129 (February (2)) (2008) 888–895.

[284] L.H. Nguyen, T.V. Phi, P.Q. Phan, H.N. Vu, C. Nguyen-Duc, F. Fossard, Synthesis of multi-walled carbon nanotubes for NH3 gas detection, Phys. E: Low-Dimen. Syst. Nanostruct. 37 (March (1–2)) (2007) 54–57.

[285] P. Mishra, P. Balyan, Harsh, S.S. Islam, Role of electric field on sensing mechanism of carbon nanotube based ammonia gas sensor, Sens. Lett. 11 (8) (2013) 1460–1464.

[286] S. Kim, H.R. Lee, Y.J. Yun, S. Ji, K. Yoo, W.S. Yun, J.Y. Koo, D.H. Ha, Effects of polymer coating on the adsorption of gas molecules on carbon nanotube networks, Appl. Phys. Lett. 91 (9) (2007).

[287] J. Ali, A. Kumar, S. Husain, M. Kumari, Harsh, M. Husain, Characterization and field emission studies of uniformly distributed multi-walled carbon nanotubes (MWCNTS) film grown by low-pressure chemical vapour deposition (LPCVD), Curr. Nanosci. 7 (June (3)) (2011) 333–336.

[288] D.A. Zilli, P.R. Bonelli, A.L. Cukierman, Synthesis of Multi-walled Carbon Nanotubes by Floating Catalyst Chemical Vapor Deposition and Their Utility for Hydrogen Sensing at Room Temperature, Nova Science Publishers, Inc., 2013, pp. 297–332.

[289] K.Y. Wang, W.L. Tsai, P.Y. Yang, C.H. Chou, C.Y. Liao, Y.R. Li, H.C. Cheng, Flexible atmospheric-pressure gas ionization sensors with horizontally aligned carbon nanotube electrodes, J. Nanosci. Nanotechnol. 16 (December (12)) (2016) 12860–12865.

[290] J.D. Kim, B.S. Kang, T.W. Noh, J.G. Yoon, S.I. Baik, Y.W. Kim, Controlling the nanostructure of RuO_2/carbon nanotube composites by gas annealing, J. Electrochem. Soc. 152 (2) (2005).

[291] E. Ahn, H. Jung, N. Le Hung, D. Oh, H. Kim, D. Kim, No gas sensing characteristics of layered composites of carbon nanotubes coated with Al-doped Zno, Korean J. Mater. Res. 19 (November (11)) (2009) 631–636.

[292] S.Y. Park, H. Jung, E. Ahn, L.H. Nguyen, Y. Kang, H. Kim, D. Kim, NO gas sensing properties of ZnO-carbon nanotube composites, Korean J. Mater Res. 18 (12) (2008) 655–659.

[293] T. Ueda, H. Norimatsu, M.M.H. Bhuiyan, T. Ikegami, K. Ebihara, NO sensing property of carbon nanotube based thin film gas sensors prepared by chemical vapor deposition techniques, Jap. J. Appl. Phys. 45 (October (10b)) (2006) 8393–8397.

[294] W. Ding, R. Hayashi, K. Ochi, J. Suehiro, K. Imasaka, M. Hara, N. Sano, E. Nagao, T. Minagawa, Analysis of PD-generated SF6 decomposition gases adsorbed on carbon nanotubes, IEEE Trans. Dielectr. Electr. Insul. 13 (December (6)) (2006) 1200–1207.

[295] H. Kang, S. Lim, N. Park, K.Y. Chun, S. Baik, Improvement of the Sensitivity of Carbon Nanotube Sensors by Benzene Functionalization for Detecting Dissociated SF6 Species, Sens. Actuator B: Chem. (2010) 433–434.

[296] Y. Wang, X. Cao, J. Li, N. Chen, A new cataluminescence gas sensor based on SiO_2 nanotubes fabricated using carbon nanotube templates, Talanta 84 (May (3)) (2011) 977–982.

[297] M. Farbod, M.H. Joula, M. Vaezi, Promoting effect of adding carbon nanotubes on sensing characteristics of ZnO hollow sphere-based gas sensors to detect volatile organic compounds, Mater. Chem. Phys. 176 (June) (2016) 12–23.

[298] G. Peng, U. Tisch, H. Haick, Detection of nonpolar molecules by means of carrier scattering in random networks of carbon nanotubes: toward diagnosis of diseases via breath samples, Nano Lett. 9 (April (4)) (2009) 1362–1368.

[299] H. Haick, P. Gang, U. Tisch, Y. Zilberman, W. Pisula, X. Feng, K. Müllen, Sniffing Out Cancer in the Breath: Detection of Non-polar Volatile Compounds Through Carrier Scattering in Random Networks of Carbon Nanotubes, 2009, pp. 741809.

[300] Z. Zhu, W. Song, K. Burugapalli, F. Moussy, Y.L. Li, X.H. Zhong, Nano-yarn carbon nanotube fiber based enzymatic glucose biosensor, Nanotechnology 21 (16) (2010).

[301] R.J. Wu, Y.C. Huang, M.R. Yu, T.H. Lin, S.L. Hung, Application of m-CNTs/NaClO4/Ppy to a fast response, room working temperature ethanol sensor, Sens. Actuators B: Chem. 134 (August (1)) (2008) 213–218.

[302] L. Mahdavian, M. Monajjemi, N. Mangkorntong, Sensor response to alcohol and chemical mechanism of carbon nanotube gas sensors, Fuller. Nanotub. Carb. Nanostruct. 17 (5) (2009) 484–495.

[303] D. Das, A. Das, M. Reghunath, K.K. Nanda, Phosphine-free avenue to Co2P nanoparticle encapsulated N,P co-doped CNTs: A novel non-enzymatic glucose sensor and an efficient electrocatalyst for oxygen evolution reaction, Green Chem. 19 (5) (2017) 1327–1335.

[304] C. Tasaltin and F. Basarir, “Preparation of flexible VOC sensor based on carbon nanotubes and gold nanoparticles.” Sensors Actuators B Chem., 194, 173 (2014).

[305] S. Zhang, H. Zhang, G. Yao, F. Liao, M. Gao, Z. Huang, K. Li, and Y. Lin, “Highly stretchable, sensitive, and flexible strain sensors based on silver nanoparticles/carbon nanotubes composites.” J. Alloys Compd., 652, 48 (2015).

[306] U. Yaqoob, D. T. Phan, A. S. M. I. Uddin, and G. S. Chung, “Highly flexible room temperature NO_2 sensor based on MWCNTs-WO3 nanoparticles hybrid on a PET substrate.” Sensors Actuators, B Chem., 221, 760 (2015).

[307] B. Kim, Y. H. Lee, J. H. Ryu, and K. Do Suh, “Enhanced colloidal properties of single-wall carbon nanotubes in α-terpineol and texanol.” Colloids Surfaces A Physicochem. Eng. Asp., 272, 161 (2006).

[308] M. Asad, M. H. Sheikhi, M. Pourfath, and M. Moradi, “High sensitive and selective flexible H2S gas sensors based on Cu nanoparticle decorated SWCNTs.” Sensors Actuators, B Chem., 210, 1 (2015).

[309] E. Cagatay, P. Kohler, P. Lugli, and A. Abdellah, “Flexible capacitive tactile sensors based on carbon nanotube thin films.” IEEE Sens. J., 15, 3225 (2015).

[310] P. Wan, X. Wen, C. Sun, B. K. Chandran, H. Zhang, X. M. Sun, and X. Chen, “Flexible transparent films based on nanocomposite networks of polyaniline and carbon nanotubes for high-performance gas sensing.” Small, 11, 5409 (2015).

[311] J. H. Kim, J. Y. Hwang, H. R. Hwang, H. S. Kim, J. H. Lee, J. W. Seo, U. S. Shin, and S. H. Lee, “Simple and cost-effective method of highly conductive and elastic carbon nanotube/polydimethylsiloxane composite for wearable electronics.” Sci. Rep., 8 (2018).

[312] P. J. Glatkowski, “Carbon nanotube based transparent conductive coatings.” Carbon Nanotub., 48, 2146 (2003).

[313] Y. M. Haddara and M. M. R. Howlader, “Integration of heterogeneous materials for wearable sensors.” Polymers, 10 (2018).

[314] Z. D. Lin, S. J. Young, and S. J. Chang, “CO_2 gas sensors based on carbon nanotube thin films using a simple transfer method on flexible substrate.” IEEE Sens. J., 15, 7017 (2015).

[315] U. Yaqoob, A. S. M. I. Uddin, and G. S. Chung, “A high-performance flexible NO_2sensor based on WO3NPs decorated on MWCNTs and RGO hybrids on PI/ PET substrates.” Sensors Actuators, B Chem., 224, 738 (2016).

[316] J. C. Chiou, C. C. Wu, Y. C. Huang, S. C. Chang, and T. M. Lin, “Effects of operating temperature on droplet casting of flexible polymer/multi-walled carbon nanotube composite gas sensors.” Sensors (Switzerland), 17, 1 (2017).

[317] C. Hua, Y. Shang, Y. Wang, J. Xu, Y. Zhang, X. Li, and A. Cao, “A flexible gas sensor based on single-walled carbon nanotube-Fe2O3composite film.” Appl. Surf. Sci., 405, 405 (2017).

[318] L. Xue, W. Wang, Y. Guo, G. Liu, and P. Wan, “Flexible polyaniline/carbon nanotube nanocomposite film-based electronic gas sensors.” Sensors Actuators, B Chem., 244, 47 (2017).

[319] X. Wang, Y. Li, J. Pionteck, Z. Zhou, W. Weng, X. Luo, Z. Qin, B. Voit, and M. Zhu, “Flexible poly(styrene-butadiene-styrene)/carbon nanotube fiber based vapor sensors with high sensitivity, wide detection range, and fast response.” Sensors Actuators, B Chem., 256, 896 (2018).

[320] B. Paul K, A. K. Panigrahi, V. Singh, and S. G. Singh, “A multi-walled carbon nanotube–zinc oxide nanofiber based flexible chemiresistive biosensor for malaria biomarker detection.” Analyst, 142, 2128 (2017).

[321] Z. Huang, M. Gao, T. Pan, X. Wei, C. Chen, and Y. Lin, “Interface engineered carbon nanotubes with SiO_2 for flexible infrared detectors.” Appl. Surf. Sci., 413, 308 (2017).

[322] J. B. Andrews, J. A. Cardenas, C. J. Lim, S. G. Noyce, J. Mullett, and A. D. Franklin, “Fully printed and flexible carbon nanotube transistors for pressure sensing in automobile tires.” IEEE Sens. J., 18, 7875 (2018).

[323] X. Xuan and J. Y. Park, “A miniaturized and flexible cadmium and lead ion detection sensor based on micro-patterned reduced graphene oxide/carbon nanotube/bismuth composite electrodes.” Sensors Actuators B Chem., 255, 1220 (2018).

[324] P. B. Agarwal, B. Alam, D. S. Sharma, S. Sharma, S. Mandal, and A. Agarwal, "Flexible and printed electronics flexible NO_2 gas sensor based on single walled carbon nanotubes on PTFE substrate." Flex. Print. Electron., 3, 035001 (2018).

[325] Y. Jung, M. G. Shin, H. J. Tak, K. K. Jung, and J. S. Ko, "Flexible pressure sensor made using PDMS containing carbon nanotubes." in Proceedings of the IEEE International Conference on Micro Electro Mechanical Systems (MEMS), 2018, 501 (2018).

[326] G. L. Goh, S. Agarwala, Y. J. Tan, and W. Y. Yeong, "A low cost and flexible carbon nanotube pH sensor fabricated using aerosol jet technology for live cell applications." Sensors Actuators, B Chem., 260, 227 (2018).

[327] M. Jian, K. Xia, Q. Wang, Z. Yin, H. Wang, C. Wang, H. Xie, M. Zhang, and Y. Zhang, "Flexible and highly sensitive pressure sensors based on bionic hierarchical structures." Adv. Funct. Mater., 27, 1606066 (2017).

[328] L. Kumar, I. Rawal, A. Kaur, and S. Annapoorni, "Flexible room temperature ammonia sensor based on polyaniline." Sensors Actuators B Chem., 240, 408 (2017).

[329] D. Zhang, H. Chang, P. Li, R. Liu, and Q. Xue, "Fabrication and characterization of an ultrasensitive humidity sensor based on metal oxide/graphene hybrid nanocomposite." Sensors Actuators B Chem., 225, 233 (2016).

[330] J. N. Gavgani, A. Hasani, M. Nouri, M. Mahyari, and A. Salehi, "Highly sensitive and flexible ammonia sensor based on S and N co-doped graphene quantum dots/ polyaniline hybrid at room temperature." Sensors Actuators B Chem., 229, 239 (2016).

[331] S. Gong, W. Schwalb, Y. Wang, Y. Chen, Y. Tang, J. Si, B. Shirinzadeh, and W. Cheng, "A wearable and highly sensitive pressure sensor with ultrathin gold nanowires." Nat. Commun., 5 (2014).

[332] B. Liu et al., "A flexible NO_2 gas sensor based on polypyrrole/nitrogen-doped multiwall carbon nanotube operating at room temperature." Sensors Actuators, B Chem., 295, 86 (2019).

[333] R. Zhang et al., "Facile one-step preparation of laminated PDMS based flexible strain sensors with high conductivity and sensitivity via filler sedimentation." Compos. Sci. Technol., 186, 1 (2020).

[334] W. Xu, T. Yang, F. Qin, D. Gong, Y. Du, and G. Dai, "A sprayed graphene pattern-based flexible strain sensor with high sensitivity and fast response." Sensors (Switzerland), 19, 1 (2019).

[335] X. Sun et al., "Carbon nanotubes reinforced hydrogel as flexible strain sensor with high stretchability and mechanically toughness." Chem. Eng. J., 382, 122832 (2020).

[336] S. Min, G. Lee, and S. Ahn, "Direct printing of highly sensitive, stretchable, and durable strain sensor based on silver nanoparticles/multi-walled carbon nanotubes composites." Compos. Part B, 161, 395 (2019).

[337] P. Zhu et al., "Flexible and highly sensitive humidity sensor based on cellulose nanofibers and carbon nanotube composite film." Langmuir, 35, 4834 (2019).

[338] Y. Zhou, G. Liu, X. Zhu, Y. Guo, Ultrasensitive NO 2 gas sensing based on rGO/ MoS 2 nanocomposite film at low temperature, Sens. Actuators B Chem. 251 (2) (2017) 280–290.

[339] Q. Lu, Y. Yu, Q. Ma, B. Chen, H. Zhang, 2D transition-metal-dichalcogenidenanosheet-based composites for photocatalytic and electrocatalytic hydrogen evolution reactions, Adv. Mater. 28 (10) (2016) 1917–1933.

[340] Y. Shi, H. Li, L.J. Li, Recent advances in controlled synthesis of two-dimensional transition metal dichalcogenides via vapour deposition techniques, Chem. Soc. Rev. 44 (9) (2015) 2744–2756.

[341] Y. Wang, et al., "Strain-induced direct–indirect bandgap transition and phonon modulation in monolayer WS2, Nano Res. 8 (8) (2015) 2562–2572.

[342] A. Ambrosi, M. Pumera, Electrochemical exfoliation of MoS2 crystal for hydrogen electrogeneration, Chem. Eur J. (2018) 18551–18555.

[343] A. Ambrosi, Z. Sofer, M. Pumera, Lithium intercalation compound dramatically influences the electrochemical properties of exfoliated MoS2, Small 11 (5) (2015) 605–612.

[344] T.A. Shifa, et al., Engineering the electronic structure of 2D WS2 nanosheets using Co incorporation as Cox W(1-x) S2 for conspicuously enhanced hydrogen generation, Small 12 (28) (2016) 3802–3809.

[345] C.C. Cheng, et al., Activating basal-plane catalytic activity of two-dimensional MoS2monolayer with remote hydrogen plasma, Nano Energy 30 (2016) 846–852.

[346] G. Zhao, P. Li, K. Rui, Y. Chen, S.X. Dou, W. Sun, CoSe2/MoSe2 heterostructures with enriched water adsorption/dissociation sites towards enhanced alkaline hydrogen evolution reaction, Chem. Eur J. 24 (43) (2018) 11158–11165.

[347] J. Luxa, V. Mazanek, ◆ D. Bou◆sa, D. Sedmidubský, M. Pumera, Z. Sofer, Grapheneamorphous transition-metal chalcogenide (MoSx, WSx) composites as highly efficient hybrid electrocatalysts for the hydrogen evolution reaction, ChemElectroChem 3 (4) (2016) 565–571.

[348] S. Pourbeyram, J. Abdollahpour, M. Soltanpour, Green synthesis of copper oxide nanoparticles decorated reduced graphene oxide for high sensitive detection of glucose, Mater. Sci. Eng. C 94 (October 2018) (2019) 850–857.

[349] V. Kumar, et al., Enhanced electron transfer mediated detection of hydrogen peroxide using a silver nanoparticle-reduced graphene oxide-polyaniline fabricated electrochemical sensor, RSC Adv. 8 (2) (2018) 619–631.

[350] Z. Li, Y. Liu, D. Guo, J. Guo, Y. Su, Room-temperature synthesis of CuO/reduced graphene oxide nanohybrids for high-performance NO_2 gas sensor, Sens. Actuators B Chem. 271 (October 2017) (2018) 306–310.

[351] C.-S. Lee, S. Yu, T. Kim, One-step electrochemical fabrication of reduced graphene oxide/gold nanoparticles nanocomposite-modified electrode for simultaneous detection of dopamine, ascorbic acid, and uric acid, Nanomaterials 8 (1) (2017) 17.

[352] P. Bollella, et al., Beyond graphene: electrochemical sensors and biosensors for biomarkers detection, Biosens. Bioelectron. 89 (2017) 152–166.

[353] C. Tan, Z. Lai, H. Zhang, Ultrathin two-dimensional multinary layered metal chalcogenide nanomaterials, Adv. Mater. 29 (37) (2017) 1–25.

[354] C. Tan, et al., Preparation of high-percentage 1T-phase transition metal dichalcogenide nanodots for electrochemical hydrogen evolution, Adv. Mater. 30 (9) (2018) 1–9.

[355] Z. Wang, B. Mi, Environmental applications of 2D molybdenum disulfide (MoS2) nanosheets, Environ. Sci. Technol. 51 (15) (2017) 8229–8244.

[356] M. Donarelli, L. Ottaviano, "2D materials for gas sensing applications: a review on graphene oxide, MoS_2, WS_2 and phosphorene, Sensors 18 (11) (2018).

[357] B. Cho, et al., Metal decoration effects on the gas-sensing properties of 2D hybridstructures on flexible substrates, Sensors 15 (10) (2015) 24903–24913.

[358] C. Liu, B, L. Chen, G. Liu, A.N. Abbas, M. Fathi, Zhou, High-performance chemical sensing using Schottky-contacted chemical vapor deposition grown monolayer MoS2 transistors, ACS Nano 8 (5) (2014) 5304–5314.

[359] Y. Niu, R. Wang, W. Jiao, G. Ding, L. Hao, F. Yang, MoS 2 graphene fiber based gas sensing devices, Carbon N. Y. 95 (2) (2015) 34–41.

[360] Y. Dan, Y. Lu, N.J. Kybert, Z. Luo, A.T.C. Johnson, Intrinsic response of graphene vapor sensors, Nano Lett. 9 (4) (2009) 1472–1475.

[361] H. Li, et al., "Fabrication of single- and multilayer MoS2 film-based field-effect transistors for sensing NO at room temperature, Small 8 (1) (2012) 63–67.

[362] G. Lu, L.E. Ocola, J. Chen1, Gas detection using low-temperature reduced graphene oxide sheets, Appl. Phys. Lett. 94 (2009), 083111.

[363] B. Cho, et al., Chemical sensing of 2D graphene/MoS2 heterostructure device, ACS Appl. Mater. Interfaces 7 (30) (2015) 16775–16780.

[364] P. Prezioso, Stefano Francesco, et al., Graphene oxide as a practical solution to high sensitivity gas sensing, J. Phys. Chem. C 117 (20) (2013) 10683–10690.

[365] R. Kumar, N. Goel, M. Kumar, UV-activated MoS2 based fast and reversible NO_2 sensor at room temperature, ACS Sens. 2 (11) (2017) 1744–1752.

[366] A. Agrawal, R. Kumar, S. Venkatesan, A. Zakhidov, G. Yang, J. Bao, M. Kumar, M. Kumar, Photo-activated mixed in-plane and edge-enriched p-type, ACS Sens. 3 (5) (2018) 998–1004.

[367] J.Z. Ou, et al., Physisorption-based charge transfer in two-dimensional SnS2 for selective and reversible NO_2 gas sensing, ACS Nano 9 (10) (2015) 10313–10323.

[368] U.A. Mos, et al., Charge-transfer-based gas Sensing Using atomic-layer MoS2, Sci. Rep. 5 (2015) 8052.

[369] A.Y. Polyakov, et al., Gold decoration and photoresistive response to nitrogen dioxide of WS 2 nanotubes, Chem. Eur J. 24 (71) (2018) 18952–18962.

[370] M. Ma, et al., A novel wireless gas sensor based on LTCC technology, Sens. Actuators B Chem. 239 (2017) 711–717.

[371] J.Z. Ou, et al., Physisorption-based charge transfer in two-dimensional SnS2 for selective and reversible NO_2 gas sensing, ACS Nano 9 (10) (2015) 10313–10323.

[372] H. Khan, et al., Quasi physisorptive two dimensional tungsten oxide nanosheets with extraordinary sensitivity and selectivity to NO_2, Nanoscale 9 (48) (2017) 19162–19175.

[373] C. Wang, X. Li, C. Feng, Y. Sun, G. Lu, Nanosheets assembled hierarchical flowerlike WO3 nanostructures: synthesis, characterization, and their gas sensing properties, Sens. Actuators B Chem. 210 (2015) 75–81.

[374] L. Fan, B. Zhu, P.C. Su, C. He, Nanomaterials and technologies for low temperature solid oxide fuel cells: recent advances, challenges and opportunities, Nano Energy 45 (October 2017) (2018) 148–176.

[375] G. Korotcenkov, Gas response control through structural and chemical modification of metal oxide films: state of the art and approaches, Sens. Actuators B Chem. 107 (1) (2005) 209–232. SPEC. ISS.

[376] C. Li, Z. Luo, T. Wang, J. Gong, Surface, bulk, and interface: rational design of hematite architecture toward efficient photo-electrochemical water splitting, Adv. Mater. 30 (30) (2018) 1–23.

[377] M.D. Regulacio, Y. Wang, Z.W. Seh, M.-Y. Han, Tailoring porosity in copper-based multinary sulfide nanostructures for energy, biomedical, catalytic, and sensing applications, ACS Appl. Nano Mater. 1 (7) (2018) 3042–3062.

[378] S. Liu, B. Yu, H. Zhang, T. Fei, T. Zhang, Enhancing NO 2 gas sensing performances at room temperature based on reduced graphene oxide-ZnO nanoparticles hybrids, Sens. Actuators B Chem. 202 (2) (2014) 272–278.

[379] G. Lu, J. Xu, J. Sun, Y. Yu, Y. Zhang, F. Liu, UV-enhanced room temperature NO 2 sensor using ZnO nanorods modified with SnO 2 nanoparticles, Sens. Actuators B Chem. 162 (1) (2012) 82–88.

[380] C. Manh, H. Viet, N. Van Duy, N. Duc, Comparative effects of synthesis parameters on the NO 2 gas-sensing performance of on-chip grown ZnO and Zn 2 SnO 4 nanowire sensors, J. Alloy. Comp. 765 (2) (2018) 1237–1242.

[381] X. Chen, et al., Synthesis of ZnO nanowires/Au nanoparticles hybrid by a facile one- pot method and their enhanced NO 2 sensing properties, J. Alloy. Comp. 783 (2019) 503–512.

[382] S. Bai, et al., Reverse microemulsion in situ crystallizing growth of ZnO nanorods and application for NO 2 sensor, Sens. Actuators B Chem. 190 (2014) 760–767.

[383] J. Lee, A. Katoch, J. Kim, S.S. Kim, Effect of Au nanoparticle size on the gassensing performance of p-CuO nanowires, Sens. Actuators B Chem. 222 (2016) 307–314.

[384] S.K. Shaikh, V.V. Ganbavale, S.V. Mohite, U.M. Patil, K.Y. Rajpure, ZnO nanorod based highly selective visible blind ultra-violet photodetector and highly sensitive NO 2 gas sensor, Superlattice Microstruct. 120 (May) (2018) 170–186.

[385] S.A. Vanalakar, M.G. Gang, V.L. Patil, T.D. Dongale, Enhanced gas-sensing response of zinc oxide nanorods synthesized via hydrothermal route for nitrogen dioxide gas, J. Electron. Mater. 48 (1) (2019) 589–595.

[386] W. Chebil, et al., Structural, optical and NO_2 gas sensing properties of ZnMgO thin films prepared by the sol gel method, Phys. B Phys. Condens. Matter 505 (2) (2017) 9–16.

[387] A. Aziz, N. Tiwale, S.A. Hodge, S. Attwood, G. Divitini, M.E. Welland, Core-shell electrospun polycrystalline ZnO nanofibres for ultra-sensitive NO 2 gas sensing, ACS Appl. Mater. Interfaces 10 (50) (2018) 43817–43823.

[388] X. Li, et al., Vitamin C-assisted synthesis and gas sensing properties of coaxial in 2 O 3 nanorod bundles, Sens. Actuators B Chem. 220 (2015) 68–74.

[389] J. M, G.L. Qiuyue Yang, Xiaobiao Cui, Jiangyang Liu, Jing Zhao, Yinglin Wang, Yuan Gao, Peng Sun, A low temperature operating gas sensor with high response to NO 2 based on ordered mesoporous, New J. Chem. 40 (2016) 2376–2382.

[390] B. Xiao, Q. Zhao, D. Wang, M. Zhang, Facile synthesis of nanoparticle packed in 2 O 3 nanospheres for highly sensitive NO 2 sensing, New J. Chem. 41 (16) (2017) 8530–8535.

[391] C. Woong, et al., Highly selective and sensitive detection of NO 2 using rGO-In 2 O 3 structure on flexible substrate at low temperature, Sens. Actuators B Chem. 255 (2) (2018) 1671–1679.

[392] Z. Wang, et al., The enhanced NO_2 sensing properties of SnO_2 nanoparticles/ reduced graphene oxide composite, J. Colloid Interface Sci. 537 (2) (2019) 228–237.

[393] G. Neri, A. Bonavita, G. Micali, G. Rizzo, E. Callone, G. Carturan, Resistive CO gas sensors based on In2O3 and InSnOx nanopowders synthesized via starch-aided sol-gel process for automotive applications, Sens. Actuators B Chem. 132 (1) (2008) 224–233.

[394] R. You, D.D. Han, F. Liu, Y.L. Zhang, G. Lu, Fabrication of flexible roomtemperature NO_2 sensors by direct laser writing of In2O3 and graphene oxide composites, Sens. Actuators B Chem. 277 (2) (2018) 114–120.

[395] W. Yang, P. Wan, X. Zhou, J. Hu, Y. Guan, L. Feng, Additive-free synthesis of In2O3 cubes embedded into graphene sheets and their enhanced NO_2 sensing performance at room temperature, ACS Appl. Mater. Interfaces 6 (23) (2014) 21093–21100.

[396] H.Y. Lee, Y.C. Heish, C.T. Lee, High sensitivity detection of nitrogen oxide gas at room temperature using zinc oxide-reduced graphene oxide sensing membrane, J. Alloy. Comp. 773 (2019) 950–954.

[397] T. Han, S. Gao, Z. Wang, T. Fei, S. Liu, T. Zhang, Investigation of the effect of oxygen-containing groups on reduced graphene oxide-based room-temperature NO_2 sensor, J. Alloy. Comp. 801 (2019) 142–150.

[398] H. Yan, et al., Effects of the oxidation degree of graphene oxide on the adsorption of methylene blue, J. Hazard Mater. 268 (2014) 191–198.

[399] D.C. Marcano, D.V. Kosynkin, J.M. Berlin, A. Sinitskii, Z. Sun, A. Slesarev, et al., Improved synthesis of graphene oxide, ACS Nano 4 (2010) 4806–4814.

[400] A. Giampiccolo, et al., Sol gel graphene/TiO_2 nanoparticles for the photocatalytic-assisted sensing and abatement of NO_2, Appl. Catal. B Environ. 243 (October 2018) (2019) 183–194.

Chapter 5: Sensitive detection of Nitrogen Dioxide using gold nanoparticles decorated Single Walled Carbon Nanotubes

5.1 Introduction

The main feature of individual SWNT sensors, besides their small size is that they operate at room temperature with higher sensitivity. SWNTs possess several properties that are very essential for gas sensors. They have all their atoms on the surface, endowing them with the highest specific surface area possible together with graphene. Therefore, all the carbon atoms in the nanotube can, in principle, interact with the analytic gas, while simultaneously supporting charge transport in the device. Thus, adsorbates and electrostatic charges and dipoles close to the nanotube can greatly impact charge transport. At the same time, the carbon nanotube lattice is held together by strong sp2 C-C bonds, which provide the necessary chemical stability to the carbon nanotube. An individual SWNTs sensor can be used to detect different types of molecules [1].

Detecting gas molecules is basic to environmental monitoring [2], control on chemical processing [3], space mission [4], agricultural and medical applications [1]. This type of device is very important because there are many gases which are harmful to organic life, such as humans and animals. One of the gases to be verified is nitrogen dioxide (NO_2). Even in small concentrations, it irritates the respiratory tract in large concentration causes pulmonary edema. NO_2 create disturbance mainly in the airways and lungs, but also causes changes in blood composition, in particular, reduces the content of haemoglobin in blood. At low concentration of only 0.23 mg/m3, one feels the presence of this gas, but its adverse effects observed in healthy individuals at concentrations of NO_2 in all 0.56 mg/m3, which is four times lower than the detection threshold. People with chronic lung diseases experience difficulty in breathing

even at a concentration of 0.38 mg/m3. Among all harmful gasses, NO_2 is a well-known toxic gas and air pollutant and monitoring its concentration is crucial for air quality monitoring. Prolonged exposure to low concentration of NO_2 capable of causing several health hazards such as coronary artery disease as well as stroke [5-6]. The sensitivity of SWNTs towards NO_2 at atmospheric temperature as reported [1] is particularly interesting. The sensing of NO_2 is important to monitor environmental pollution resulting from combustion or automotive emission [7-8]. In recent times, the accidents in the oil, coal, gas industries have been increases, which claim the lives of hundreds of people. Every year many people lose their life due to hazardous gas leakage [14].

Many research groups have discussed sensing mechanism of NO_2 based on CNT. In order to improves the sensing performance, and more challengingly, how to improve sensitivity of sensor for different gas species. One promising way is the functionalization [4, 9] of carbon nanotubes. Many characteristics of CNTs are superior to most other materials. Thus, for example, Young's modulus, which depends on the diameter and chirality of a CNT defect, can reach 1.8TPa, while when the conventional carbon fibres, it is comparable to 800GPa. The bulk compressibility of CNTs is quite high and amounts to 0.024GPa-1. If bent CNT also exhibit exceptional flexibility, their electrical conductivity depends on the magnetic field induction [10]. The magnetic properties of CNTs are remarkably different from the properties of diamond and graphite. The first measurements of the magnetic susceptibility showed that it greatly decreases with decreasing temperature of 300K. CNTs exhibit anisotropy magnetic property. With these properties, CNTs have broad application prospects, but their successful use is necessary to deal with some problems [2, 4, 10]. For example, CNT through the possession of large surface energy, tend to form agglomerates, reaching up to tens or

hundreds of micrometres. This leads to deterioration of the properties of CNTs in comparison with those that would be typical for homogeneous distribution. Solution to this problem can be achieved using various methods. CNT mechanical processing time must also be limited; since it increases the density of surface defects is increased [11]. Therefore, in addition to mechanical processing methods use the chemical treating CNTs to achieve more efficient dispersibility and impart additional properties. For example, using metal catalysts in the form of nanoparticles to decorate CNT, promotes the interaction with specific gas species. In this experiment CNTs have been functionalize by gold decoration.

Existing gas sensors are based on metal oxide semiconductor. However they have a low sensitivity, high operating temperature and reaction time and substantial recovery. To ensure effective monitoring of air quality status it is necessary to improve the characteristics of gas sensors that can detect danger in advance. Development of NO_2 sensors based on carbon nanotubes due to their unique properties will provide an opportunity to find a solution to these critical problems. To increase the sensitivity and selectivity to specific gas, as well as their reliability in various condition. The extraordinary property of SWNTs towards NO_2 sensing attracts not only academicians but also industrials to make low power NO_2 gas sensor. In present work, I am trying to solve above mentioned problems, for same, SWNTs grown sample is decorated with gold nanoparticles and also I have done detailed study on various effect of Au decoration on sensor characteristics.

5.2 Experiment

SWNTs used in this sensor have been grown by standard Chemical vapor Deposition (CVD) technique [10,13, 14]. CVD technique is one of the best technologies for CNTs growth on silicon wafers.

I grow SWNTs on 5X5 mm chromium coated silicon wafer by standard CVD method [10, 13, 15]. Deposited SWNTs are decorated by gold. Gold is coated over sample by sputtering system. After that two electrodes are made by standard lithography technique as shown in Figure 5.1.

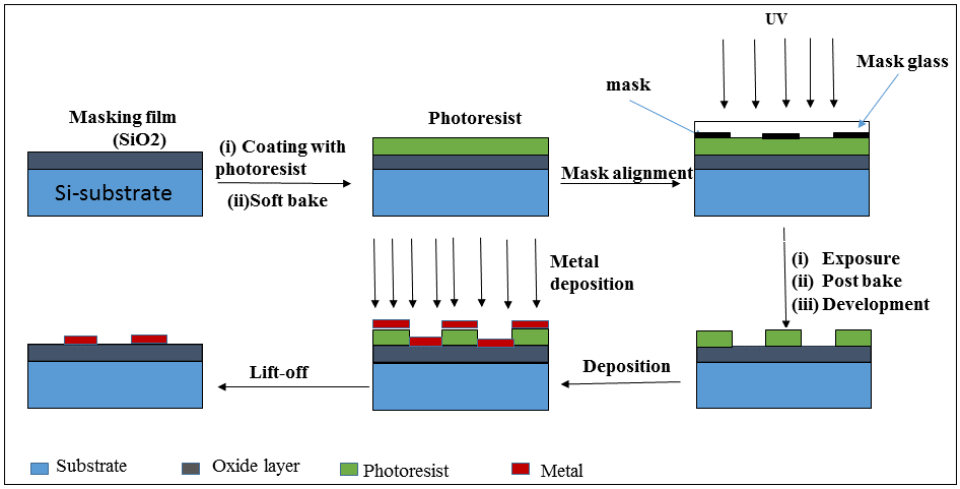

Figure 5. 1: Phases of lithographical process.

Formation of sensor electrode has the following successive processes: lithography, deposition and etching. Typical lithography process includes a set of operations that can be divided into three phases (Figure 5.1):

- Forming a continuous uniform layer of resist on the substrate surface;

- Once the surface has been coated with photoresist, the substrate is exposed to UV light;

- Once exposed, the substrate is immersed in a developer solution.

NO_2 sensor research work carried out based on a CNT in a special chamber with one side connected to the gas distributor and on the other with the release into the environment. The gas supply comes from the two cylinders: the first bottle contains only air, the second air cylinder + NO_2 concentration of 100ppm. The camera also has outputs for connection of an oscilloscope, multimeter that allows you to measure the change in resistance of the sensor in real time. Restoring the sensor is carried out by exposure to UV radiation. The flow of UV rays sent directly to the camera cell by limiting their distribution area. The calculation and measurement of the concentration of nitrogen dioxide (NO_2) to obtain the experimental data; regulation of the inlet gas concentration is done by standard mass flow controller and change in the resistance is measured by using multimeter/oscilloscope.

5.3 Results and discussion

Figure 5.2 shows the scanning electron microscopy (FESEM) image of pristine SWNTs grown over silicon substrate, in which I clearly observe a dense horizontal network of SWNTs over all substrate. The present SWNTs on substrate also verify by Raman spectroscopy (Figure 5.4). In Raman spectra, a sharp peak in the range of 200cm-1 to 300cm-1 is verifying the existence of SWNTs on silicon substrate. Figure 5.3 shows the FESEM image of Au decorated SWNTs surface, where I can see nonuniform particles of gold is distributed on every CNT. First, I had done sensing experiment without UV supported recovery. And I found that the recovery time is more than 12 hours, which is impractical and does not meet all the tasks to be performed by the sensor. For the functional operation of the sensor it is necessary to its full recovery after each cycle

of gas exposure. To expedite this process, I need to give the adsorbed gas molecules enough energy to break chemical bonds and their desorption from the surface of the CNTs. To achieve such an effect is possible by heating or exposing the sensor with UV exposure. Exposure to UV light is more advantageous way compared with heating, since, firstly, quantum energy UV radiation allows strong enough to destroy the chemical bonds, thereby accelerating the desorption process several times; Second, importantly, the use of UV lamps easier to operate [15-20]. After that i performed a series of experiment to monitor the response of the sensor with different concentrations of NO_2, followed by reduction by means of UV radiation (see Figure 5.5 to Figure 5.6). To see the various effect of gold decoration on sensing property firstly I performed the sensing experiment on pristine SWNTs with the concentration of NO_2 is 40ppm level and found initial resistance Ri = 65.06KΩ. After the start of gas supply to the resistance test chamber starts to decrease gradually. The response of the sensor is a 1 ~ 3 seconds. After 5 minutes the gas flow was stopped, the camera only did the air flow and also produces ultraviolet light. Almost immediate increase in resistance was noted. Full recovery of the sensor to the initial position was 4 minutes 30 seconds. Now same experiment was repeated for gold decorated SWNTs sample with kept all sensing parameter same as before.

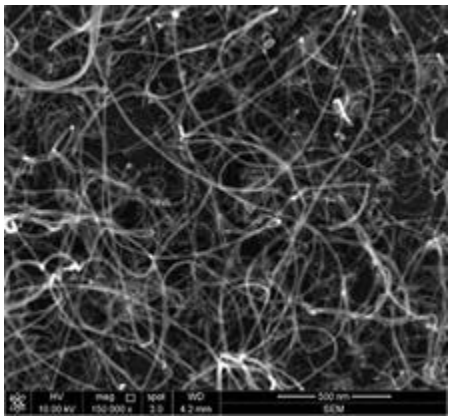

Figure 5. 2: FESEM image of pristine SWNTs.

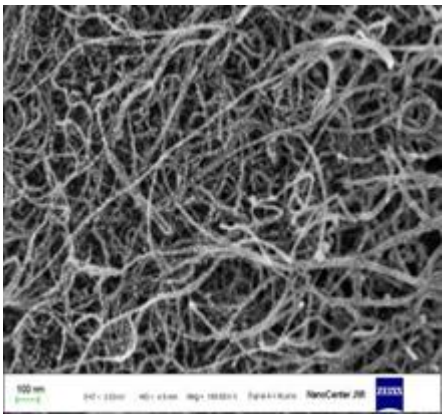

Figure 5. 3: FESEM image of gold decorated SWNTs.

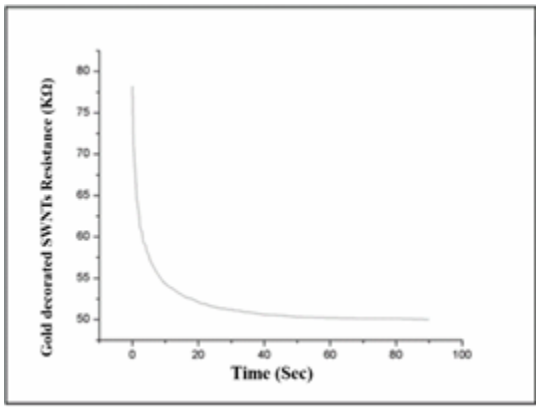

Figure 5. 4: Raman spectra of pristine SWNTs.

It is observed that initial resistance Ri = 78.2KΩ sharply decreased to drag reduction occurred more rapidly than without gold sample. Comparison between NO_2 gas sensor without gold coated and with gold coated has been shown in the Figure 5.6 The sensitivity for each case can be calculated by formula:

$$S = \frac{R_0 - R_{NO2}}{R_0} X\ 100\% \qquad (1)$$

Where –S is the sensitivity of the sensor; R_0 is the sensor resistance before you start working; R_{NO2} is the resistance of the sensor at the end of the experiment. And I can see the sensor sensitivity for pristine type sensor approximately 30percent and for gold decorated sensor around 38 percent approximately. The comparison between both type of sensor also shown in Figure 5.6 and it is clearly observed from figure that gold decorated sensor have better sensitivity as compare to pristine SWNTs sensor. The possible reason for better sensitivity is that gold decorated CNTs have larger surface area as compare to pristine CNTs and hence the area for gas molecules interaction with sample is also larger.

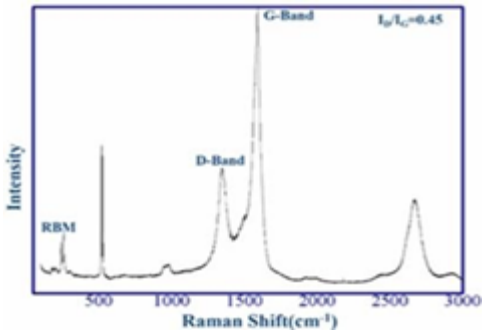

Figure 5. 5: Resistance Vs time for Au decorated SWNTs sensor.

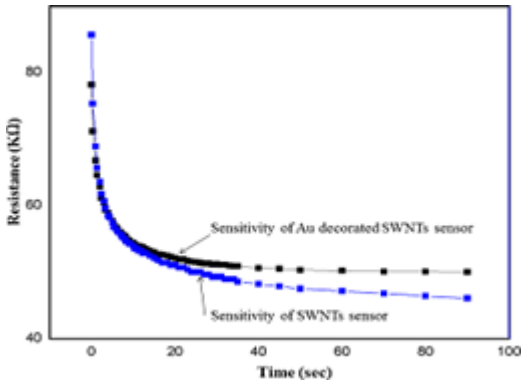

Figure 5. 6: Plot of the comparison between response of SWNT NO_2 sensor and Au-modified SWNT NO_2 sensor. Au-modified SWNT NO_2 sensor showed increase in sensitivity as compared with without gold coated SWNTs NO_2 sensor.

5.4 Conclusion

I have successfully developed a good quality NO_2 sensor. Based on the results of observations it can be argued that the sensor has an almost instantaneous reaction rate to the feed gas and the selected recovery technique using UV radiation has advantages over previous technologies by small time and ease of use. The change in sensitivity of SWNT sensor is induced by the coating of Au layer. The chemical pattern clearly demonstrates a significantly higher sensitivity of the Au-modified SWNT sensor compared with the un-functionalized SWNT sensor for NO_2 gas.

5.5 References

[1] Kong J. Nanotube Molecular Wires as Chemical Sensors. Science 2000; 287(5453): 622–625.

[2] Zanolli Z, Leghrib R, Felten A, Pireaux J-J, Llobet E, Charlier J-C. Gas sensing with au-decorated carbon nanotubes. ACS Nano 2011; 5(6).

[3] Zeng Q, Luna J, Bayazitoglu Y, Wilson K, Imam MA, BarreraEV. Metal Coated Functionalized Single-Walled Carbon Nanotubes for Composites Application. Mater. Sci. Forum 2007; 561–565: 655–658.

[4] Sun Y-P, Fu K, Lin Y, Huang W. Functionalized Carbon Nanotubes: Properties and Applications. Acc. Chem. Res. 2002; 35(12): 1096–1104.

[5] Vallejos S, Grácia I, Chmela O, Figueras E, Hubálek J, Cané C. Chemoresistive micromachined gas sensors based on functionalized metal oxide nanowires: Performance and reliability. Sensors Actuators B Chem. 2016; 235: 525–534.

[6] Suehiro J, Zhou G, Hara M. Fabrication of a carbon nanotube-based gas sensor using dielectrophoresis and its application for ammonia detection by impedance spectroscopy. J. Phys. D. Appl. Phys. 2003; 36(21): L109– L114.

[7] Tran TH, Lee J-W, Lee K, Lee YD, Ju B-K. The gas sensing properties of single-walled carbon nanotubes deposited on an aminosilane monolayer. Sensors Actuators B Chem. 2008; 129(1): 67–71.

[8] Penza M, Rossi R, Alvisi M, Signore MA, Cassano G, Dimaio D, Pentassuglia R, Piscopiello E, Serra E, Falconieri M. Characterization of metal-modified and vertically-aligned carbon nanotube films for functionally enhanced gas sensor applications. Thin Solid Films 2009; 517(22).

[9] Derycke V, Auvray S, Borghetti J, Chung C-L, Lefèvre R, Lopez-Bezanilla A, Nguyen K, Robert G, Schmidt G, Anghel C, Chimot N, Lyonnais S, Streiff S, Campidelli S, Chenevier P, Filoramo A, Goffman MF, Goux-Capes L, Latil S, Blase X, Triozon F, Roche S, Bourgoin J-P. Carbon nanotube chemistry and assembly for electronic devices. Comptes Rendus Phys. 2009; 10(4): 330–347.

[10] Mishra P, Pavelyev VS, Patel R, Islam SS. Resistive sensing of gaseous nitrogen dioxide using a dispersion of single-walled carbon nanotubes in an ionic liquid. Mater. Res. Bull. 2016; 78: 53–57.

[11] Meng L, Fu C, Lu Q. Advanced technology for functionalization of carbon nanotubes. Prog. Nat. Sci. 2009; 19(7): 801–810.

[12] Lee K, Lee J-W, Dong K-Y, Ju B-K. Gas sensing properties of single-wall carbon nanotubes dispersed with dimethylformamide. Sensors Actuators B Chem. 2008; 135(1): 214–218.

[13] Tripathi N, Mishra P, Joshi B, Islam SS. Precise control over physical characteristics of Carbon Nanotubes by differential variation of Argon flow rate during Chemical Vapor Deposition processing: A systematic study on growth kinetics. Mater. Sci. Semicond. Process 2015; 35: 207–215.

[14] Tripathi N, Mishra P, Joshi B, Islam SS. Catalyst free, excellent quality and narrow diameter of CNT growth on Al2O3 by a thermal CVD technique. Phys. E Low-dimensional Syst. Nanostructures 2017; 62: 43–47.

[15] Penza M, Rossi R, Alvisi M, Cassano G, Serra E. Functional characterization of carbon nanotube networked films functionalized with tuned loading of Au nanoclusters for gas sensing applications. Sensors Actuators, B Chem. 2009; 140(1).

[16] Brahim S, Colbern S, Gump R, Grigorian L. Tailoring gas sensing properties of carbon nanotubes. J. Appl. Phys. 2008; 104(2): 24502.

[17] Mishra P, Harsh, Islam SS. Trace level ammonia sensing by SWCNTs (network/film) based resistive sensor using a simple approach in sensor development and design. Int. Nano Lett. 2013; 3(1): 46.

[18] Peng N, Zhang Q, Chow CL, Tan OK, Marzari N. Sensing mechanisms for carbon nanotube based NH3 gas detection.. Nano Lett. 2009; 9(4): 1626–1630.

[19] Huang XJ, Choi YK. Chemical sensors based on nanostructured materials. 2007; 122(2): 659–671.

[20] Van PTH, Thanh NH, Van Quang V, Van Duy N, Hoa ND, Van Hieu N. Scalable fabrication of high-performance NO_2 gas sensors based on tungsten oxide nanowires by on-chip growth and RuO_2-functionalization. ACS Appl. Mater. Interfaces 2014; 6(15): 12022–12030.

Chapter 6: Thin film chemiresistive gas sensor on single-walled carbon nanotubes-functionalized with polyethylenimine (PEI) for NO_2 gas sensing

6.1 Introduction

The world health organization (WHO) 2016 report suggests that the 90% population of the world inhales the polluted air and is polluted beyond the limits specified by the WHO. The major components of this polluted air are nitrogen dioxide (NO_2), Sulphur dioxide (SO_2), ozone (O_3), carbon monoxide (CO), volatile organic compounds (VOCs) and particulate matter (PM) [1]. Owing to globalization and rapid growth in the human population, there is a tremendous increase in the concentration of different greenhouse gases like CO_2, H_2S, H_2O and NO_2, which leads to various respiratory diseases [2]. Although all of these gases are noxious to humans and to the environment, but the most crucial is the increase in the consolidation of toxic NO_2 gases. The overexposure of NO_2 in small concentration causes irritation in the human respiratory tract and in large concentration may lead to pulmonary disease and in the extreme case can cause loss of human life [3]. It can also cause a change in the blood composition, in particular, reduces the content of hemoglobin in blood [4]. The main source of the NO_2 gases is traffic and fossil fuel consumption processes. We can feel the presence of NO_2 gas when the concentration is 0.23mg m^{-3}, but its adverse effect can be observed in healthy individual at the concentration of 0.056mg m^{-3}, which is four times lower than the detection threshold. The people with chronic lung disease experience difficulty in breathing even at the concentration of 0.038mg m^{-3} NO_2 gases. Therefore, the detection to reduce the concentration of NO_2 under an ambient condition at room temperature is of great importance.

Conventional sensing material, such as metal oxide semiconductors have poor sensitivity at room temperature and requires an additional power supply source and microfabrication

techniques for the normal functioning of the sensor. Some examples of metal oxide semiconductor-based NO_2 gas sensors are titanium dioxide (TiO_2), zinc oxide (ZnO), copper (II) phthalocyanine (CuPc) [5] and copper oxide (CuO) [6]. Metal oxide semiconductors-based gas sensors have been extensively used, but for particular detectors, the high operating temperature has restricted the development of such sensors because it requires high cost as well as the complicated configurations [7, 8].

On the other hand, carbon nanotubes (CNTs) are one-dimensional (1-D) nanomaterial, which attract more consideration because they have high sensitivity for gases at room temperature [9, 10]. It has been found that CNTs; are encouraging detecting material, which retains electrical properties and is extremely responsive to a low concentration of gases, such as carbon dioxide (CO_2), nitrogen oxide (NOx) and ammonia (NH_3) at room temperature. Besides, CNTs as ultra-sensitive sensing materials, also outperform the conventional sensing material, such as metal oxide semiconductor in terms of vast assimilative capability, large surface-area-to-volume ratio, low weight and rapid response time, resulting in momentous variations in electrical properties, such as resistance and capacitance [11, 12]. After the breakthrough of CNTs by Iijima [13], CNTs have shown great potential and emerged as one of the most promising materials for a wide range of engineering applications, such as optoelectronics [14, 15], sensors [16,17,18,19] and actuators [16,17,18]. CNTs are incredible structures having an array of fascinating magnetic, electrical and mechanical characteristics. The essential requirements of a good sensor are fast response, high selectivity, high volume production, low cost and high reliability.

As a sensing material, CNTs can be exploited in two different ways, for enhancing the sensitivity and selectivity. CNTs are repeatedly decorated with new elements such as metals. Conversely, CNTs can be integrated with other sensing materials, for instance, metal oxide

semiconductor to enhance their sensitivity [20]. It has been established that there is a variation in electrical conductivity of conducting polymers when it is exposed to diverse organic and inorganic gases [21]. There are many conducting polymers, for instance, polyaniline (Pani), polypyrrole (PPy), polythiophene and the various derivatives of different polymers, which can be used as sensing materials [22]. Currently, many researchers tried to increase the sensitivity of CNTs-based gas sensors in various different ways, such as by depositing layers of different metals or by functionalizing with polymers [23].

In the present work, I have analyzed the growth and development of single-walled carbon nanotubes-polyethylenimine (SWCNTs-PEI) functionalized-based resistive gas sensor for toxic NO_2 gas detection. An elaborate study of the sensor was done for various parameters such as sensitivity, reversibility and response–recovery time. I have investigated the effect of functionalization on the sensitivity of the SWCNTs-based resistive gas sensors with the polyethyleneimine (PEI, Aldrich Chemicals) at room temperature.

6.2 Experimental

6.2.1 Sensors

The SWCNTs sensor was grown by using the standard thermal CVD method. The SWCNTs films were deposited on a SiO_2/Si substrate by using standard thermal chemical vapour deposition (CVD) method and co-sputtering was used for preparing the catalyst. The two planer Au electrodes were deposited on the as-grown SWCNTs surface by sputtering method followed by patterning with the standard lift-off method. The catalyst used for growing SWCNTs is achieved by co-sputtering of Fe–Mo metals (0.5 nm width) on a subsidiary cover of Al metal (10 nm width) [24]. The catalyst was annealed for 30 min in Ar/H2 atmosphere at 900∘ C temperature. The mass flow controller was used to control the supply of carrier gas Ar/H2 and the precursor gas

C_2H_2 (acetylene) into the chamber. For SWCNTs growth, the rate of flow of Ar/H_2 and C_2H_2 gases are kept at 30 and 5 sccm, respectively, and this gas flow is maintained for 5 min. The growth pressure was maintained at 50 Torr [24]. The two planer Au electrodes were deposited on the as-grown SWCNTs surface by sputtering method followed by patterning with standard lift-off method. The sensing area comprising SWCNTs were grown by thermal CVD system on SiO_2/Si substrate, and the electrodes made up of gold pattern structure with 60μm channel length was fabricated by a standard photolithography technique. The methods of physical treatment of the CNTs are not sufficiently effective, so the other option is to change the chemical properties of the surface through chemical functionalization. PEI, from Sigma Aldrich, is adsorbed on the surface of SWCNTs network by immersing in a PEI/methanol solution. The sensors were dipped for 15 min, 1 and 2 h in a 20 wt.% solution of PEI polymer. The sensors are taken out from the solution and the excess PEI is removed by rinsing the sample with the methanol. So as to remove the excess methanol present over the sample, it was then heated up to a temperature of 80°C for 15 min, leaving behind a pure PEI-coated SWCNTs film without methanol.

6.2.2 **Measurements**

The PEI functionalized SWCNTs sample is placed inside a closed chamber, with one side connected to the gas distribution and the other side is open to the environment. The gas supply comes from the two gas cylinders: the first gas cylinder contains only air, while the other gas cylinder contains NO_2. The NO_2 gas (100 ppm, balanced nitrogen) used in the experiment as purchased from Linde Industrial Gases, Russia. The enclosed sample chamber also has a connection for connecting multimeter that allows recording the real-time change in the resistance of the samples when it is exposed to the NO_2 gases. The power density of the UV light used in the experiment is 10 W. The MKS standard mass flow controller (MFC) has been used for accurately

controlling the NO_2 concentrations in the various ppm-levels. The schematic diagram of the setup for NO_2 gas sensing (Figure 6.1). The change in the resistance of the SWCNTs sensor was recorded for various NO_2 gas concentrations, such as 20 and 50 ppm. In addition, to examine the repeatability of the sensor, the behavior of the SWCNTs sensor for same NO_2 gas concentration was recorded for repetitive cycles. Similarly, the behavior of PEI-doped SWCNTs sensors was also recorded in the presence of various concentrations of NO_2 gas and also under the same concentration of NO_2 gas for repetitive cycles. Inside the chamber, there is a platform for holding the gas sensor samples with two pointed electrodes, which are connected with the multimeter (UNIT-T UT803). UV light illumination is used to enhance the recovery of the gas sensor in case of pristine SWCNTs sensor, whereas in case of PEI functionalized SWCNTs, I did not use UV light, hence the recovery is slow.

6.2.3 **Characterization**

A field emission electron microscopy (Nova NanoSEM 450, FEI and ZEISS sigma FESEM, India) of SWNTs-PEI as shown in Figure 6.2 was done to study the surface morphologies, orientation and dimensions of SWNTs-PEI bilayer sensor film. The samples were mounted on the double-sided tape and the high-resolution images of SWCNTs and SWCNTs-PEI were taken as shown respectively, in Figure 6.2a and Figure 6.2b. In Figure 6.2, I can see the uniform dispersion of the bilayer of SWCNTs-PEI and there are many spots which resemble island shape. The presence of cavities at the tip of the isle shaped spot helps in the adsorption of NO_2 molecules on the surface of the gas sensor. The PEI polymer layer essentially operates as a transitional charge transmit strip from the SWNTs to the electron acceptors. Basically, the polymer PEI accelerate the charge transfer mechanism. A lot of work has been reported, which have acknowledged the binding energy and charge transfer for NO_2 gas molecules [11, 25]. Transmission of charged particles takes

place from the surface of PEI functionalized SWCNTs to the acceptors when the NO_2 gas molecules are adsorbed on the surface of PEI, PEI acting as a transitional layer.

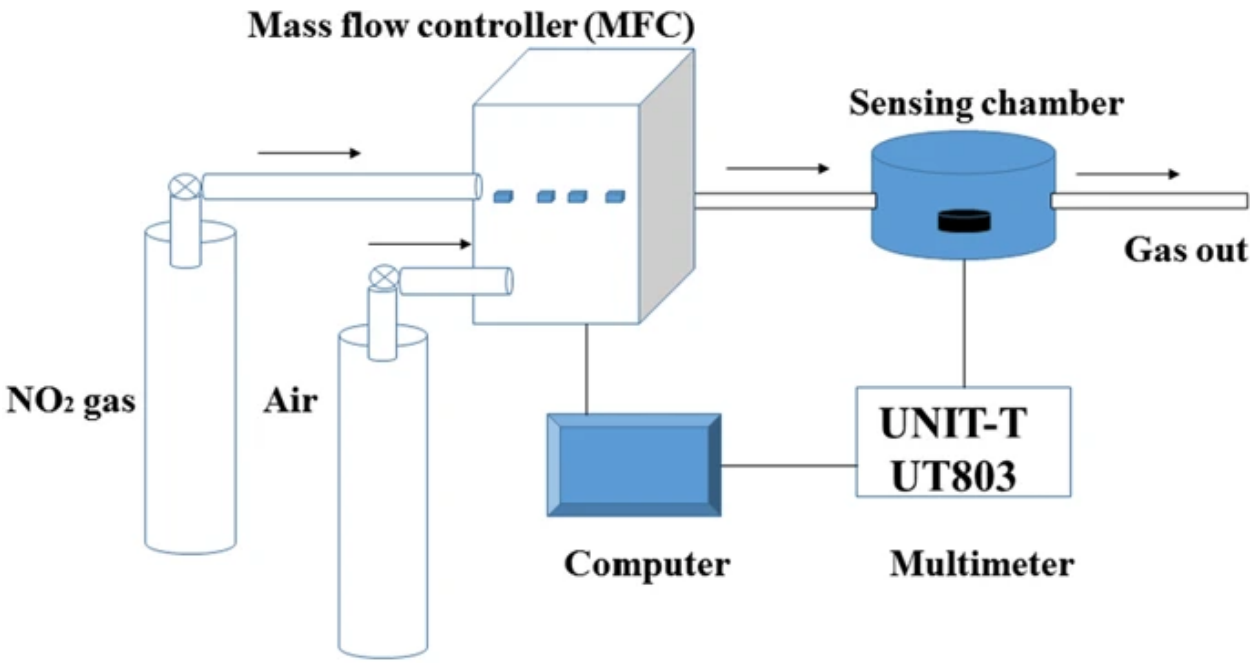

Figure 6. 1: Schematic diagram of the setup for NO_2 gas sensing.

The IRS spectroscopy of the PEI-SWCNTs composites is shown in Figure 6.3. The IR bands indicate two peaks at 1360cm^{-1} and 1720cm^{-1}, which shows the presence of imide moieties and carbonyl in the five-membered ring structure of PEI, respectively. The strong bond at 1039cm^{-1} is the confirmatory band of the PEI polymer for its conductivity and is a measure of the degree of delocalized electrons. This bond is evident for the high conductivity, which ascribed to the C–H in-plane vibration. The bond at 1360cm^{-1} is the representative of C=C*C*=*C* bonds, the C–C vibration occurs due to the internal defects. The other bonds observed at 2937cm^{-1} and 3318cm^{-1} are characteristic of C–H and O–H stretches, respectively. O–H vibrations are observed due to the amorphous carbon, which can easily form a bond with atmospheric air [26].

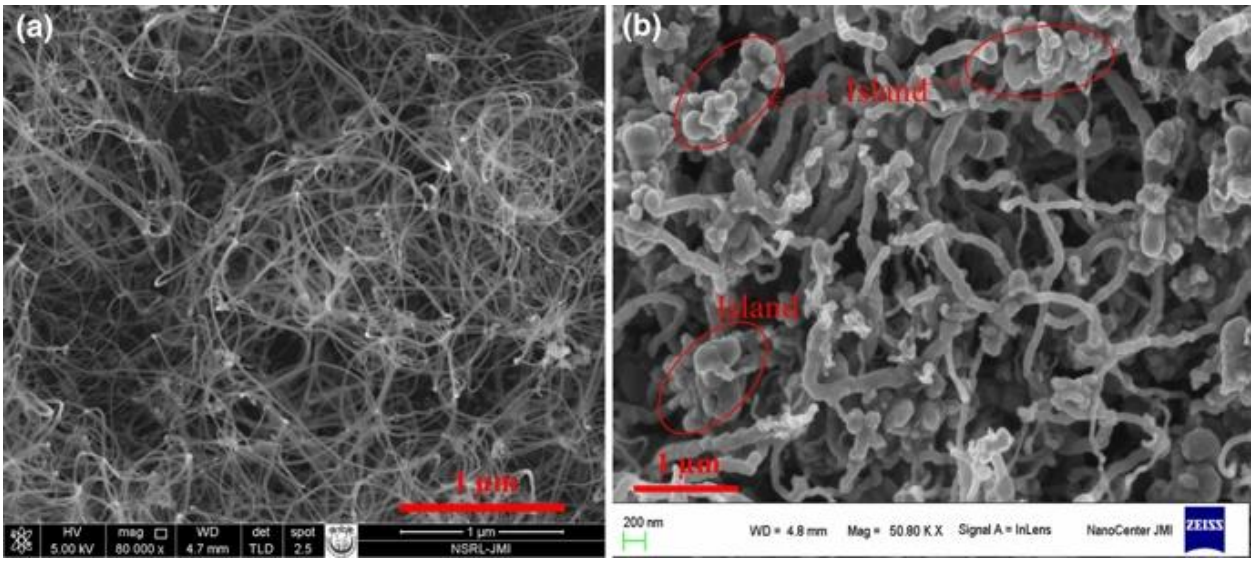

Figure 6. 2: SEM micrograph of gas sensor films. (a) Surface micrograph of the pristine SWCNT sensor. (b) Surface of PEI functionalized SWCNT sensor.

Raman spectroscopy (NTEGRA Spectra NT-MDT) was performed to observe the characteristic vibrational modes of SWCNTs and the subsequent effect of PEI functionalization and the spectra. Raman spectra measured on both pristine and PEI functionalized SWCNTs film is shown in Figure 6.4. Radial breathing mode (RBM) of the sample was observed at 198cm^{-1}. As the frequency of RBM is inversely proportional to the reciprocal of the diameter, it can be used to determine nanotube diameter. The RBM also provides information on chirality and thus, the electronic properties of the nanotube. Because single excitation energy was used in our experiment, only nanotubes resonant with this particular energy will demonstrate a peak at the RBM frequency. The nanotube diameter can be determined by $V_{RBM}=248/\omega$ [27], where V_{RBM} is Raman frequency shift of the RBM in cm$^{-1.}$ From measured RBM, calculated SWCNT diameter is 1.25 nm. The characteristic graphene band was observed at 1590cm^{-1}, the broadening of G band appeared because of the small diameter of SWCNTs. Defect-related D-band was observed at 1352cm^{-1}. The

low intensity of the D band signifies a smaller number of defects in samples. Further, the decrease in the peak intensities of the functionalized SWCNTs as compared to pristine SWCNTs endorses the surface coverage by PEI on SWCNTs resulting in some modification on the surface [26].

6.3 Results and discussion

Investigations were done to understand the consequences of PEI functionalized SWCNTs gas senor samples on the NO_2 sensing. Figure 6.5 shows the sensing response and recovery curve of SWCNTs sensor towards the NO_2 gas molecules. Initially, when the NO_2 gas molecules start flowing into the closed chamber, the resistance of the sensors starts decreasing from the baseline i.e. 36.44KΩ. However, once the analyte gas flow is stopped into the chamber, de-adsorption of the NO_2 molecules from the surface of SWCNTs starts taking place and consequently, causes an increase in the resistance of the sample. Many researchers have reported that due to significant binding energy at the adsorption sites, the natural recovery of the sensor is slow as compared to the response. Figure 6.5 explains the repeatability and recoverability in case of pristine SWCNT sensor. The major challenge faced was the recovery of the sensor. The fast recovery was accomplished by the use of UV illumination.

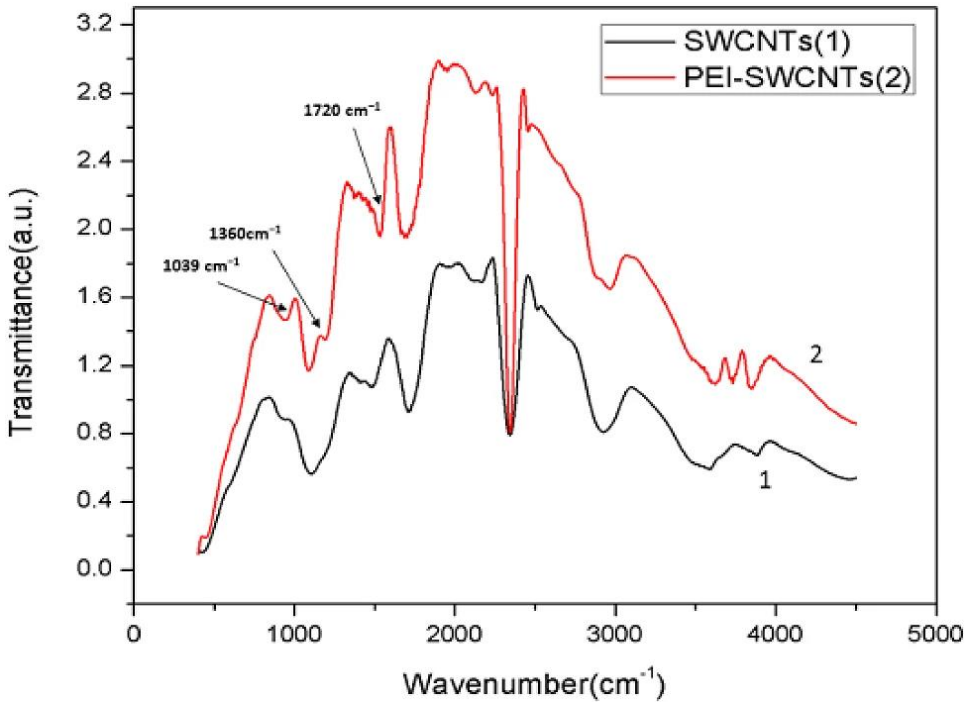

Figure 6. 3: IRS spectroscopy comparison of pure SWCNTs and PEI-SWCNTs composites.

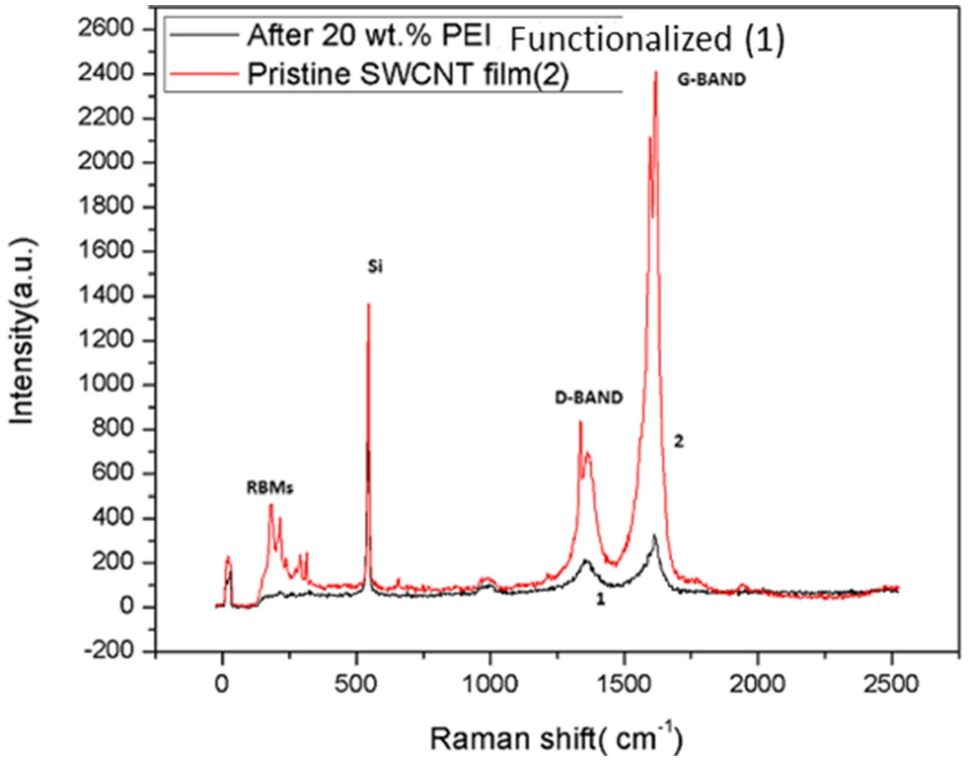

Figure 6. 4: Raman Spectroscopy: (1) PEI-functionalized SWCNTs sensor and (2) pristine SWCNTs sensor.

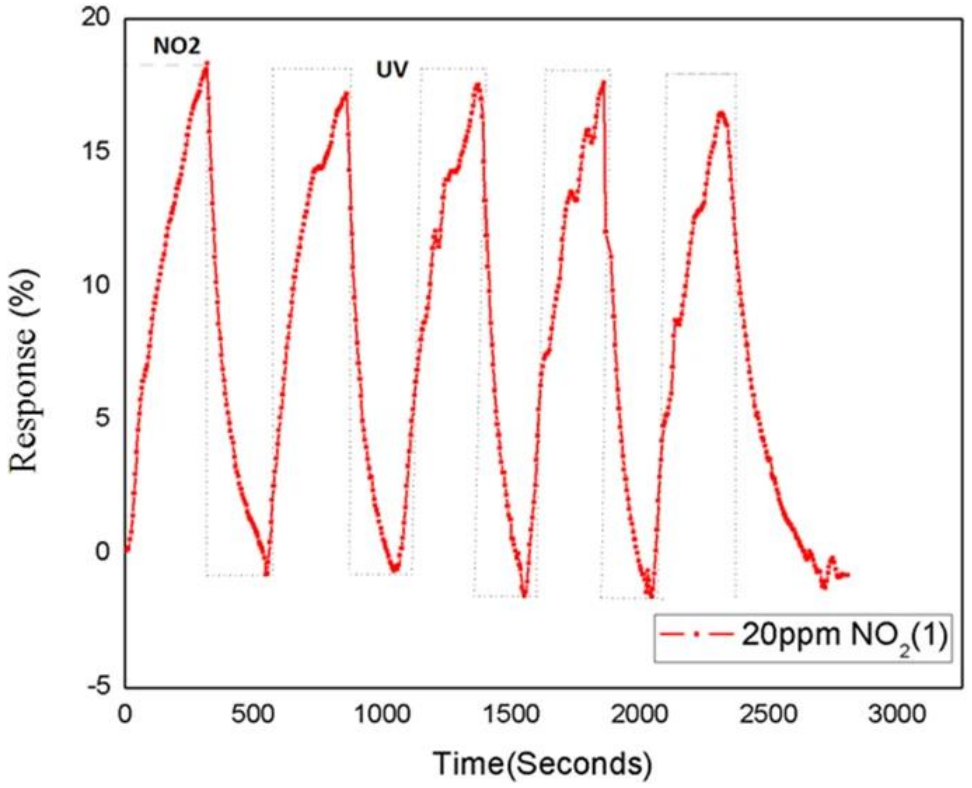

Figure 6. 5: It shows the repeatability for NO_2 gases of the SWCNTs sensor.

It is evident from Figure 6.5 that as the NO_2 gas flow continues, there is a continuous decrease in the resistance of the sensor. It can also be seen that after some time, the resistance become stable and desorption of analytes takes a longer time at the ambient conditions. Therefore, to establish the decreasing curve, two different concentrations of NO_2 analytes were passed through the closed chamber in which the gas sensor was placed. Figure 6.6 and Figure 6.7 show the comparison between the sensitivity of SWCNT resistive gas sensors for various concentrations of NO_2 gases. It is evident from the graph that as the concentration of NO_2 increases correspondingly, there is an

increase in response percentage. The sensitivity of chemiresistive gas sensors can be calculated as the ratio of the initial resistance of the sensor in the air to the resistance in the presence of gas.

$$S\ (\%) = (Ra - Rg)/Ra * 100, \quad (1)$$

Where *S* is the sensitivity of the gas sensor, Ra the initial resistance in the presence of air and Rg the final resistance in the presence of analyte gas NO_2.

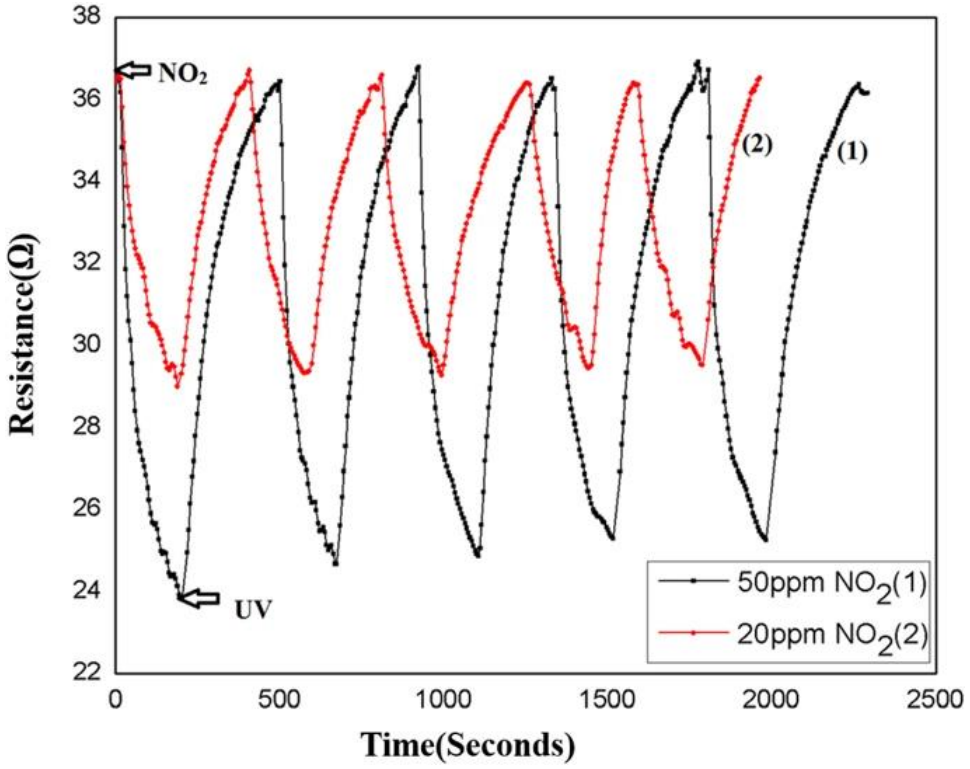

Figure 6. 6: SWCNTs sensor response for various concentrations of NO_2 gases, such as 20 and 50 ppm.

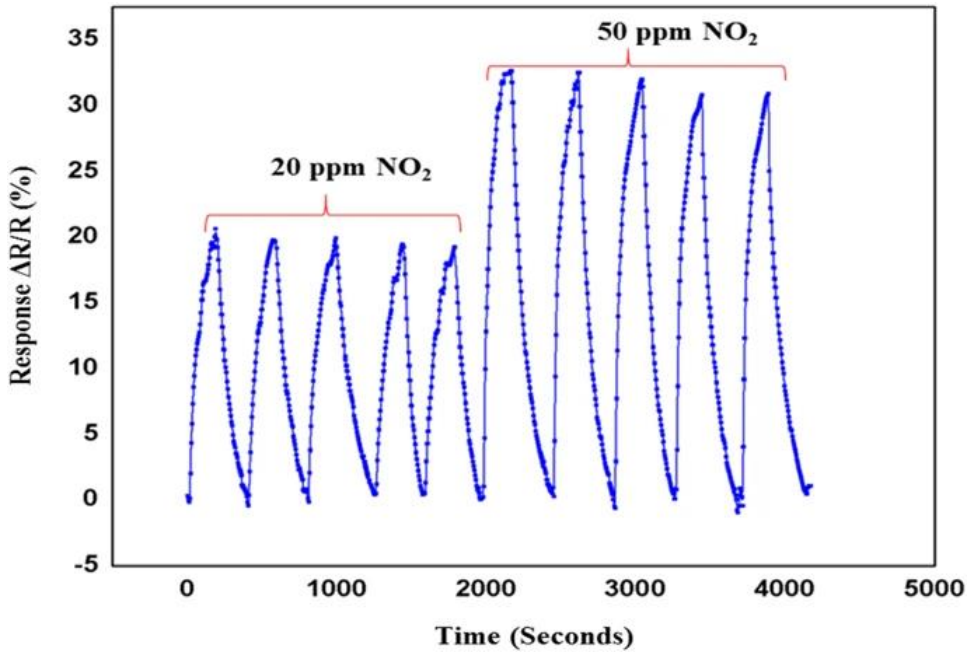

Figure 6. 7: Response ΔR/R (%) for various concentrations of NO_2 gases, such as 20 and 50 ppm.

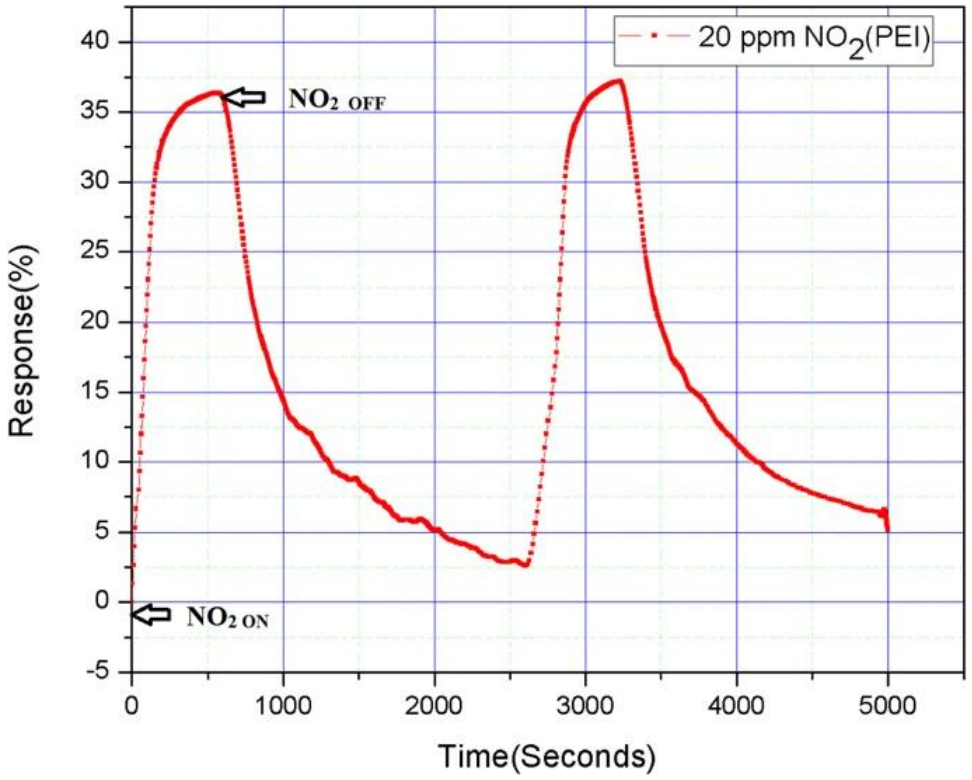

Figure 6. 8: Response of PEI-functionalized SWCNTs resistive gas sensor in the presence of NO_2 gases.

The sensitivity of the resistive gas sensor based on SWCNTs was calculated using equation (1) and it was found to be 20.12%. The sensitivity of the SWCNTs sensor can be improved by properly functionalizing the sensor with the PEI polymer. PEI is a polymer with the repeating units of the amine group and two carbon aliphatic spacers. PEI acts as a transitional charge transfer layer from SWCNTs to the electron acceptor. There is a considerable amount of increase in the sensitivity of the gas sensor functionalized with PEI as compared to the bare CNT sensors. I have been successful in effort to develop a PEI functionalized SWCNTs sensor with much better sensitivity. The functionalization resistive gas sensor based on SWCNTs has shown a substantial increase in the sensitivity and was found as 37.00% for 20 ppm NO_2 gas detection. The semiconducting pristine SWCNTs sensor shows p-type behavior prior to PEI functionalization and it can be corroborated with the decrease in the resistance in the presence of NO_2 gas. The adsorption of PEI on the sidewalls of SWCNTs after functionalization is irreversible and it cannot be completely removed even after extensive rinsing in ethanol. This is in complete agreement with the other recent findings of the irreversible polymer wrapping around SWCNTs [28,29,30]. So, to control the functionalization level of SWCNTs network, the sensors were immersed in a solution of 20 wt.% PEI/methanol for 15 min, 1 and 2 h, respectively. There was a substantial increase in the sensitivity of the modified sensor. It was found that the initial resistance of the sensors kept on increasing as the sensors were immersed for a longer time. This behavior can be due to the donor effect of PEI on the p-type of SWCNT channel. The results concur with the first observation; this tendency is presumably by the virtue of accumulation of extra acceptor molecules resulting from the PEI functionalization of the SWCNTs surface of the gas sensors. There is a decrease in the channel resistance of p-type of SWCNTs because NO_2 acts as electron acceptors.

The response of the SWCNT sensor in the presence of NO_2 gas was found to be 20.12%. On the other hand, when the SWCNT sensor was functionalized with PEI polymer, then, the response of the doped SWCNT sensor increased up to 37% as shown in Figure 6.8. The charge transfer takes place from the SWNT surface to the NO_2 gas molecules with PEI polymer acting as an intermediate layer. An efficient molecular photodesorption of NO_2 gas from the surface of SWCNTs in the presence of UV illumination is achieved [31, 32]. A comparison table comparing the performance of the developed sensor with the other sensors developed for NO_2 gas sensing has been included and shown in table 7.1.

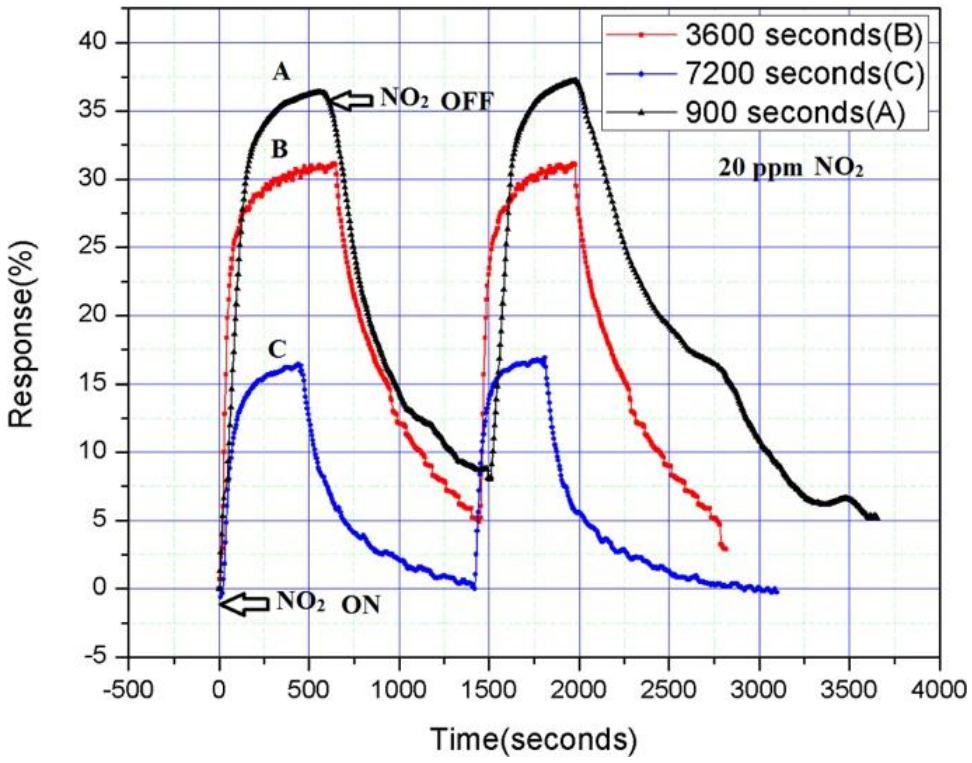

Figure 6. 9: Comparison of PEI-functionalized SWCNTs sensor response for the various durations of immersion of sensor in PEI/methanol solution.

At atmospheric conditions, the nature of SWCNTs is p-type [33,34,35]. In the case of pristine SWCNTs, when NO_2 gas interacts with SWNTs, the gas molecules withdraw electron and

thus, increases the majority carriers, which decreases the resistance strenuously [36, 37]. The strong carbon–carbon bonding in CNTs suppresses their reactivity and limits their sensing capability. Structural defects increase the chemical reactivity of carbon nanotubes [38, 39]. Pristine SWCNTs have fewer defects and hence, only a small number of gas molecules adsorbed on the surface during exposure. During the PEI functionalization process, additional defects (removal of carbon atoms, breaking of C=C*C*=*C* bonds) are created on the sidewalls as well as on the ends of SWCNTs. Functional groups, such as amine groups are preferably attached to these defects' sites, which further facilitates the adsorption of NO_2 gas molecules. As a result, more NO_2 gas molecules are adsorbed on the SWCNTs sensor, contributing to increased charge transfer between CNTs and NO_2 gas molecules. This results in a large change in the resistance of the sensor. Thus, the sensitivity of the PEI functionalized SWCNTs NO_2 gas sensor is enhanced. Also, the degree of enhancement in the sensitivity of SWCNTs depends on the type of functional group and the amount of functional group attached. The influence of moisture on the actual gas sensing response is found to be insignificant. The exposure of relative humidity (RH) does not make any sensible change in the baseline resistance of the sensor. I performed experiments at 5, 10, 20 wt% of PEI. Our sensor gave the best result for 20 wt% of PEI.However, as the immersion duration of SWCNT sensor into the PEI/methanol solution increases sensitivity, and recoverability of the sensor decreases as shown in Figure 6.9. There are two proposed reasons for the decrease in sensitivity and recoverability. The first reason is the accumulation of PEI polymer layer on the surface of SWCNTs after long hours of immersion. This deposition of a thick layer of PEI on the SWCNT surface decreases the sensitivity of SWCNT by reducing the charge transfer between the SWCNT layer and NO_2 molecules as shown in Figure 6.9.

Table 6. 1: Comparison of different materials based on NO_2 gas sensor performances.

Materials	NO_2 concentration	Sensitivity/response (%)	Response time	Operating temperature (°C)	References
ZnO	1–30 ppm	3.3	25 s	250	[40]
Silicon/ZnO	200 ppb	35	50 s	25	[41]
MoS_2–Au	2.5 ppm	30	4 min	RT	[42]
RGO–MoS_2–CdS	0.2 ppm	27.4	25 s	75	[43]
MoS_2/ZnO NWs	50 ppm	31.2	5 min	200	[44]
MoS_2/PSi NWs	50 ppm	28.4	—	RT	[45]
F-SWCNTs/Ps	—	36	11 s	RT	[46]
SWCNTs/Ps	—	13.5	13 s	100	[46]
F-SWCNTs	50 ppm	37	4 min	RT	This work

6.4 Conclusion

I have developed a chemiresistive SWCNTs-PEI functionalized gas sensor by using a thermal CVD method. The higher adhesive coefficient for the electron-withdrawing NO_2 of PEI-coated SWCNTs than untreated SWCNTs. At room temperature, PEI-SWCNTs-coated resistive gas sensor demonstrated elevated sensing behaviour and swift reaction to NO_2. Furthermore, owing to room temperature operation of the resistive gas sensor can be encouragingly exploited in the environment observation. A detector was successfully developed to detect low concentration (ppm) of NO_2 and by an accurate selection of thermal treatment, the complete recovery of the sensor was achieved. More importantly, it was found that with the increase in the duration of functionalization, the sensitivity of the SWCNTs is enhanced. By controlling the basicity and the functionalization concentration of SWCNTs network, the PEI-SWCNT sensors can be extended to various domains and the selectivity of the sensor can be configured based on various chemical environments. The achieved results are important as they demonstrate that the sensitivity of a SWCNTs gas sensor can be enhanced by the presence of attached amine group. However, apart from sensitivity, selectivity is also a challenge for a reliable CNT gas sensor development. As NO_2

gas sensors are intended to be deployed in both open and closed environments, the study of the effect of temperature and humidity is very important for calibration, interface circuitry and working room temperature SWCNT nitrogen dioxide sensor device. The optimization of the resistive gas sensor based on SWCNTs would be examined profoundly in future analysis.

6.5 References

[1] WHO, "WHO releases country estimates on air pollution exposure and health impact," *WHO*, 2016. [Online]. Available: http://www.who.int/mediacentre/news/releases/2016/air-pollution-estimates/en/#.

[2] Pan X, Zhao X, Bermak A, and Fan Z 2016 *IEEE Elect. Dev. Lett.*, **37**,92.

[3] Cullinan P, Muñoz X, Suojalehto H, Agius R, Jindal S, Sigsgaard T, Blomberg A, Charpin D, Annesi-Maesano I, Gulati M, Kim Y, Frank A. L, Akgün M, Fishwick D, De la Hoz R. E, and Moitra S. 2017 *The Lancet Respiratory Medicine*, **5** 445.

[4] Liddle L, Monaghan C, Burleigh M. C, McIlvenna L. C, Muggeridge D. J, and Easton C, 2018 *Nitric Oxide - Biol. Chem.*,**72** 59.

[5] Antisari M. V, Marazzi R, and Krsmanovic R 2003 *Carbon N. Y.*, **41** 2393.

[6] Teymourzadeh M and Kangarlou H 2012 *World Appl. Sci. J.*, **18** 879.

[7] Lee A. P and Reedy B. J 1999 *Sensors Actuators, B Chem.*, **60** 35.

[8] Martinelli E, Polese D, Catini A, Amico A. D', and Di Natale C 2012 *Sensors Actuators, B Chem.*,**161** 534.

[9] Wei B. Y, Hsu M. C,Su P. G, Lin H. M, Wu R. J, and Lai H. J 2004 *Sensors Actuators, B Chem.*,**101** 81.

[10] Van Hieu N, Thuy L. T. B, and Chien N. D 2008 *Sensors Actuators, B Chem.*, **129** 888.

[11] Ghoorchian A and Alizadeh N 2018 *Sensors Actuators, B Chem.*, **255** 826.

[12] Sayago I, Fernández M. J, Fontecha J. L, Horrillo M. C, Vera C, Obieta I, and Bustero I 2012 *Sensors Actuators, B Chem.*, **175** 67.

[13] S. Iijima 1991 *Nature;* **354** 56.

[14] Abdulla S, Mathew T. L, and Pullithadathil B 2015 *Sensors Actuators, B Chem.*, **221** 1523.

[15] Chen L, Chen Z, Huang Z, Huang Z, Wang Y, Li H, Zhou H, and Kuang Y 2015 *J. Phys. Chem. C*, **119** 28757.

[16] Shen J, Zhu Y, Yang X, and Li C 2012 *Chem. Commun.*, **48** 3686.

[17] Yamada T, Hayamizu Y, Yamamoto Y, Yomogida Y, Izadi-Najafabadi A, Futaba D. N, and Hata K 2011 *Nat. Nanotechnol.*,**6** 296.

[18] Lipomi D. J, Vosgueritchian M, Tee B. C. K, Hellstrom S. L, Lee J. A, Fox C. H, and Bao Z, 2011 *Nat. Nanotechnol.*,**6** 788.

[19] Rafiee M, Rafiee J, Wang Z, Song H, Yu Z, and Koratkar N 2009 *ACS Nano*,**3** 3884.

[20] Balint R, Cassidy N. J, and Cartmell S. H 2014 *Acta Biomater.*,**10** 2341.

[21] Inoue S and Matsumura Y 2009 *Chem. Phys. Lett.*,**469** 125.

[22] Lupi C, Felli F, Brotzu A, Caponera M. A, and Paolozzi A 2008 *IEEE Sensors Journal*,**8** 1299.

[23] Körösi L, Mogyorósi K, Kun R, Németh J, and Dékány I 2004 *Prog. Colloid Polym. Sci.*,**125** 27.

[24] Mishra P, Harsh, and Islam S. S 2013 *Int. Nano Lett.*,**3** 46.

[25] Battie Y, Ducloux O, Thobois P, Dorval N, Lauret J. S., Loiseau A., 2011 *Carbon*,**49** 3544.

[26] Hussain S., Jha P., Chouksey A., Raman R., Islam S. S, Islam T., Choudhary P. K, 2011 *Journal of Modern Physics*, **2** 538.

[27] Jorio A., Saito R., Hafner J. H., 2001 *Phys Rev Lett*. **86** 6.

[28] Kong J and Dai H 2001 *J. Phys. Chem. B*, **105** 2890.

[29] Shim M, Javey A, Kam N. W. S, and Dai H, 2001 *Jour. of the Amer. Chem. Soci.*, **123** 11512.

[30] Connell M. J. O, Boul P, Ericson L. M, Hu C, Wang Y, Haroz E, Kuper C, Tour J, Ausman K. D, and Smalley R. E, 2001 *Chemical physics letter*.,**342** 265.

[31] Karthigeyan A, Minami N, and Iakoubovskii K, 2008 *Jpn. J. Appl. Phys.*, **47** 7440.

[32] Jeon J. Y, Kang B. C, Byun Y. T, and Ha T. J, 2019 *Nanoscale*, **11** 1587.

[33] Fukumaru T, Fujigaya T, and Nakashima N, 2015 *Sci. Rep.*, **5**, 1.

[34] Geier M. L, McMorrow J. J, Xu W, Zhu J, Kim C. H, Marks T. J., and Hersam M. C., 2015 *Nat. Nanotechnol.*,**10** 944.

[35] Takenobu T, Takano T, Shiraishi M, Murakami Y, Ata M, Kataura H, Achiba Y, and Iwasa Y, 2003 *Nat. Mater.*, **2** 683.

[36] Kumar D, et al., 2016 *Materials Chemistry and Physics*,**177** 276.

[37] Evans G.P, Buckley D.J, Skipper N.T, Parkin I.P, 2014 *RSC Adv.*, **4** 51395.

[38] Terrones M, Terrones H, 1996 *Fullerene Science and Technology*, **4** 517.

[39] Crespi V. H, Cohen M. L, Rubio A, 1997 *Physical Review Letters*, **79** 2093.

[40] Chen X *et al.*, 2018 *Appl. Surf. Sci.*, **435** 1096.

[41] Betty C. A, Sehra K, Barick K. C, and Choudhury S, 2018 *Anal. Chim. Acta*, **1039** 82.

[42] Yong Zhou Y. G, Cheng Z, Xiaogang L, 2018 *Appl. Phys. Lett.*, **113** 082103.

[43] Shao S, Che L, Chen Y, Lai M, Huang S, and Koehn R, 2019 *J. Alloys Compd.*, **774** 1.

[44] Zhao S, Wang G, Liao J, Lv S, Zhu Z, and Li Z, 2018 *Appl. Surf. Sci.*, **456** 808.

[45] Zhao S, Li Z, Wang G, Liao J, Lv S, and Zhu Z, 2018 *RSC Adv.*, **8** 11070.

[46] Naje A. N. and Mahmood W. K, 2018 *IOP Conf. Ser. Mater. Sci. Eng.*, **454** 1.

Chapter 7: Conclusion, Summary and Future Scope

7.1 Main Results and Conclusions

An important scientific and technical problem of detecting hazardous gas NO_2 has been solved in this work.

1) Single walled carbon nanotubes (SWCNTs) have been successfully grown using Chemical Vapor Deposition (CVD) method.
2) The as-grown SWCNTs gas sensor were decorated with Au nanoparticles. The sensing response analysis exhibited that the Au decorated sensor has better/comparable sensing response of 38% towards NO_2 gas in comparision to previous reported sensors.
3) The Polyethylenimine (PEI) polymer were used for functionalizing the SWCNTs surface. The result analysis shows that the PEI functionalized sensor showed better better/comparable sensitivity of 37% to wards NO_2 gas, and also shows better/comparable response/recovery time and repeatability.
4) The analysis of the gas sensing behavior of sensors with surface decoration of SWCNTs with Au nanoparticles and surface functionalization with polymer Polyethylenimine (PEI) revealed that the surface modification has improved the sensing parameters such as sensitivity, response/recovery times, repeatability and more importantly the sensor works at room temperature.

7.2 Summary

The present thesis deals with the fabrication of Carbon Nanotubes (single walled) using Chemical Vapor deposition method and their characterization. It has been established that surface modifications of CNTs using various methods such as metal deposition and functionalization using polymer can influence the sensing behavior of the NO_2 gas detector. The SWCNTs surface functionalization resulted in the improved sensing parameters such as sensitivity, response and recovery times as well as the stability of the detector.

There are various gas sensors available to detect this poisonous gas at low temperature. Each gas sensors have their own advantages and disadvantages in their working capabilities. However, there are certain qualities in the sensor which makes it highly suitable towards the NO_2 detection. The problem with the existing detection capabilities are low stability, sensitivity, selectivity, large response and recovery times. The suitable qualities of an ideal gas sensor to detect these volatiles are listed below:

- High sensitivity to detect gas targets at low temperature
- Multiple gas detection to detect multiple gas targets
- Low cost to enable accessibility on a wide range scale
- Comparatively easier fabrication procedure for fast and low cost manufacturing
- Comparatively robust design

The focus of this research was on single walled carbon nanotubes (SWCNTs) NO_2 gas sensor which came much closer to some of these qualities compared to the other gas sensors. Thus, the SWCNTs NO_2 gas sensor is studied, analyzed, investigated and customized in this research to improve its performance and designing the sensor in a way to detect harmful gases. The designed

customized SWCNTs functionalized gas sensor has provided a platform for the detection of harmful gas with some of the above-mentioned qualities and thereby enabling the early detection of dangerous NO_2 gas.

The second chapter of the thesis gives an introduction to the Carbon Nanotubes. It starts with the basic understanding of the hybridizations in Carbon. Different allotropes of Carbon (Such as Diamond, Graphite, Graphene, Fullerenes and CNTs etc.) are discussed with their respective structure. A detailed description of Carbon Nanotubes about their structures, types, defects, their electronic and mechanical properties are present in this chapter. Different types of carbon nanotubes on the basis of number of walls, chirality etc. are discussed in an elaborative way. Various promising applications of CNTs are described in detail.

In the third chapter of the present thesis growth and characterization techniques of CNTs are discussed in detail with the special emphasis on Chemical Vapor Deposition. CNTs can be synthesized using arc discharge, laser ablation, Chemical Vapor Deposition method. These methods are well discussed in this chapter. Among these methods, Chemical Vapor Deposition method is the most popular method because of its versatility, less complexity. The high yield of good quality carbon nanotubes can be synthesized by this method. This method can be modified according to the requirement. Different variants of CNTs are being used by the researchers all over the world according to the specific needs. In this chapter, the variants of CVD such as Thermal CVD, Low Pressure CVD, and Plasma CVD etc. are discussed in details with their respective pros and cons. Characterization is an important part of the experimental research. The details of Characterization techniques which is used in the present study are also included in the present chapter. Microscopic techniques such as Scanning Electron Microscopy, Transmission Electron Microscopy and Atomic Force Microscopy are discussed with their basic principles. Raman

Spectroscopy has been proven to be the best spectroscopic technique for the investigation of the quality of CNTs. It is discussed in detail with the explanations of different bands (G-band, D-band etc.) which originate in the Raman spectrum due to the molecular vibrations associated with the specific structures of CNTs.

In the fourth chapter of the present thesis presents the literature survey of carbon nanotubes-based gas sensors. This chapter also includes literature survey of carbon nanotubes based flexible sensors. It also has survey about the 2D TMD materials based NO_2 gas sensor.

The fifth chapter discusses the role of metal deposition on the surface of SWCNTs. The conclusion of our work is that I successfully developed a good quality NO_2 sensor. Based on the results of observations it can be argued that the sensor has an almost instantaneous reaction rate to the feed gas and the selected recovery technique using UV radiation has advantages over previous technologies by small time and ease of use. The change insensitivity of SWNT sensor is induced by the coating of Au layer. The chemical pattern clearly demonstrates a significantly higher sensitivity of the Au-modified SWNT sensor compared with the un-functionalized SWNT sensor for NO_2 gas. By analyzing the results of Au deposited SWCNTs, it is established that the metal deposition has increased the NO_2 gas sensing property of the sensor. It is concluded that SWCNTs sensing response towards NO_2 gas can be improved by metal deposition.

In the sixth and the last chapter the functionalization of SWCNTs with polymer PEI has been discussed. I have developed a chemiresistive SWCNTs-PEI functionalized gas sensor by using a thermal CVD method. The higher adhesive coefficient for the electron-withdrawing NO_2 of PEI-coated SWCNTs than untreated SWCNTs. At room temperature, PEI-SWCNTs-coated resistive gas sensor demonstrated elevated sensing behaviour and swift reaction to NO_2. Furthermore, owing to room temperature operation of the resistive gas sensor can be encouragingly exploited in

the environment observation. A detector was successfully developed to detect low concentration (ppm) of NO_2 and by an accurate selection of thermal treatment, the complete recovery of the sensor was achieved. More importantly, it was found that with the increase in the duration of functionalization, the sensitivity of the SWCNTs is enhanced.

7.3 Future Scope

The major problem with most of the gas sensors is the process of designing them to be particularly sensitive with the target gas. Studies have suggested that there are three possible solutions to tackle this limitation which are,

- Designing a large array of sensors and using particular sections of these arrays with different sensing materials to target different gases.
- Implementing micro heater unit in the sensor and changing the temperature of the sensing materials and influencing the sensing material to be more sensitive to various gases at different temperature cycles.
- Implementing sensitive materials which are particularly more sensitive to the NO_2 poisonous gas.

The highly sensitive gas sensor design has been already designed in this research. Also, TMDs such as MoS_2, WS_2, and TiS_2 can be used for obtaing gas sensor for improving selectivity and other important sensing parameters.